UNIVERSITY OF CALIFORNIA SAN DIEGO

Synthesis and Characterization of Fluorescent Molecular Rotors

A Thesis submitted in partial satisfaction of the
requirements for the degree
Master of Science

in

Chemistry

by

Jamie Y. Lam

Committee in charge:

Professor Emmanuel Theodorakis, Chair
Professor Joseph O'Connor
Professor Jerry Yang

2020

The Thesis of Jamie Y. Lam is approved, and is acceptable in quality and form for publication on microfilm and electronically:

_____

_____

_____

Chair

University of California San Diego

2020

TABLE OF CONTENTS

LIST OF FIGURES AND TABLES

LIST OF SCHEMES

LIST OF SPECTRA

ACKNOWLEDGEMENTS

I especially want to thank Professor Emmanuel Theodorakis for giving me the opportunity to do research and for teaching me about synthesis. Thank you for your attentiveness and availability as a PI, and for teaching me how to critically think as a Chemist. Your genuine, never-ending excitement to hear research updates, as well as your willingness to work alongside me in lab when I need help, are things that I will always appreciate.

Thank you to Professor Jerry Yang and Rachel Ehrlich for their support and guidance on working with the amyloids portion of this project. Thank you to Professor Gürol Süel and Kaito Kikuchi for their excitement to test new dyes and compiling such great videos for the bacterial electrophysiology studies. Thank you to Professor James Lee and Tao Teng for testing our ratiometric dyes and working with us to understand their spectroscopic properties. Thank you to Professor Joseph O'Connor for his mentorship as I started working at UCSD, and to Professor Patricia Jennings for allowing me to use her fluorometer until our lab was able to acquire one.

Thank you to Professor Yitzhak Tor and his lab, especially Kaivin, Marcela, Kfir, Deyuan, Paul, and Phil, for allowing me to attend their group meetings and for teaching me about fluorescence.

Thank you to my lab mates Alex, Bank, Kevin, and Nan for their mentorship and guidance as I learned how to do synthesis and work independently. I have truly enjoyed struggling and growing alongside each of you.

To my parents, thank you for always supporting me in my search to discover my interests and passions. Your steadfast prayers, financial, and emotional support mean the world to me, more than I can ever express in words.

Finally, thank you to Professors Alex John, Yao Olive Li, Gabriel Davidov, Michael Page, and Frances Flores for cultivating my love for research and science at Cal Poly Pomona. To Dr. John especially,

thank you for being an amazing mentor and for being the first to take a chance on a random Food Science student who had an interest in Organic Chemistry. You have inspired me to get to where I am today.

This thesis contains material coauthored by Kikuchi, Kaito; Ehrlich, Rachel; Teng, Tao; Tharamak, Sorachat; Lee, James; Yang, Jerry; Süel, Gürol; Theodorakis, Emmanuel; and Lam, Jamie. The thesis author was the secondary author of these materials.

Kikuchi, Kaito; Lam, Jamie; Süel, Gürol; Theodorakis, Emmanuel. Figures 2.5, 2.6, and 2.7. Mr. Kikuchi was the principal researcher on these figures.

Ehrlich, Rachel; Lam, Jamie; Yang, Jerry; Theodorakis, Emmanuel. Figure 2.8. Ms. Ehrlich was the principal researcher on this figure.

Teng, Tao; Lam, Jamie; Lee, James; Theodorakis, Emmanuel. Figures 3.5 and 3.6. Mr. Teng was the principal researcher on these figures.

Tharamak, Sorachat; Lam, Jamie; Theodorakis, Emmanuel. Schemes E4 and E5, synthesis of final compounds QN1-BTZ/BTZM and QN2-BTZ/BTZM, and Spectra 22-41. Mr. Tharamak was the principal researcher of these schemes, compounds, and spectra.

ABSTRACT OF THE THESIS

Synthesis and Characterization of Fluorescent Molecular Rotors

by

Jamie Y. Lam

Master of Science in Chemistry

University of California San Diego, 2020

Professor Emmanuel Theodorakis, Chair

Small molecule fluorescent probes provide a non-invasive way to obtain accurate microviscosity measurements for biological analyses, especially when bulk measurements are not

feasible. A family of push-pull fluorescent dyes, inspired by the benzothiazole motif of Thioflavin T, are reported, along with preliminary data on their use for visualizing long-range bacterial signaling and binding affinities for amyloids. By altering the π-wire through increased conjugation and heteroatom substitution, a red-shifted ThT analogue was successfully synthesized.

Synthetic analogues of previously reported fluorescent probes were also synthesized. Increasing the π-wire from phenyl to naphthyl induced a bathochromic shift. It was also observed that switching from an ester to an amide altered photophysical properties in both sets of analogues. There was a slight hypsochromic shift due to the amide, likely attributed to the slight decrease in electron-withdrawing character of the acceptor group. Moreover, the emission intensity of the FRET donor decreased in the amide ratiometric system as compared to that of its ester counterpart, potentially indicating an enhancement of energy transfer between the donor and acceptor pair. These studies point towards ways to optimize the chemical structures of various fluorescent probes for specific applications.

CHAPTER 1: Introduction to fluorescent molecular rotors

The use of fluorescent probes has garnered interest in recent years, as it is a non-invasive method for the imaging of various environmental properties and biological processes. These probes are small molecules, typically containing an aromatic moiety, that absorb light at a certain wavelength and emit light of lower energy and thus, at a longer wavelength than the absorbed light— a process known as fluorescence. Fluorescence is usually described using the Jablonski diagram (Figure 1.2), in which the light source provides a photon, at a specific wavelength λ_{ex}, to excite an electron from the ground state (S_0) to the excited state (S_1).[1–3] This excited state is a short-lived species, which exists for a finite time known as the excited state lifetime. In order to relax from the excited state back to the ground state, the molecule can undergo non-radiative or radiative relaxation. Non-radiative pathways of relaxation include collisional quenching, rotational relaxation, and Förster resonance energy transfer (FRET).[4] Radiative relaxation leads to emission at a specific wavelength λ_{em}, which is typically red-shifted (lower energy) from the λ_{ex} due to some energy loss in the excited state. The efficiency of light absorption is quantified by the molar extinction coefficient, ε, whereas the efficiency of emission of absorbed photons is denoted by the quantum yield, Φ. The brightness of fluorescent dyes or proteins can therefore be quantified by the product of these two factors.[5,6] Another important consideration for fluorescent probes is the Stokes shift, which takes into account the difference in energy between the emission and excitation.[7,8] This energy difference is important for minimizing the background noise between the emission and excitation.

Fluorescence can either be exploited for biological assays through the use of fluorescent proteins, conjugation of protein to a fluorophore, or the introduction of small molecule probes to a system.[9–11] There are naturally occurring biological fluorophores, such as aromatic amino acids,

flavins, and fluorescent proteins. These native fluorophores can be used as biomarkers to observe changes in their local environments, such as changes in protein conformations or enzymatic reactions. Another option is to use genetically modified proteins that are specific for a chemical moiety and exploit that affinity for labelling purposes. Several of these methods, such as halo tagging and snap tagging, have become widely popular because simple linker groups can be added to fluorophores to increase their specific localization, as well as increase the stability of the dye by preventing any conformational changes during cellular uptake.[12] The alternative is to exclusively use small molecule fluorescent probes, which can have varying degrees of structural inspirations; some of these small fluorophores are designed from biological structures and introduce modifications to alter or increase fluorescence while still keeping biological functionality intact, whereas others are designed to be exogenously introduced, with localization being directed by various functional groups. A category of these exogenous small molecule fluorescent probes, coined fluorescent molecular rotors (FMRs), detect changes in microscopic environments.[13–16]

FMRs, sometimes referred to as push-pull dyes, contain a distinct structure of donor (D), π-system (π), and acceptor (A). Because of this unique D-π-A system, push-pull dyes have been mainly used to evaluate biological landscapes, such as monitoring changes in viscosity, polarity, or pH.

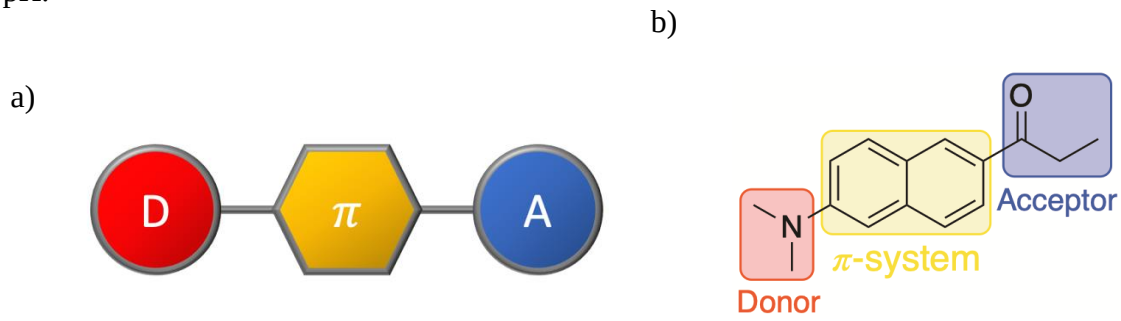

Figure 1.1. (a) Generic structure of push-pull dyes (b) Structure of prodan with D-π-A outlined.

There are several classes of FMRs, such as boron dipyrromethene (BODIPY)-based, dioxaborine-based, cyanine/hemi-cyanine-based, porphyrin-based, and thiophene-based dyes[17]. The free rotation of FMRs in non-viscous environments allows the excited molecule to adopt a twisted intramolecular charge transfer (TICT) state, resulting in the dissipation of energy in the form of non-radiative relaxation (i.e., rotational relaxation), which quenches the emission of the fluorophore.[18,19] However, in highly viscous environments, the rotation of the FMR is restricted, therefore allowing for the release of energy in the form of fluorescence. The intensity of fluorescence can be correlated with the viscosity of the environment using a calibration curve, thus giving rise to the use of FMRs in the determination of microviscosity in disease states, detection of amyloids, and visualization of organelles. Other novel uses for FMRs include the detection of volatile organic compounds (VOCs) and the monitoring of polymerization reactions.

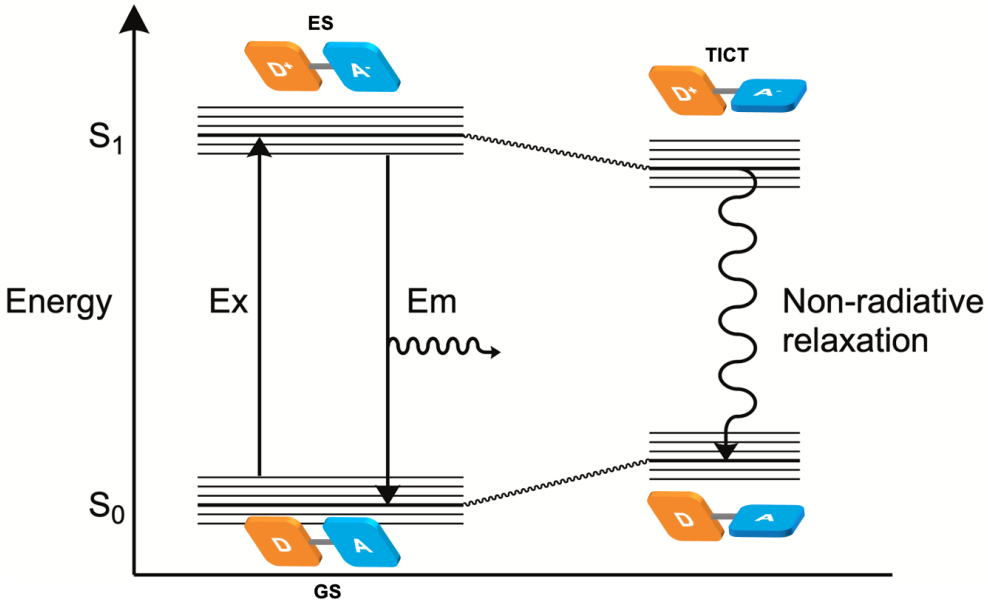

Figure 1.2. Jablonski diagram modified for FMRs with a single emission band.

Push-pull systems can be specifically designed by altering the D, π, or A portions to obtain desired optical and biological properties. For instance, dyes can typically be red-shifted by

increasing the D and/or A strength, or by increasing the amount of conjugation in the π component[20,21]. Red-shifted dyes are a valuable characteristic, as they allow greater contrast against naturally fluorescent biological compounds, which tend to be blue-shifted in comparison, and also prevent phototoxicity from the light source by using light of lower energy. Changes to the D-π-A system can also affect other parameters, such as binding and self-aggregation. As previously mentioned, targeting groups can be incorporated into dye design as well, which can direct the localization of the dye to different cellular compartments.

In the following section, three families of FMRs— BODIPY, dioxaborine, and cyanines— will be highlighted.

1. Examples of FMR scaffolds and their derivatives

BODIPY fluorescent dyes contain a boron dipyrromethene core for the donor (Figure 1.3a), which provides several advantages such as high quantum yields, large molar extinction coefficients, and sharp emission peaks[22,23]. Because of these advantages, BODIPY-based dyes are commonly used for imaging, since they can be tuned to be within the range that can penetrate tissue and eliminate background fluorescence signals. By attaching a targeting group, triphenyl phosphonium, to a previously reported BODIPY dye, Su *et al* synthesized a FMR (Figure 1.3b) to report mitochondrial viscosity; this dye had notably high sensitivity for solvent viscosity, especially in comparison to others in the 0.6 cP to 950 cP range.[24] López-Duarte *et al* reported the first FMR to selectively visualize the viscosity of the plasma membrane of live cells by synthesizing a BODIPY dye with a double positive charge[25] (Figure 1.3c); the double positive charge of this dye prevents endocytosis, thus allowing it to localize in the plasma membrane.

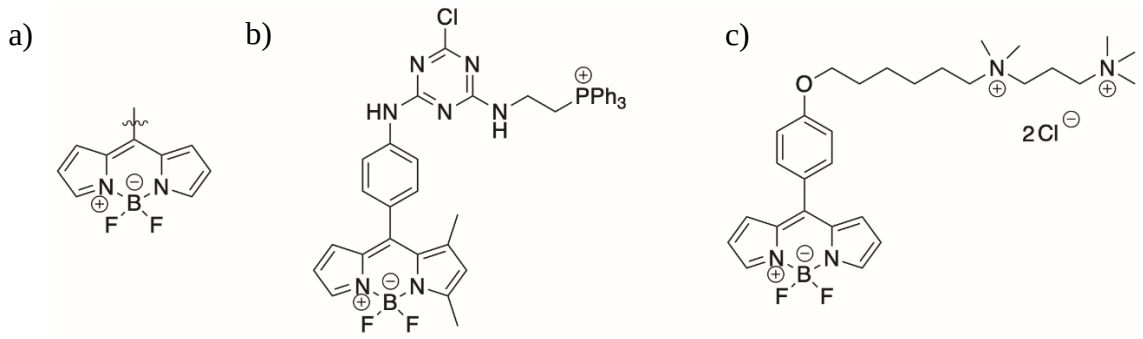

Figure 1.3. Examples of BODIPY-based FMRs.

Dioxaborine-based fluorescent dyes contain ketone and enol functionalities, bridged by a boron. Like BODIPY-based dyes, they exhibit far-red to near-infrared absorption and emission profiles, and high quantum yields.[26] Karpenko *et al* conjugated a DBX Red carboxylic acid derivative to carbetocin, a ligand for the oxytocin G protein-coupled receptor (Figure 1.4a) to allow for receptor imaging.[27] Furthermore, by taking advantage of the fact that FMRs are not very emissive in aqueous environments, they were able to conduct the imaging via no-wash conditions while preserving good contrast. A class of dioxaborine FMRs are coined CRANAD dyes and are based on the structure of curcumin. It was first reported by Ran *et al*, in which two derivatives, CRANAD-1 and CRANAD-2 (Figures 1.4b and 1.4c, respectively) were synthesized.[28] CRANAD-1 retains the overall structure of curcumin, with the added difluoroboronate to the diketone to observe the anticipated red-shifting effect— a hypothesis inspired from the classical BODIPY scaffold (Figure 1.3a). CRANAD-2 removes the methoxy groups of CRANAD-1, and replaces the hydroxyl groups for dimethyl amino donors, which are strongly donating auxochromes and shift the fluorescence to longer wavelengths.

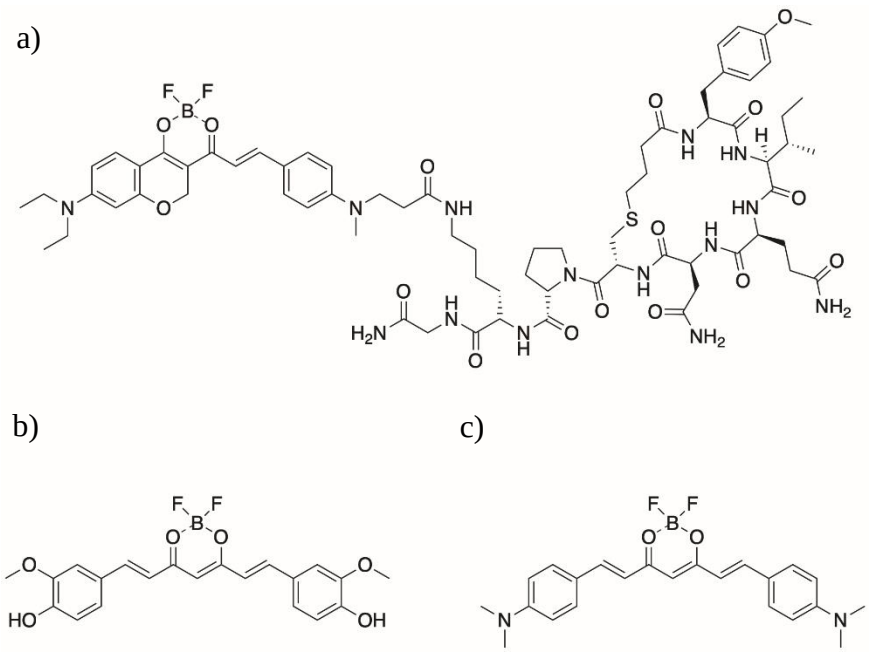

Figure 1.4. Examples of dioxaborine-based FMRs.

Cyanine- and hemi-cyanine-based fluorescent dyes have the general structure of a 3° amine connected to a 4° amine salt via a conjugated linker (Figure 1.5a). In cyanines, both the amine entities are cyclically caged by a hydrocarbon chain, whereas in hemi-cyanines, only one of the amines is cyclically caged and the other is free rotating. These cyclically caged structures can be elaborated with the insertion of heteroatoms and extended to include aromatic groups, which allow the amines to exist as various functional groups such as indoles, thiazoles, benzothiazoles, imidazoles, and oxazoles. Cyanines have found utility as membrane-potential fluorescent probes, specifically as slow response probes, which are translocated across cellular membranes and demonstrate fluorescence depending on their localization during membrane potential changes.[29] These membrane potential probes are commercially available, consisting of indole (DiI), thiazole (DiS), and oxazole (DiO) cyanines, and their nomenclature typically includes $C_{\#}(\#)$ after the denotation of the functional group, with the subscript indicating the free carbon chain on the nitrogen, and the number in parentheses indicating the number of carbons in the conjugated linker

(e.g., $DiSC_3(5)$, Figure 1.5d). They are also commonly used for imaging, as some cyanines have shown good affinity for binding to DNA and the nucleus.

Recently, Kang *et al* used an NHS derivative of Cy3 (Figure 1.5c) to demonstrate increased viscosity at the oil-water interface of microdroplets, an environment where there has been observed differences in chemical thermodynamics as compared to bulk solutions.[30] As the rapid *cis-trans* isomerization is restricted at the interface, fluorescence lifetime is also increased due to the decrease in non-radiative relaxation methods. Peng *et al* introduced an aldehyde auxiliary to the conjugated linker to create a ratiometric cyanine dye (Figure 1.5b) for cellular viscosity, which circumvents potential issues with dye concentration and allows this probe to be used for both ratiometric measurements and lifetime imaging.[31]

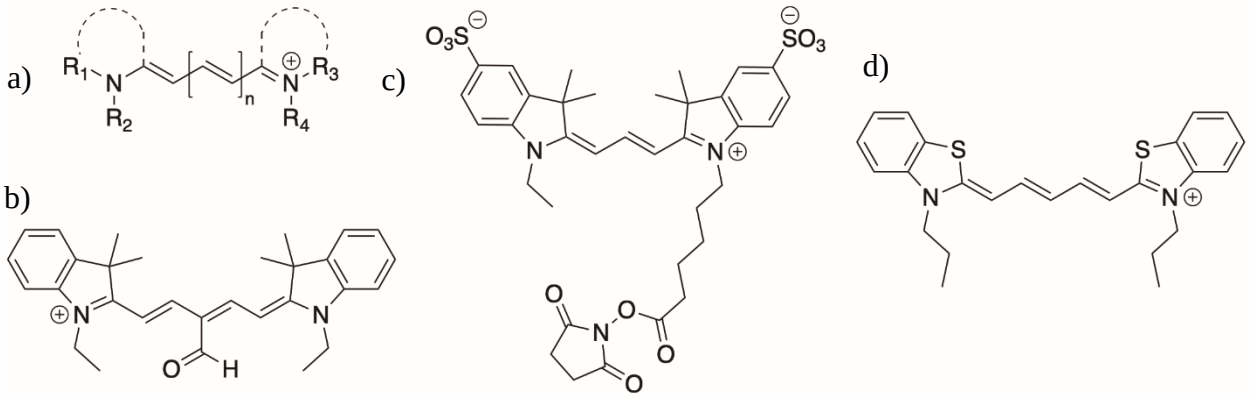

Figure 1.5. Examples of cyanine-based FMRs.

2. Applications of FMRs

FMRs lend themselves to a wide variety of applications since they demonstrate an increase in fluorescence intensity in constricted environments, either from microviscosity changes or binding to a protein. Moreover, by attaching targeting groups to FMRs, their localization to specific organelles can be directed, therefore allowing the imaging or determination of viscosity at specific sites. Among the first examples of push-pull dyes utilized for viscosity sensing was the

hydrophobic dye 9-(2,2-dicyanovinyl) julolidine (DCVJ); Kung and Reed explored the use of DCVJ for determining the microviscosity of sodium dodecyl sulfate micelles and dipalmitoyl phosphatidylcholine vesicles, as well as to follow tubulin polymorphs and assembly based on the changes in fluorescence of DCVJ.[32,33] The hydrophobic nature of DCVJ limits its use for probing hydrophilic microenvironments, giving rise to derivatizations of this classical FMR. One example of a hydrophilic DCVJ derivative is 9-(2-carboxy-2-cyanovinyl) julolidine (CCVJ), which increases hydrophilicity by changing one of the cyano-groups to a carboxylic acid moiety. This carboxylic acid moiety can also be used to create various ester derivatives, further demonstrating the versatility of D-π-A fluorescent probes.

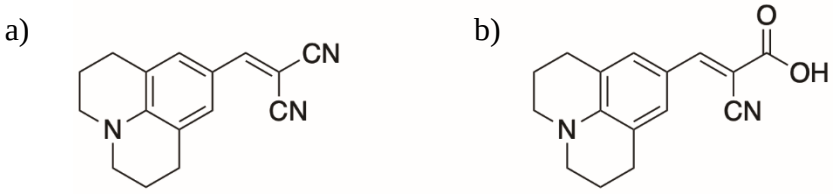

Figure 1.6. Structures of (a) DCVJ and (b) CCVJ.

Targeting specific organelles is crucial in biological analyses since the viscosity of cellular compartments can be correlated with various disease states, as this change in cell viscosity affects various metabolic processes within the cell. For instance, probes that typically target the mitochondria are cationic with an overall lipophilic structure, often containing aromatic rings. Known targeting groups include triphenyl phosphonium, cyanines, rhodamines, and cationic quinoline and pyridines.[12] This targeting is possible due to the negative membrane potential of the inside of the mitochondria, arising from the proton motive force.

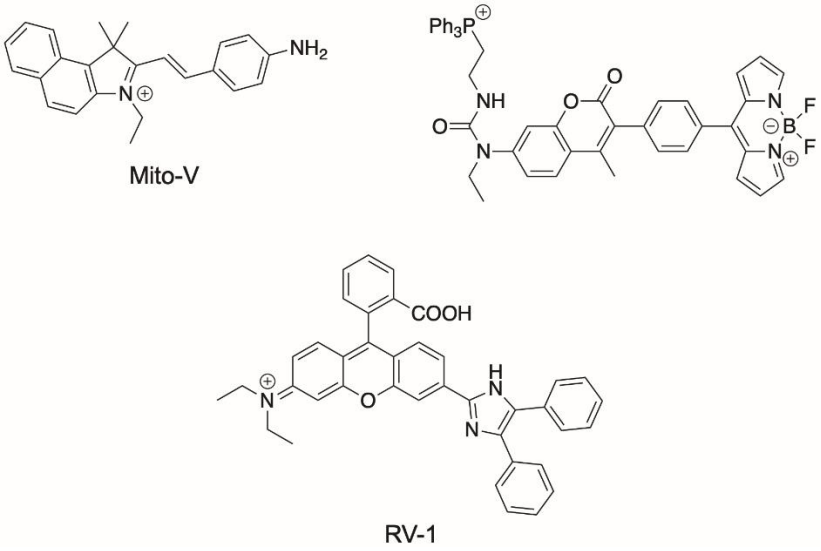

Figure 1.7. Examples of fluorescent probes developed to monitor mitochondrial viscosity.[34–36]

Another application for FMRs is the detection of amyloid plaques. The extracellular accumulation of amyloids in the brain is indicative of many neurodegenerative diseases, such as Alzheimer's, Parkinson's, and Huntington's disease. FMRs show significant increases in brightness when bound to an amyloid, as binding to the β-sheet structures of amyloids restricts rotational relaxation, thus increasing the quantum yield. Several chemical scaffolds have been investigated for the detection of amyloid aggregates (Figure 1.8), such as thiazole, stilbene, curcumin, thiophene, alkatriene, and BODIPY cores.[37]

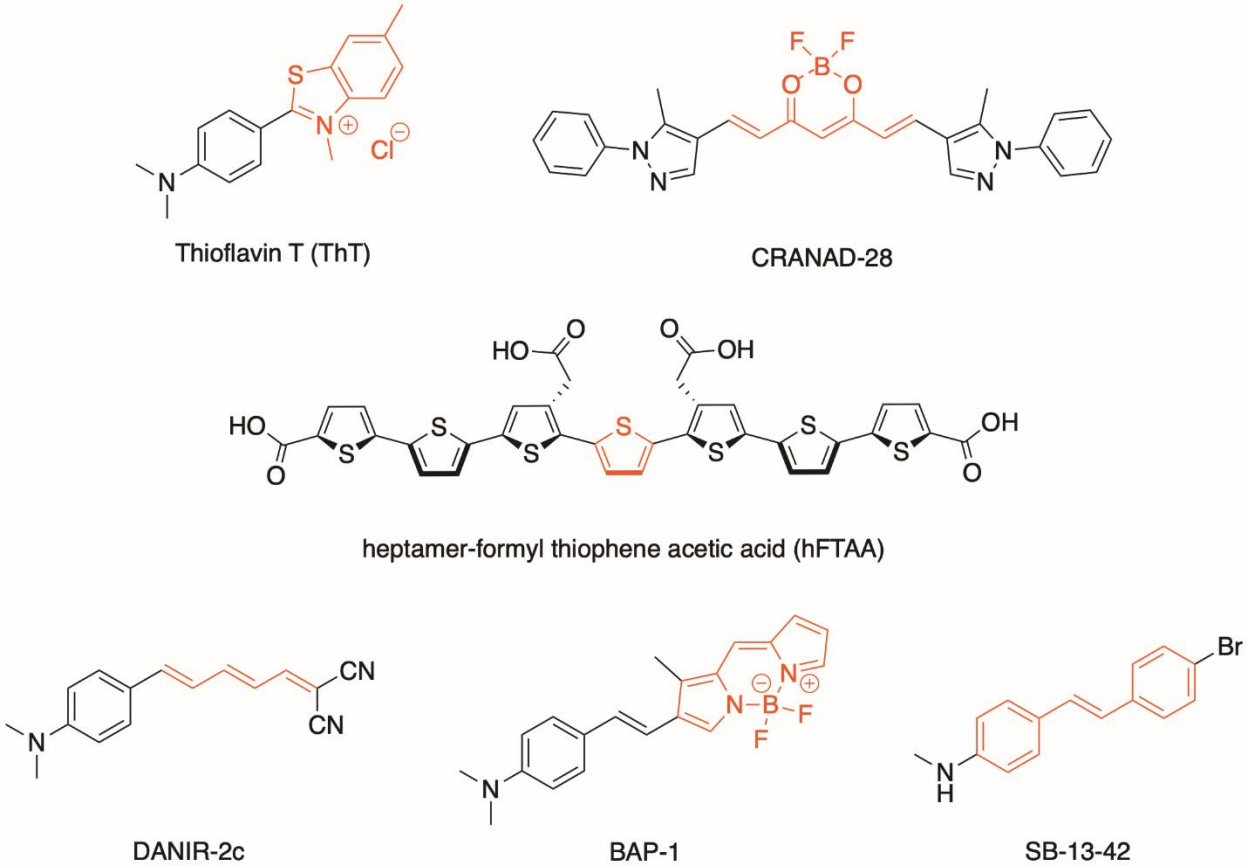

Figure 1.8. Examples of FMRs that have shown promise in binding to amyloids. Functional group scaffolds are highlighted in red.[38–42]

Fluorescent probes have been incorporated into polymer matrices, where they have been used for the detection of VOCs. In a highly ordered polymer, the fluorescence intensity of FMRs is high since their rotation is restricted. Pucci *et al* incorporated FMRs into polystyrene-based polymers and exposed them to VOCs, noting the decrease in fluorescence intensity due to VOC-induced plasticization; polystyrene is porous, and these micro-channels can be filled with solvent vapors upon exposure, therefore locally solvating the FMRs and allowing non-radiative decay as the primary mechanism of relaxation.[43,44]

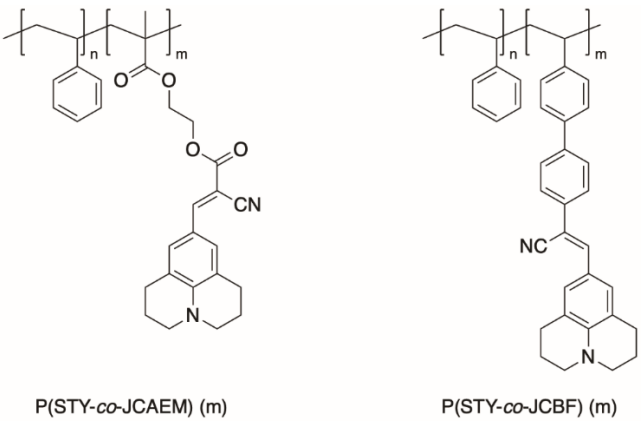

Figure 1.9. Julolidine-based FMRs reported by Pucci *et al* for the detection of VOCs.

The progression of polymerization reactions when synthesizing polymers can also be monitored by FMRs. As polymerization progresses, there is a drop in polarity due to conversion of unsaturated to saturated bonds, thus leading to a slight hypsochromic shift. Moreover, the viscosity of the microenvironment is increased as the polymer grows, thus also increasing the fluorescence intensity of the FMR by restricting free rotation. Various probes have been developed for the monitoring of polymerization reactions, taking advantage of different fluorescent properties such as excimer formation, quenching, or emission shifts that result from progression.[45] Ortyl *et al* synthesized several 2-amino-4,6-diphenyl-pyridine-3-carbonitrile derivatives (Figure 1.10b) and compared their sensitivity and utility to several reference FMRs (Figure 1.10a).[46] It was determined that when R_1 = CN and R_2 = OCH_3, the push-pull system was optimized and there was increased sensitivity to microenvironmental changes, in addition to having the most red-shifted absorbance and emission. Interestingly, these probes were demonstrated to not only be effective in monitoring free radical and thiol-ene photopolymerzation, but also served a role in aiding the photoinitiation of the reactions by acting as photosensitizers.

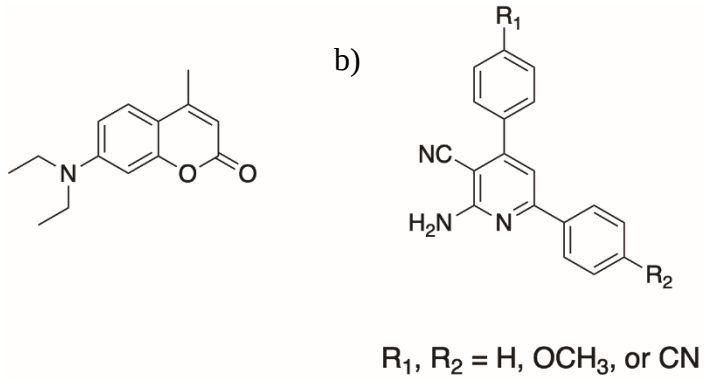

Figure 1.10. FMRs for the monitoring of polymerization.

Accurately measuring microscale viscosities is crucial to the understanding of biological processes. Classical methods of measuring viscosity using viscometers, such as rotational viscometers, vibrational viscometers, falling ball viscometers, or falling piston viscometers, are impractical at a cellular level, therefore highlighting the significant role FMRs play in research. In particular, FMRs with the classical push-pull structure are easily tunable in terms of spectroscopic properties, and encompass a wide array of possible D, π, and A moieties. Cellular targeting and water solubilizing groups can be incorporated into FMR design to direct localization, allowing information to be obtained on specific organelles. Aside from biology, FMRs have found use in other fields, such as materials chemistry[47] and atmospheric chemistry[48], and have shown potential for applications in the food industry[49]. Because of their wide range of applications and ability to be fine-tuned towards specific sensing needs, FMRs present themselves as a valuable tool and interesting field for further development.

CHAPTER 2: Thioflavin T analogues

1. Introduction

The buildup of insoluble protein aggregates, known as amyloids, is responsible for the development of neurodegenerative diseases such as Alzheimer's and Parkinson's disease, and the extracellular accumulation of amyloids is indicative of these diseases, even prior to the onset of clinical symptoms. The push-pull dye Thioflavin T (ThT, Figure 2.1) has been the standard for the detection of amyloids, as it is not very emissive when unbound, but shows a drastic increase in fluorescence intensity when in the presence of amyloids.

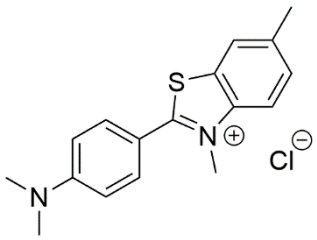

Figure 2.1. Structure of ThT.

One major issue with ThT is its emission— it is below the near-red and infra-red range of 650-900 nm, which helps minimize background fluorescence from native fluorophores and allows for adequate tissue penetration. Because of this, there have been recent efforts to synthesize fluorescent probes with near-red or infra-red emission, while still maintaining good binding affinity to amyloids, notable fluorescence changes upon binding, high quantum yields, blood brain barrier permeability, and low toxicity.[37]

Additionally, although it is hypothesized that the accumulation of amyloids is involved in the onset of neurodegenerative diseases, the exact structure of the different amyloids themselves have yet to be elucidated. ThT is hypothesized to bind along the long edges of the amyloid fibril β-sheets, in which it interacts with aromatic residues of amino acids, in addition to forming key

hydrophobic interactions with nonpolar sidechains of leucine and tyrosine.[50] Although ThT has been considered the standard for amyloid detection, recent efforts have been directed towards synthesizing dyes that are specific for certain amyloid fibrils, such as amyloid-beta (Aβ) and α-synuclein, for the diagnosis and differentiation of specific neurodegenerative diseases. Because the aggregation of amyloids occurs prior to clinical symptoms of neurodegenerative diseases, the development of fluorescent probes to accurately distinguish between different amyloids is crucial for monitoring purposes and deciding upon proper treatment.

Recently, it was reported that bacterial colonies communicate similarly to the signaling of neurons, therefore introducing the field of bacterial electrophysiology. Since the membrane potential within the bacterial cells is highly negative, cationic dyes like ThT are readily translocated across the bacterial membrane. Bacterial biofilms grow outwards, so when cells in the interior of the bacterial biofilm undergo metabolic stress due to the lack of glutamate, they release potassium ions, causing the surrounding bacterial cells in the biofilm to depolarize then hyperpolarize; since glutamate and potassium are both charged, the potassium flux hampers the uptake of glutamate for neighboring cells, causing metabolic stress and the corresponding release of potassium.[51] This cascade continues until the edge of the bacterial biofilm, which decreases the consumption of the outer bacterial cells and increases nutrient availability for the interior cells. Once the interior cells are no longer under metabolic stress, the potassium flux stops, allowing the biofilm to continue expanding from the resuming of outer bacterial metabolism. This overall altruistic process serves as long-range signaling across the biofilm, in which bacterial metabolic stress can be distributed between the inner and outer membrane regions.[52,53]

By incorporating a fluorescent dye into the cellular membrane, the metabolism and signaling can be visualized by the oscillation of fluorescence of the bacterial biofilm, where firing

cells are fluorescent and those that are not do not fluoresce. This oscillation of fluorescence is observed due to heterogeneous signaling, as there is minimal gain beyond a certain threshold of firing cells due to the cost of individual bacterial cell growth; this observation is described by percolation theory.[54] For the purpose of studying long-range bacterial signaling, the drawback of ThT is that it is excited and emits in the blue range, therefore leading to phototoxicity and making a red-shifted fluorescent probe desirable. Other qualities that are valuable in these Nernstian dyes are their S/N ratio, a short equilibration time, and having minimal effects on bacterial physiology.[55] In terms of photophysical properties, brightness is important in increasing the S/N ratio, since adding high concentrations of the dyes can start to affect the membrane potential.

With the robustness of ThT and the drawback of excitation and emission wavelength in mind, several derivatives of ThT have been synthesized. However, they all involve drastic structural changes, such as the addition of other auxiliary groups or introducing a completely new A to the D-π-A system. In this work, we opted to shift the excitation and emission wavelengths via changes strictly to π, thereby preserving the unique benzothiazole or benzothiazolium A of ThT in the derivatives.

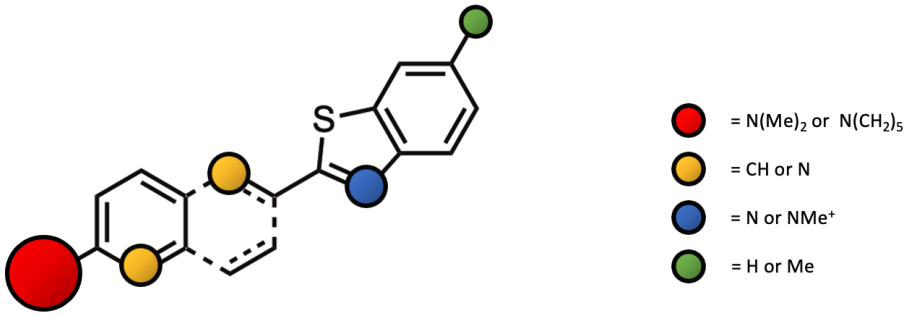

Figure 2.2. ThT modifications involved in this work.

2. Results and Discussion

A family of push-pull dyes was synthesized, inspired by the benzothiazolium acceptor of ThT. This family of dyes consists of structural changes to the D-π-A and includes their benzothiazole (BTZ) and benzothiazolium (BTZM) counterparts, which are the non-methylated and methylated species, respectively.

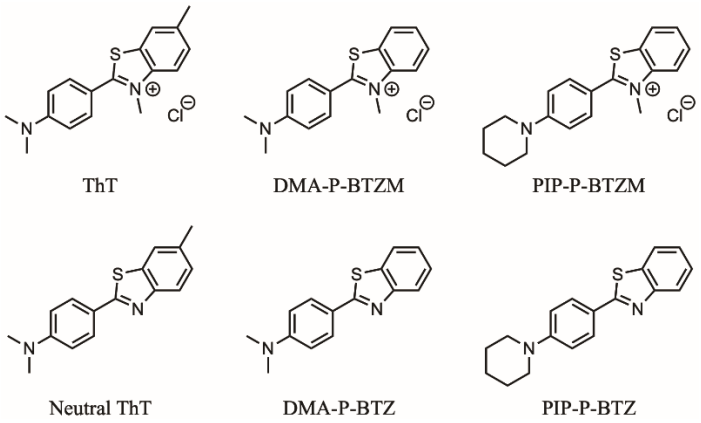

Figure 2.3. Synthesized dyes with changes to the D and A portions of ThT.

The first generation (Figure 2.3) of this family consists of control dyes, in which sequential changes were made to the D and A of ThT, dictated by the availability and feasibility of synthesis. The 2-amino-5-methylbenzenethiol needed for cyclization with the aldehyde is expensive, so a set of controls (DMA-P-BTZM and DMA-P-BTZ) was synthesized using 2-aminobenzenethiol, a more cost-efficient option. The dimethylamino donor was swapped for a piperidinyl group (PIP-P-BTZM and PIP-P-BTZ), since the piperidine could easily be installed by a Buchwald-Hartwig cross-coupling reaction. Piperidine was not expected to have much change upon the excitation or emission profiles of the ThT derivatives, as it is not a constrained ring and remains a dialkylated nitrogen that is not caged to the π-system. In regards to the D and A alterations, it appears that both the methyl group on the A and dimethylamino D moiety were installed in the industrial

synthesis out of ease, since retrosynthetic analysis of dehydrothiotoluidine leads to what seems to be a dimerization of *p*-toluidine, therefore not necessarily being crucial for functionality.

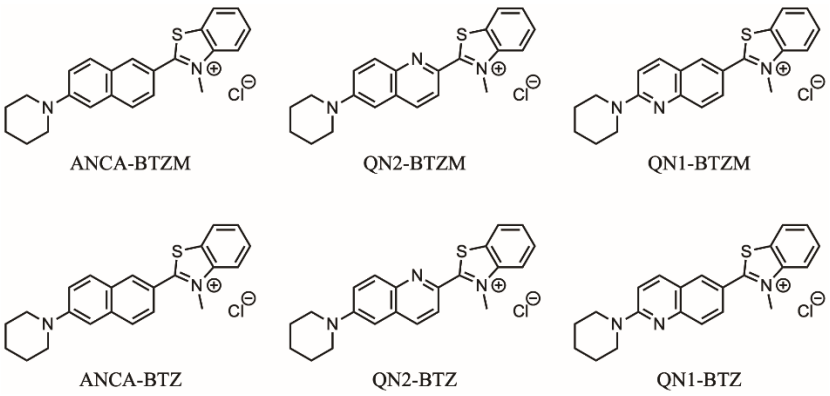

Figure 2.4. Synthesized dyes with changes to π of ThT.

The second generation of dyes (Figure 2.4) focuses on changes to the π of ThT. It is known that extending the conjugation of the push-pull system causes the emission to be red-shifted, since the increased conjugation lowers the HOMO-LUMO energy gap[56]. In previous studies, it was discovered that the incorporation of nitrogen atoms in the naphthalene ring could either red- or blue-shift the probes due to their effect on HOMO and LUMO by altering the electron density by the acceptor or donor. As a result, the BTZ and BTZM analogues of quinolines QN1 and QN2, with the number denoting the ring location of the nitrogen atom, were synthesized to observe their effects upon the optical properties of the probes.

The large scale synthesis of ThT typically involves methylation of dehydrothiotoluidine under high pressure and temperature to give ThT. Although this is a highly efficient synthesis, this method is not practical for benchtop synthesis. Instead, we opted to install the benzothiazole and benzothiazolium groups via an acid-mediated cyclization of the aldehyde with 2-aminobenzenethiol or 2-amino-5-methylbenzenethiol, and 2-(methylamino)benzenethiol, respectively. Initially, the goal was to synthesize the BTZM species from the BTZ via methylation.

However, methylation efforts using methyl iodide yielded methylation products at the wrong nitrogen (i.e., the donor).

Once synthesized, the dyes were dissolved in DMSO at a concentration of 1 mg/mL, and appropriately diluted until good resolution of excitation and emission spectra could be achieved.

Table 2.1. Photophysical properties of synthesized ThT derivatives

	λ_{ex} (nm)	λ_{em} (nm)	Stokes shift (cm^{-1})
Neutral ThT	304	425	9365
ThT	333	490	9622
DMA-P-BTZ	364	428	4108
DMA-P-BTZM	367	488	6756
PIP-P-BTZ	363	432	4400
PIP-P-BTZM	349	482	7906
ANCA-BTZ	368	493	6890
ANCA-BTZM	537	621	2519
QN1-BTZ	425	443	956
QN1-BTZM	476	546	2693
QN2-BTZ	475	519	1785
QN2-BTZM	589	652	1641

Table 2.1 shows the excitation and emission of each ThT derivative, and the normalized spectra can be seen in Figures 2.A.1 and 2.A.2, respectively. As expected, there were minimal changes to the emission spectra due to the removal of the methyl auxiliary group, as well as changing the donor from a dimethylamino to piperidinyl group (Figure 2.A.3 and 2.A.4). ANCA-BTZM demonstrated the expected bathochromic shift due to the extension of conjugation (Figure 2.A.5). The QN1 derivatives showed a notable hypsochromic shift in comparison to the ANCA derivatives due to decreasing electron density around the donor, while QN2 showed a bathochromic shift by decreasing electron density around the acceptor (Figure 2.A.6). The BTZM

species have longer emission wavelengths as well, highlighting the effect of A strength (degree of electron deficiency).

2.1 Bacterial cell studies

To ensure that all changes in optical properties were due to the changes from π, the 5 controls were further evaluated qualitatively, through visualization in bacteria.

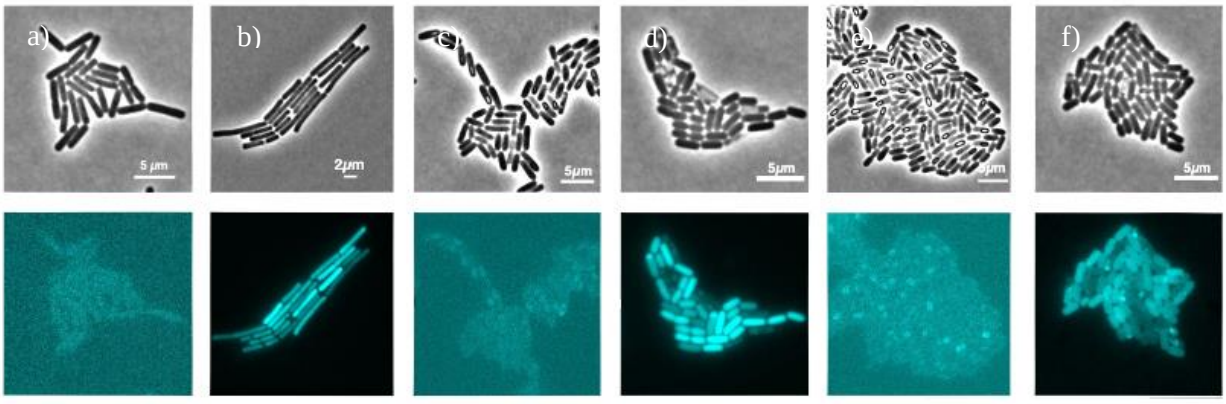

Figure 2.5. ThT and control dyes in *Bacillus subtilis*. (a) neutral ThT (b) ThT (c) DMA-P-BTZ (d) DMA-P-BTZM (e) PIP-P-BTZ (f) PIP-P-BTZM. Kikuchi, Kaito; Lam, Jamie; Süel, Gürol; Theodorakis, Emmanuel. Figure 2.5. Mr. Kikuchi was the principal researcher on these figures.

As shown in Figure 2.5, the removal of the methyl from the BTZ and BTZM moieties did not have much effect on the activity of the dyes, nor did changing the donor from dimethylamine to piperidine. As a result, changes to the optical properties for the subsequently synthesized dyes were attributed to the changes in π length and heteroatom substitutions.

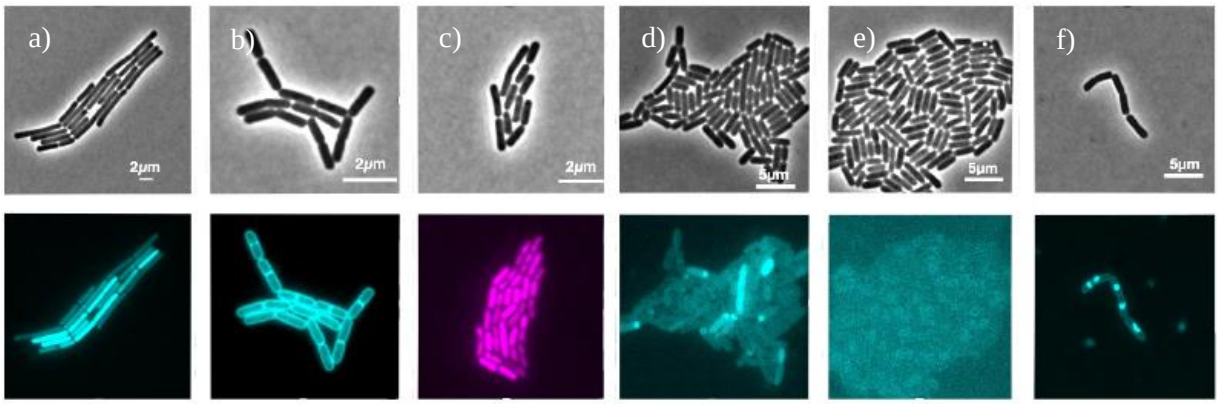

Figure 2.6. ThT and π derivatives in *Bacillus subtilis*. (a) ThT (b) ANCA-BTZ (c) ANCA-BTZM (d) QN1-BTZM (e) QN1-BTZ (f) QN2-BTZ (QN2-BTZM omitted). Kikuchi, Kaito; Lam, Jamie; Süel, Gürol; Theodorakis, Emmanuel. Figure 2.6. Mr. Kikuchi was the principal researcher on these figures.

Although the photophysical properties of QN2 were desirable in terms of the furthest bathochromic shift in wavelength, both QN1- and QN2-BTZ and BTZM were toxic to bacterial cells. Quinoline derivatives, like bedaquiline, have demonstrated antibacterial properties[57], so the quinoline scaffold of the QN1 and QN2 derivatives may cause toxicity. Interestingly, ANCA-BTZ showed better S/N than its phenyl π counterparts and seemed to only bind to the outside of the cell. This was hypothesized to be the cell wall, as Gram-positive bacteria, like *Bacillus subtilis*, have a thick layer of peptidoglycan (PG) on the outside of the cell. Similar to crystal violet in a Gram stain, the dye would be better retained in the thick layer of PG of Gram-positive bacteria, whereas Gram-negative bacteria, like *Escherichia coli*, have a layer of lipopolysaccharide (LPS) covering a thin layer of PG, and do not retain crystal violet.

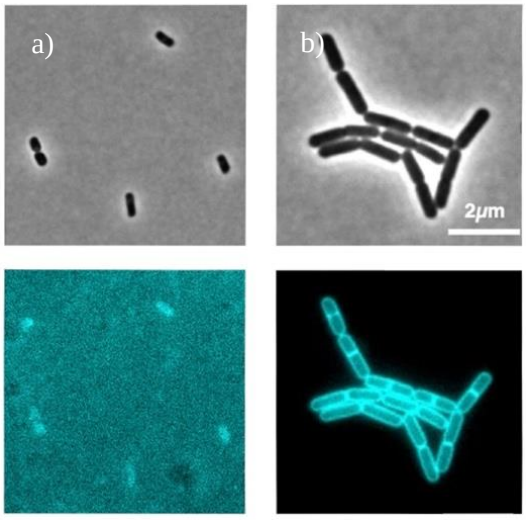

Figure 2.7. ANCA-BTZ in (a) *E. coli* and (b) *B. subtilis*. Kikuchi, Kaito; Lam, Jamie; Süel, Gürol; Theodorakis, Emmanuel. Figure 2.7. Mr. Kikuchi was the principal researcher on these figures.

As seen in Figure 2.7, ANCA-BTZ stained *B. subtilis* with good contrast but not *E. coli*, reinforcing the hypothesis that the dye was localizing in the cell wall. To further confirm this, testing on other strains of Gram-positive and Gram-negative bacteria would be necessary, as well as cell wall perturbing studies to demonstrate ANCA-BTZ can accurately track changes to the cell wall. Nonetheless, this is an interesting preliminary finding, since fluorescent Gram staining techniques could provide clinical benefits, such as potentially expediting diagnosis or differentiating Gram-positive bacteria from a mixture of colonies. Gram staining requires heat fixing of cells, therefore making it impossible to perform the Gram classification on live bacteria, whereas a fluorescent dye that discriminates between these two types of bacteria could provide both classification and monitoring of bacterial growth in real-time.

2.2 Amyloid binding studies

ANCA-BTZM showed an increase in fluorescence intensity when in the presence of α-synuclein. This supports the suggestion that the pi-stacking and aromatic sidechains may play a role in the binding of these molecular rotors to amyloids, in which the constriction of their rotation

results in an enhanced fluorescence. However, the fold increase of ANCA-BTZM in comparison to ThT is significantly less, specifically 9.5 ± 2.1 RFU and 58.0 ± 4.5 RFU, respectively.

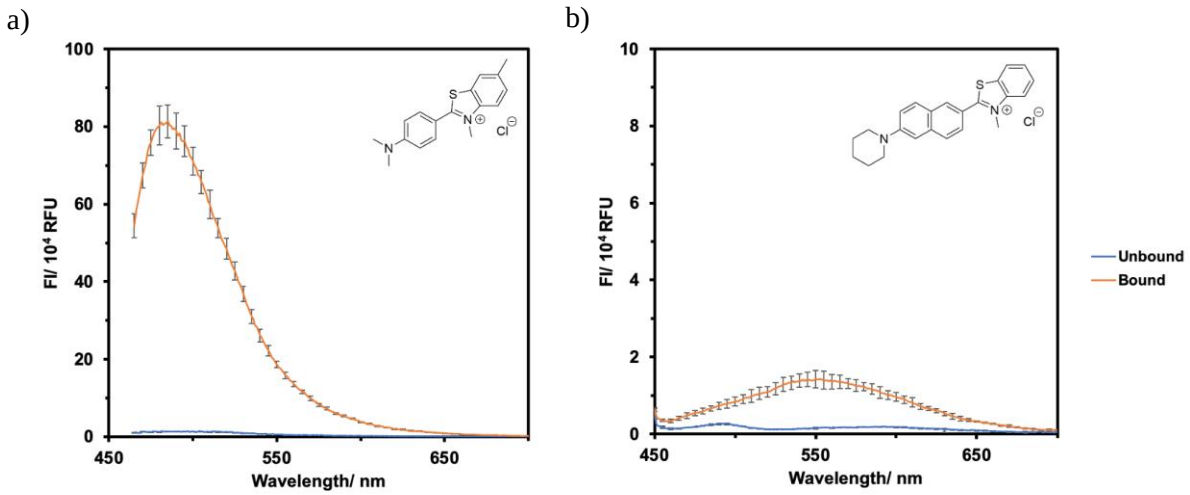

Figure 2.8. Fluorescence changes upon binding with α-synuclein. (a) ThT (b) ANCA-BTZM. Ehrlich, Rachel; Lam, Jamie; Yang, Jerry; Theodorakis, Emmanuel. Figure 2.8. Ms. Ehrlich was the principal researcher on this figure.

It remains unclear whether these results are due to decreased binding of ANCA-BTZM to α-synuclein or differences in photophysical properties (i.e., molar absorptivity, quantum yield, and brightness), so further experiments to determine K_d, the binding affinity, of ANCA-BTZM to α-synuclein would be beneficial.

3. Conclusion

In summary, it was demonstrated that changes to the π-system of push-pull dyes can result in hypsochromic or bathochromic shifts. Although the quinolines provide intriguing paths of derivatization, they cannot be further explored for use in bacteria due to their similarity to anti-bacterial drugs. ANCA-BTZM showed promising results in the bacterial electrophysiology studies as a red-shifted ThT derivative, but alterations must be made to increase brightness prior to further biological studies. This probe also showed an increase in fluorescence when in the presence of amyloids, suggesting that it binds similarly to ThT.

4. Future directions

When developing a probe with biological applications, having good contrast is crucial. Future developments involving ANCA-BTZM, which showed the most promise in both the bacterial and amyloid-binding studies, will be focused on increasing brightness, potentially through changing the donor to an azetidine group, which has been shown to improve quantum yields of push-pull dyes[58,59]. Structure activity relationships could also be examined by screening different donor groups, such as pyrrolidine or azocane, to observe the effect of increased lone pair availability and increased rotational bulk. Another approach is to mimic the structure of julolidine by preventing the rotation of the donor group by fusing the nitrogen to the naphthalene via a six-membered hydrocarbon bridge. By hindering rotation at one site, adoption of the TICT state should be less probable, therefore increasing quantum yields. This may also help increase the intensity by introducing a mild electron-donating group at a location in which the resonance travels through the π-wire.

Although ANCA-BTZM has accomplished the goal of making a bathochromically shifted ThT derivative, changes to the π-system may also be investigated to synthesize a dye in the tissue-penetrating range. BODIPY-based and rhodamine-based dyes have become popular due to their potential to achieve near-red to infra-red emissions, and may provide a good starting point for the alteration of ANCA-BTZM. Moreover, it is known that heavy atoms, like silicon, cause red-shifting when incorporated into a dye structure[60]. It is unknown what the effect of such a bulky group will be on the bacteria or the binding capability to amyloids, but this alteration provides an interesting possibility for derivatization while preserving the benzothiazolium moiety.

Another key point of interest is investigating ANCA-BTZM and QN2-BTZM for their binding selectivity. Preliminary studies have indicated ANCA-BTZM binds to α-synuclein. Since

the only change between the two structures is the heteroatom substitution of nitrogen in the second aromatic ring, differing results may be attributed to the binding pocket not accommodating a basic site. Testing these two dyes on another amyloid, such as Aβ, may demonstrate a difference in binding sites if QN2-BTZM or ANCA-BTZM are able to show differences in fluorescence intensity.

5. Appendix

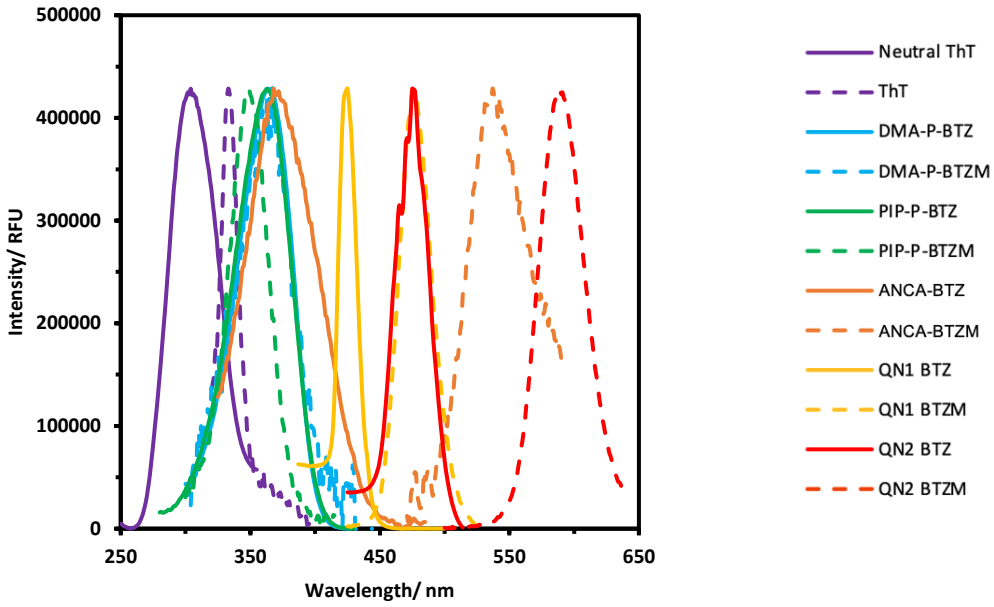

Figure 2.A.1. Normalized excitation spectra for ThT derivatives.

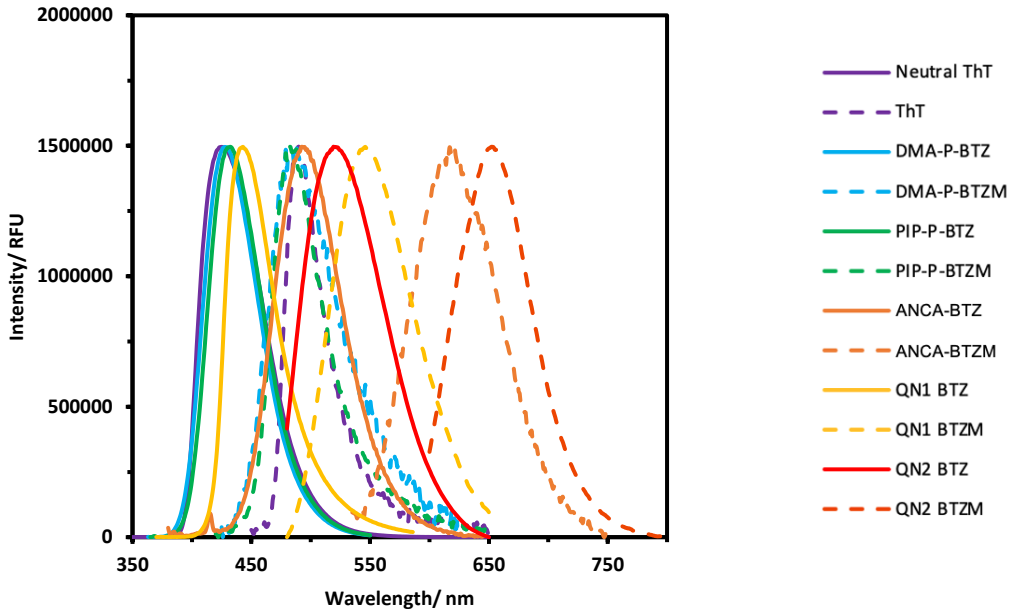

Figure 2.A.2. Normalized emission spectra for ThT derivatives.

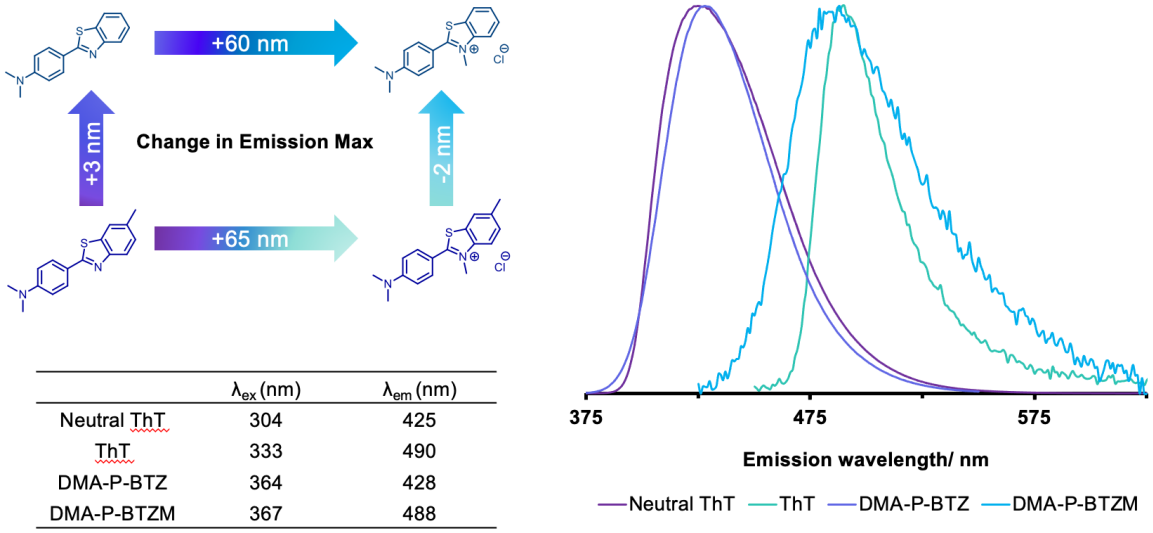

	λ_{ex} (nm)	λ_{em} (nm)
Neutral ThT	304	425
ThT	333	490
DMA-P-BTZ	364	428
DMA-P-BTZM	367	488

Figure 2.A.3. Effect of removing the auxiliary methyl group.

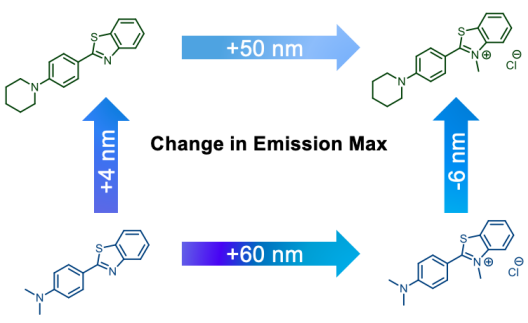

	λ_{ex} (nm)	λ_{em} (nm)
DMA-P-BTZ	364	428
DMA-P-BTZM	367	488
PIP-P-BTZ	363	432
PIP-P-BTZM	349	482

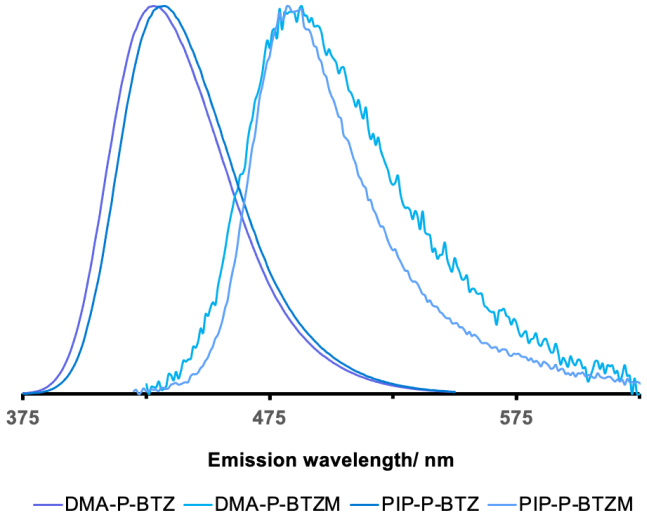

Figure 2.A.4. Effect of switching the donor group.

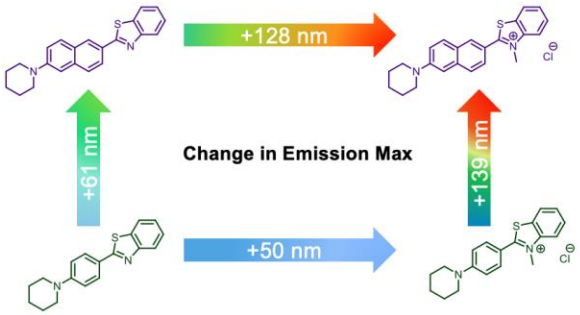

	λ_{ex} (nm)	λ_{em} (nm)
PIP-P-BTZ	363	432
PIP-P-BTZM	349	482
ANCA-BTZ	368	493
ANCA-BTZM	537	621

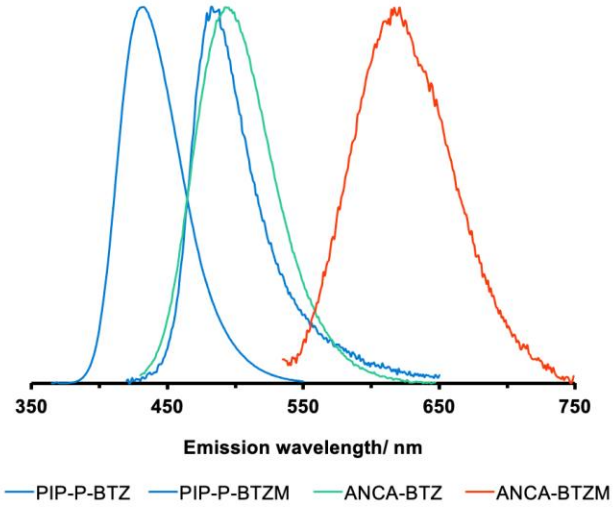

Figure 2.A.5. Effect of extending π-conjugation.

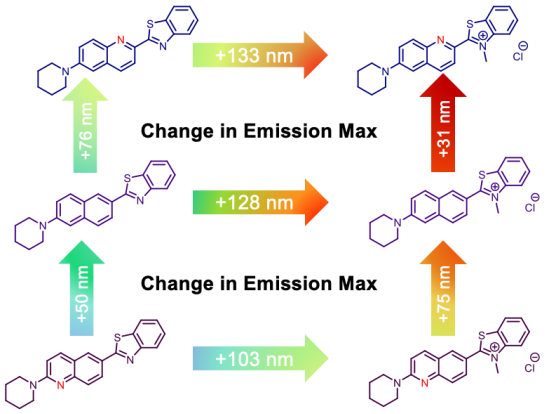

	λ_{ex} (nm)	λ_{em} (nm)
ANCA-BTZ	368	493
ANCA-BTZM	537	621
QN1-BTZ	425	443
QN1-BTZM	476	546
QN2-BTZ	475	519
QN2-BTZM	589	652

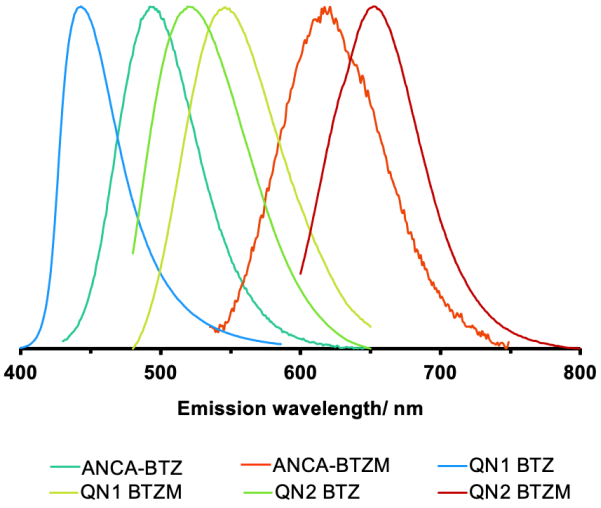

Figure 2.A.6. Effect of nitrogen placement in the conjugation path.

CHAPTER 3: Amide modifications of previously reported dyes

1. Introduction

It is known that amides are more stable than esters, due to the decreased electronegativity of the nitrogen atom that in turn, increases the efficiency of its lone pair engagement in stabilizing the partial positive charge of the carbonyl group— resonance stabilization prevails here. This logic can be translated to a biological perspective, where fluorescent probes with amides are more resistant to degradation by hydrolysis than their ester counterparts. Two previously reported probes, ARCAM-1 and ANCA-11, differed only by their amide or ester linkage. However, there was a notable difference in stability in the live animal models, as well as an approximate 8-fold increase in fluorescence in the amide derivative when in the presence of amyloids[61].

The use of FMRs as viscosity sensors can be useful, but when quantifying the viscosity of complex biological systems, having an internal reference fluorophore is extremely useful. Steady-state fluorescence (i.e., emission intensity) can be used for simple measurements or detection, but for quantitative measurements of complex systems, such as determining microscale viscosities in biological systems, dye concentration and fluid optical properties become significant factors in observed emission intensity.[62] The use of a ratiometric dye, rather than a simple FMR, would aid in circumventing the aforementioned factors. Ratiometric dyes are molecules that have dual emissions, and these emission intensities can be used to calculate a ratio that normalizes the observed emission intensity, thus acting as an internal reference and providing a more accurate measurement. A previously reported ratiometric dye, henceforth referenced in this work as dye 24, was synthesized using coumarin as the reference dye which, when excited, emits at the excitation of the viscosity sensitive dye— a phenomena called Förster resonance energy transfer (FRET). FRET relies heavily on the distance between the donor and acceptor molecules, in addition to the

overlap between the emission of the donor and the excitation of the acceptor[62]. The viscosity sensitive portion of the dye was a thiophene containing an ester-linkage to the carbon-chain bridge connecting to the reference fluorophore. The dye, but with the amide, was synthesized to observe changes upon the biological stability of the ratiometric dye.

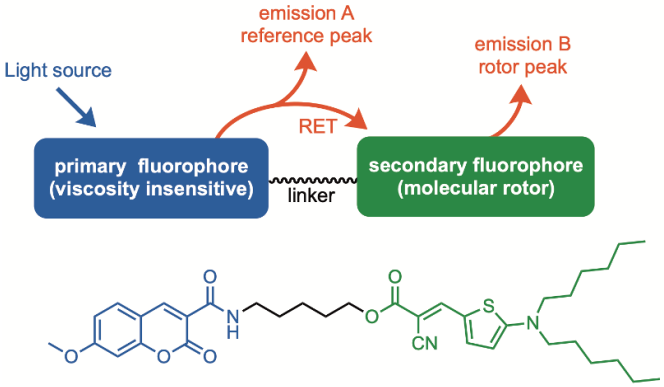

Figure 3.1. General schematic of FRET with representative molecule dye 24.

In addition, a previous FMR, coined EAT08[63], was used for the determination of bacterial biofilm signaling, with around 20-30% signal-to-noise (S/N). In efforts to increase the contrast, as well as red shift the dyes for aforementioned reasons, a series of EAT08 analogues was synthesized.

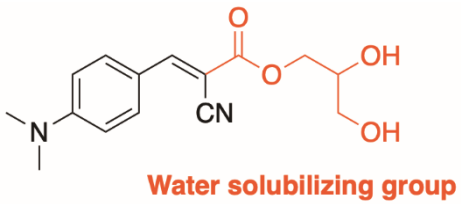

Figure 3.2. Structure of EAT08.

EAT08 is a derivative of CCVJ (Figure 1.6b) in which the julolidine moiety is swapped for a free rotating dimethylamino group, and the uncharged water solubilizing group (WSG) is the glycerol ester. Increasing the hydrophilicity of fluorescent probes helps with solubility and taking

viscosity measurements of aqueous environments, such as certain domains of the cytoplasm, blood plasma, and colloidal systems.

2. Results and Discussion

2.1 EAT08 analogues

The published synthesis[63] for the WSG consists of an esterification of cyanoacetic acid with solketal via a DCC coupling, catalyzed by DMAP. The cyanoester acceptor unit is then attached to the donor and π-system via a Knoevenagel condensation using DBU to afford the protected EAT08. The deprotection of the acetonide was achieved via an acidic resin.

The key reaction of all the EAT08 analogues was the Knoevenagel condensation, done with piperidine rather than DBU. Instead of the acidic resin, a simple deprotection of the acetonide using aq. HCl and methanol was performed to avoid a heterogeneous solution. The amide linker was synthesized starting with solketal, which was tosylated to create a better leaving group, then azidated with sodium azide. The azide was then hydrogenated to afford the amine, which was reacted with methyl cyanoacetate to yield the amide derivative of the WSG.

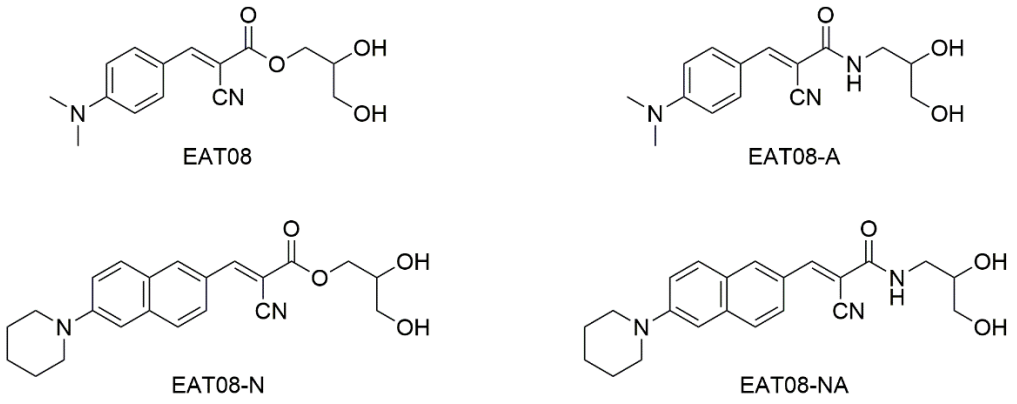

Figure 3.3. Synthesized EAT08 analogues.

The switching of π from a phenyl to naphthyl results in increased emission intensity. This is seen both quantitatively and qualitatively, shown in Figures 3.A.1 and 3.A.2.

Table 3.1. Photophysical properties for synthesized EAT08 analogues

	λ_{abs} (nm)	λ_{em} (nm)	Stokes shift (cm^{-1})
EAT08	432	492	2823
EAT08-P	434	492	2716
EAT08-A	392	481	4720
EAT08-AP	394	484	4720
EAT08-N	446	614	6135
EAT08-NP	450	612	5882
EAT08-NA	410	587	7354
EAT08-NAP	410	589	7412

As seen in Table 3.1, an unexpected change was in the slight hypsochromic shift due to switching the water solubilizing group from an ester to an amide. This may be attributed to the donation of electron density from the nitrogen into the carbonyl, therefore decreasing the electron-withdrawing character in comparison to the ester. Although the excited state of the dye typically resonates into the cyano group, the decreased electron deficiency in the general proximity of the acceptor, especially when still in conjugation with the π-system, could increase the energy gap between HOMO and LUMO and result in a hypsochromic shift. This is similar to the nitrogen-doping of naphthalene from Chapter 2, where the perturbations in electron density in proximity to the donor and acceptor, especially in the π-system, resulted in emission wavelength shifts.

2.2 Ratiometric dyes

Ratiometric dye 24 was synthesized following the reported procedure.[64] The cyanoester of dye 24 was synthesized first by a Boc-protection of 5-aminopropanol, followed by a DCC coupling

with cyanoacetic acid to afford the protected cyanoester. The cyanoamide of JL227 was achieved by the Boc-protection of cadaverine, followed by an EDC coupling with cyanoacetic acid.

The synthesis of the viscosity sensitive FRET acceptor was achieved by an S_N^{Ar} on 5-bromothiophene-2-carbaldehyde using dihexylamine, then a Knoevenagel condensation with the protected cyanoester or cyanoamide to yield the FRET acceptor with the hydrocarbon linker. This hydrocarbon linker was deprotected with TFA to yield the free amine, which was reacted with the activated FRET donor, the NHS-ester of 7-methoxycoumarin-2-carboxylic acid, to yield the final ratiometric dyes.

a)

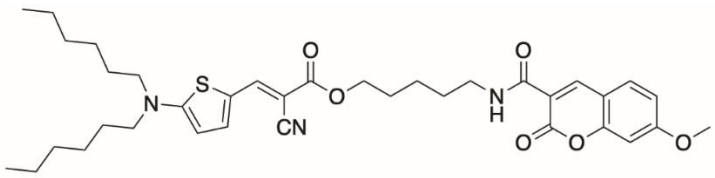

b)

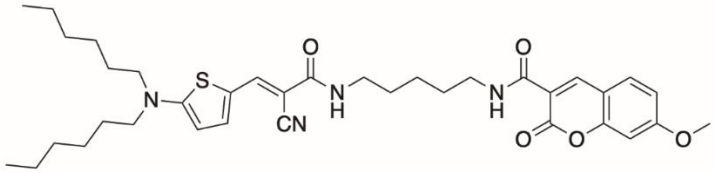

Figure 3.4. Synthesized ratiometric dyes that use FRET. (a) dye 24 (b) JL227.

The fluorescence excitation and emission of the two ratiometric dyes were obtained, as well as their excitation-emission-matrices (Figure 3.A.3). When comparing the two dyes, the molar absorptivity of the ester is higher than the amide, yet the emission intensity of the FRET donor is also higher in the ester-containing ratiometric dye than the amide. Although the excited state of the viscosity sensitive FRET acceptor resonates into the cyano group, it is still conjugated to the ester or amide of the linker, thus explaining the slight differences in absorbance and emission. This change may cause an optimization of the energy transfer in terms of distance and orientation in

space, thus resulting in the decreased emission of the FRET donor. As to the differences in emission intensity ratios, the quantum yield of the amide might be lower, thus resulting in a similar emission to the ester. Another potential reason for this difference of the emission intensity ratios may be solubility and polarity of the dyes, which may induce aggregation and self-quenching.

The ratiometric dyes were tested for their utility in determining the cytosolic viscosity of human cerebral microvascular endothelial cells in response to actin polymerization or depolymerization.

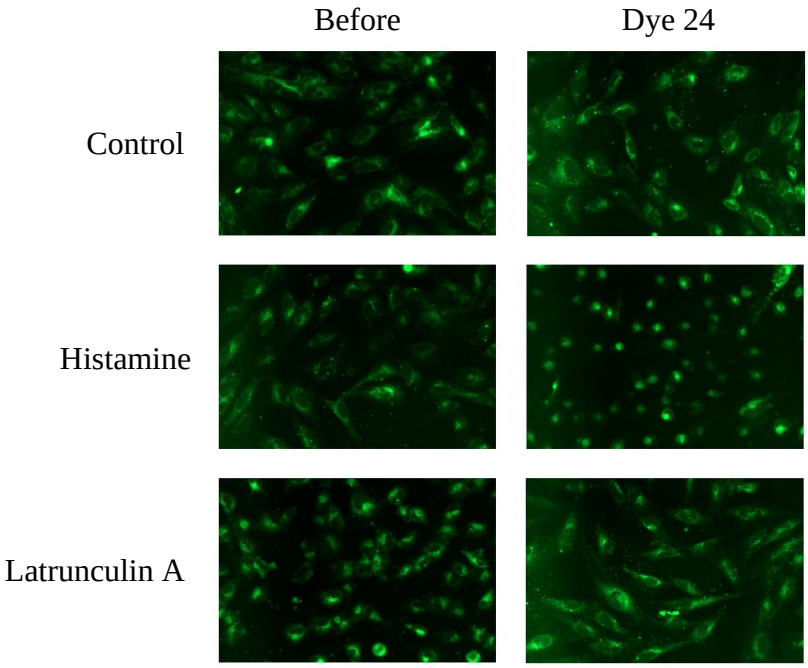

Figure 3.5. Ratiometric dye 24 in cells. On the left are the cells prior to staining, and on the right are cells after staining. Teng, Tao; Lam, Jamie; Lee, James; Theodorakis, Emmanuel. Figure 3.5. Mr. Teng was the principal researcher on this figure.

Histamines trigger the polymerization of actin in cells[65], which in turn increase the viscosity of the cytosol and increase the emission intensity of the acceptor. On the other hand, Latrunculin A causes the depolymerization of actin[66], therefore decreasing the viscosity of the cytosol and resulting in a decrease in the emission intensity of the acceptor in comparison to the

control. Preliminary studies, shown in Figure 3.5, demonstrate a clear difference in fluorescence and morphology between the control, histamine, and latrunculin A samples.

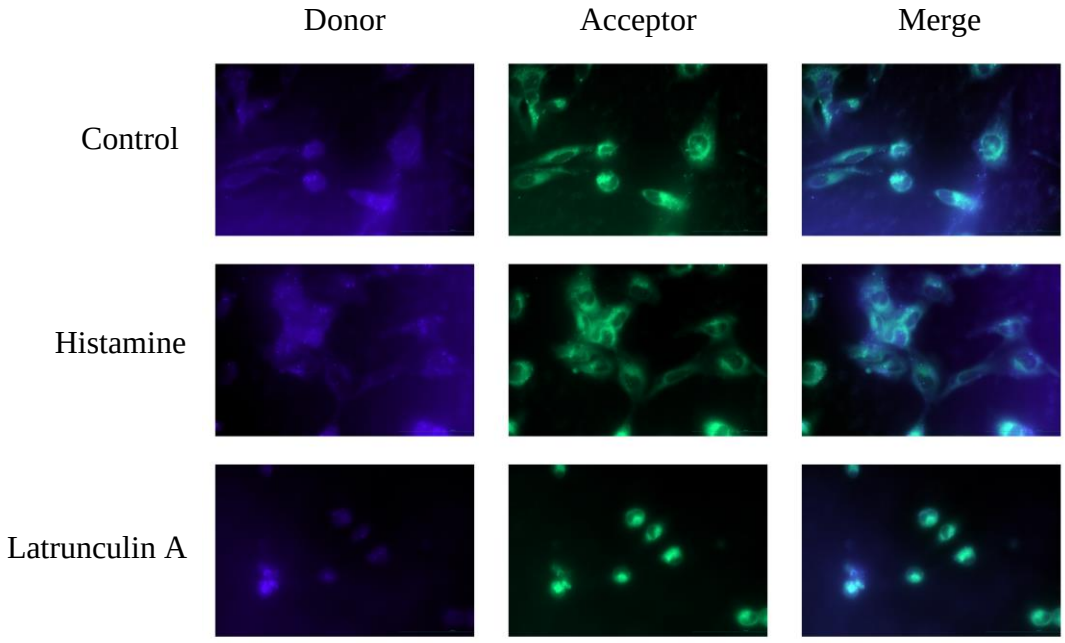

Figure 3.6. Ratiometric dye JL227 in cells. Teng, Tao; Lam, Jamie; Lee, James; Theodorakis, Emmanuel. Figure 3.6. Mr. Teng was the principal researcher on this figure.

In JL227, the acceptor is much brighter in comparison to the donor, as seen in Figure 3.A.3d and Figure 3.6, which unexpectedly differs from dye 24. Despite the same distance of the linker and the same donor, as well as the same overall structure for the acceptor, the change of the ester linkage to an amide linkage resulted in the decreased emission signal of the coumarin. In the case of using the donor as a reference to accurately quantify the viscosity of the cells, having such a low fluorescence intensity of the donor emission is undesirable.

3. Conclusion

In summary, there is a notable effect when changing part of the acceptor from an ester to an amide. Despite preliminary experiments showing more stability of amides *in vivo*, the probes must first be evaluated for their photophysical properties. The amide results in the acceptor having less electron-withdrawing characteristics overall, thus causing a slight hypsochromic shift in the

emission spectra. Moreover, it appears that the amide may enhance energy transfer between the donor and acceptor pairs of the ratiometric dye.

4. Future Directions

The naphthyl derivatives of EAT08 show greater fluorescence intensity than their phenyl counterparts, and therefore may increase the contrast when tested in bacterial cells.

Other experiments should be done to understand the effect of the amide and ester linkage upon spectroscopic properties, especially differences in molar absorptivity and effect on coumarin emission. The photophysical properties, especially quantum yield, should be looked at for the individual dyes that are not linked, to draw more conclusive information regarding the differences in observed FRET.

In terms of synthetic design, caging a point of rotation in the donor coumarin could potentially increase fluorescence emission intensity. By incorporating a julolidine-like structure for the donor, the brightness might be increased due to less non-radiative decay. However, this increase in emission intensity may just be absorbed by the acceptor, so increasing the distance between the donor and acceptor by changing the hydrocarbon spacer or even altering the FRET donor molecule would be interesting to investigate, as FRET relies heavily on distance and the overlap of donor emission and acceptor excitation.[67]

5. Appendix

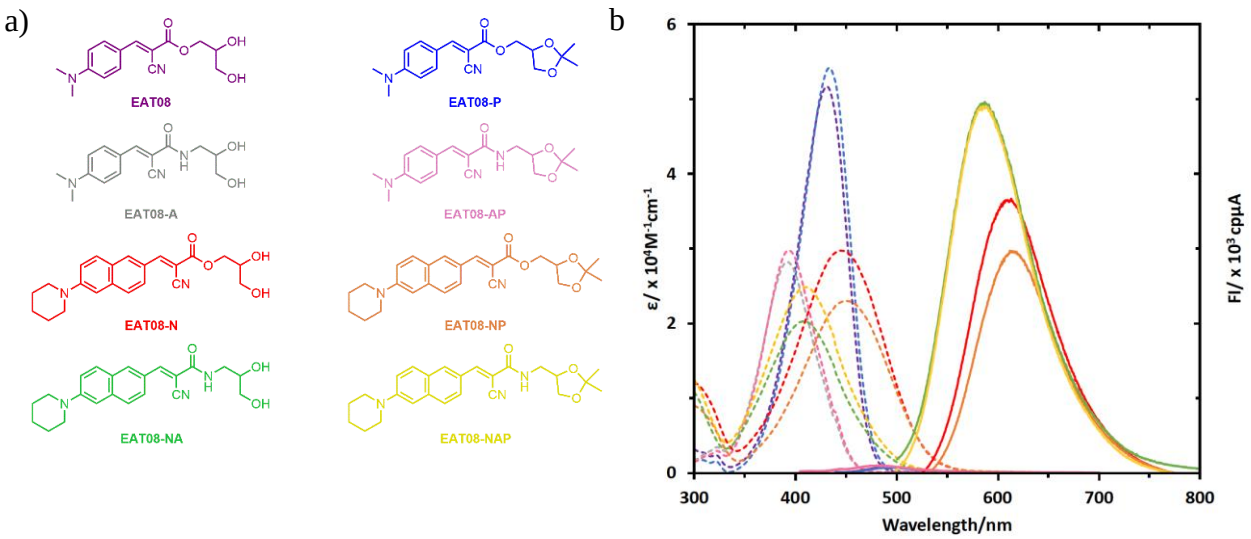

Figure 3.A.1. Spectroscopic data for the EAT08 analogues. (a) Structures of EAT analogues (b) Wavelength vs molar absorptivity and fluorescence intensity; molar absorptivity is denoted by a dashed line and emission is denoted by a solid line.

Figure 3.A.2. Image of EAT08 analogues in solution. Analogues are dissolved to a concentration of 4 mM in DMSO. From left to right: EAT08, EAT08-P, EAT08-A, EAT08-AP, EAT08-N, EAT08-NP, EAT08-NA, EAT08-NAP.

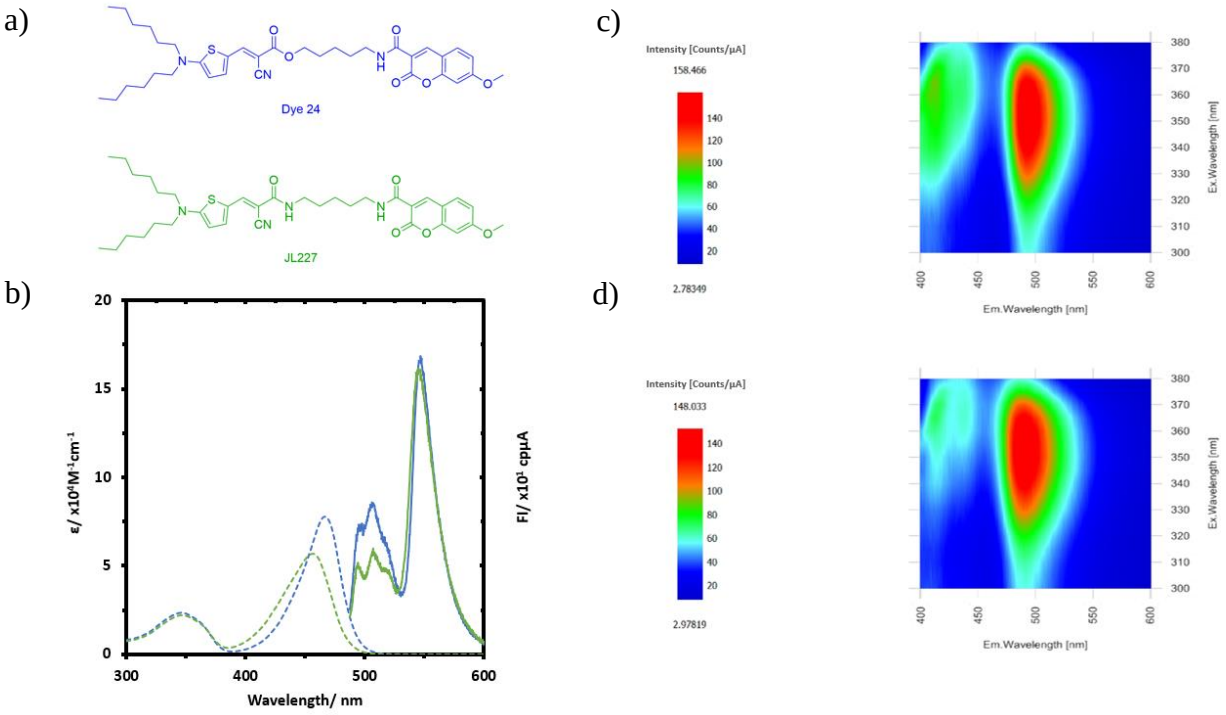

Figure 3.A.3. Spectroscopic data for the ratiometric dyes. (a) Structures of ratiometric dyes (b) Wavelength vs molar absorptivity and fluorescence intensity; molar absorptivity is denoted by a dashed line and emission is denoted by a solid line (c) EEM of dye 24 (d) EEM of JL227.

EXPERIMENTAL

Experimental Procedures

Chapter 2

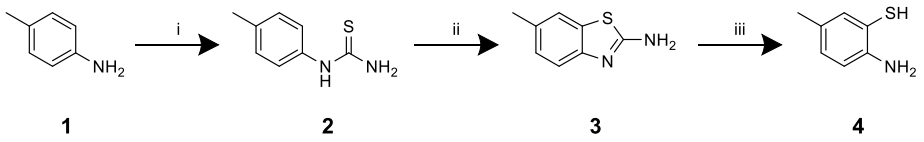

Scheme E1. Synthesis of BTZ linker for neutral ThT. (i) 1.0 eq **1**, 1.1 eq ammonium thiocyanate, dil. sulfuric acid, 20h, 85°C, 61%; (ii) 1.0 eq **2**, 0.1 eq HBr, conc. sulfuric acid, 2h, 80°C, 57%; (iii) 1.0 eq **3**, 40% NaOH, 20h, 100°C, 31%.

1-(p-tolyl)thiourea (Compound **2**): To dilute H_2SO_4 (10.0 mL) was added **1** (5.00 g, 46.66 mmol, 1.0 equiv.) and ammonium thiocyanate (3.91 g, 51.33 mmol, 1.1 equiv.) in one portion. The reaction was allowed to stir overnight at 85°C. Upon completion toluene (10.0 mL) was added, and the reaction mixture was refluxed for 1h. Solution was neutralized with ammonium hydroxide and filtered to yield **2** as a white solid (61% yield). R_f = 0.36 (1:9 EtOAc:DCM); ^{1}H NMR (300 MHz, $CDCl_3$): δ 7.87 (bs, 1H), 7.24 (d, J = 8.2 Hz, 2H), 7.12 (d, J = 8.3 Hz, 2H), 6.03 (bs, 2H), 2.37 (s, 3H).

6-methylbenzo[d]thiazol-2-amine (Compound **3**): To a solution of **2** (2.00 g, 12.03 mmol, 1.0 equiv.) in conc. H_2SO_4 (4.0 mL) was added 48% HBr (0.08 mL, 1.20 mmol, 0.1 equiv.), slowly. Reaction was allowed to stir at 80°C for 2h. The reaction was diluted with cold water, neutralized with ammonium hydroxide, then extracted with EtOAc (3 x 15.0 mL) to afford **3** as a pale yellow solid (57% yield). R_f = 0.10 (1:9 EtOAc:DCM); ^{1}H NMR (300 MHz, $CDCl_3$): δ 7.44 (d, J = 8.19, 1H), 7.41-7.40 (m, 1H), 7.12 (dq, J = 8.2, 0.6 Hz, 1H), 5.07 (bs, 2H), 2.40 (s, 3H).

2-amino-5-methylbenzenethiol (Compound **4**): To a solution of 40% NaOH (12.5 mL) was added **3** (1.00 g, 6.09 mmol, 1.0 equiv.), and the reaction was heated to 100°C for 20h. Upon completion,

the solution was neutralized with acetic acid then filtered to yield **4** as an off-white solid (31% yield). R_f = 0.76 (100% EtOAc); ^{1}H NMR (300 MHz, $CDCl_3$): δ 6.99-6.95 (m, 2H), 6.64 (d, J = 7.9 Hz, 1H), 4.18 (s, 2H), 2.13 (s, 3H).

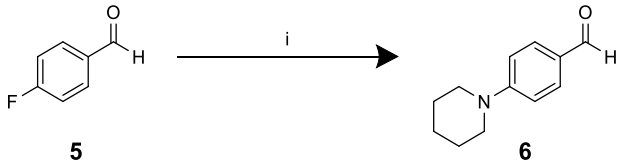

Scheme E2. Synthesis of PIP-P aldehyde. (i) 1.0 eq **5**, 1.1 eq piperidine, 1.25 eq K_2CO_3, DMF, 20h, 150°C, 92%.

4-(piperidin-1-yl)benzaldehyde (Compound **6**): To a vial of **5** (0.50 mL, 4.66 mmol, 1.0 equiv.) in DMF (5.0 mL) was added piperidine (0.51 mL, 5.13 mmol, 1.1 equiv.) and potassium carbonate (0.81 g, 5.83 mmol, 1.25 equiv.). The vial was sealed and refluxed at 150°C for 20h in a heating block. Upon completion, the reaction was poured into cold water, and the precipitate was collected then purified via flash chromatography (10-30% EtoAc/hexanes) to yield **6** as a white solid (92% yield). R_f = 0.70 (1:19 EtOAc:DCM); ^{1}H NMR (500 MHz, $CDCl_3$): δ 9.63 (s, 1H), 7.61 (d, J = 8.8 Hz, 2H), 6.76 (d, J = 8.8 Hz, 2H), 3.27 (t, J = 4.8 Hz, 4H), 1.54 (m, 6H); ^{13}C NMR (125 MHz, $CDCl_3$): δ 189.76, 154.84, 131.65, 125.77, 112.94, 48.00, 25.02, 24.05.

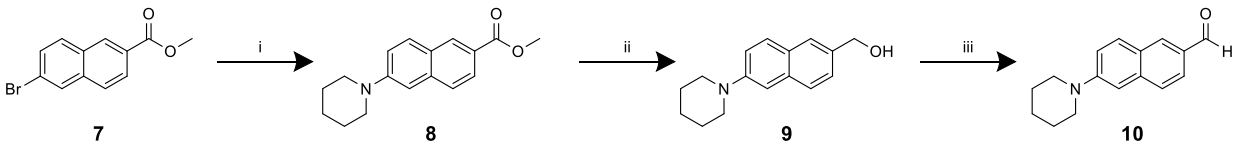

Scheme E3. Synthesis of ANCA aldehyde. (i) 1.0 eq **7**, 1.1 eq piperidine, 0.15 eq BINAP, 0.01 eq $Pd(OAc)_2$, 1.3 eq cesium carbonate, toluene, 24h, 100°C, 78%; (ii) 1.0 eq **8**, 3.0 eq 1.0 M DIBAL-H in hex, THF, 24h, 25°C, 95%; (iii) 1.0 eq **9**, 3.0 eq IBX, DCM, 24h, 25°C, 71%.

Methyl 6-(piperidin-1-yl)-2-naphthoate (Compound **8**): To a solution of anhydrous, degassed toluene (8.0 mL) was added palladium acetate (8.5 mg, 0.04 mmol, 0.01 equiv.), racemic BINAP (35 mg, 0.06 mmol, 0.15 equiv), and cesium carbonate (1.6 g, 4.9 mmol, 1.3 equiv.). The

heterogenous mixture was allowed to stir for 15 min at 100°C. After cooling to room temperature, piperidine (0.42 mL, 4.2 mmol, 1.1 equiv.) and **7** (1.00 g, 3.8 mmol, 1.0 equiv.) were added, and the reaction was allowed to stir overnight at 100°C. Following completion, the reaction was poured into sodium bicarbonate and extracted with EtOAc (3 x 10.0 mL). The organic layer was washed with brine, dried with $MgSO_4$, concentrated under reduced pressure, and purified via flash chromatography (0-50% DCM/hexanes) to provide **8** (78% yield). R_f = 0.40 (1:1 hexane:DCM); ^{1}H NMR (500 MHz, $CDCl_3$): δ 8.45 (d, J = 1.3 Hz, 1H), 7.95 (dd, J = 8.6, 1.7 Hz, 1H), 7.78 (d, J = 9.1 Hz, 1H), 7.65 (d, J = 8.7 Hz, 1H), 7.30 (dd, J = 9.1, 2.5 Hz, 1H), 7.09 (d, J = 2.3 Hz, 1H), 3.41 – 3.27 (m, 4H), 1.82 – 1.60 (m, 6H); ^{13}C NMR (125 MHz, $CDCl_3$): δ 167.72, 151.63, 137.49, 130.83, 130.24, 126.73, 126.56, 125.83, 124.19, 119.91 109.08, 52.07, 50.12, 25.77, 24.47.

(6-(piperidin-1-yl)naphthalen-2-yl)methanol (Compound **9**): To a solution of 1.0 M DIBAL-H in hexanes (6.7 mL, 6.7 mmol, 3.0 equiv.) under argon at 0°C was added a solution of **8** (0.6 g, 2.2 mmol, 1.0 equiv.) in anhydrous THF (7.5 mL), dropwise. The reaction was warmed to room temperature and allowed to stir overnight. Upon completion, the reaction was cooled to 0°C and MeOH was added dropwise until bubbling ceased, followed by the addition of saturated sodium potassium tartrate to create a jelly-like solution. Solution stirred vigorously until layers separated. The reaction was then extracted with EtOAc (3 x 20.0 mL), washed with ammonium chloride and brine, dried with $MgSO_4$, concentrated under reduced pressure, then purified via flash chromatography (0-40% EtOAc/hexanes) to provide **9** (95% yield). R_f = 0.20 (7:3 hexane:EtOAc); ^{1}H NMR (500 MHz, CDCl3): δ 7.69 (d, J = 3.4 Hz, 1H), 7.66 (d, J = 2.4 Hz, 2H), 7.39 (dd, J = 8.3, 1.8 Hz, 1H), 7.29 (dd, J = 9.0, 2.5 Hz, 1H), 7.12 (d, J = 1.8 Hz, 1H), 4.79 (s, 2H), 3.26 (t, 4H), 1.82 – 1.56 (m, 6H); ^{13}C NMR (125 MHz, $CDCl_3$): δ 150.19, 135.71, 134.29, 128.58, 128.21, 127.20, 125.77, 125.48, 120.50, 110.47, 65.68, 51.13, 25.92, 24.41.

6-(piperidin-1-yl)-2-naphthaldehyde (Compound **10**): To a solution of **9** (0.2 g, 0.8 mmol, 1.0 equiv.) in anhydrous DCM (11.0 mL) at 0°C was added IBX (0.7 g, 2.5 mmol, 3.0 equiv.), and the solution was allowed to stir for 30 min. The reaction was then warmed to room temperature and stirred overnight. Following completion of the reaction, aq. $NaHCO_3$ (10.0 mL) was added and the product was extracted with EtOAc (3 x 10.0 mL), washed with brine, dried with $MgSO_4$, concentrated under reduced pressure, then purified via flash chromatography (0-20% EtOAc/hexanes) to provide **10** (71% yield). R_f = 0.56 (7:3 hexane:EtOAc); ^{1}H NMR (500 MHz, $CDCl_3$): δ 10.03 (s, 1H), 8.16 (s, 1H), 7.92 – 7.74 (m, 2H), 7.68 (d, J = 8.6 Hz, 1H), 7.33 (dd, J = 9.1, 2.5 Hz, 1H), 7.09 (d, J = 2.4 Hz, 1H), 3.48 – 3.29 (m, 4H), 1.82 – 1.62 (m, 6H); ^{13}C NMR (125 MHz, $CDCl_3$): δ 191.72, 151.80, 138.42, 134.29, 131.18, 130.33, 127.12, 126.16, 123.20, 119.32, 108.61, 49.38, 25.43, 24.22.

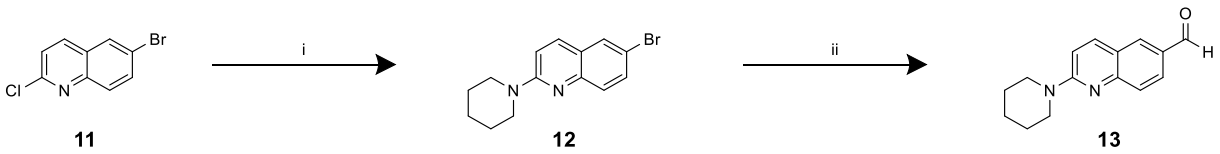

11 **12** **13**

Scheme E4. Synthesis of QN1 aldehyde. (i) 1.0 eq **11**, 5.5 eq piperidine, ACN, 1h, 100°C, 82%; (ii) 1.0 eq **12**, 1.2 eq n-BuLi, THF, 1h, –78 °C; then DMF 1h, –78 °C, 58%. Tharamak, Sorachat; Lam, Jamie; Theodorakis, Emmanuel. Scheme E4. Mr. Tharamak was the principal researcher of this scheme.

6-bromo-2-(piperidin-1-yl)quinoline (Compound **12**): To a vial of **11** (1.0 g, 4.4 mmol, 1.0 equiv.) in ACN (8.0 mL) was added piperidine (2.0 mL, 22.0 mmol, 5.5 equiv.). The reaction was then heated to 100°C for 1h. To the cooled reaction was added aq. $NaHCO_3$, then the organic layer was extracted with EtOAc. The combined layers were dried with $NaSO_4$ and concentrated under reduced pressure to provide **12** as a brownish-white solid (82% yield). R_f = 0.44 (1:9 EtOAc:hexanes); ^{1}H NMR (400 MHz, $CDCl_3$): δ 10.18 (s, 1H), 8.32 (d, J = 1.8 Hz, 1H), 8.22-8.18 (m, 1H), 8.15-8.10 (m, 2H), 7.65-7.60 (m, 1H); ^{13}C NMR (101 MHz, $CDCl_3$): δ 191.30, 151.26,

145.34, 139.59, 134.77, 133.14, 130.16, 128.37, 127.38, 126.70; HRMS (ESI-TOF) calc'd for $[C_{14}H_{16}BrN_2]^+$ $[M+H]^+$: 291.0491; found 291.0490.

2-(piperidin-1-yl)quinoline-6-carbaldehyde (Compound **13**): A solution of **12** (289 mg, 0.99 mmol, 1.0 equiv) in anhydrous THF (4.0 mL) under argon was cooled to -78°C, then 1.6 M n-BuLi in hexanes (0.74 mL, 1.19 mmol, 1.2 equiv.) was added over a period of 30m. Dry DMF was subsequently added dropwise over a period of 10m, and the reaction was allowed to slowly warm to RT. The reaction was quenched with 1M HCl, then basified with aq. $NaHCO_3$ and extracted with EtOAc. The collected organic layers were concentrated under reduced pressure, then purified via flash chromatography (10-40% EtOAc/hexanes) to afford a brownish-orange solid (58% yield). R_f = 0.56 (1:1 EtOAc:hexanes); ^{1}H NMR (500 MHz, $CDCl_3$): δ 10.00 (s, 1H), 8.04 (d, J = 1.9 Hz, 1H), 7.98 (dd, J = 8.7, 2.0 Hz, 1H), 7.91 (dd, J = 9.2, 0.7 Hz, 1H), 7.66 (d, J = 8.7 Hz, 1H), 7.02 (d, J = 9.3 Hz, 1H), 3.81-3.78 (m, 4H), 1.75-1.67 (m, 6H); ^{13}C NMR (125 MHz, $CDCl_3$): δ 191.44, 158.41, 152.20, 138.33, 132.97, 130.24, 127.74, 127.07, 121.67, 110.29, 45.96, 25.88, 24.79; HRMS (ESI-TOF) calc'd for $[C_{15}H_{17}N_2O]^+$ $[M+H]$+: 241.1335; found 241.1333.

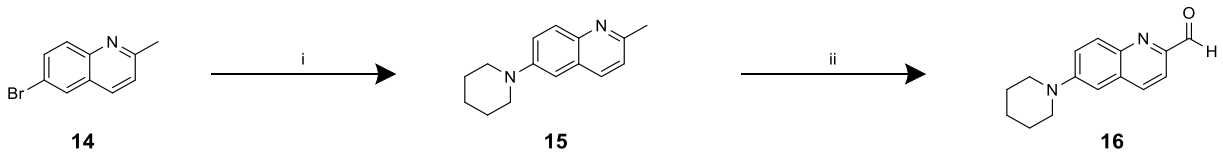

Scheme E5. Synthesis of QN2 aldehyde. (i) 1.0 eq **14**, 1.3 eq piperidine, 0.2 eq $Pd(OAc)_2$, 0.12 eq CyJohnPhos, 1.3 eq t-BuOK, toluene, 20h, 120°C, 53%; (ii) 1.0 eq **15**, 3.0 eq SeO_2, 1,4-dioxane, 2h, 110°C, 52%. Tharamak, Sorachat; Lam, Jamie; Theodorakis, Emmanuel. Scheme E5. Mr. Tharamak was the principal researcher of this scheme.

2-methyl-6-(piperidin-1-yl)quinoline (Compound **15**): To dry, degassed toluene (10.0 mL) was added $Pd(OAc)_2$ (225 mg, 1.0 mmol, 0.2 equiv.) and CyJohnPhos (210 mg, 0.6 mmol, 0.12 equiv). The solution was allowed to stir for 30m, then **14** (1.1 g, 5.0 mmol, 1.0 equiv.), piperidine (0.64 mL, 6.5 mmol, 1.3 equiv,), and t-BuOK (729 mg, 6.5 mmol, 1.3 equiv.) were added. The reaction

was flushed with argon, heated to 120°C, and allowed to stir overnight. Upon completion, the reaction was cooled to RT, concentrated under reduced pressure, and purified via flash chromatography (10-50% EtOAc/hexanes) to yield a yellow solid (53%). R_f = 0.30 (1:9 EtOAc:hexanes); ^{1}H NMR (400 MHz, $CDCl_3$): δ 7.86 (d, J= 9.2 Hz, 2H), 7.46 (dd, J= 6.4 Hz, 2.8 Hz 1H), 7.17 (d, J= 8.4), 7.0 (d, J= 2.8 Hz), 3.24 (t, J= 5.2 Hz, 4H), 2.68 (s, 3H), 1.75 (m, 4H), 1.61 (m, 2H); ^{13}C NMR (101 MHz, $CDCl_3$): δ 155.6, 149.6, 143.2, 134.9, 129.0, 127.5, 123.2, 122.0, 109.3, 50.7, 25.8, 25.0, 24.2; HRMS (ESI-TOF) calc'd for $[C_{15}H_{19}N_2]^+$ $[M+H]^+$: 227.1543; found 227.1542

6-(piperidin-1-yl)quinoline-2-carbaldehyde (Compound **16**): To a solution of **15** (274 mg, 1.2 mmol, 1.0 equiv.) in anhydrous 1,4-dioxane was added SeO_2 (403 mg, 3.6 mmol, 3.0 equiv.). The reaction was refluxed at 110°C for 2h. The heterogeneous mixture was filtered hot through celite, then concentrated under reduced pressure and purified via flash chromatography (30-50% EtOAc/hexanes) to afford a yellow solid (52%). ^{1}H NMR (400 MHz, $CDCl_3$): δ 8.03 (t, J= 8.4 Hz, 2H), 7.91 (d, J= 8.8 Hz, 1H), 7.56 (dd, J= 6.4 Hz, 2.6 Hz, 1H), 6.99 (d, J=2.8, 1H), 3.41 (m, 4H), 1.74 (m, 4H), 1.67 (m, 2.08); ^{13}C NMR (101 MHz, $CDCl_3$): 193.5, 151.4, 149.5, 142.7, 134.7, 132.1, 131.0, 122.9, 118.0, 107.2, 49.4, 25.5, 24.2; HRMS (ESI-TOF) calc'd for $[C_{15}H_{17}N_2O]^+$ $[M+H]^+$: 241.1335; found 241.3333.

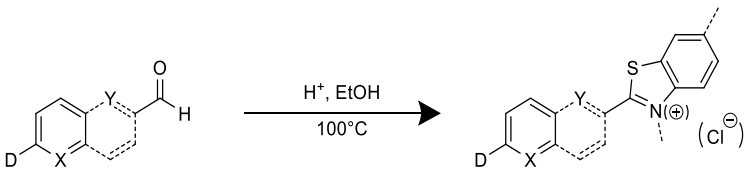

Scheme E6. General synthetic scheme for the installation of BTZ and BTZM groups. Tharamak, Sorachat; Lam, Jamie; Theodorakis, Emmanuel. Compounds QN1-BTZ/BTZM and QN2-BTZ/BTZM. Mr. Tharamak was the principal researcher of these compounds.

General procedure for the synthesis of benzothiazoles

To a 2.0-5.0 mL microwave vial was added the appropriate aldehyde (1.0 equiv.) and aminobenzothiol (1.2 equiv.) in EtOH (2.0-3.0 mL). A few beads of Amberlite-IR120 were added, and the reaction was subjected to microwave radiation at 100°C for 3h. The precipitate was collected via filtration to provide the BTZ.

Neutral ThT (Compound **17**): Pale yellow solid (40% yield); R_f = 0.84 (1:9 EtOAc:DCM); ^{1}H NMR (500 MHz, $CDCl_3$): δ 7.94 (d, J = 8.9 Hz, 2H), 7.86 (d, J = 8.3 Hz, 1H), 7.63 (s, 1H), 6.25 (dd, J = 0.8, 8.6 Hz, 1H), 6.74 (d, J = 8.9 Hz, 2H), 3.05 (s, 6H), 2.47 (s, 3H); ^{13}C NMR (125 MHz, $CDCl_3$): δ: 167.95, 152.54, 152.14, 134.75, 134.35, 128.82, 127.62, 121.87, 121.60, 121.33, 111.80, 40.33, 21.63; HRMS (ESI-TOF) calc'd for $[C_{16}H_{17}N_2S]^+$ $[M+H]^+$: 269.1107; found 269.1106.

DMA-P-BTZ (Compound **18**): Pale yellow solid (46% yield); R_f = 0.81 (1:9 EtOAc:DCM); ^{1}H NMR (500 MHz, $CDCl_3$): δ 7.99 (d, J = 8.3 Hz, 1H), 7.96 (d, J = 9.2 Hz, 2H), 7.84 (d, J = 8.0 Hz, 1H), 7.44 (t, J = 7.7 Hz, 1H), 7.30 (t, J = 7.6 Hz, 1H), 6.74 (d, J = 8.9 Hz, 2H), 3.05 (s, 6H); ^{13}C NMR (125 MHz, $CDCl_3$): δ: 168.94, 154.53, 152.28, 134.66, 128.97, 126.09, 124.30, 122.38, 121.47, 111.78, 40.28; HRMS (ESI-TOF) calc'd for $[C_{15}H_{15}N_2S]^+$ $[M+H]^+$: 255.0950; found 255.0951.

PIP-P-BTZ (Compound **19**): Pale yellow solid (37% yield); R_f = 0.84 (1:9 EtOAc:DCM); ^{1}H NMR (300 MHz, $CDCl_3$): δ 7.99 (d, J = 7.6 Hz, 1H), 7.96 (d, J = 9.0 Hz, 2H), 7.85 (d, J = 7.9 Hz, 1H), 7.44 (ddd, J = 8.2, 7.3, 1.3 Hz, 1H), 7.34-7.29 (m, 1H), 6.96 (d, J = 8.8 Hz, 2H), 3.35-3.31 (m, 4H), 1.71-1.64 (m, 6H); ^{13}C NMR (125 MHz, $CDCl_3$): δ: 168.60, 154.46, 153.59, 134.74, 128.90, 126.14, 124.47, 123.26, 122.55, 121.51, 114.95, 49.29, 25.56, 24.43; HRMS (ESI-TOF) calc'd for $[C_{18}H_{19}N_2S]^+$ $[M+H]^+$: 295.1263; found 295.1262.

ANCA-BTZ (Compound **20**): Yellow-green solid (83% yield); ^{1}H NMR (300 MHz, $CDCl_3$): δ 8.42 (s, 1H), 8.15-8.03 (m, 2H), 7.91 (d, J = 7.3 Hz, 1H), 7.82 (d, J = 9.2 Hz, 1H), 7.74 (d, J = 8.7 Hz, 1H), 7.53-7.44 (m, 1H), 7.42-7.29 (m, 2H), 7.12 (d, J = 2.2 Hz, 1H), 3.34 (t, J = 6.0 Hz, 4H), 1.84-1.61 (m, 6H); ^{13}C NMR (125 MHz, $CDCl_3$): δ 168.87, 154.40, 151.17, 136.46, 135.02, 129.73, 128.06, 127.53, 127.38, 126.37, 124.98, 124.91, 122.99, 121.69, 120.40, 109.54, 50.35, 25.84, 24.49; HRMS (ESI-TOF) calc'd for $[C_{22}H_{21}N_2S]^+$ $[M+H]^+$: 345.1420; found 345.1417.

QN1-BTZ (Compound **21**): Light yellow solid (57% yield); ^{1}H NMR (300 MHz, $CDCl_3$): δ 8.31 (d, J = 2.0 Hz, 1H), 8.22 (dd, J = 8.8, 2.1 Hz, 1H), 8.06 (d, J = 8.2 Hz, 1H), 7.92 (t, J = 8.7 Hz, 2H), 7.73 (d, J = 8.8 Hz, 1H), 7.55-7.44 (m, 1H), 7.42-7.33 (m, 1H), 7.03 (d, J = 9.3 Hz, 1H), 3.79 (br, 4H), 1.71 (s, 6H); ^{13}C NMR (125 MHz, $CDCl_3$): δ 168.43, 158.02, 154.38, 150.06, 137.90, 135.04, 128.37, 127.08, 126.99, 126.88, 126.37, 124.95, 122.94, 122.48, 121.67, 110.55, 46.16, 25.96, 24.94; HRMS (ESI-TOF) calc'd for C21H20N3S+ [M+H]+: 346.1372; found 346.1375.

QN2-BTZ (Compound **22**): Yellow solid (60% yield); ^{1}H NMR (300 MHz, $CDCl_3$): δ 8.36 (d, J = 8.6 Hz, 1H), 8.09 (t, J = 8.4 Hz, 2H), 8.03 (d, J = 9.4 Hz, 1H), 7.97 (d, J = 7.2 Hz, 1H), 7.52 (ddd, J = 9.4, 8.9, 2.1 Hz, 2H), 7.45-7.37 (m, 1H), 7.04 (d, J = 2.7 Hz, 1H), 3.37 (t, J = 2.7 Hz, 4H), 1.84-1.62 (m, 6H); ^{13}C NMR (125 MHz, $CDCl_3$): δ 170.59, 154.53, 150.85, 148.12, 143.10, 136.33, 135.15, 130.74, 130.41, 126.25, 125.57, 123.53, 123.34, 122.07, 118.70, 108.41, 50.17, 25.78, 24.42; HRMS (ESI-TOF) calc'd for $[C_{21}H_{20}N_3S]^+$ $[M+H]^+$: 346.1372; found 346.1371.

General procedure for the synthesis of benzothiazoliums

The aldehyde (1.0 equiv.) and aminobenzothiol (1.2 equiv.) were dissolved in EtOH that was bubbled with O_2, and HCl in 1,4-dioxanes was added (3.0 equiv.). The reaction was stirred at 100°C for 2h. Upon completion, the solution was concentrated, diluted in the minimum amount of MeOH, and precipitated with EtOAc.

DMA-P-BTZM (Compound **23**): Dark yellow solid (38% yield); ^{1}H NMR (300 MHz, MeOD): δ 8.19 (dd, J = 26.7, 8.3 Hz, 2H), 7.83 (tt, J = 15.3, 7.7 Hz, 4H), 7.02 (d, J = 8.9 Hz, 2H), 4.34 (s, 3H), 3.18 (s, 6H); ^{13}C NMR (125 MHz, MeOD): δ: 155.87, 144.47, 133.51, 130.74, 129.76, 129.19, 124.67, 117.64, 113.29, 112.32, 40.19, 38.80; HRMS (ESI-TOF) calc'd for $[C_{16}H_{17}N_2S]^+$ $[M]^+$: 269.1107; found 269.1108.

PIP-P-BTZM (Compound **24**): Dark yellow solid (16% yield); ^{1}H NMR (300 MHz, MeOD): δ 8.19 (dd, J = 26.7, 8.2 Hz, 2H), 7.97-7.70 (m, 4H), 7.17 (d, J = 8.9 Hz, 2H), 4.33 (s, 3H), 3.59-3.57 (m, 4H), 1.73 (m, 6H); ^{13}C NMR (125 MHz, MeOD): δ: 174.81, 151.62, 144.20. 133.89, 131.27, 130.78, 129.86, 125.10, 120.04, 118.28, 54.06, 38.86, 25.53, 23.64; HRMS (ESI-TOF) calc'd for $[C_{19}H_{21}N_2S]^+$ $[M]^+$: 309.1420; found 309.1418.

ANCA-BTZM (Compound **25**): Red solid (14% yield); ^{1}H NMR (300 MHz, MeOD): δ 8.59 (s, 1H), 8.42 (d, J = 8.2 Hz, 1H), 8.36 (d, J = 8.5 Hz, 1H), 8.26 (dd, J = 8.8, 3.1 Hz, 2H), 8.19-7.79 (m, 5H), 4.43 (s, 3H), 3.70 (t, J = 6.0 Hz, 4H), 2.28-1.95 (m, J = 4.6 Hz, 4H), 1.90-1.74 (m, J = 5.2 Hz, 2H); ^{13}C NMR (75 MHz, MeOD): δ 175.87, 144.19, 137.56, 137.50, 133.26, 132.78, 131.41, 131.25, 130.64, 130.59, 130.06, 127.36, 125.19, 123.08, 121.71, 118.47, 117.70, 54.88, 38.94, 25.55, 23.56; HRMS (ESI-TOF) calc'd for $[C_{23}H_{23}N_2S]^+$ $[M\text{-}Cl]^+$: 359.1576; found 359.1575.

QN1-BTZM (Compound **26**): Muddy yellow solid (90% yield); ^{1}H NMR (300 MHz, MeOD): δ 8.60-8.26 (m, 6H), 8.05 (t, J = 7.8 Hz, 1H), 7.94 (t, J = 7.7 Hz, 1H), 7.74 (d, J = 9.8 Hz, 1H), 4.42 (s, 3H), 4.06 (br, 4H), 1.90 (br, 6H); ^{13}C NMR (125 MHz, MeOD): δ 174.58, 153.23, 144.13, 143.69, 141.29, 134.32, 132.95, 131.65, 131.51, 130.37, 125.33, 123.26, 122.49, 120.36, 118.67, 115.71, 38.88, 26.91, 24.52; HRMS (ESI-TOF) calc'd for $[C_{22}H_{22}N_3S]^+$ $[M\text{-}Cl]^+$: 360.1529; found 360.1525.

QN2-BTZM (Compound **27**): Dark red solid (38% yield); ^{1}H NMR (300 MHz, MeOD): δ 8.78 (t, J = 12.4 Hz, 1H), 8.58-8.24 (m, 5H), 8.25-8.15 (m, 1H), 8.05 (t, J = 7.9 Hz, 1H), 7.95 (t, J = 7.7 Hz, 1H), 4.76 (s, 3H), 3.78 (br, 4H), 2.08 (br, J = 4.4 Hz, 4H), 1.86 (br, 2H); ^{13}C NMR (75 MHz, MeOD): δ 173.32, 147.54, 146.34, 145.87, 144.89, 140.23, 133.72, 131.81, 131.63, 130.84, 130.64, 125.70, 125.49, 124.56, 118.74, 56.64, 39.80, 25.16, 22.85; HRMS (ESI-TOF) calc'd for $[C_{22}H_{22}N_3S]^+$ $[M\text{-}Cl]^+$: 360.1529; found 360.1525.

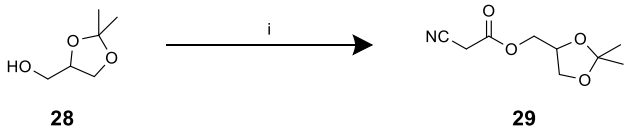

Scheme E7. Synthesis of ester WSG for EAT08 analogues. (i) 1.0 eq **28**, 1.0 eq cyanoacetic acid, 1.0 eq DCC, 0.1 eq DMAP, DCM, 2h, 25°C, 83%.

(2,2-dimethyl-1,3-dioxolan-4-yl)methyl 2-cyanoacetate (Compound **29**): To a solution of cyanoacetic acid (0.5 g, 5.9 mmol, 1.0 equiv.), **28** (0.73 mL, 5.9 mmol, 1.0 equiv.), and DMAP (72 mg, 0.59 mmol, 0.1 equiv.) in DCM (6.0 mL) at 0°C was added a solution of DCC (1.2 g, 5.9 mmol, 1.0 equiv.) in DCM (6.0 mL), dropwise. The solution was allowed to warm to RT and stir for 2h. Upon completion, the reaction was concentrated under reduced pressure and filtered to provide **29** as a pale yellow oil (83%); R_f = 0.31 (7:3 hexanes:EtOAc); ^{1}H NMR (300 MHz, $CDCl_3$): δ 4.34 (p, J = 3.3 Hz, 1H), (dq, J = 2.58, 6.8 Hz, 2H), 4.09 (dd, J = 4.0, 5.1 Hz, 1H), 3.76 (dd, J = 3.5, 5.1 Hz, 1H), 3.51 (s, 2H), 1.43 (s, 3H), 1.36 (s, 3H).

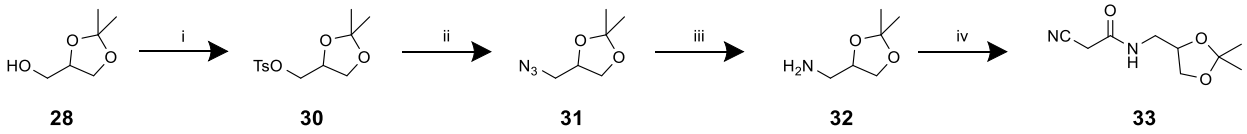

Scheme E8. Synthesis of amide WSG for EAT08 analogues. (i) 1.0 eq **28**, 1.5 eq TEA, 1.1 eq TsCl, 0.02 eq DMAP, DCM, 20h, 25°C, 98%; (ii) 1.0 eq **30**, 2.0 eq NaN_3, DMF, 20h, 80°C, 44% (iii) 1.0 eq **31**, 0.15 eq Pd/C, H_2, MeOH, 26h, 25°C, 48%; (iv) 1.0 eq **32**, 1.5 eq methyl cyanoacetate, 0.003 eq DMAP, EtOH, 16h, 80°C, 83%.

(2,2-dimethyl-1,3-dioxolan-4-yl)methyl 4-methylbenzenesulfonate (Compound **30**): A solution of **28** (5.0 g, 37.8 mmol, 1.0 equiv.) in DCM (50.0 mL) was cooled to 0°C, and TEA (7.9 mL, 56.6 mmol, 1.5 equiv.), TsCl (7.9 g, 41.61 mmol, 1.1 equiv.), and DMAP (92 mg, 0.76 mmol, 0.02 equiv.) were added. The reaction was stirred overnight at RT, the concentrated and purified via flash chromatography (10-30% EtOAc/hexanes) to provide a clear oil (98%); R_f = 0.40 (7:3 hexanes:EtOAc); ^{1}H NMR (300 MHz, $CDCl_3$): δ 7.79 (d, J = 8.3 Hz, 2H), 7.35 (d, J = 8.1 Hz, 2H),

4.31-4.23 (m, 1H), 4.06-3.94 (m, 3H), 3.76 (dd, J = 8.8, 5.1 Hz, 1H), 2.45 (s, 3H), 1.33 (s, 3H), 1.31 (s, 3H).

4-(azidomethyl)-2,2-dimethyl-1,3-dioxolane (Compound **31**): To a solution of **30** (2.1 g, 7.2 mmol, 1.0 equiv.) in DMF (50.0 mL) was added sodium azide (938 mg, 14.4 mmol, 2.0 equiv.). The reaction was heated to 80°C and stirred overnight. Upon completion, the reaction was diluted with water and poured into ice. The product was extracted with EtOAc and the combined organic layers were washed with brine, dried with $MgSO_4$, then concentrated under reduced pressure to provide a clear oil (44%); R_f = 0.54 (7:3 hexanes:EtOAc); ^{1}H NMR (300 MHz, $CDCl_3$): δ 4.31-4.23 (m, 1H), 4.06 (dd, J = 8.3, 6.5 Hz, 1H), 3.77 (dd, J = 8.4, 6.0 Hz, 1H), 3.35 (ddd, J = 18.3, 12.8, 5.1 Hz, 2H), 1.47 (s, 3H), 1.36 (s, 3H).

(2,2-dimethyl-1,3-dioxolan-4-yl)methanamine (Compound **32**): To a flask was added the **31** (1.0 g, 6.4 mmol, 1.0 equiv.) and Pd/C (102 mg, 1.0 mmol, 0.15 equiv.) in MeOH (15.0 mL). The flask was bubbled with H_2 and allowed to stir at RT for 26h at RT. Upon completion, the reaction was filtered through celite and concentrated under reduced pressure. The crude oil was diluted with DCM and washed with brine, dried with $MgSO_4$, and concentrated under reduced pressure to afford a light-yellow oil (48%). R_f = 0.13 (1:9 MeOH:EtOAc); ^{1}H NMR (300 MHz, $CDCl_3$): δ 4.16-4.01 (m, 1H), 4.05-4.01 (m, 1H), 3.66 (t, J = 7.2 Hz, 1H), 2.83-2.75 (m, 2H), 1.42 (s, 3H), 1.35 (s, 3H), 1.28 (bs, 2H).

2-cyano-N-((2,2-dimethyl-1,3-dioxolan-4-yl)methyl)acetamide (Compound **33**): To a flask of EtOH (0.3 mL) was added the **32** (0.1 g, 0.76 mmol, 1.0 equiv.), methyl cyanoacetate (0.1 mL, 1.1 mmol, 1.5 equiv.), and DMAP (0.3 mg, 0.002 mmol, 0.003 equiv.). The reaction was heated to 80°C and stirred for 16h. Upon completion, the reaction was concentrated and purified via flash chromatography (30-60% EtOAc/hexanes) to provide a light yellow oil (83%). R_f = 0.11 (7:3

hexanes:EtOAc); ^{1}H NMR (500 MHz, $CDCl_3$): δ 6.45 (bs, 1H), 4.29-4.24 (m, 1H), 4.07 (dd, J = 8.5, 6.6 Hz, 1H), 3.65 (dd, J = 8.6, 6.0 Hz, 1H), 3.58 (ddd, J = 13.9, 5.7, 3.4 Hz, 1H), 3.40 (s, 2H), 3.36 (dt, J = 13.9, 6.0 Hz, 1H), 1.46 (s, 3H), 1.35 (s, 3H).

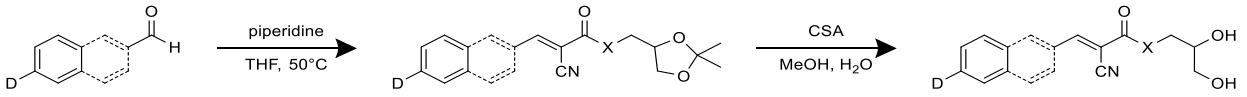

Scheme E9. General synthesis for condensation and deprotection of EAT08 analogues.

General procedure for Knoevenagel condensation

To a solution of the aldehyde (0.10 mmol, 1.0 equiv.) and the cyanoamide or cyanoester (0.12 mmol, 1.1 equiv.) in anhydrous THF (0.5 mL) was added piperidine (0.2 mg, 0.003 mmol, 0.025 equiv.). The solution was heated to 50°C and stirred for 16h. Upon completion, the solution was concentrated and purified via flash chromatography (0-30% EtOAc/hexanes).

EAT08-P (Compound **34**): Yellow solid (65%); R_f = 0.21 (7:3 hexanes:EtOAc); ^{1}H NMR (500 MHz, $CDCl_3$): δ 8.08 (s, 1H), 7.94 (d, J = 8.9 Hz, 2H), 6.69 (d, J = 9.0 Hz, 2H), 4.43-4.38 (m, 1H), 4.35-4.29 (m, 2H), 4.13 (dd, J = 8.5, 6.4 Hz, 1H), 3.89 (dd, J = 8.5, 6.0 Hz, 1H), 3.11 (s, 6H), 1.46 (s, 3H), 1.38 (s, 3H); ^{13}C NMR (125 MHz, $CDCl_3$): δ 164.25, 155.18, 153.87, 134.40, 119.41, 117.42, 111.65, 109.98, 93.29, 73.56, 66.56, 65.53, 40.17, 26.83, 25.62.

EAT08-AP (Compound **35**): Yellow-lime solid (50%); R_f = 0.61 (100% EtOAc); ^{1}H NMR (500 MHz, $CDCl_3$): δ 8.14 (s, 1H), 7.87 (d, J = 8.7 Hz, 2H), 6.68 (d, J = 8.7 Hz, 2H), 6.60 (bs, 1H), 4.32-4.29 (m, 1H), 4.06 (t, J = 7.4 Hz, 1H), 3.69-3.66 (m, 1H), 3.65-3.61 (m, 1H), 3.56-3.51 (m, 1H), 3.08 (s, 6H), 1.48 (s, 3H), 1.35 (s, 3H); ^{13}C NMR (125 MHz, $CDCl_3$): δ 162.58, 153.34, 152.82, 133.61, 119.62, 118.85, 111.58, 109.70, 95.26, 74.39, 66.71, 42.15, 40.10, 26.82, 25.27; HRMS (ESI-TOF) calc'd for $[C_{18}H_{24}N_3O_3]^+$ $[M+H]^+$: 330.1812; found 330.1809.

EAT08-NP (Compound **36**): Orange solid (67%); R_f = 0.24 (8:2 hexanes:EtOAc); ^{1}H NMR (500 MHz, $CDCl_3$): δ 8.38 (s, 1H), 8.17 (s, 1H), 8.05 (dd, J = 8.7, 1.5 Hz, 1H), 7.75 (d, J = 9.1 Hz, 1H), 7.65 (d, J = 8.8 Hz, 1H), 7.29 (dd, J = 9.1, 2.3 Hz, 1H), 7.05 (d, J = 1.9 Hz, 1H), 6.72 (t, J = 5.5 Hz, 1H), 4.36-4.32 (m, 1H), 4.09 (dd, J = 8.4, 6.6 Hz, 1H), 3.72-3.64 (m, 2H), 3.57 (dt, J = 14.0, 5.8 Hz, 1H), 3.40-3.37 (m, 4H), 1.76-1.72 (m, 4H), 1.68-1.65 (m, 2H), 1.50 (s, 3H), 1.37 (s, 3H); ^{13}C NMR (125 MHz, $CDCl_3$): δ 163.42, 155.98, 152.17, 138.05, 135.05, 130.87, 127.46, 126.59, 126.23, 125.76, 119.46, 116.46, 110.09, 108.54, 98.41, 73.48, 66.49, 65.95, 49.52, 26.85, 25.66, 25.60, 34.50; HRMS (ESI-TOF) calc'd for $[C_{25}H_{29}N_2O_4]^+$ $[M+H]^+$: 421.2122; found 421.2120.

EAT08-NAP (Compound **37**): Yellow solid (62%); R_f = 0.22 (7:3 hexanes:EtOAc); ^{1}H NMR (500 MHz, $CDCl_3$): δ 8.38 (s, 1H), 8.17 (s, 1H), 8.05 (d, J = 8.7 Hz, 1H), 7.75 (d, 9.1 Hz, 1H), 7.65 (d, J = 8.8 Hz, 1H), 7.29 (dd, J = 9.1, 2.3 Hz, 1H), 7.05 (d, J = 1.9 Hz, 1H), 6.72 (t, J = 5.5 Hz, 1H), 4.36-4.32 (m, 1H), 4.09 (dd, J = 8.4, 6.6 Hz, 1H), 3.72-3.64 (m, 2H), 3.57 (dt, J = 14.0, 5.8, 1H), 3.38 (t, J = 5.1 Hz, 4H), 1.76-1.72 (m, 4H), 1.68-1.65 (m, 2H), 1.50 (s, 3H), 1.37 (s, 3H); ^{13}C NMR (125 MHz, $CDCl_3$): δ 161.67, 153.52, 151.95, 137.56, 134.12, 130.56, 127.41, 126.76, 126.13, 125.90, 119.61, 117.99, 109.81, 108.74, 100.18, 74.26, 66.72, 49.67, 42.34, 26.84, 25.67, 25.25, 24.48; HRMS (ESI-TOF) calc'd for $[C_{25}H_{30}N_3O_3]^+$ $[M+H]^+$: 420.2282; found 420.2279.

General procedure for acetonide deprotection

The appropriate acetonide (0.1 mmol, 1.0 eq) was dissolved in MeOH (1.0 mL), and 4 drops of 2M HCl were added. The reaction was stirred at RT until completion, then aq. $NaHCO_3$ was added until the pH was basic. The solution was concentrated under reduced pressure then purified via flash chromatography (50-100% EtOAc/hexanes) to provide the corresponding diol.

EAT08 (Compound **38**): Yellow solid (75%); R_f = 0.35 (100% EtOAc); ^{1}H NMR (300 MHz, $CDCl_3$): δ 8.09 (s, 1H), 7.95 (d, J = 9.0 Hz, 2H), 6.70 (d, J = 9.1 Hz, 2H), 4.37 (qd, J = 11.3, 5.1,

2H), 4.05 (q, J = 4.3 Hz, 1H), 3.76-3.72 (m, 2H), 3.13 (s, 6H), 2.60 (d, J = 4.7 Hz, 1H), 2.06 (t, J = 5.8 Hz, 1H); ^{13}C NMR (125 MHz, $CDCl_3$): δ 164.79, 155.47, 152.98, 134.51, 119.34, 117.75, 111.67, 92.74, 70.14, 66.77, 63.41, 40.17.

EAT08-A (Compound **39**): Yellow solid (72%); R_f = 0.29 (100% EtOAc); ^{1}H NMR (500 MHz, $CDCl_3$): δ 8.16 (s, 1H), 7.89 (d, J = 9.0 Hz, 2H), 6.70 (d, J = 9.0 Hz, 2H), 6.649-6.62 (m, 1H), 3.88-3.83 (m, 1H), 3.65-3.52 (m, 4H), 3.11 (s, 6H), 2.85 (d, J = 5.7 Hz, 1H), 2.80 (t, J = 6.2 Hz, 1H); ^{13}C NMR (125 MHz, MeOD): δ 165.40, 155.04, 153.11, 134.48, 120.55, 119.00, 112.62, 96.53, 71.75, 65.20, 44.26, 40.10; HRMS (ESI-TOF) calc'd for $[C_{15}H_{20}N_3O_3]^+$ $[M+H]^+$: 290.1499; found 290.1501.

EAT08-N (Compound **40**): Red solid (85%); R_f = 0.51 (100% EtOAc); ^{1}H NMR (500 MHz, $CDCl_3$): δ 8.32 (s, 1H), 8.21 (s, 1H), 8.10 (dd, J = 1.7, 8.8 Hz, 1H), 7.76 (d, J = 9.2 Hz, 1H), 7.65 (d, J = 8.8 Hz, 1H), 7.30 (dd, J = 9.1, 2.3 Hz, 1H), 7.05 (d, J = 1.9 Hz, 1H), 4.42 (ddd, J = 17.6, 11.5, 5.4, 2H), 4.09 (dt, J = 10.0, 5.1 Hz, 1H), 3.77 (ddd, J = 16.9, 11.5, 4.6 Hz, 2H), 3.42 (t, J = 5.0 Hz, 4H), 2.67 (bs, 1H), 2.11 (bs, 1H), 1.76-1.72 (m, 4H), 1.70-1.66 (m, 2H); ^{13}C NMR (125 MHz, $CDCl_3$): δ 163.90, 156.30, 152.24, 138.16, 135.29, 130.95, 127.51, 126.56, 126.18, 125.67, 119.44, 116.68, 108.51, 97.96, 70.05, 67.13, 63.39, 49.50, 25.67, 24.51; HRMS (ESI-TOF) calc'd for $[C_{22}H_{25}N_2O_4]^+$ $[M+H]^+$: 381.1809; found 381.1807.

EAT08-NA (Compound **41**): Red-orange solid (42%); R_f = 0.34 (100% EtOAc); ^{1}H NMR (500 MHz, MeOD): δ 8.29 (s, 1H), 8.24 (s, 1H), 8.08 (d, J = 10.4 Hz, 1H) 7.77 (dd, J = 29.7, 9.0 Hz, 2H), 7.40 (dd, J = 9.1, 2.3 Hz, 1H), 7.18 (s, 1H), 3.82 (dq, J = 10.3, 5.2 Hz, 1H), 3.57 (q, J = 6.5 Hz, 3H), 3.42-3.37 (m, 5H), 1.75-1.74 (m, 4H), 1.70-1.69 (m, 2H); ^{13}C NMR (125 MHz, MeOD): δ 163.01, 152.01, 151.98, 137.45, 133.47, 129.91, 126.99, 126.87, 126.07, 124.94, 119.55, 116.63,

108.42, 101.18, 70.26, 63.83, 49.33, 43.01, 25.34, 24.11; HRMS (ESI-TOF) calc'd for $[C_{22}H_{26}N_3O_3]^+$ $[M+H]^+$: 380.1969; found 380.1968.

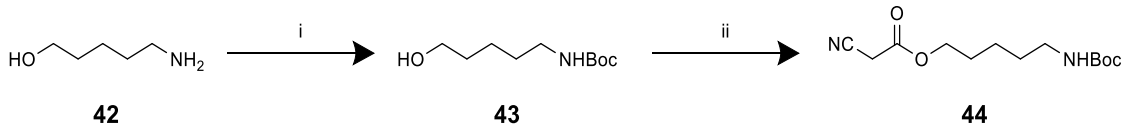

42 **43** **44**

Scheme E10. Synthesis of linker for Dye 24. (i) 1.0 eq **42**, 1.1 eq Boc anhydride, DCM, 12h, 25°C, >99%; (ii) 1.0 eq **43**, 1.0 eq cyanoacetic acid, 0.1 eq DMAP, 1.0 eq DCC, DCM, 2h, 25°C, 82%.

tert-butyl (5-hydroxypentyl)carbamate (Compound **43**): To a solution of **42** (1.0 g, 9.7 mmol, 1.0 equiv.) in DCM (10.0 mL) was added Boc anhydride (2.5 mL, 10.7 mmol, 1.1 equiv.) in DCM (10.0 mL), dropwise. The solution was allowed to stir at RT for 12h. Upon completion, the reaction was diluted with water and extracted with DCM (2 x 10.0 mL). The combined organic layers were washed with aq. $NaHCO_3$ and brine, dried with $MgSO_4$, and concentrated under reduced pressure to provide a clear oil (>99%); R_f = 0.29 (7:3 hexanes:EtOAc); ^{1}H NMR (300 MHz, $CDCl_3$): δ 3.63 (t, J = 6.4 Hz, 2H), 3.11 (t, J = 6.8 Hz, 2H), 1.60-1.55 (m, 2H), 1.50-1.47 (m, 2H), 1.43 (s, 9H), 1.40-1.35 (m, 2H).

5-((tert-butoxycarbonyl)amino)pentyl 2-cyanoacetate (Compound **44**): To a solution of cyanoacetic acid (0.6 g, 7.1 mmol, 1.0 equiv.), **43** (1.4 g, 7.1 mmol, 1.0 equiv.), and DMAP (83 mg, 0.71 mmol, 0.1 equiv.) in DCM (14.0 mL) at 0°C was added a solution of DCC (1.5 g, 7.1 mmol, 1.0 equiv.) in DCM (7.0 mL), dropwise. The solution was warmed to RT and allowed to stir for 2h. Upon completion, the solution was washed with several portions of aq. $NaHCO_3$ and aq. NH_4Cl, dried with $MgSO_4$, then concentrated under reduced pressure to yield a yellow-brown oil (82%); R_f = 0.57 (5:95 EtOAc:DCM); ^{1}H NMR (300 MHz, $CDCl_3$): δ 4.54 (bs, 1H), 4.20 (t, J = 6.5 Hz, 2H), 3.46 (s, 2H), 3.11 (m, 2H), 1.70 (dt, J = 13.8, 6.8 Hz, 2H), 1.56-1.36 (m, 13H).

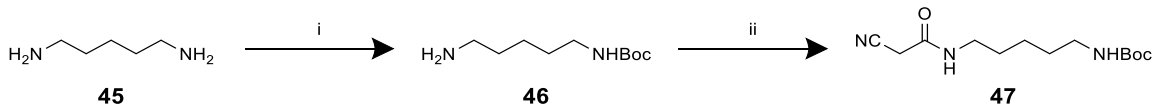

45 46 47

Scheme E11. Synthesis of linker for JL227. (i) 5.0 eq **45**, 1.0 eq Boc anhydride, DCM, 16h, 25°C, 95%; (ii) 1.0 eq **46**, 1.0 eq cyanoacetic acid, 1.3 eq EDC, 1.3 eq DMAP, DCM, 20h, 25°C, 58%.

tert-butyl (5-aminopentyl)carbamate (Compound **46**): To a flask of DCM (20.0 mL) was added **45** (2.7 mL, 22.9 mmol, 5.0 equiv.). The solution was cooled to 0°C, and a solution of Boc anhydride (1.0 g, 4.6 mmol, 1.0 equiv.) in DCM (10.0 mL) was added, dropwise. The reaction was warmed to RT and allowed to stir overnight. Upon completion, the solution was filtered through celite then concentrated under reduced pressure. The resultant oil was diluted with EtOAc and washed with portions of brine until no longer cloudy. The organic layer was dried with $MgSO_4$ and concentrated under reduced pressure to provide a cloudy white oil (95%); R_f = 0.05 (1:9 MeOH:EtOAc); ^{1}H NMR (300 MHz, $CDCl_3$): δ 4.59 (bs, 1H), 3.14-3.05 (m, 2H), 2.72 (m, 2H), 2.15 (m, 2H), 1.54-1.35 (m, 15H).

tert-butyl (5-(2-cyanoacetamido)pentyl)carbamate (Compound **47**): To a solution of **46** (1.0 g, 4.9 mmol, 1.0 equiv.) and DMAP (785 mg, 6.4 mmol, 1.3 equiv.) in anhydrous DCM (15.0 mL) was added cyanoacetic acid (420 mg, 4.9 mmol, 1.0 equiv.), followed by EDC (1.2 g, 6.4 mmol, 1.3 equiv.). The solution was allowed to stir at RT overnight. Upon completion, the mixture was quenched with 10% aq. citric acid solution (15.0 mL), washed with water, $NaHCO_3$, and brine. The organic layer was dried with $MgSO_4$, concentrated under reduced pressure, then purified via flash chromatography (100% EtOAc) to afford a yellow solid (58%); R_f = 0.64 (1:9 MeOH:EtOAc); ^{1}H NMR (300 MHz, $CDCl_3$): δ 6.34 (bs, 1H), 4.57 (bs, 1H), 3.38 (s, 2H), 3.31 (dd, J = 12.9, 6.8 Hz, 2H), 3.12 (dd, J = 12.8, 6.4 Hz, 2H), 1.58-1.48 (m, 4H), 1.44 (s, 9H), 1.41-1.33 (m, 2H).

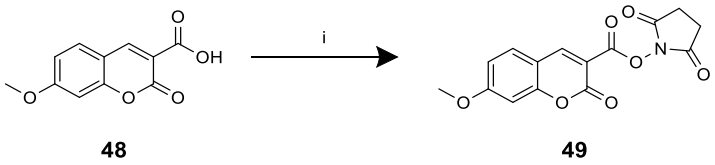

Scheme E12. Activation of coumarin for amidation. (i) 1.0 eq **48**, 1.0 eq NHS, 0.76 eq EDC, DMF, 21h, 40°C, 38%.

2,5-dioxopyrrolidin-1-yl 7-methoxy-2-oxo-2H-chromene-3-carboxylate (Compound **49**): To a flask of DMF (0.5 mL) was added NHS (26 mg, 0.23 mmol, 1.0 equiv.), EDC (33 mg, 0.17 mmol, 0.76 equiv.), and **48** (50 mg, 0.23 mmol, 1.0 equiv.). The reaction was heated to 40°C and allowed to stir overnight. Upon completion, the reaction was quenched with 10% aq. citric acid solution (0.5 mL) and extracted with EtOAc (3 x 1.0 mL). The combined organic layers were washed with brine, then concentrated under reduced pressure to yield a white solid (38% yield). R_f = 0.13 (1:9 MeOH:EtOAc); ^{1}H NMR (500 MHz, $CDCl_3$): δ 8.75 (s, 1H), 7.55 (d, J = 8.6 Hz, 1H), 6.94 (d, J = 8.4 Hz, 1H), 6.84 (s, 1H), 3.94 (s, 3H), 2.91 (s, 4H).

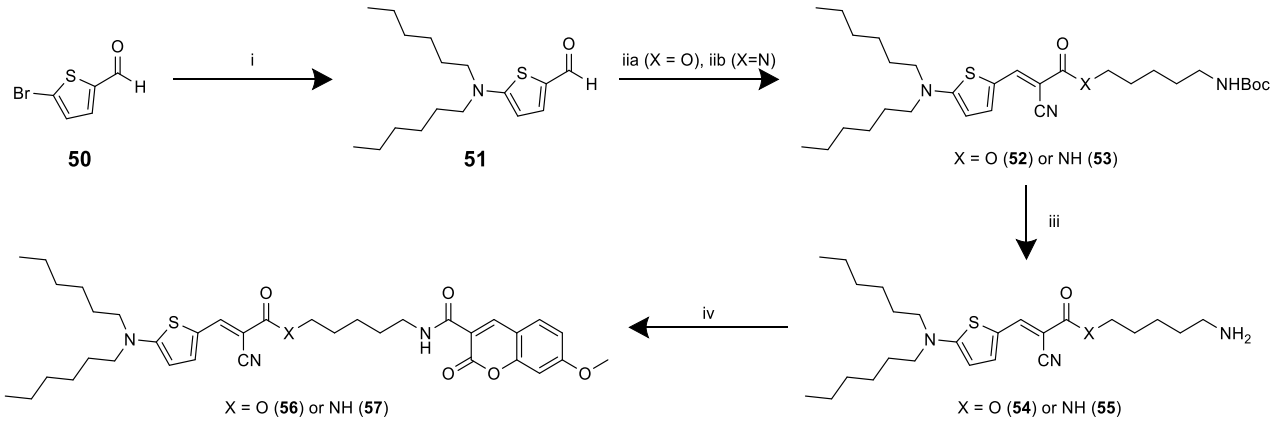

Scheme E13. Synthesis of ratiometric dyes. (i) 1.0 eq **50**, 3.0 eq dihexylamine, 0.03 eq *p*-TsOH, 18h, 100°C, 68%; (iia) 1.2 equiv **51**, 1.0 eq **44**, 1.4 eq DBU, THF, 20h, 25°C, 90%; (iib) 1.0 eq **51**, 1.25 eq **47**, 0.025 piperidine, THF, 21h, 50°C, 71%; (iii) 1.0 eq **52** or **53**, TFA, anisole, 1h, 25°C, >99%; (iv) 1.0 eq **49**, 1.1 eq **54** or **55**, 0.1 eq DMAP, 2.3 eq DIPEA, DCM, 20h, 25°C, 72%/77%*.

*ester/amide yield

5-(dihexylamino)thiophene-2-carbaldehyde (Compound **51**): To flask was added **50** (5.0 g, 26.17 mmol, 1.0 equiv.), dihexylamine (18.3 mL, 78.51 mmol, 3.0 equiv.), and *p*-TsOH (135 mg, 0.79 mmol, 0.03 equiv.). The reaction was heated to 100°C and allowed to stir overnight. Upon completion, reaction was cooled and diluted with water, then extracted with DCM. The combined organic layers were washed with aq. NH_4Cl and aq. $NaHCO_3$, washed with brine, dried with $MgSO_4$, concentrated under reduced pressure, then purified via flash chromatography (100% DCM) to afford a dark reddish-brown oil (68% yield). R_f = 0.56 (7:3 hexanes:EtOAc); ^{1}H NMR (300 MHz, $CDCl_3$): δ 9.42 (s, 1H), 7.46 (d, J= 4.4 Hz, 1H), 5.91 (d, J = 4.4 Hz, 1H), 3.33 (t, J = 7.6 Hz, 4H), 1.70-1.61 (m, 4H), 1.31 (m, 12H), 0.90 (t, J = 6.3 Hz, 6H).

5-((tert-butoxycarbonyl)amino)pentyl (E)-2-cyano-3-(5-(dihexylamino)thiophen-2-yl)acrylate (Compound **52**): To a solution of **51** (300 mg, 1.11 mmol, 1.2 equiv.) and **44** (394 mg, 1.33 mmol, 1.0 equiv.) in dry THF (7.0 mL) was added DBU (0.01 mL, 1.55 mmol, 1.4 equiv.). The reaction stirred at RT overnight. Upon completion, the solution was concentrated under reduced pressure and purified via flash chromatography (10-30% EtOAc/hexanes) to afford a viscous red oil (90% yield). R_f = 0.41 (7:3 hexane:EtOAc); ^{1}H NMR (500 MHz, $CDCl_3$): δ 7.99 (s, 1H), 7.43 (s, 1H), 5.97 (d, J = 4.6 Hz, 1H), 4.56 (bs, 1H), 4.22 (t, J = 6.5 Hz, 2H), 3.38 (t, J = 7.3 Hz, 4H), 3.12 (t, J = 6.6 Hz, 2H), 1.75-1.66 (m, 10H), 1.59-1.51 (m, 2H), 1.44 (s, 9H), 1.32 (m, 10H), 0.90 (t, J = 5.9 Hz, 6H).

tert-butyl (E)-(5-(2-cyano-3-(5-(dihexylamino)thiophen-2-yl)acrylamido)pentyl)carbamate (Compound **53**): To a solution of **51** (50 mg, 0.17 mmol, 1.0 equiv.) and **47** (57 mg, 0.21 mmol, 1.25 equiv.) in dry THF (0.8 mL) was added piperidine (0.4 μL, 0.004 mmol, 0.025 equiv.). The reaction was heated to 50°C and stirred overnight. Upon completion, the solution was concentrated under reduced pressure and purified via flash chromatography (0-30% EtOAc/hexanes) to afford

a viscous red oil (71% yield). R_f = 0.22 (7:3 hexane:EtOAc); ^{1}H NMR (300 MHz, $CDCl_3$): δ 8.09 (s, 1H), 7.38 (s, 1H), 6.03 (t, J = 5.82 Hz, 1H), 5.92 (d, J = 4.5 Hz, 1H), 4.54 (bs, 1H), 3.40-3.33 (m, 6H), 3.12 (q, J = 7.14 Hz, 2H), 1.70-1.64 (m, 4H), 1.61-1.49 (m, 6H), 1.44 (s, 9H), 1.39-1.32 (m, 12H), 0.90 (t, J = 6.1 Hz, 6H).

General BOC deprotection

To **52** or **53** (0.46 mmol, 1.0 equiv.) was added 3.5 mL of TFA solution (5:0.1:4.9 TFA:anisole:DCM). The solution was allowed to stir at RT for 1h, then concentrated under reduced pressure. Residue was washed with portions of toluene until the pH was no longer acidic.

5-aminopentyl (E)-2-cyano-3-(5-(dihexylamino)thiophen-2-yl)acrylate (Compound **54**): Viscous brown-green oil (>99% yield); R_f = 0.03 (7:3 hexanes:EtOAc); ^{1}H NMR (300 MHz, $CDCl_3$): δ 7.97 (s, 1H), 7.72 (s, 2H), 7.39 (s, 1H), 6.01 (d, J = 3.8 Hz, 1H), 4.23 (t, J = 5.4 Hz, 2H), 3.39 (t, J = 7.5 Hz, 4H), 3.08 (bs, 2H), 1.86 (m, 2H), 1.75-1.68 (m, 6H), 1.56 (m, 2H), 1.33 (m, 12H), 0.90 (m, 6H).

(E)-N-(5-aminopentyl)-2-cyano-3-(5-(dihexylamino)thiophen-2-yl)acrylamide (Compound **55**): Viscous brown-green oil (>99% yield); R_f = 0.05 (7:3 hexanes:EtOAc); ^{1}H NMR (300 MHz, $CDCl_3$): δ 8.01 (bs, 3H), 7.41 (s, 1H), 6.28 (bs, 1H), 5.95 (d, J = 4.4 Hz, 1H), 3.42-3.27 (m, 6H), 3.00 (m, 2H), 1.73-1.58 (m, 8H), 1.43 (m, 2H), 1.32 (m, 12H), 0.89 (t, J = 6.2 Hz, 6H).

General Amidation Procedure

To a solution of **54** or **55** (0.1 mmol, 1.1 equiv.) in anhydrous DCM (1.7 mL) was added DMAP (1 mg, 0.009 mmol, 0.1 equiv.), **49** (29 mg, 0.09 mmol, 1.0 equiv.), and DIPEA (0.04 mL, 0.21 mmol, 2.3 equiv.). The reaction was stirred at RT overnight and upon completion, was purified via flash chromatography to yield the ratiometric dye.

DYE 24 (Compound **56**): Purified via flash chromatography (0-30% EtOAc/hexanes) to afford yellow solid (74%); R_f = 0.37 (7:3 hexanes:EtOAc); ^{1}H NMR (300 MHz, $CDCl_3$): δ 8.83 (s, 1H), 8.78 (s, 1H), 7.99 (s, 1H), 5.57 (d, J = 8.6 Hz, 1H), 7.39 (bs, 1H), 6.93 (d, J = 8.7 Hz, 1H), 6.86 (s, 1H), 5.97 (s, 1H), 4.23 (t, J = 6.0 Hz, 2H), 3.91 (s, 3H), 3.47 (d, J = 6.2 Hz, 2H), 3.37 (t, J = 7.0 Hz, 4H), 1.81-1.74 (m, 2H), 1.66 (m, 6H), 1.51 (d, J = 7.0 Hz, 2H), 1.32 (m, 12H), 0.89 (t, 6H).

JL227 (**57**): Purified via flash chromatography (30-80% EtOAc/hexanes) to afford a yellow solid (77%); R_f = 0.63 (100% EtOAc); ^{1}H NMR (500 MHz, $CDCl_3$): δ 8.84 (s, 1H), 8.77 (t, J = 5.5 Hz, 1H), 8.09 (s, 1H), 7.57 (d, J = 8.7 Hz, 1H), 7.37 (bs, 1H), 6.92 (dd, J = 8.7, 2.4 Hz, 1H), 6.86 (d, J = 2.2 Hz, 1H), 6.06 (t, J = 5.7 Hz, 1H), 5.91 (d, J = 4.5 Hz, 1H), 3.91 (s, 3H), 3.46 (dd, J = 13.2, 6.8 Hz, 2H), 3.40-3.33 (m, 6H), 1.68-1.48 (m, 8H), 1.44 (dt, J = 15.3, 7.7, 2H), 1.31 (m, 12H), 0.89 (t, J = 6.5 Hz, 6H); ^{13}C NMR (125 MHz, $CDCl_3$): δ: 166.97, 164.83, 163.32, 162.12, 162.01, 156.73, 148.36, 144.48, 131.03, 120.10, 119.37, 114.98, 114.10, 112.58, 103.57, 100.36, 56.13, 53.90, 40.20, 39.70, 31.63, 29.58, 29.34, 27.13, 26.67, 24.42, 22.69, 14.15; HRMS (ESI-TOF) calc'd for $[C_{36}H_{49}N_4O_5S]^+$ $[M+H]^+$: 649.3418; found 649.3430.

NMR Spectra

Chapter 2

Spectrum 1. Compound 2 ^{1}H NMR

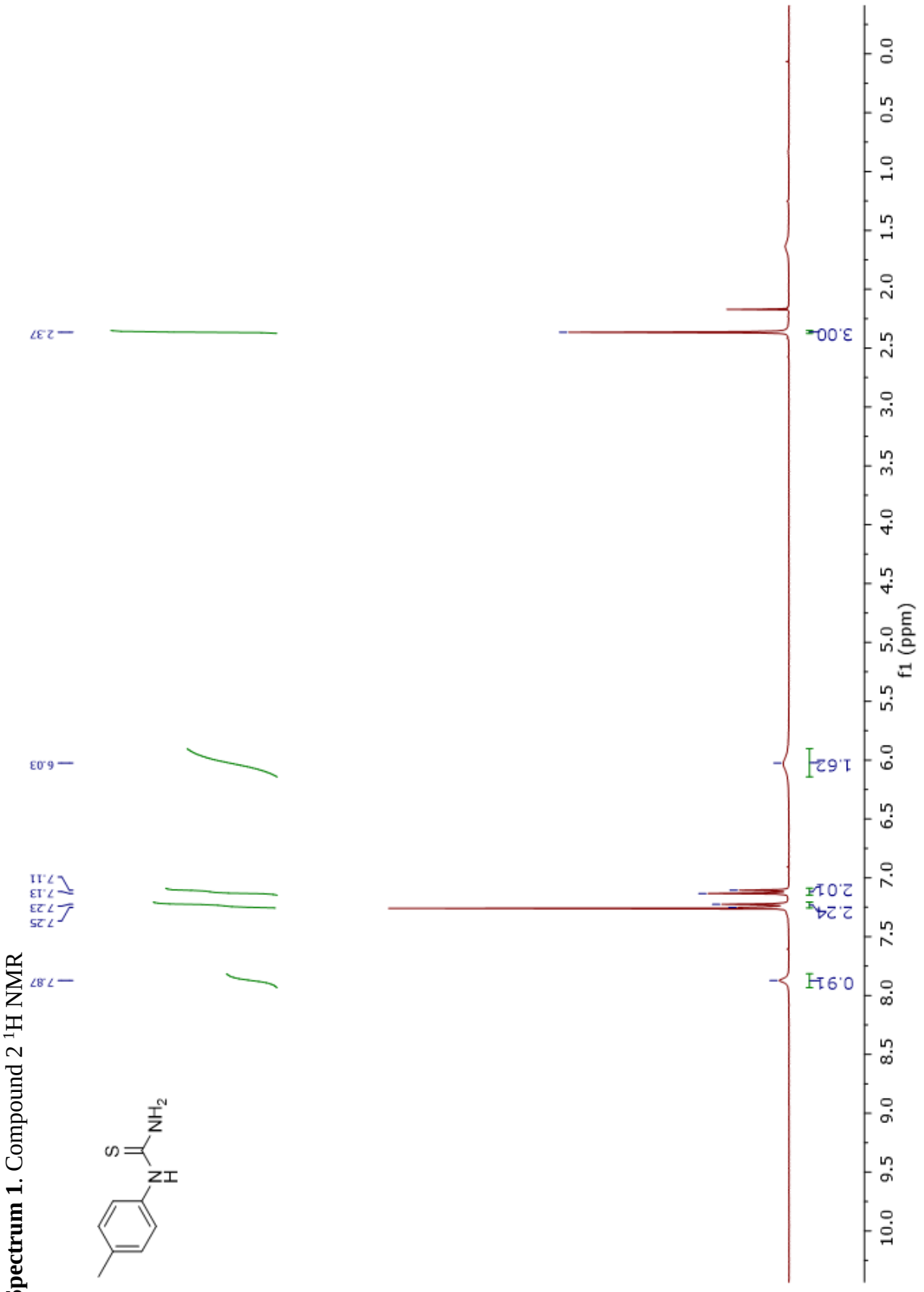

Spectrum 2. Compound 3 ^{1}H NMR

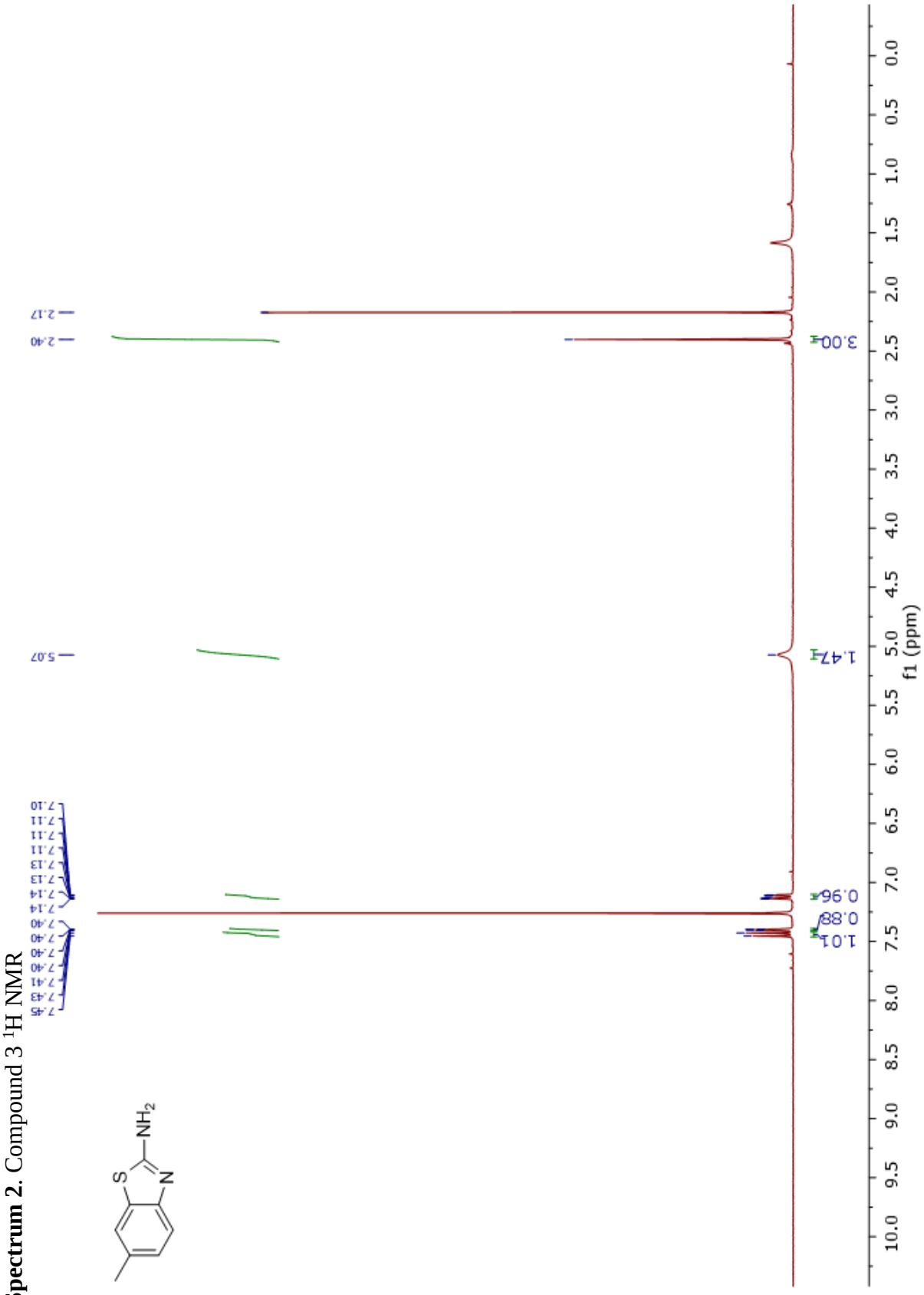

Spectrum 3. Compound 4 ^{1}H NMR

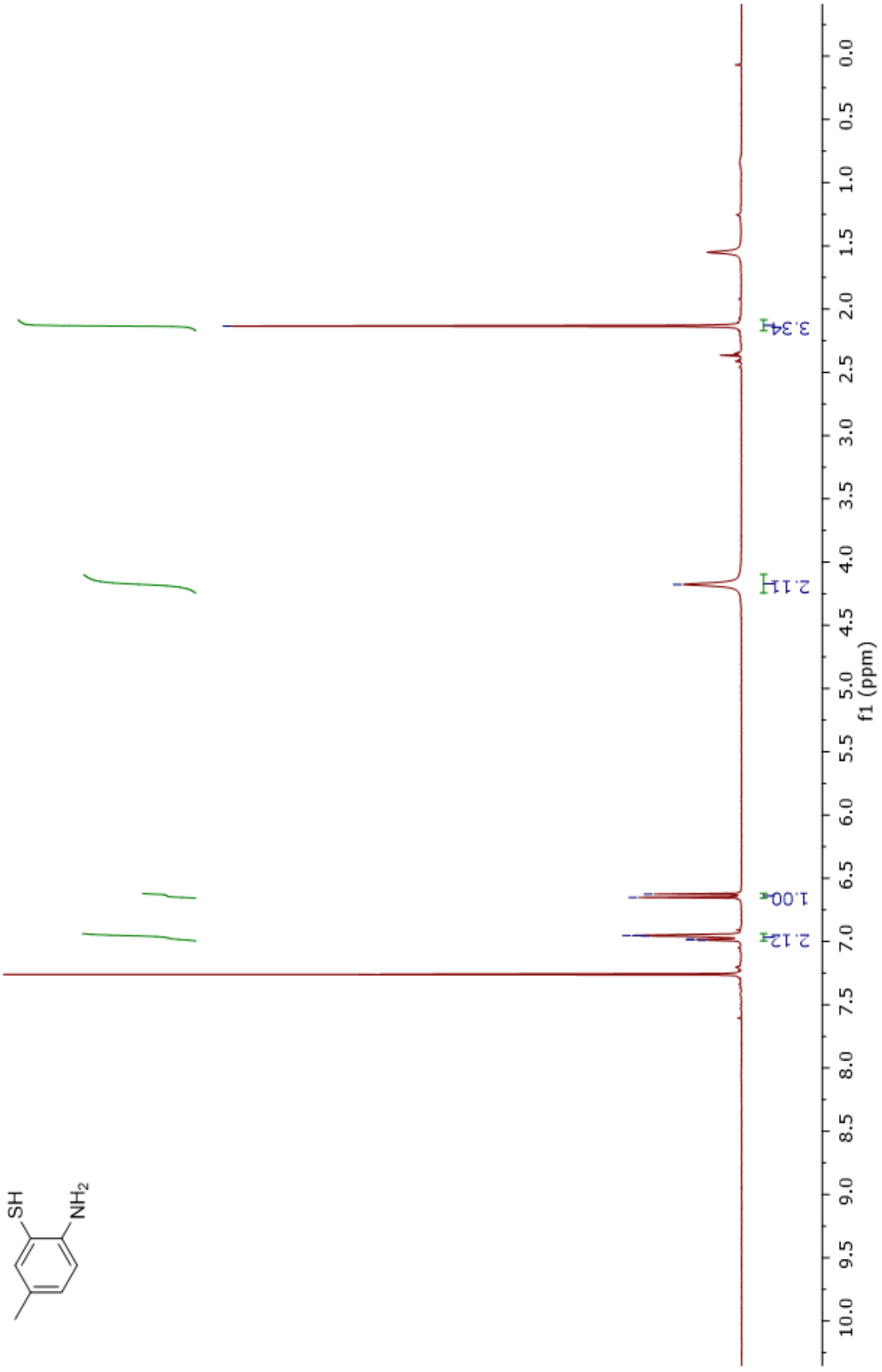

Spectrum 4. Compound 17 ^{1}H NMR

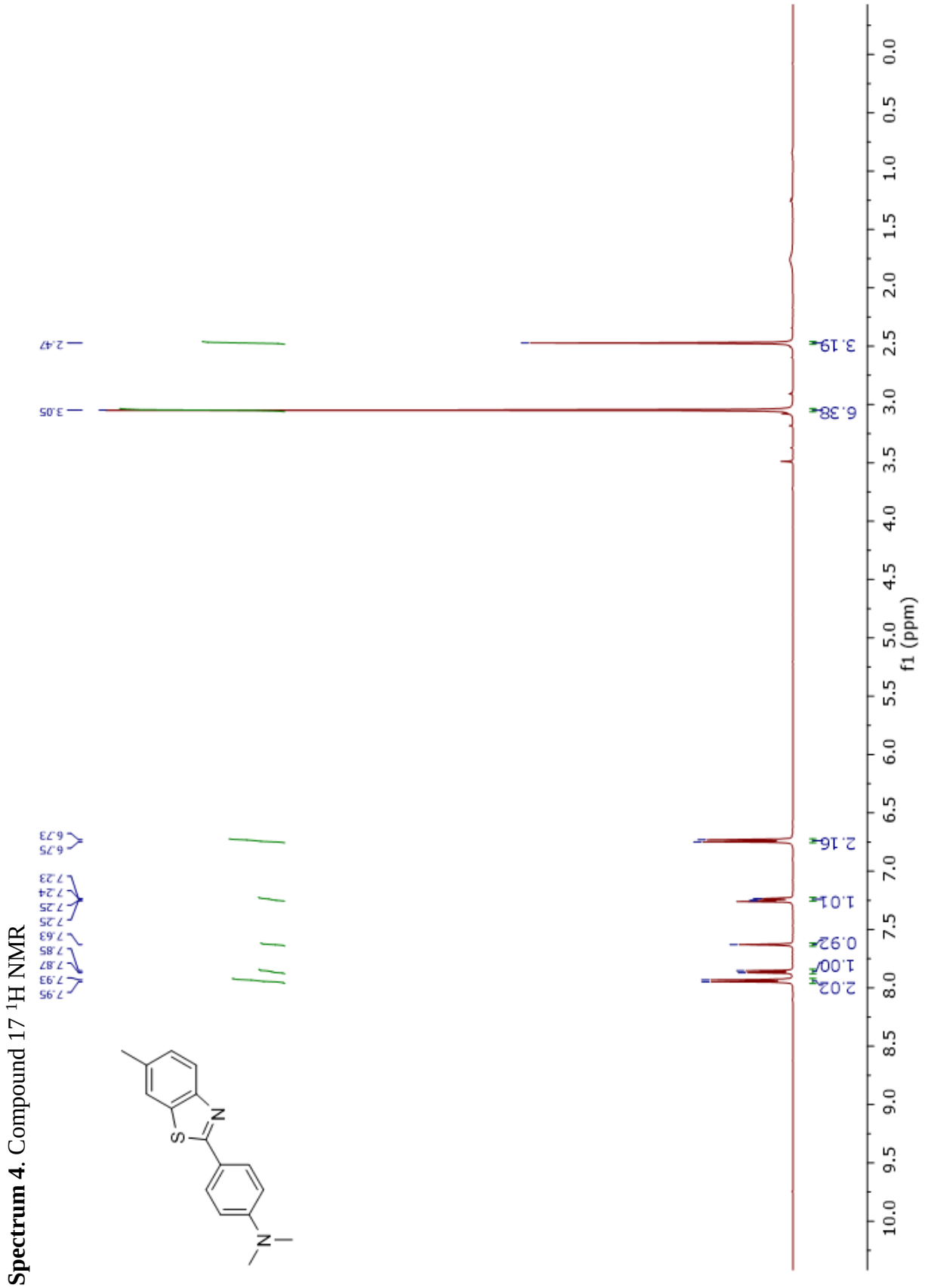

Spectrum 5. Compound 17 ^{13}C NMR

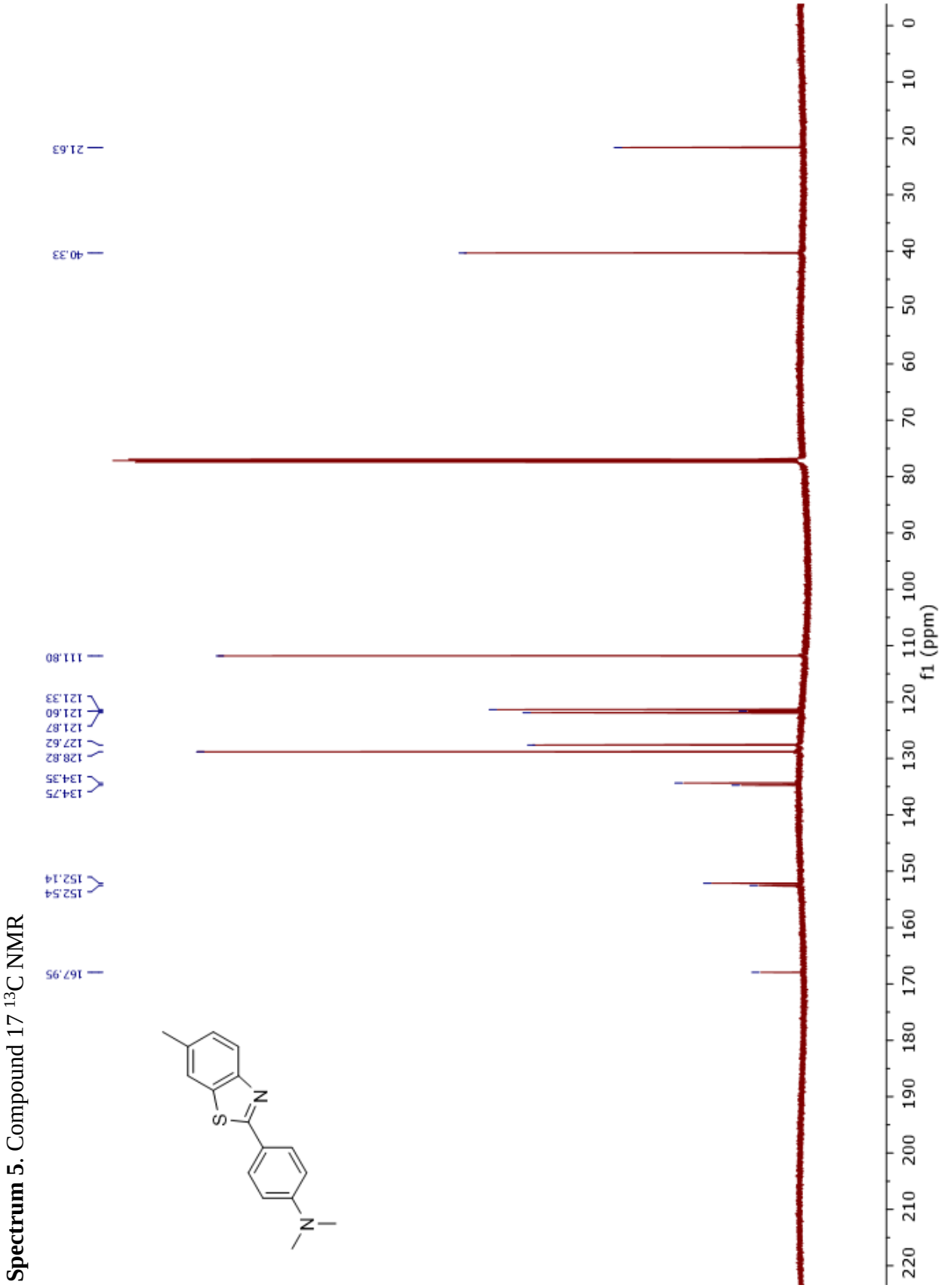

Spectrum 6. Compound 18 ^{1}H NMR

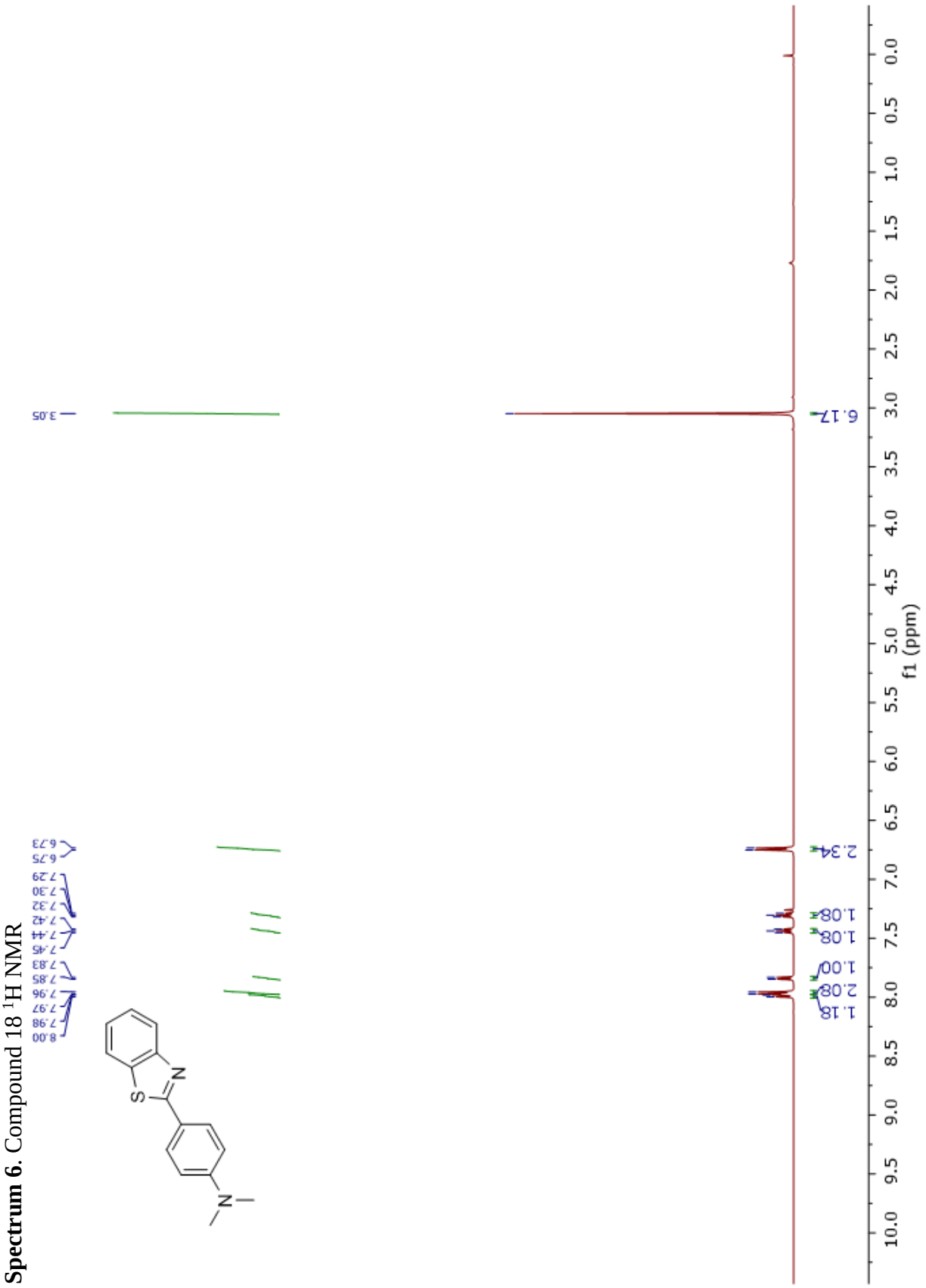

Spectrum 7. Compound 18 ^{13}C NMR

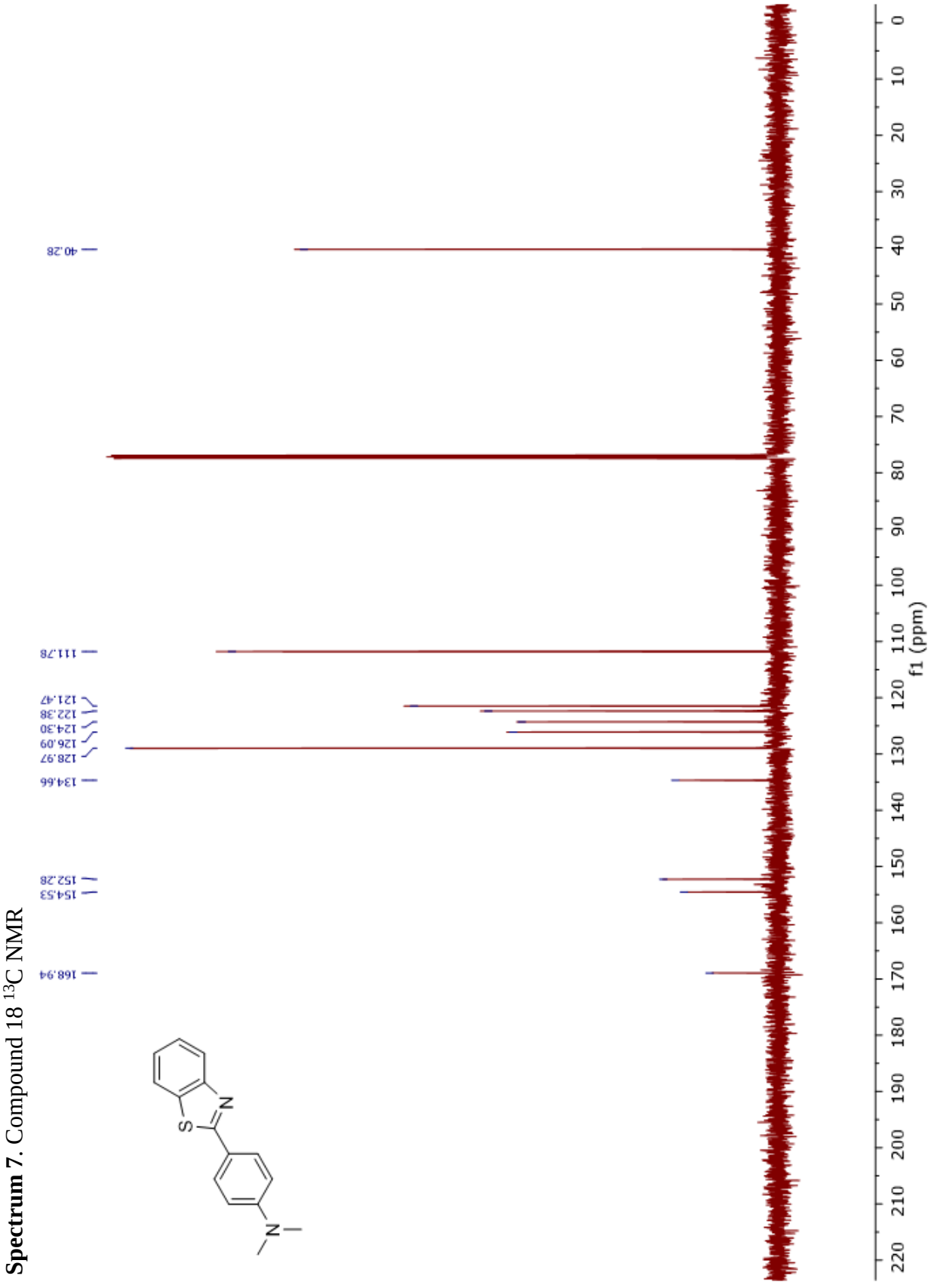

Spectrum 8. Compound 23 ^{1}H NMR

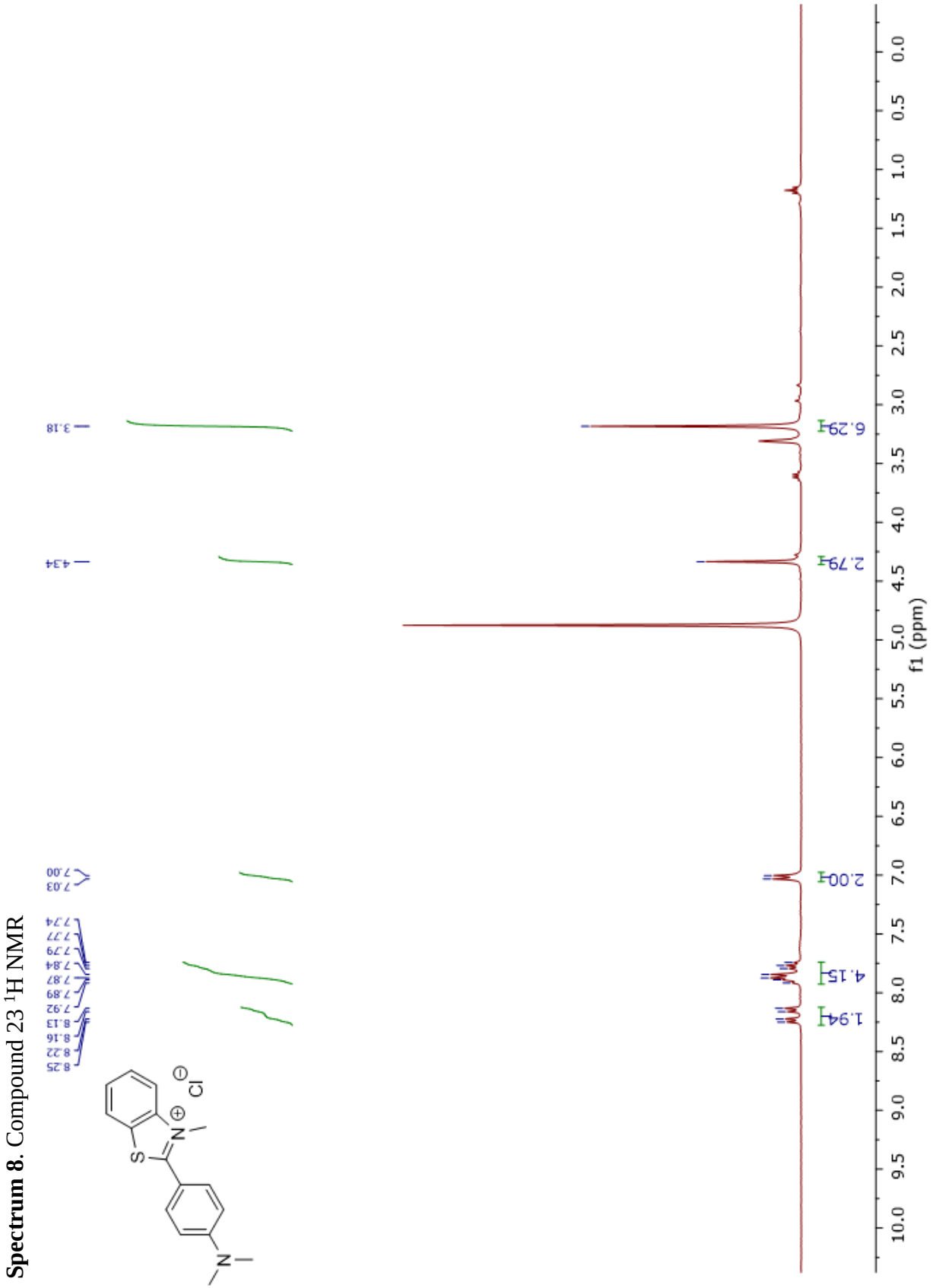

Spectrum 9. Compound 23 ^{13}C NMR

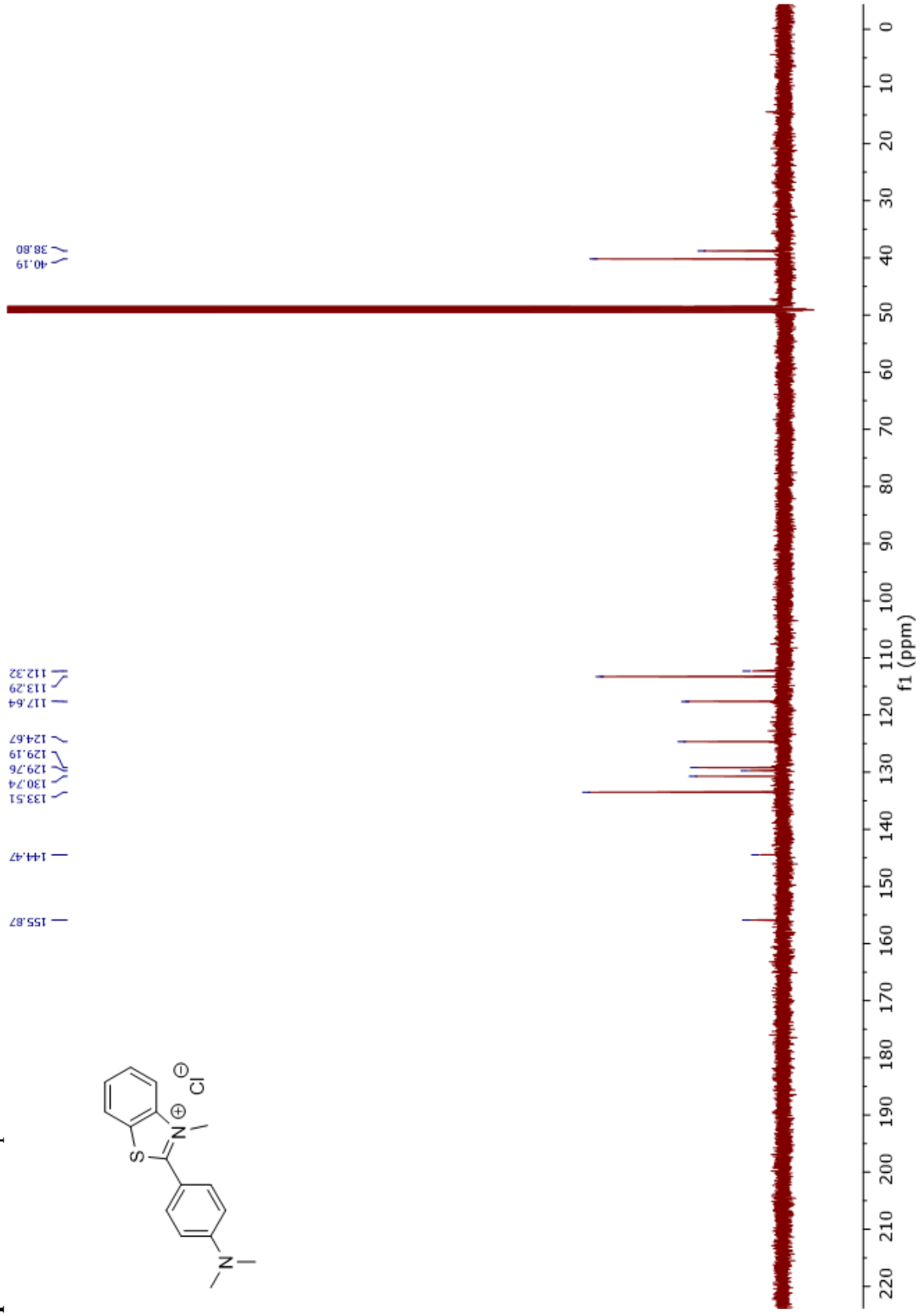

Spectrum 10. Compound 6 ^{1}H NMR

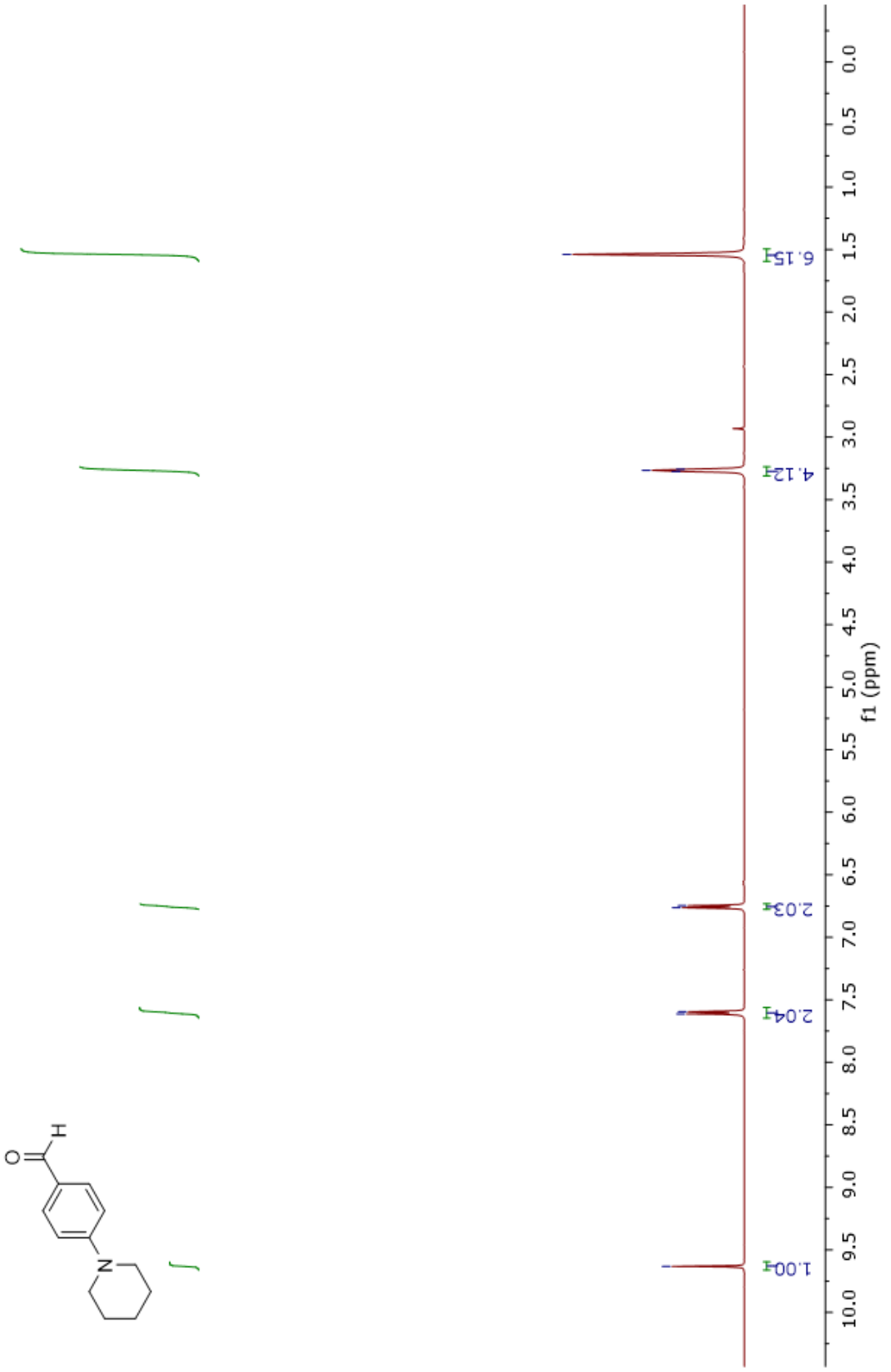

Spectrum 11. Compound 6 ^{13}C NMR

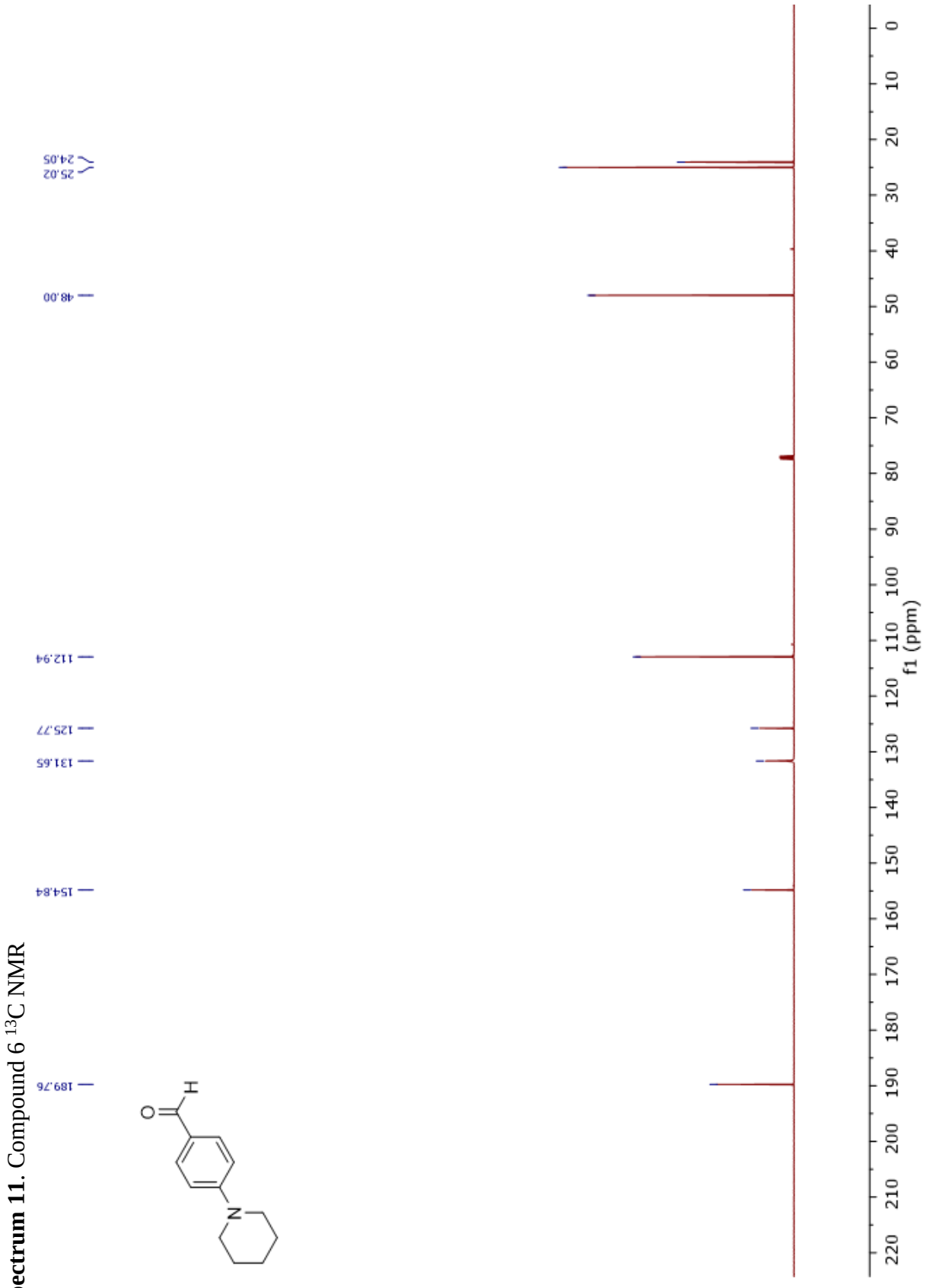

Spectrum 12. Compound 19 ^{1}H NMR

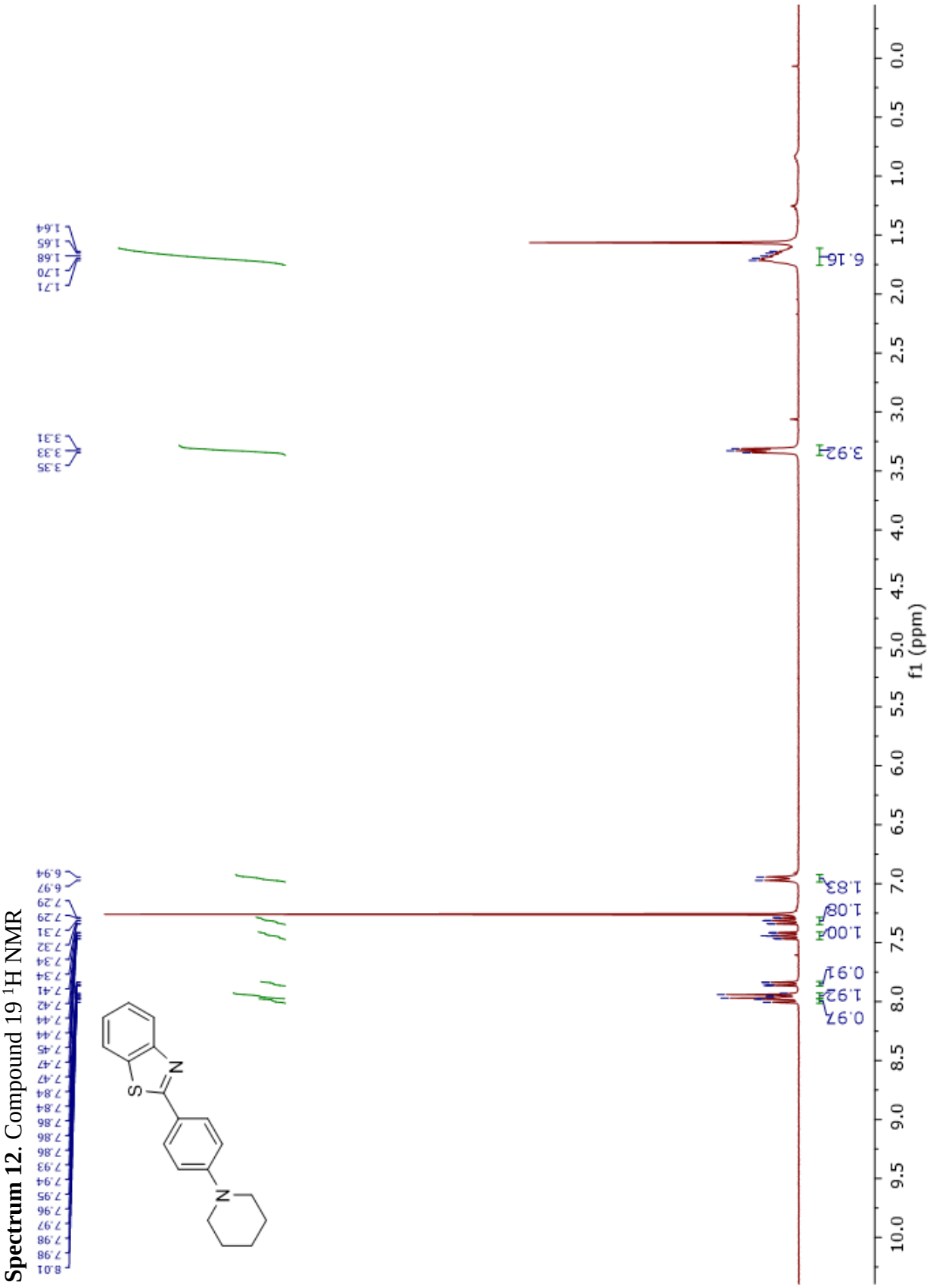

Spectrum 13. Compound 19 ^{13}C NMR

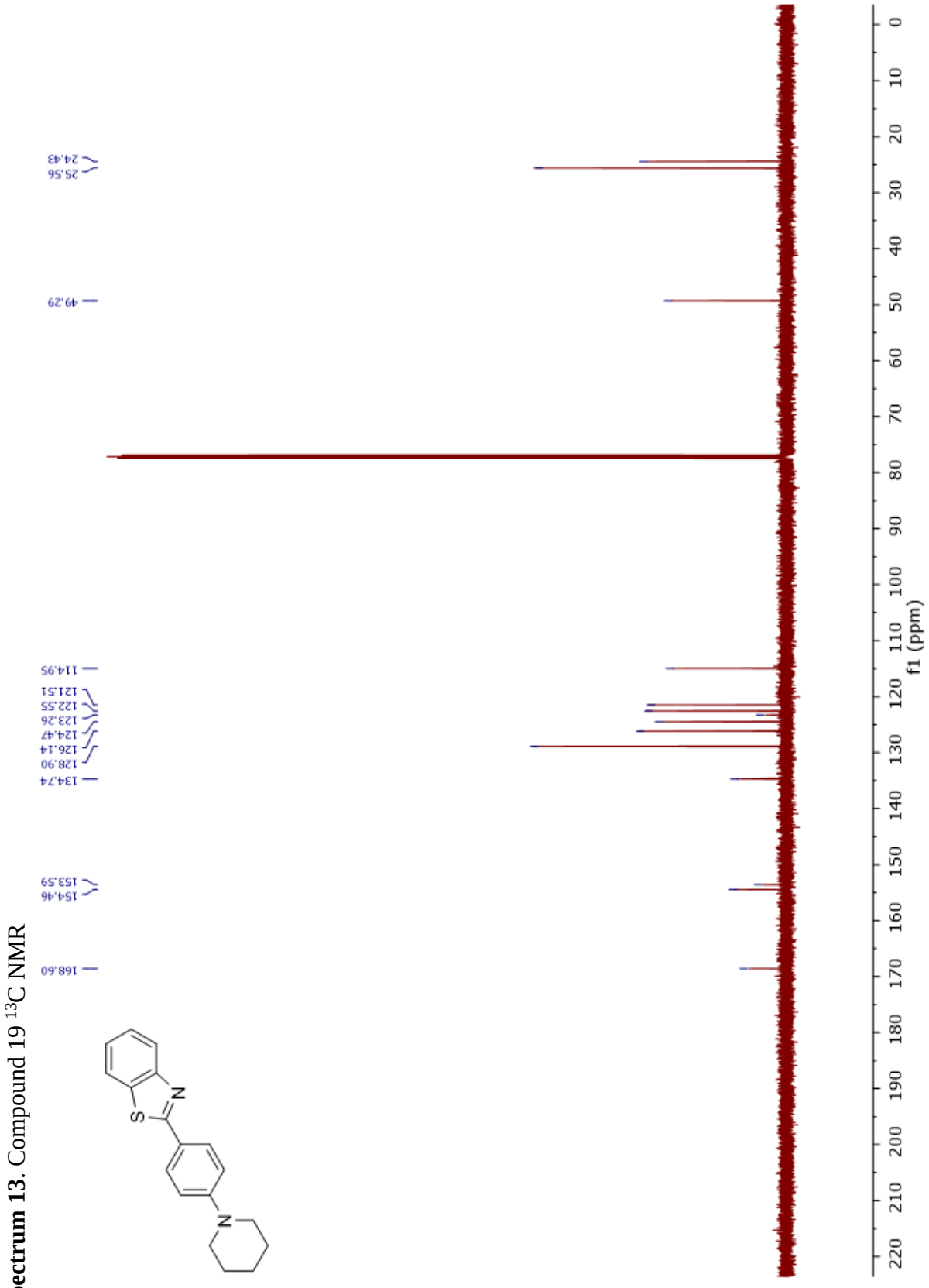

Spectrum 14. Compound 24 ^{1}H NMR

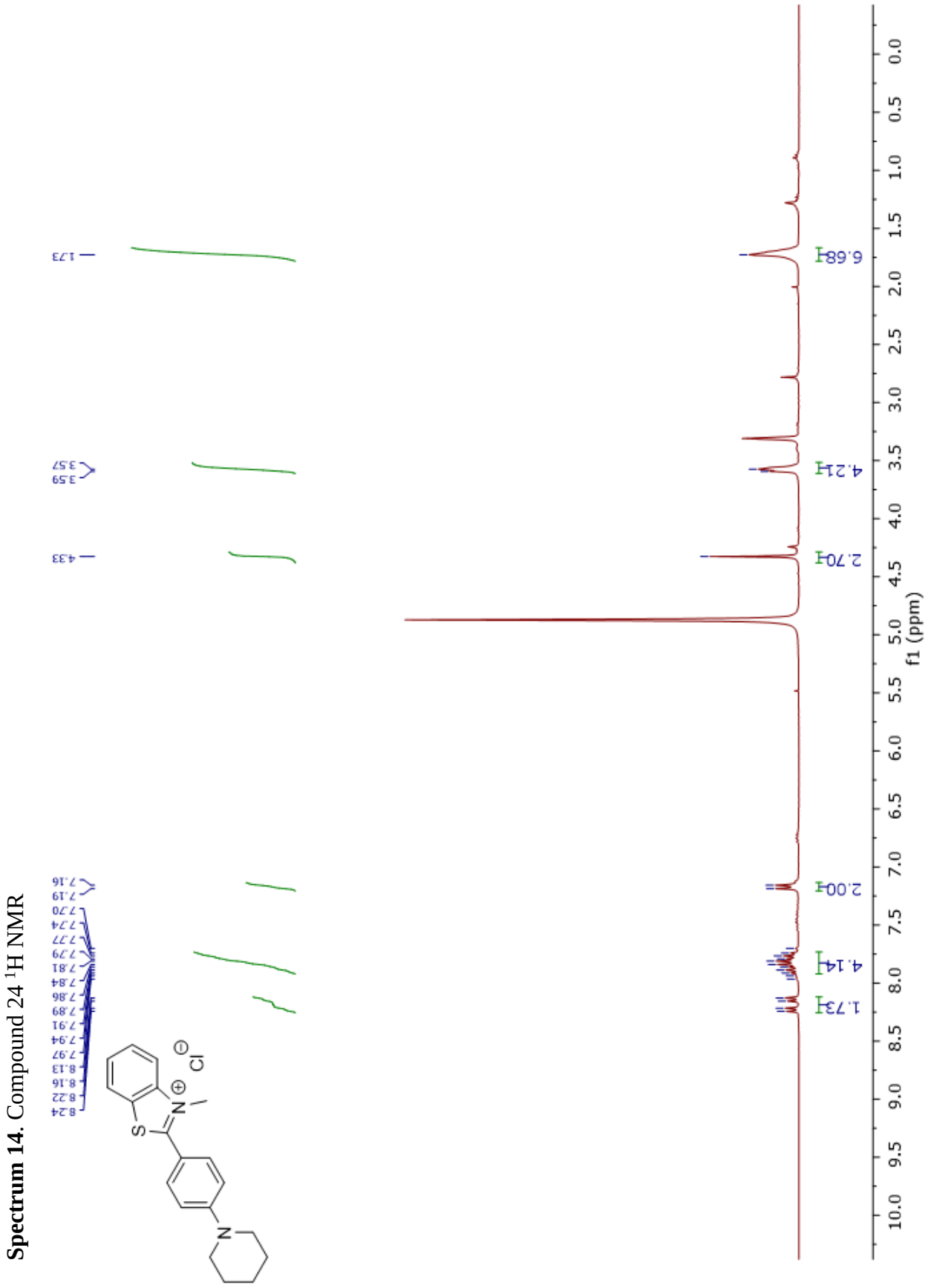

Spectrum 15. Compound 24 ^{13}C NMR

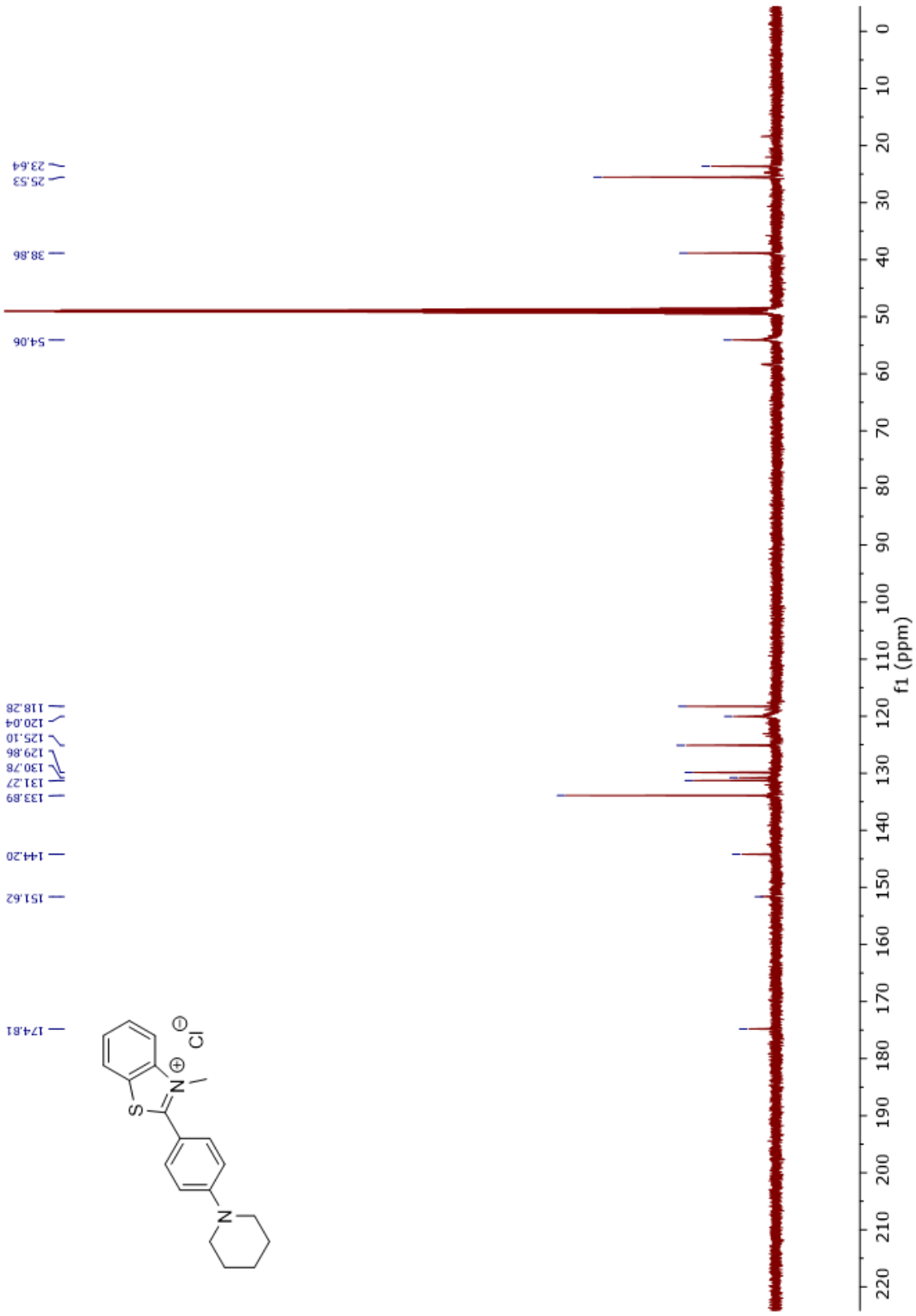

Spectrum 16. Compound 8 ^{1}H NMR

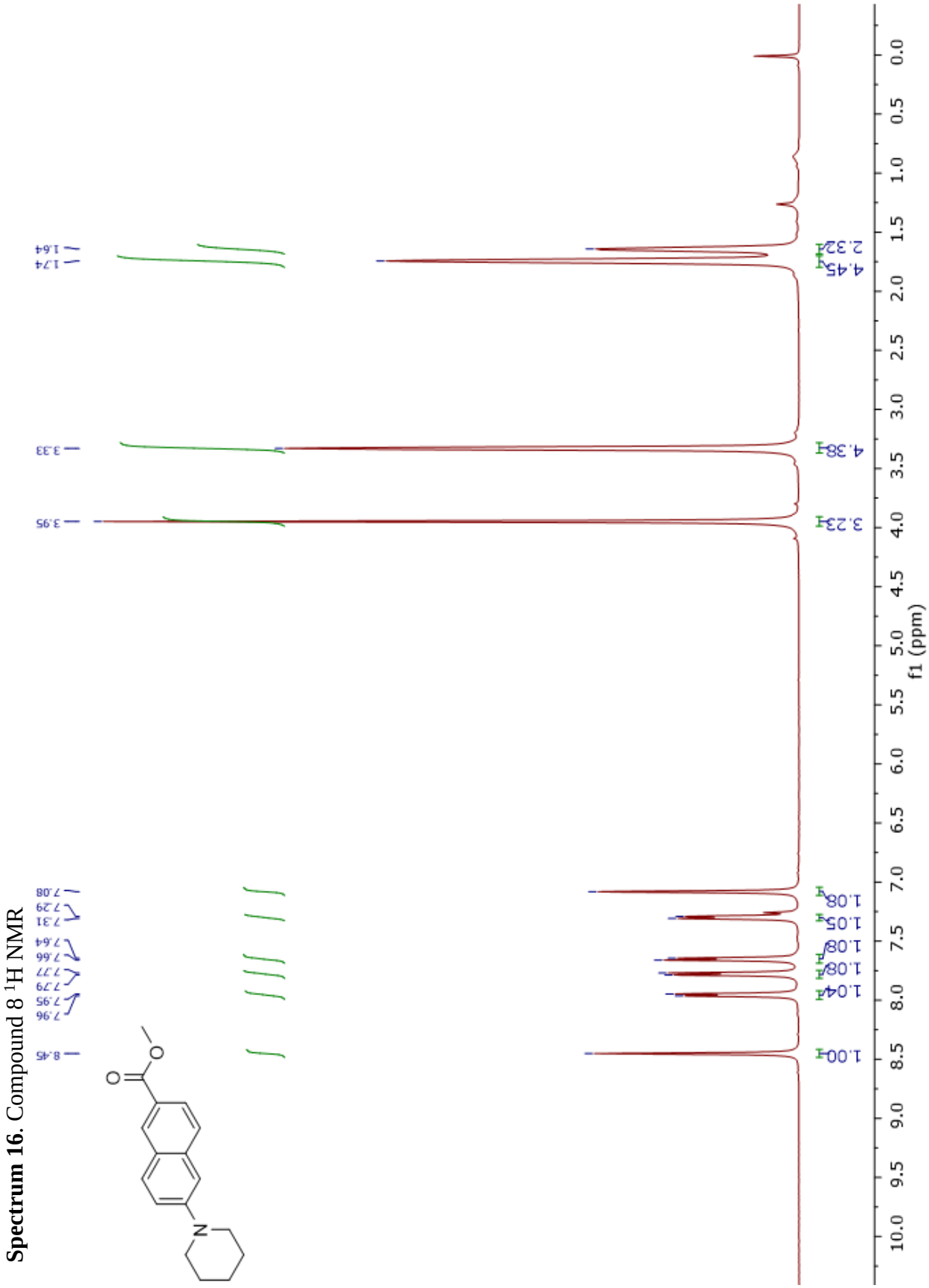

Spectrum 17. Compound 8 ^{13}C NMR

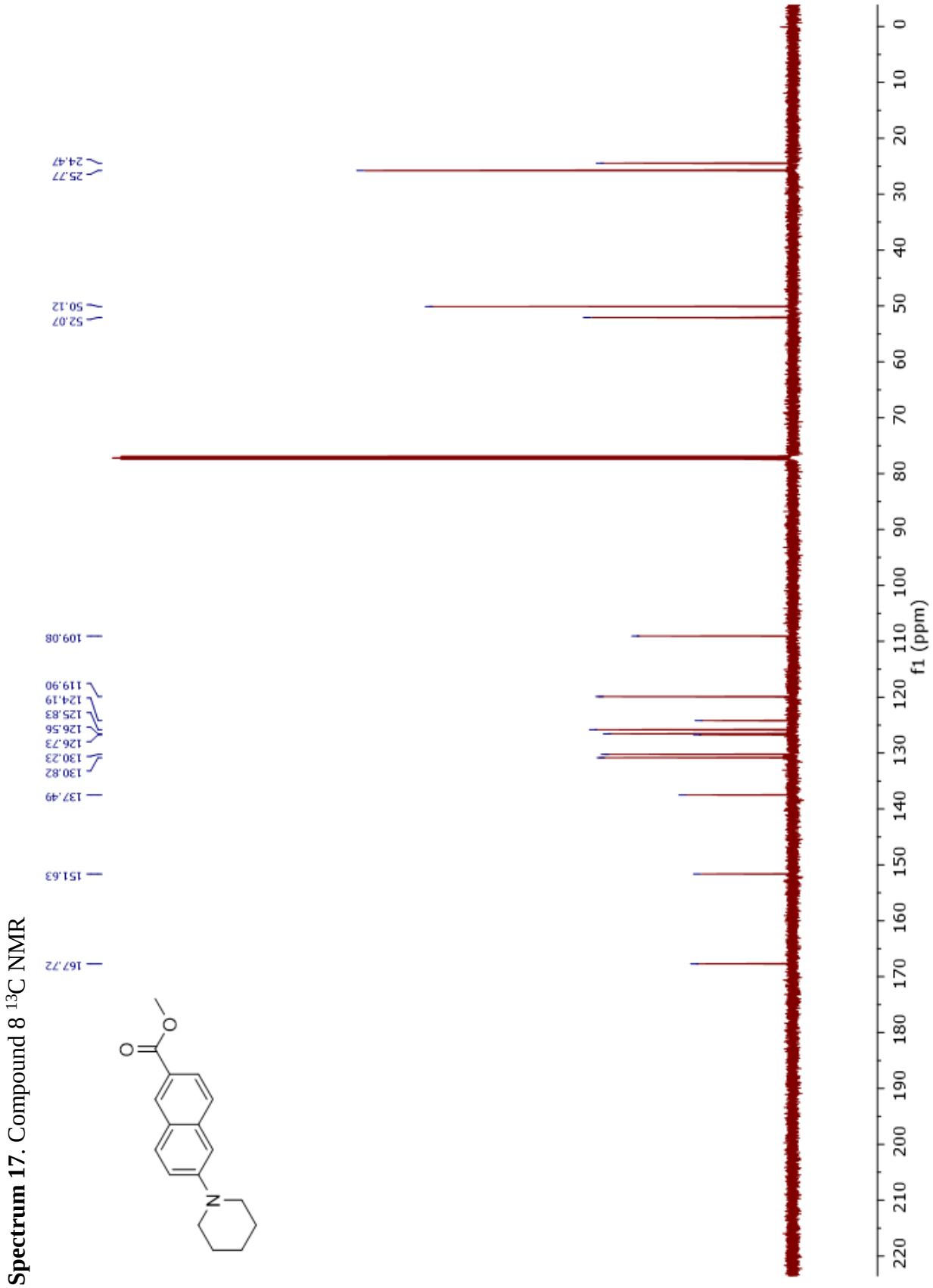

Spectrum 18. Compound 9 ^{1}H NMR

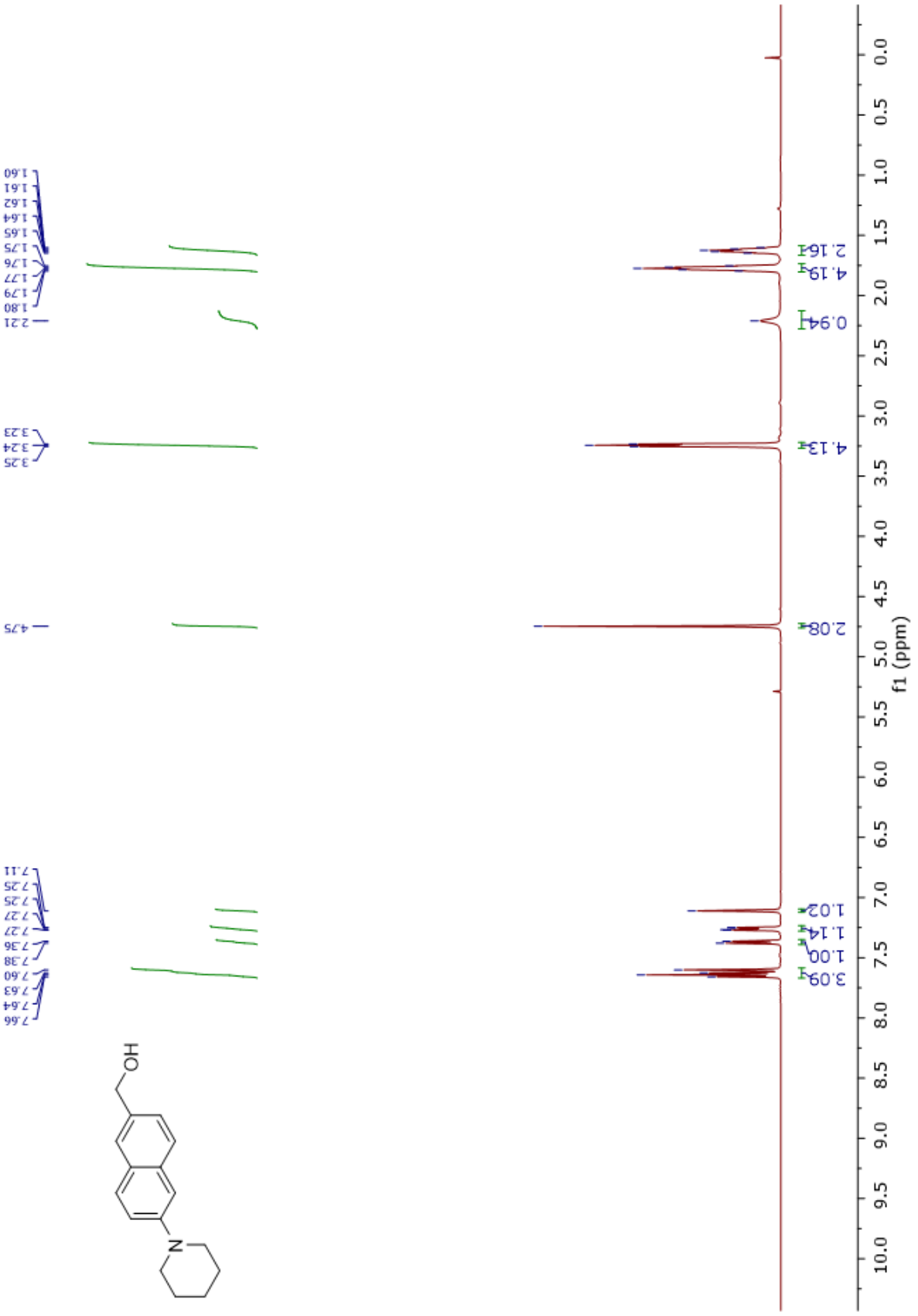

Spectrum 19. Compound 9 ^{13}C NMR

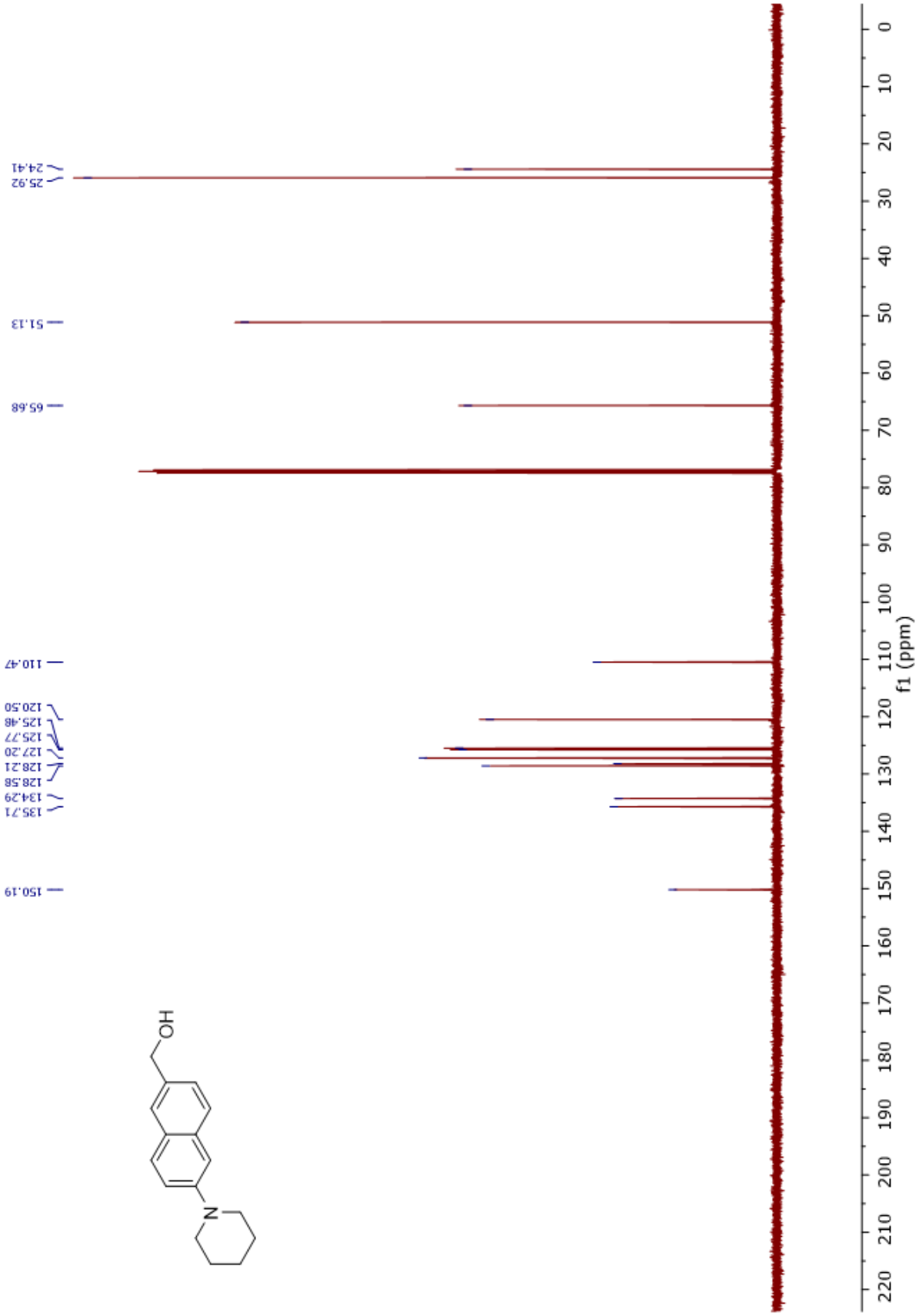

Spectrum 20. Compound 10 ^{1}H NMR

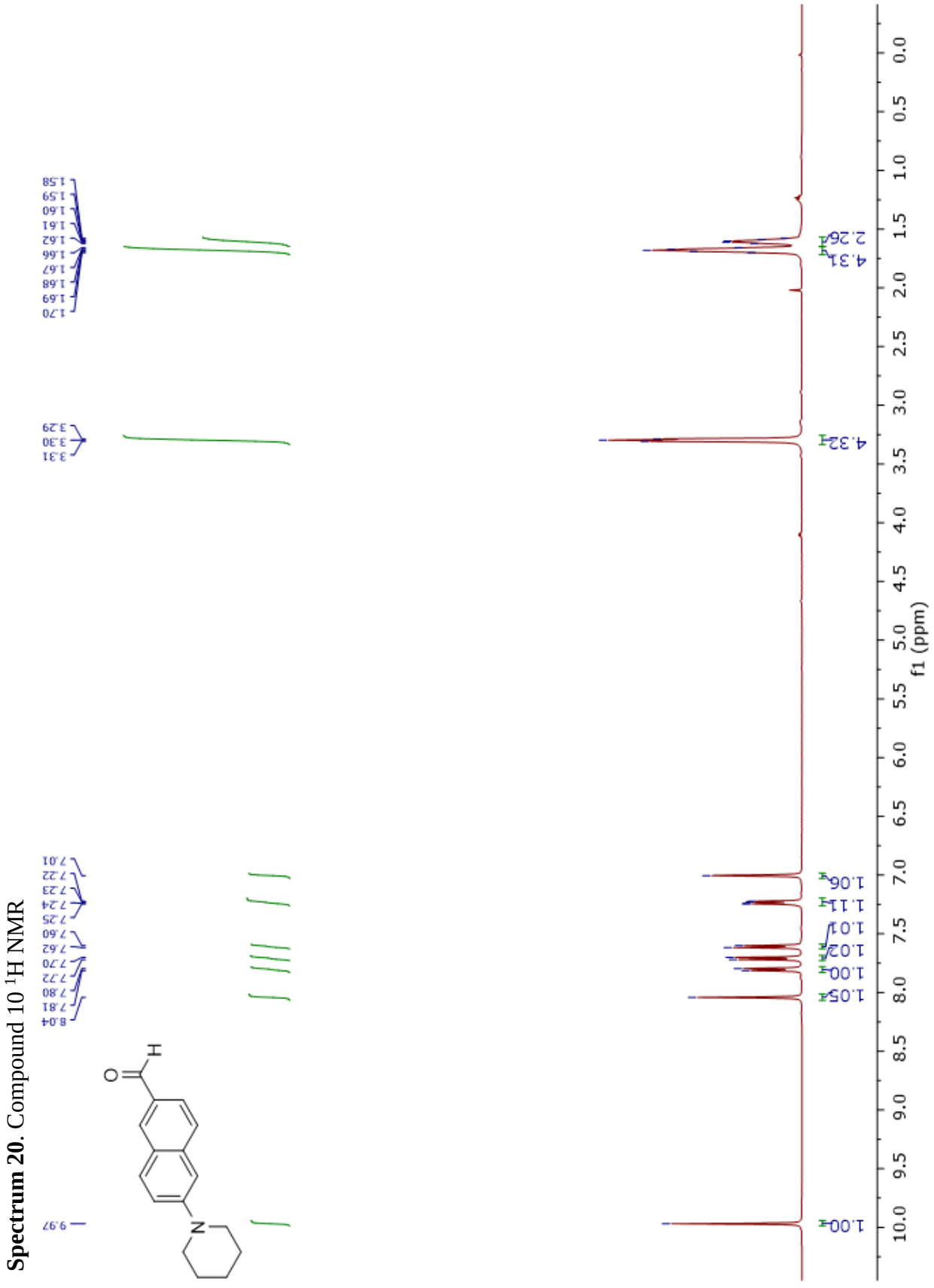

Spectrum 21. Compound 10 ^{13}C NMR

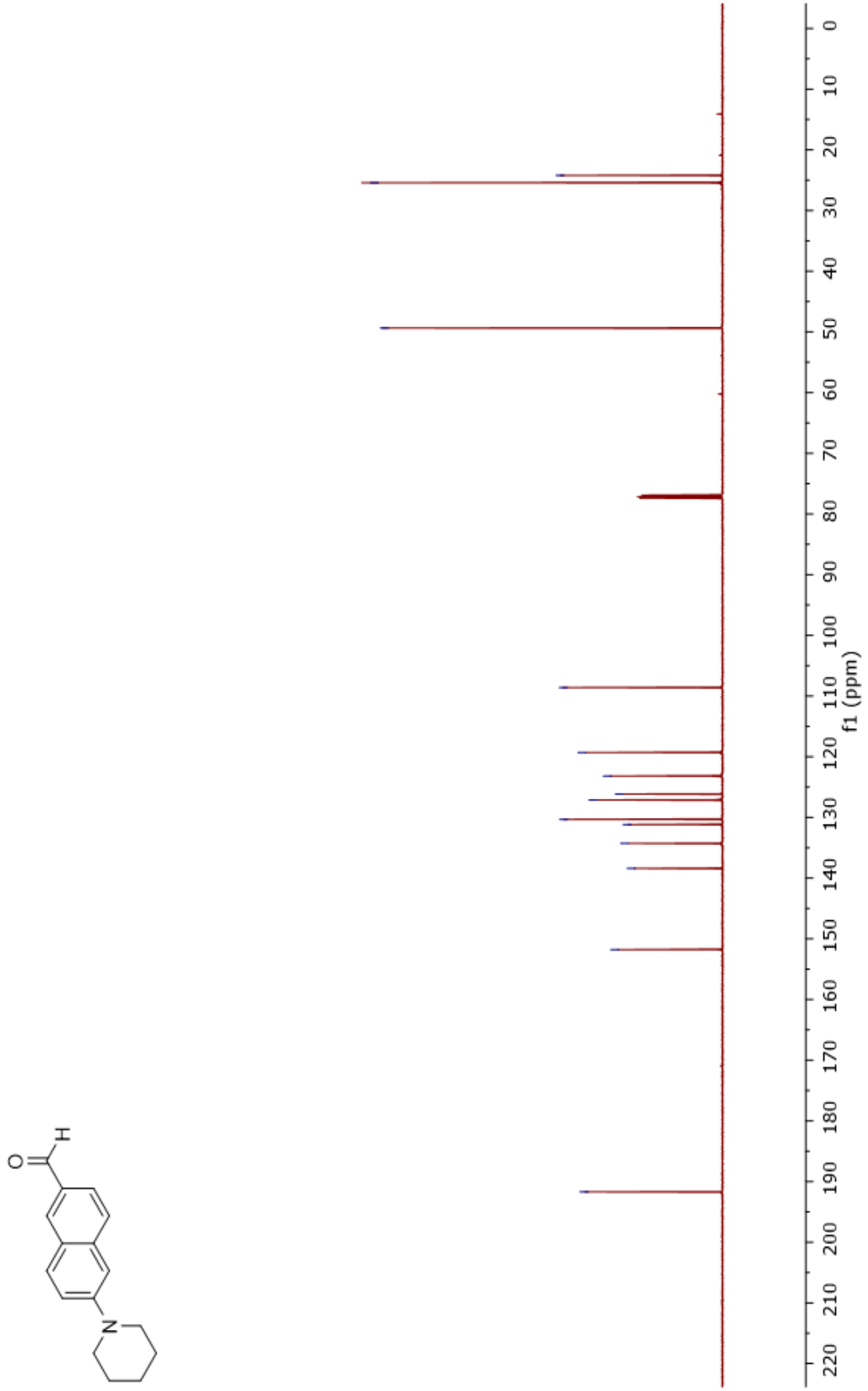

Spectrum 22. Compound 20 ^{1}H NMR. Tharamak, Sorachat; Lam, Jamie; Theodorakis, Emmanuel. Spectrum 22. Mr. Tharamak was the principal researcher of this spectrum.

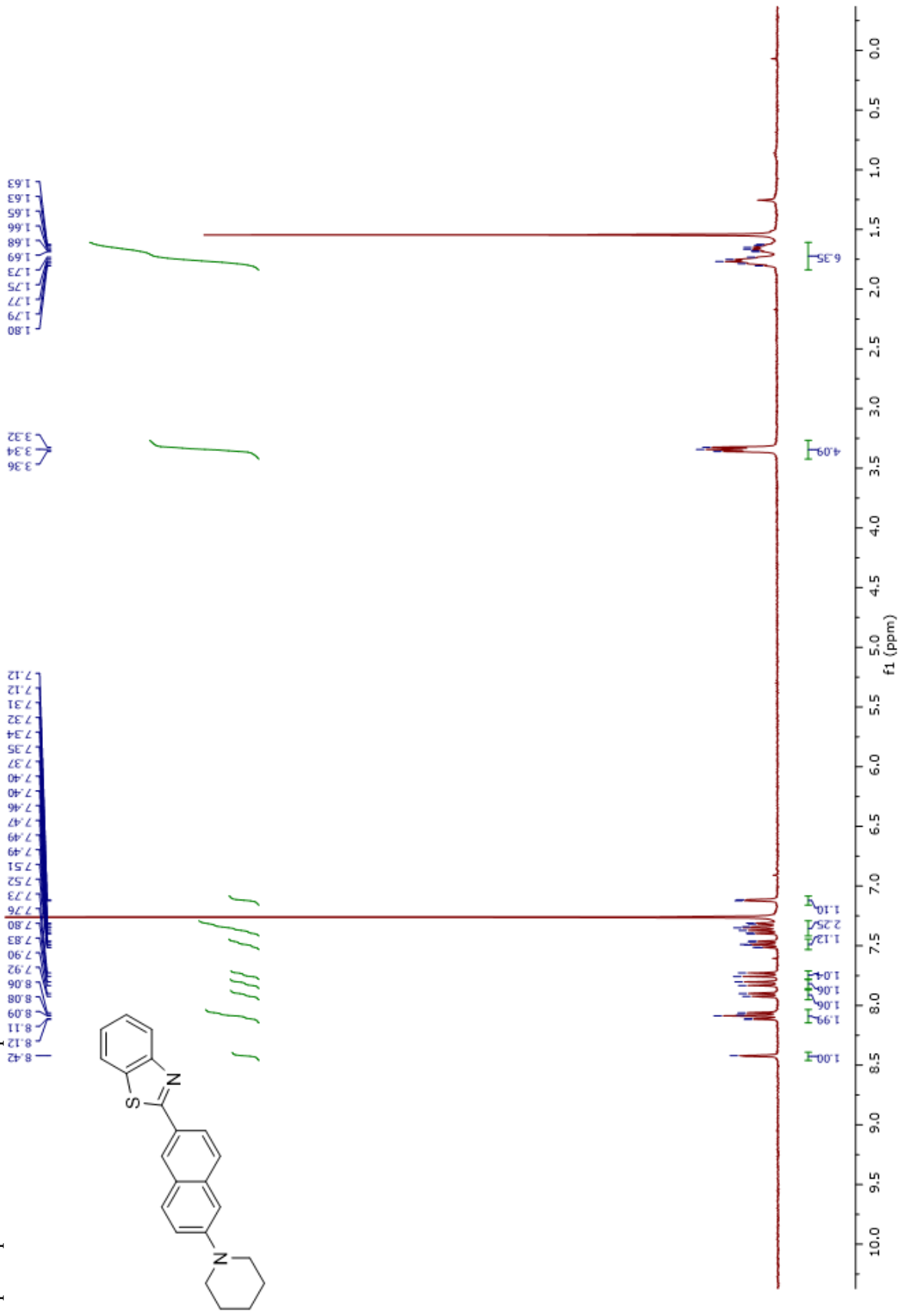

Spectrum 23. Compound 20 ^{13}C NMR. Tharamak, Sorachat; Lam, Jamie; Theodorakis, Emmanuel. Spectrum 23. Mr. Tharamak was the principal researcher of this spectrum.

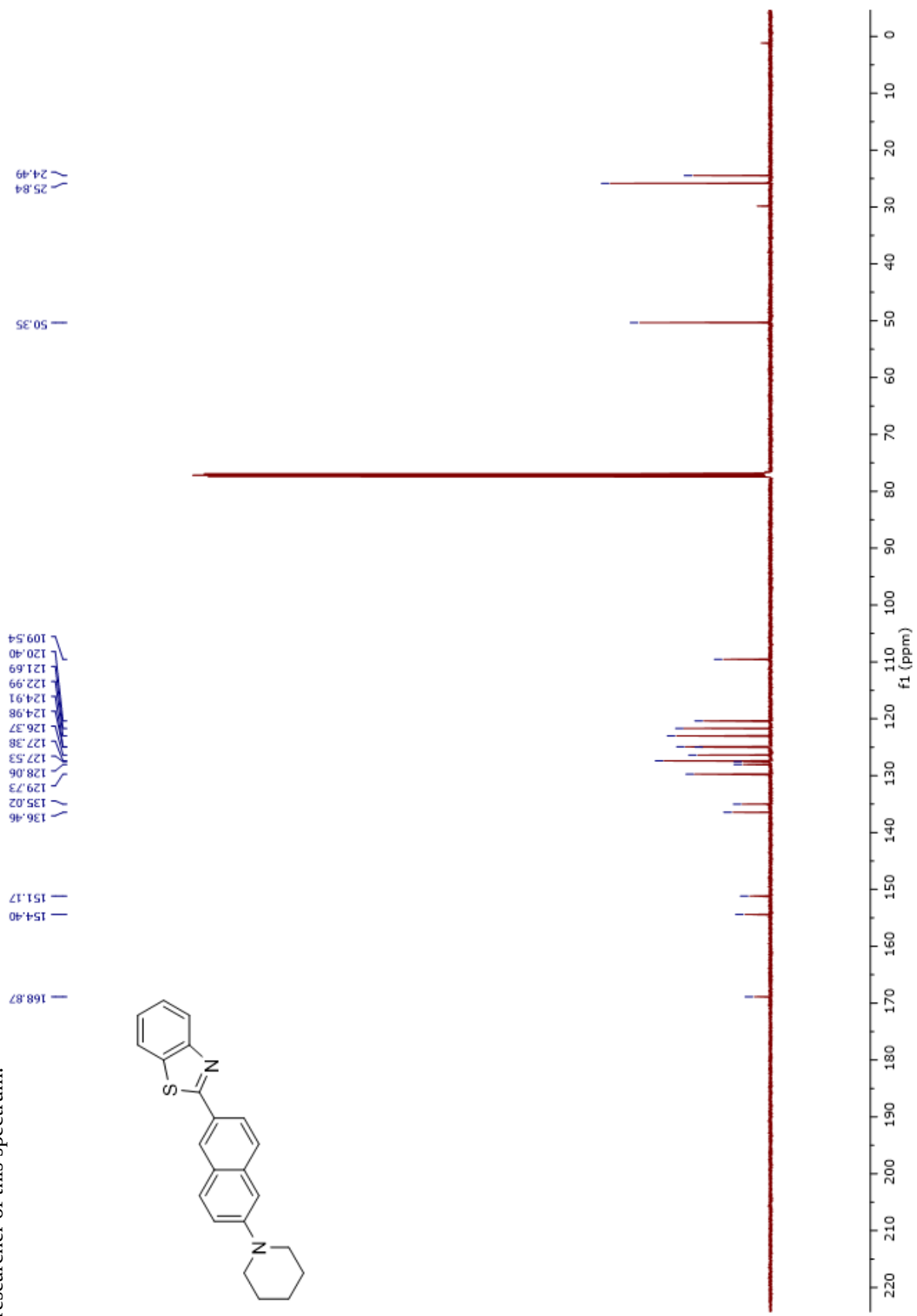

Spectrum 24. Compound 25 ^{1}H NMR. Tharamak, Sorachat; Lam, Jamie; Theodorakis, Emmanuel. Spectrum 24. Mr. Tharamak was the principal researcher of this spectrum.

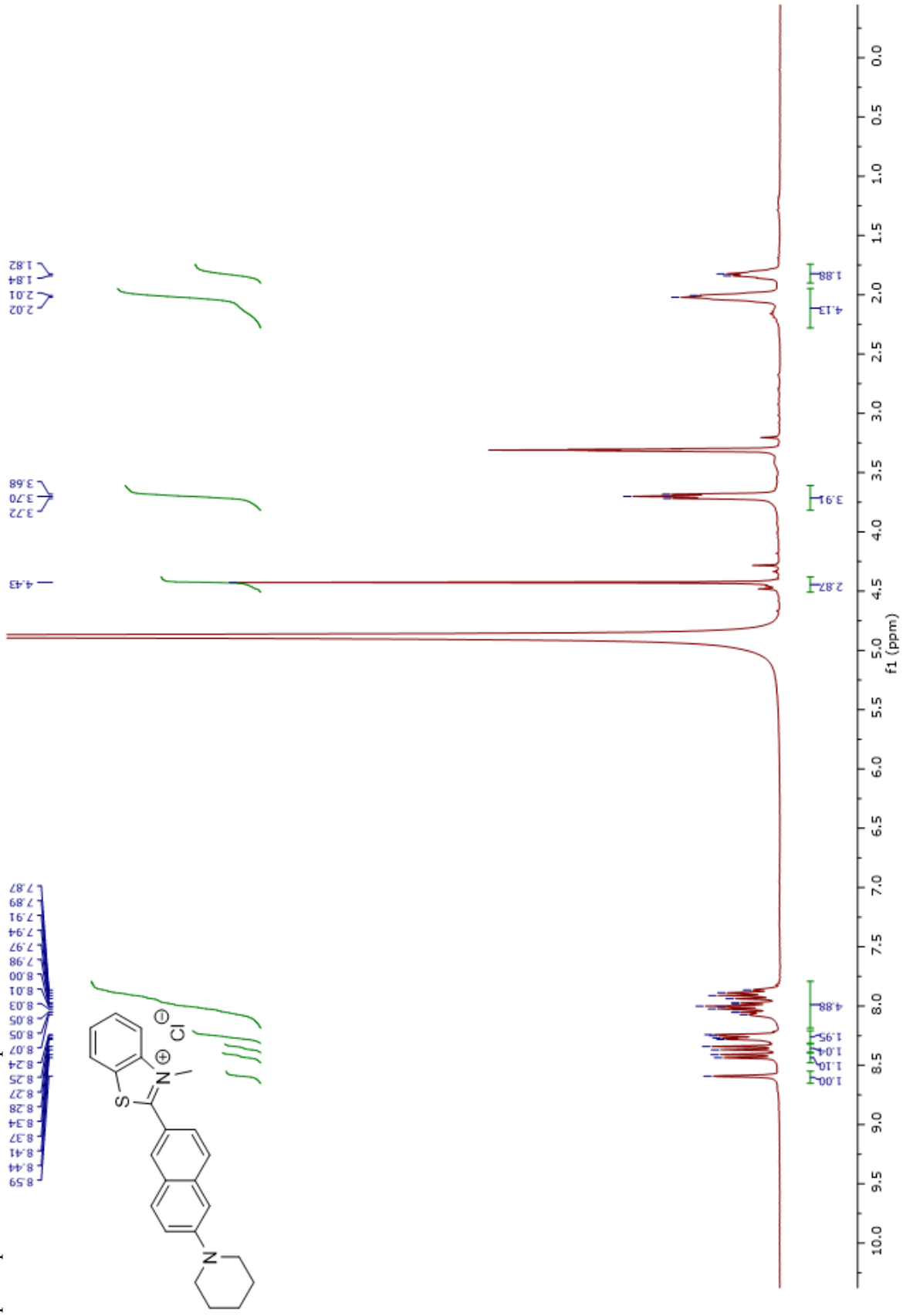

Spectrum 25. Compound 25 ^{13}C NMR. Tharamak, Sorachat; Lam, Jamie; Theodorakis, Emmanuel. Spectrum 25. Mr. Tharamak was the principal researcher of this spectrum.

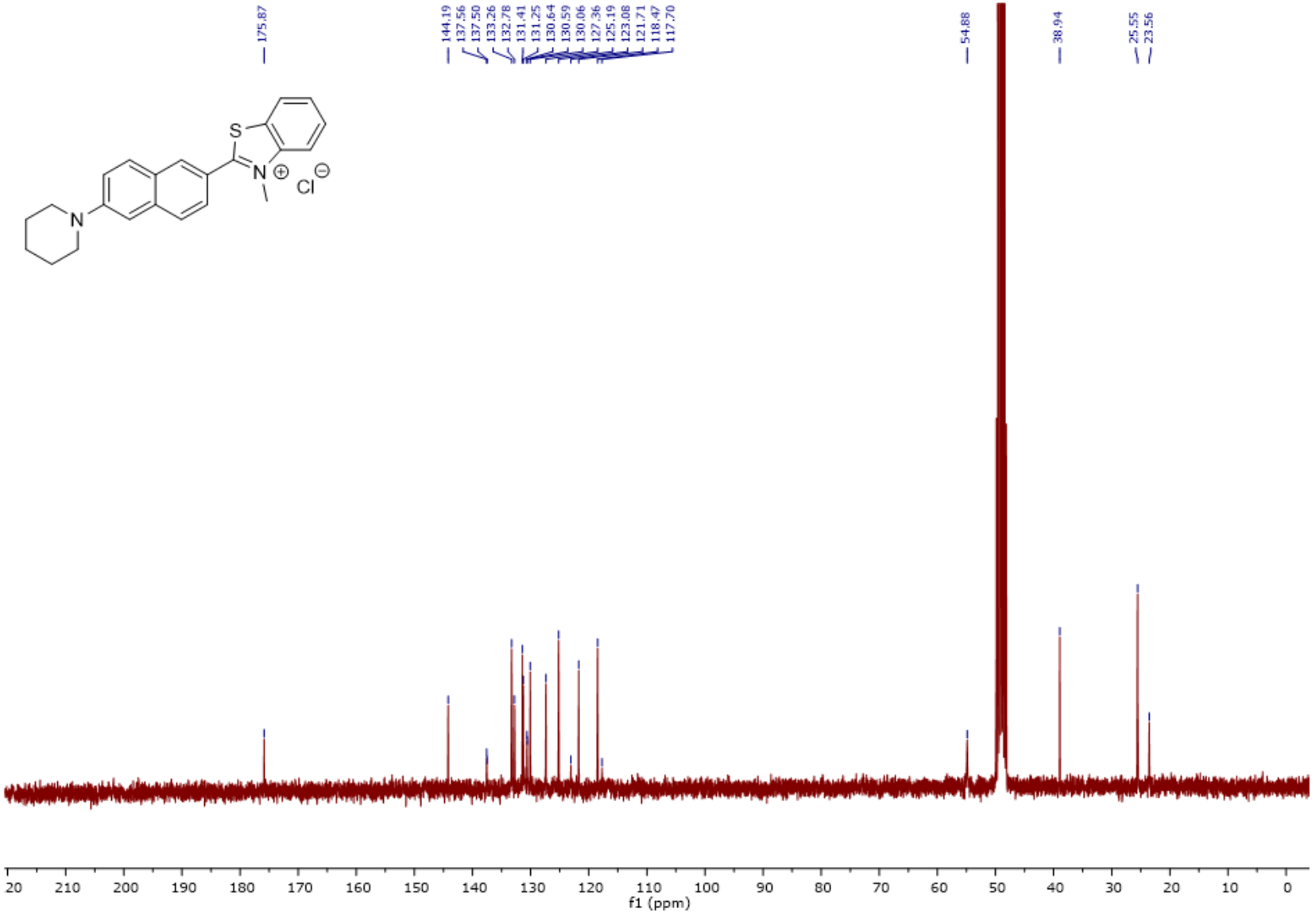

Spectrum 26. Compound 12 ^{1}H NMR. Tharamak, Sorachat; Lam, Jamie; Theodorakis, Emmanuel. Spectrum 26. Mr. Tharamak was the principal researcher of this spectrum.

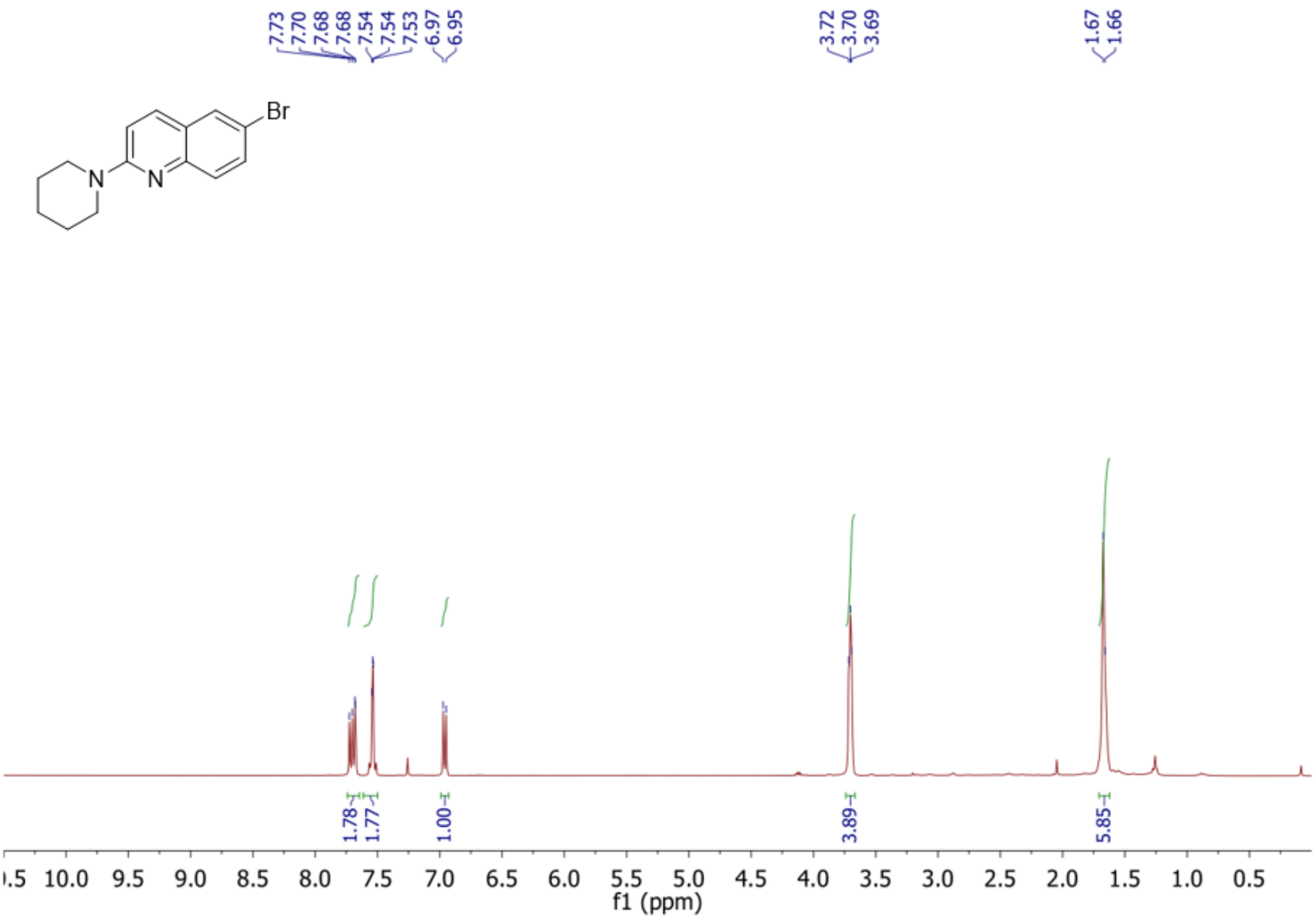

Spectrum 27. Compound 12 ^{13}C NMR. Tharamak, Sorachat; Lam, Jamie; Theodorakis, Emmanuel. Spectrum 27. Mr. Tharamak was the principal researcher of this spectrum.

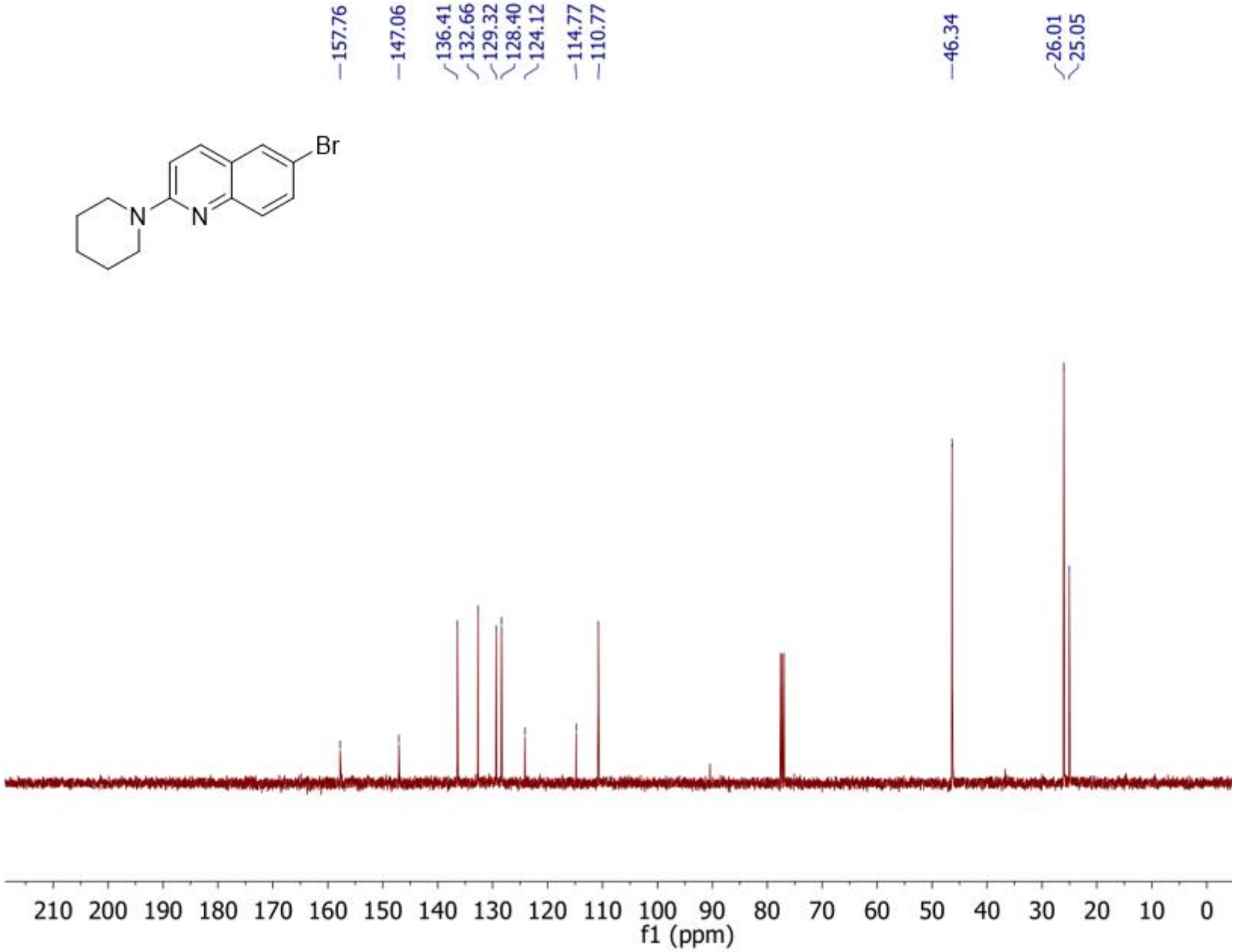

Spectrum 28. Compound 13 ^{1}H NMR. Tharamak, Sorachat; Lam, Jamie; Theodorakis, Emmanuel. Spectrum 28. Mr. Tharamak was the principal researcher of this spectrum.

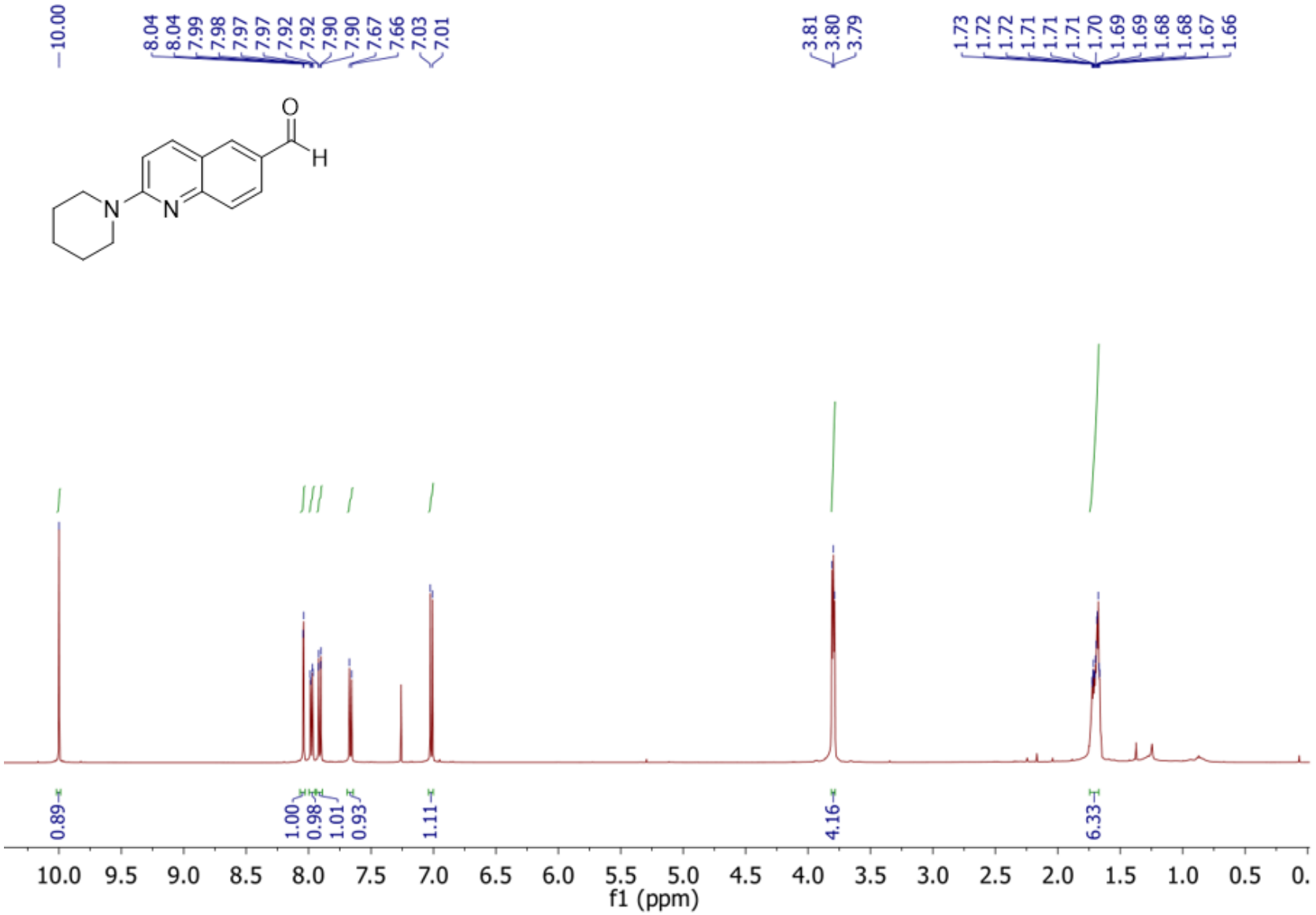

Spectrum 29. Compound 13 ^{13}C NMR. Tharamak, Sorachat; Lam, Jamie; Theodorakis, Emmanuel. Spectrum 29. Mr. Tharamak was the principal researcher of this spectrum.

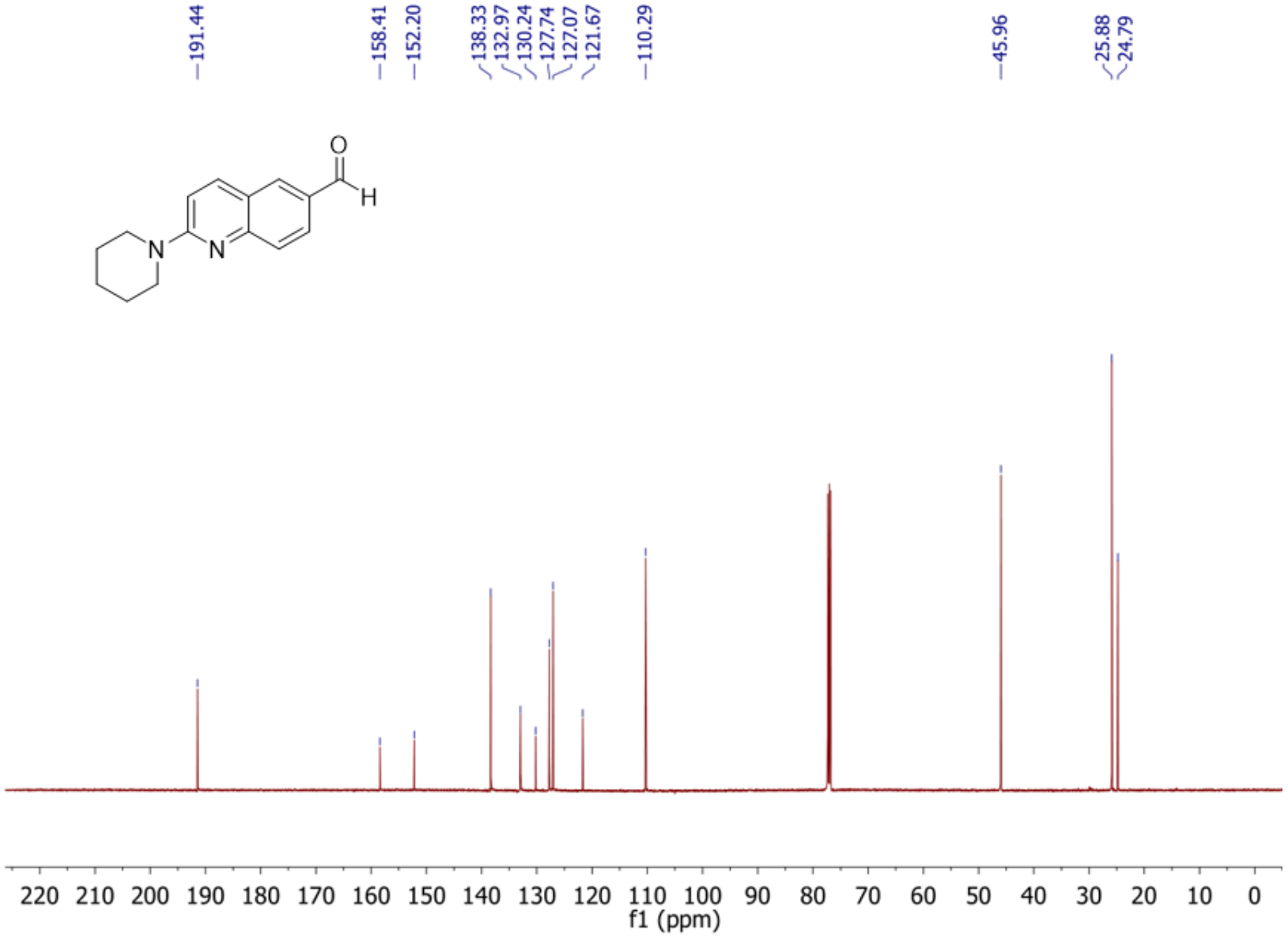

Spectrum 30. Compound 21 ^{1}H NMR. Tharamak, Sorachat; Lam, Jamie; Theodorakis, Emmanuel. Spectrum 30. Mr. Tharamak was the principal researcher of this spectrum.

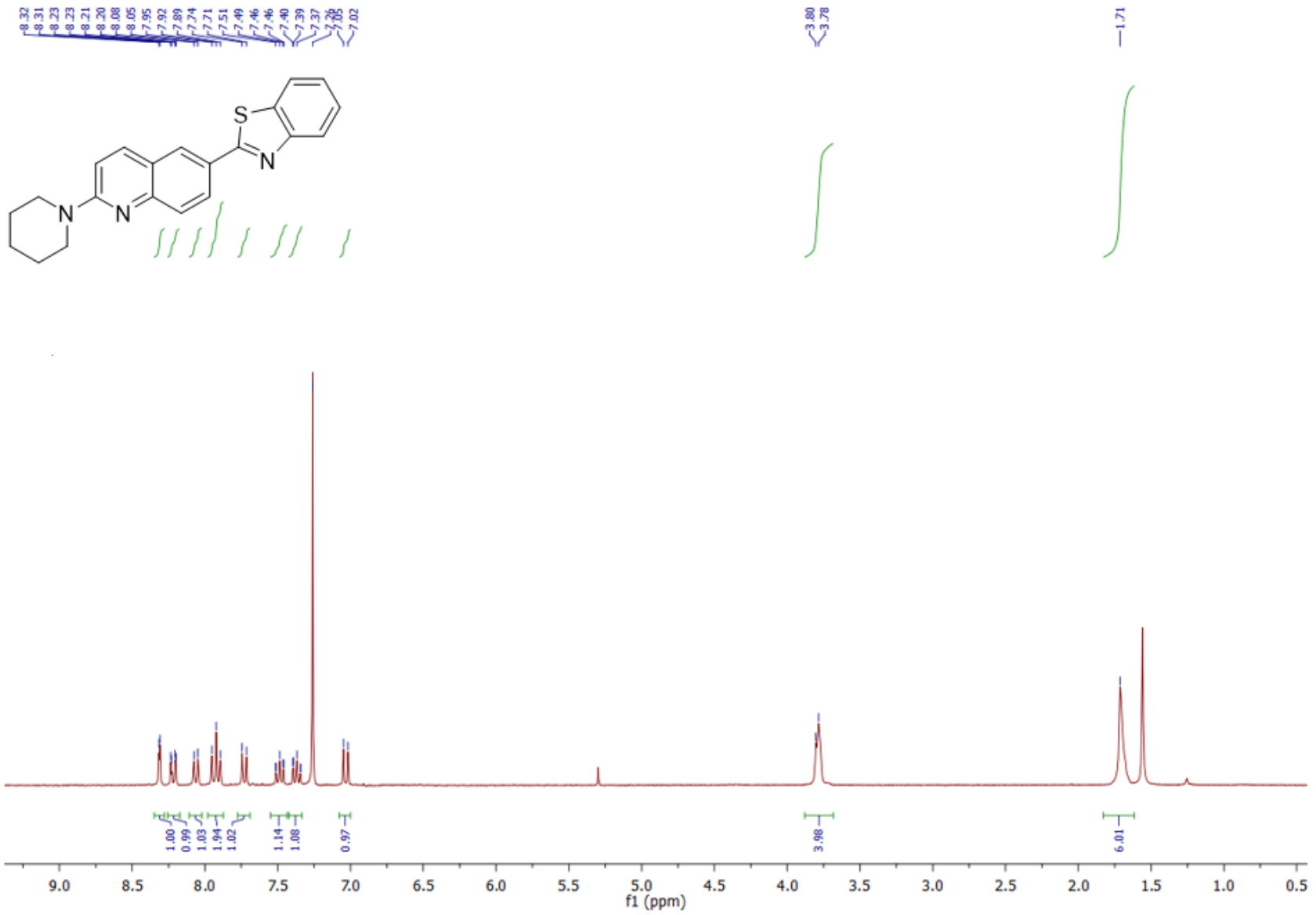

Spectrum 31. Compound 21 ^{13}C NMR. Tharamak, Sorachat; Lam, Jamie; Theodorakis, Emmanuel. Spectrum 31. Mr. Tharamak was the principal researcher of this spectrum.

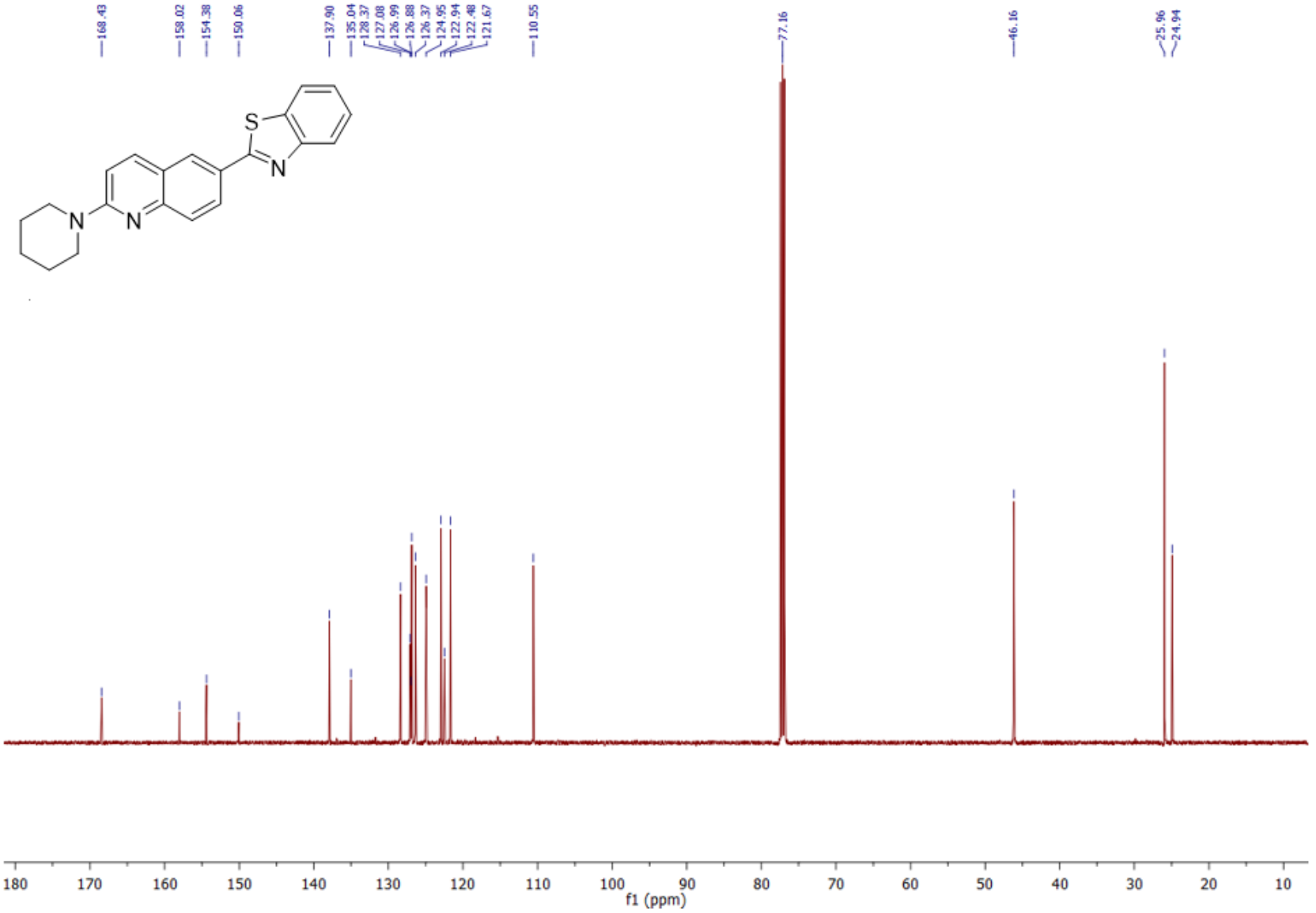

Spectrum 32. Compound 26 ^{1}H NMR. Tharamak, Sorachat; Lam, Jamie; Theodorakis, Emmanuel. Spectrum 32. Mr. Tharamak was the principal researcher of this spectrum.

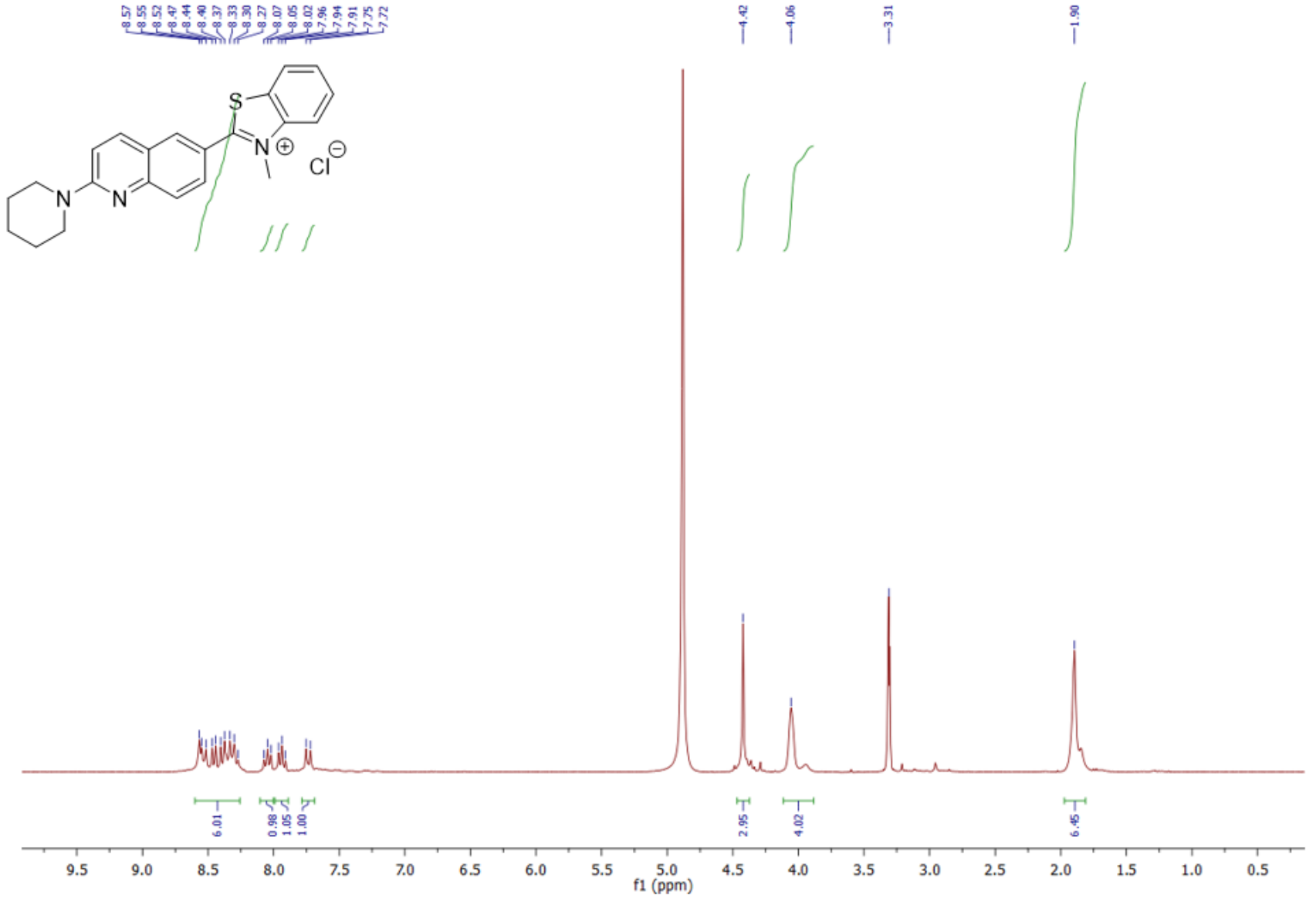

Spectrum 33. Compound 26 ^{13}C NMR. Tharamak, Sorachat; Lam, Jamie; Theodorakis, Emmanuel. Spectrum 33. Mr. Tharamak was the principal researcher of this spectrum.

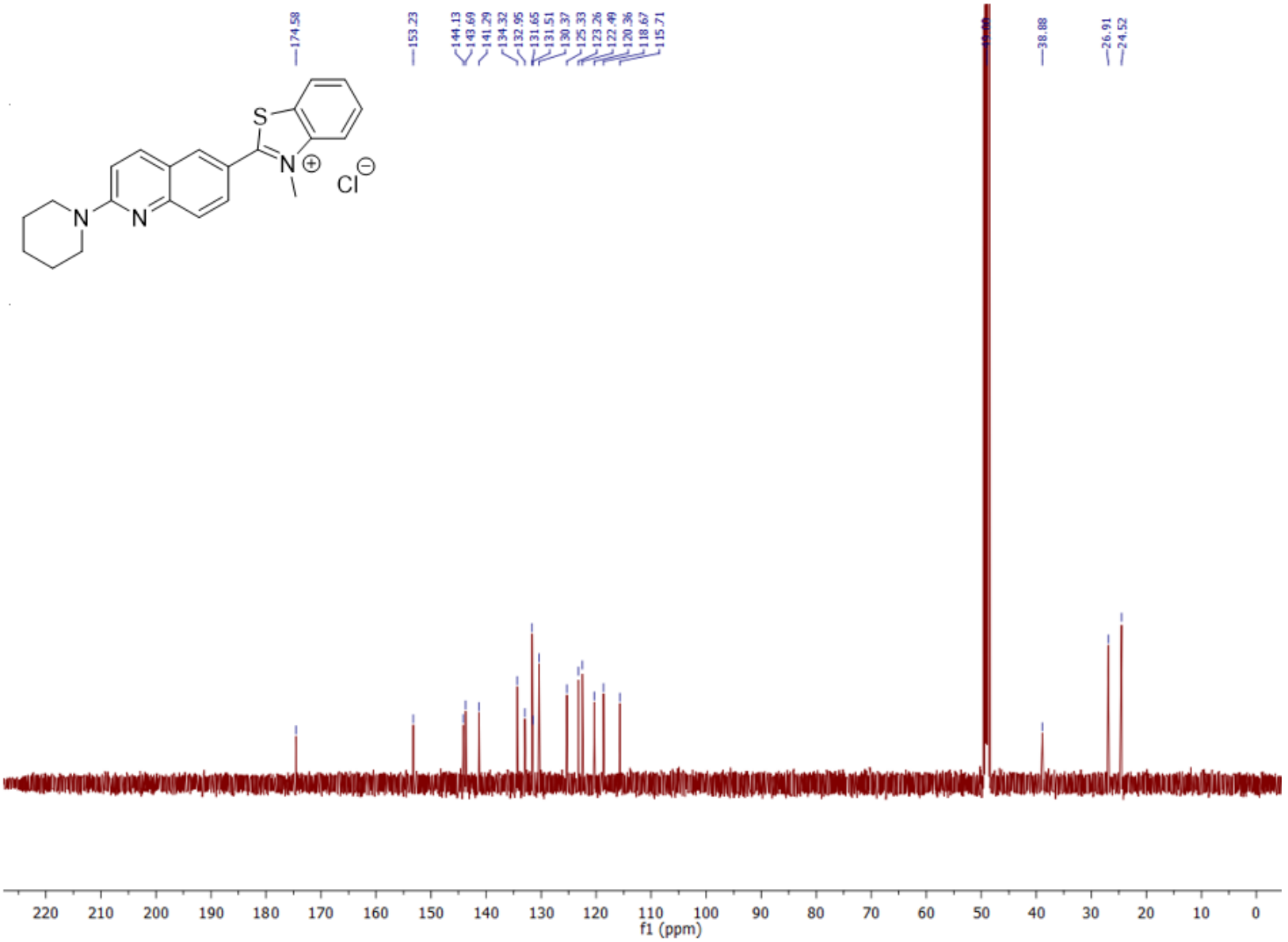

Spectrum 34. Compound 15 ^{1}H NMR. Tharamak, Sorachat; Lam, Jamie; Theodorakis, Emmanuel. Spectrum 34. Mr. Tharamak was the principal researcher of this spectrum.

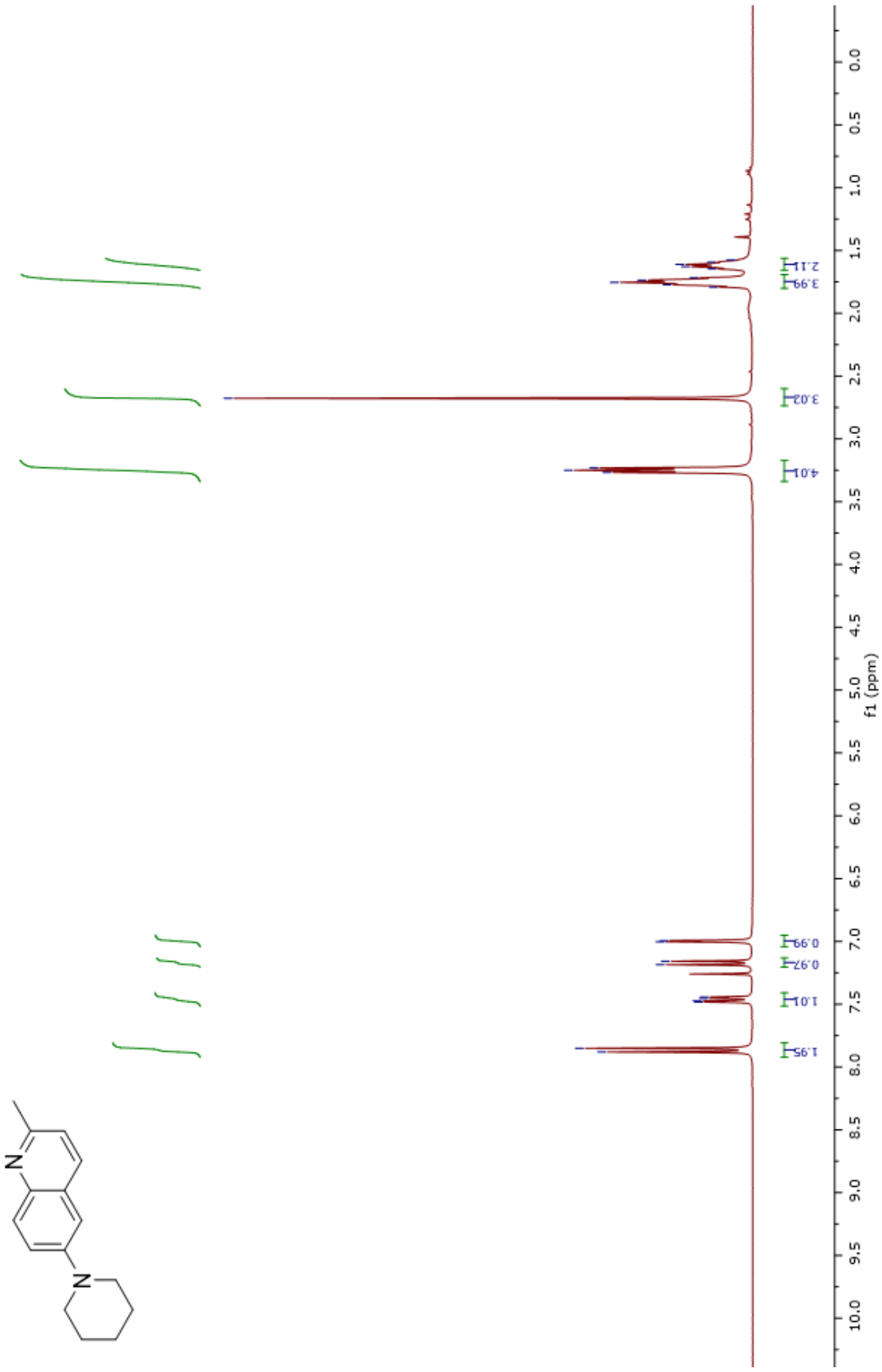

Spectrum 35. Compound 15 ^{13}C NMR. Tharamak, Sorachat; Lam, Jamie; Theodorakis, Emmanuel. Spectrum 35. Mr. Tharamak was the principal researcher of this spectrum.

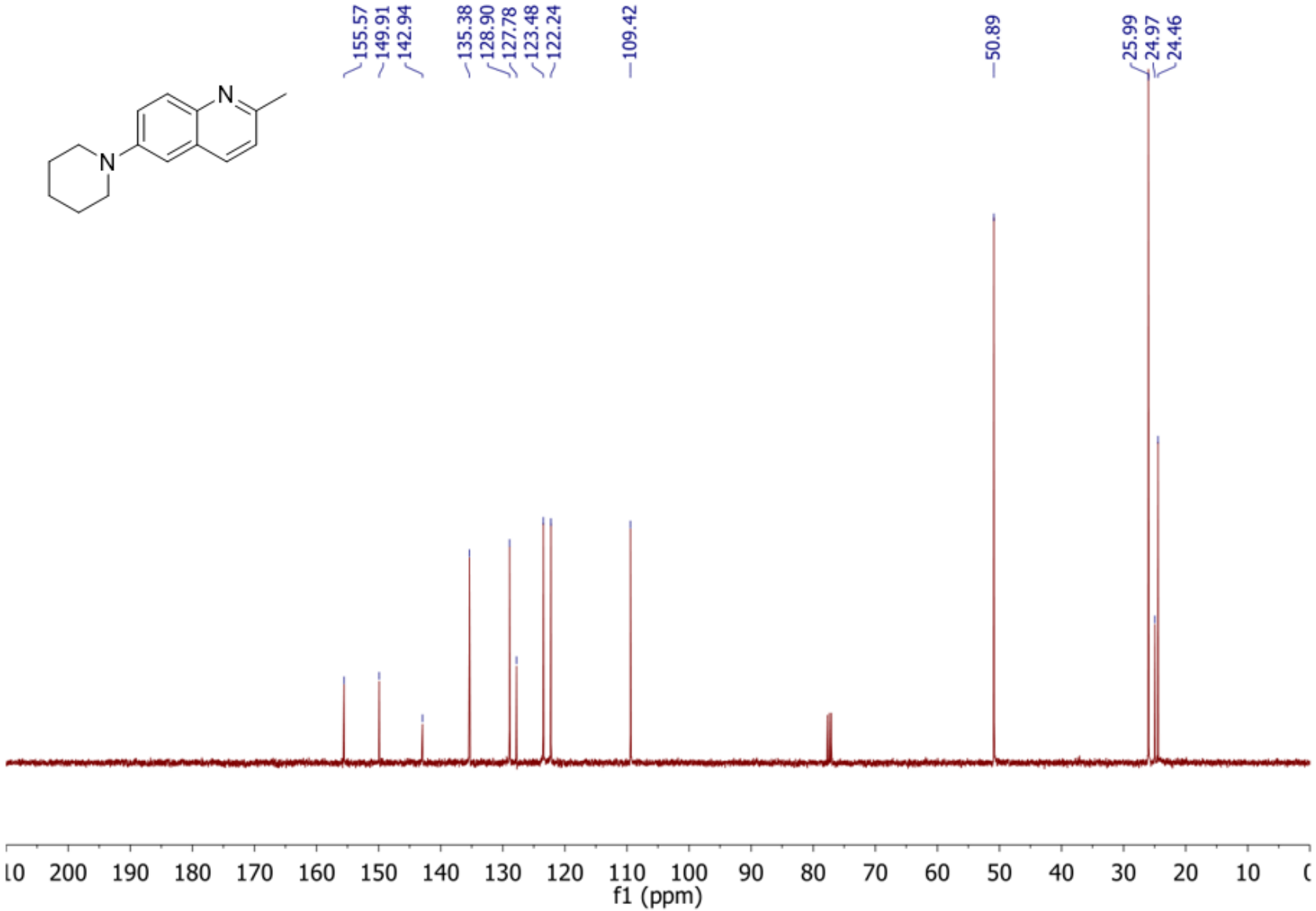

Spectrum 36. Compound 16 ^{13}C NMR. Tharamak, Sorachat; Lam, Jamie; Theodorakis, Emmanuel. Spectrum 36. Mr. Tharamak was the principal researcher of this spectrum.

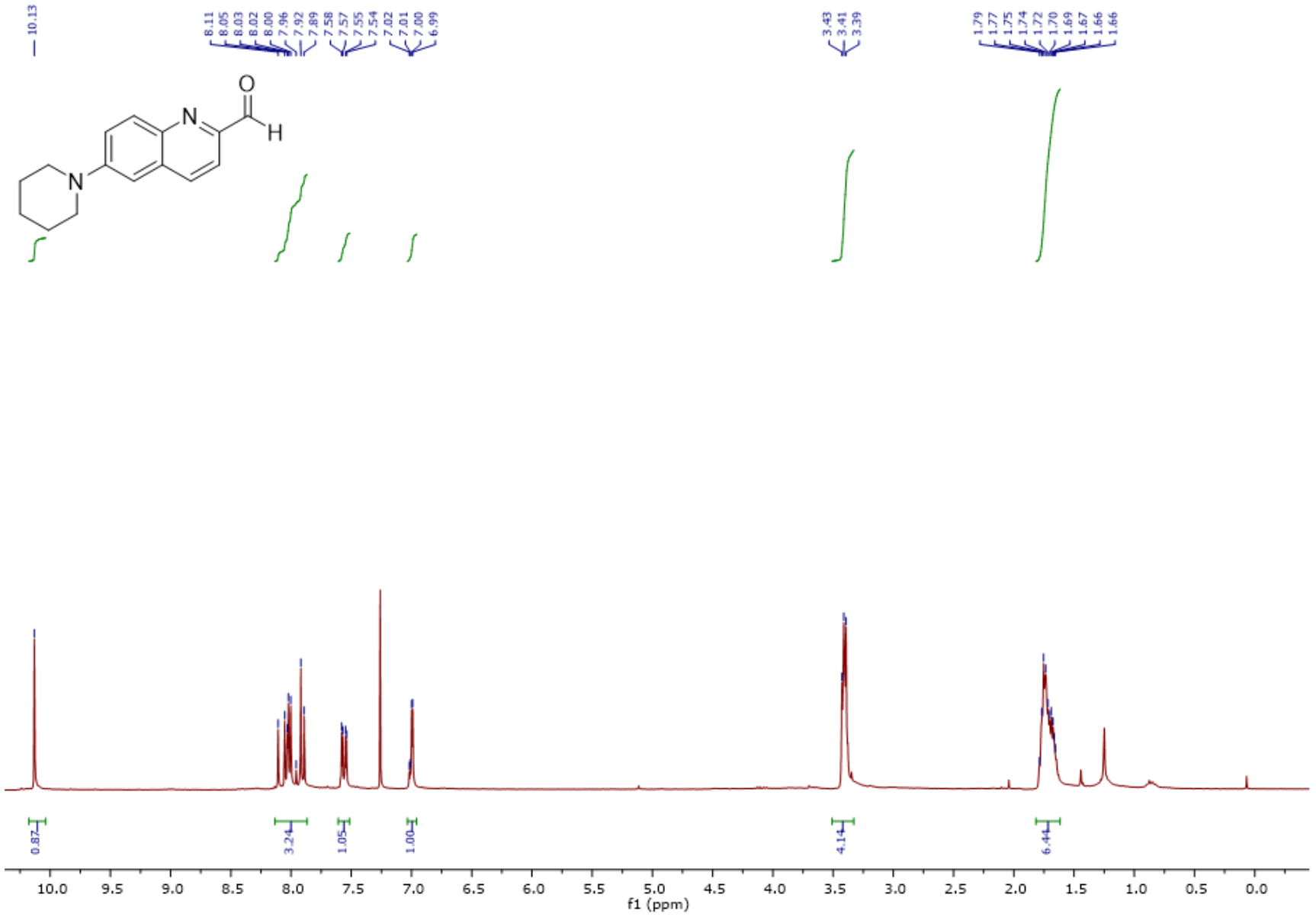

Spectrum 37. Compound 16 ^{13}C NMR. Tharamak, Sorachat; Lam, Jamie; Theodorakis, Emmanuel. Spectrum 37. Mr. Tharamak was the principal researcher of this spectrum.

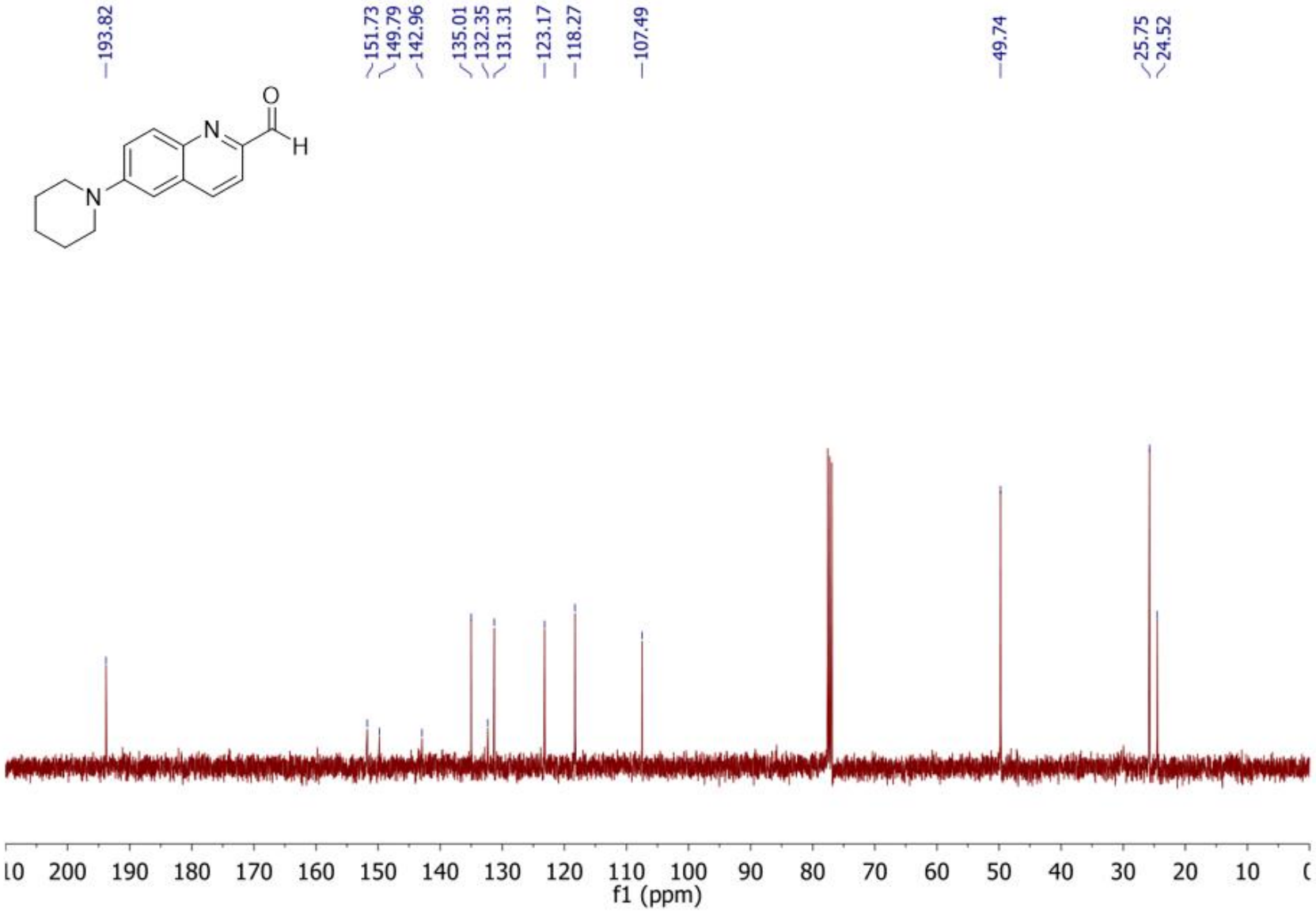

Spectrum 38. Compound 22 ^{1}H NMR. Tharamak, Sorachat; Lam, Jamie; Theodorakis, Emmanuel. Spectrum 38. Mr. Tharamak was the principal researcher of this spectrum.

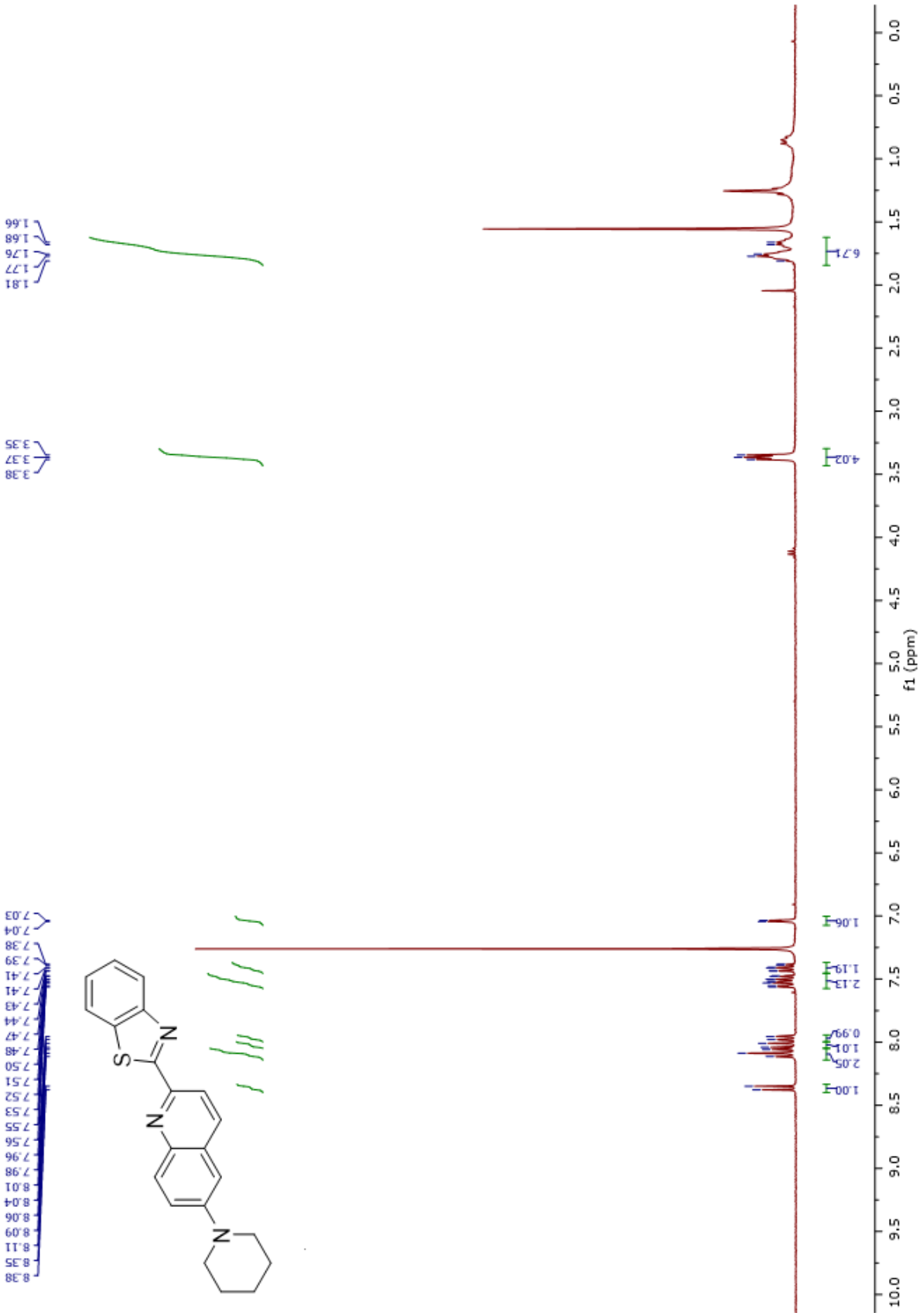

Spectrum 39. Compound 22 ^{13}C NMR. Tharamak, Sorachat; Lam, Jamie; Theodorakis, Emmanuel. Spectrum 39. Mr. Tharamak was the principal researcher of this spectrum.

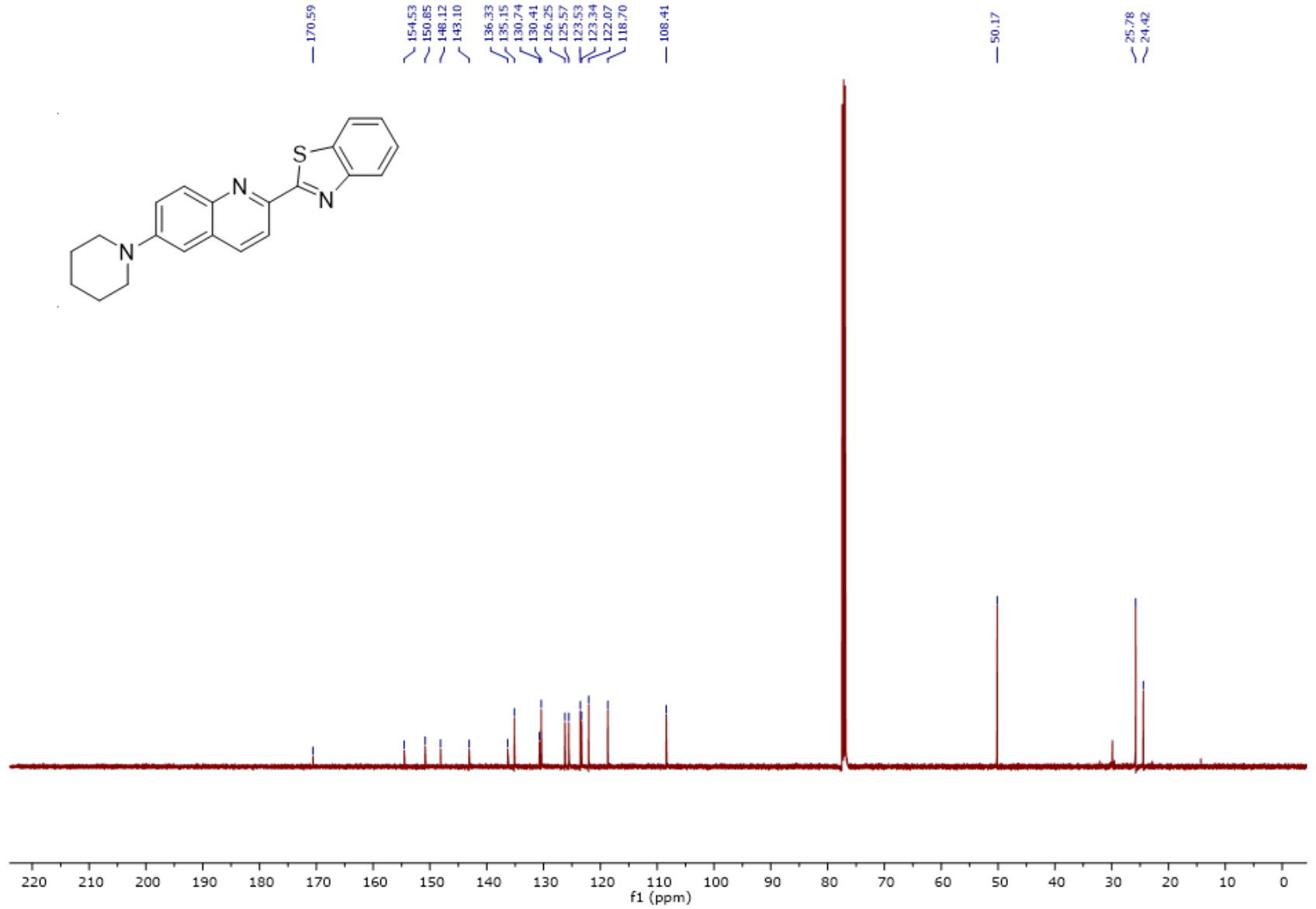

Spectrum 40. Compound 27 ^{1}H NMR. Tharamak, Sorachat; Lam, Jamie; Theodorakis, Emmanuel. Spectrum 40. Mr. Tharamak was the principal researcher of this spectrum.

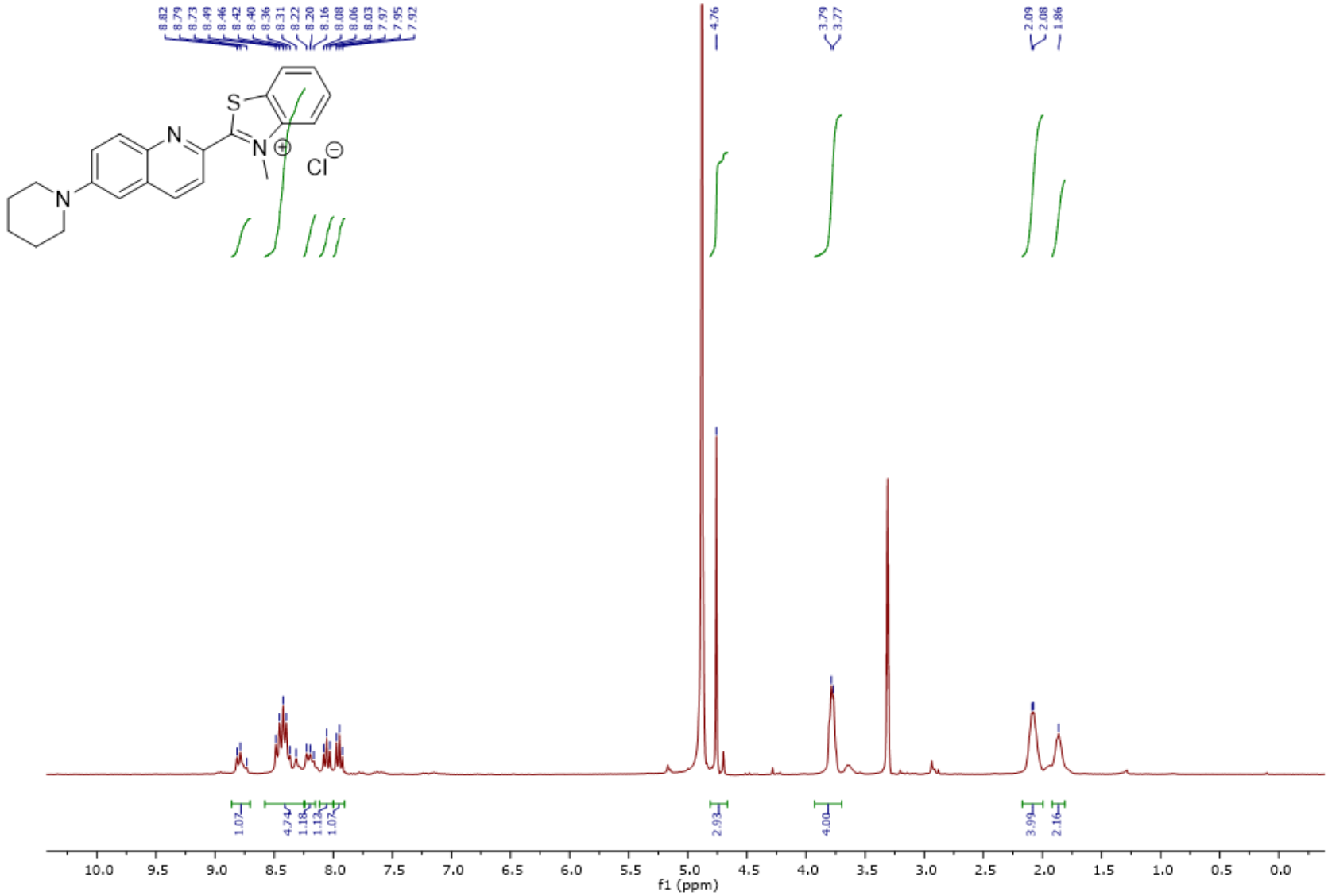

Spectrum 41. Compound 27 ^{13}C NMR. Tharamak, Sorachat; Lam, Jamie; Theodorakis, Emmanuel. Spectrum 41. Mr. Tharamak was the principal researcher of this spectrum.

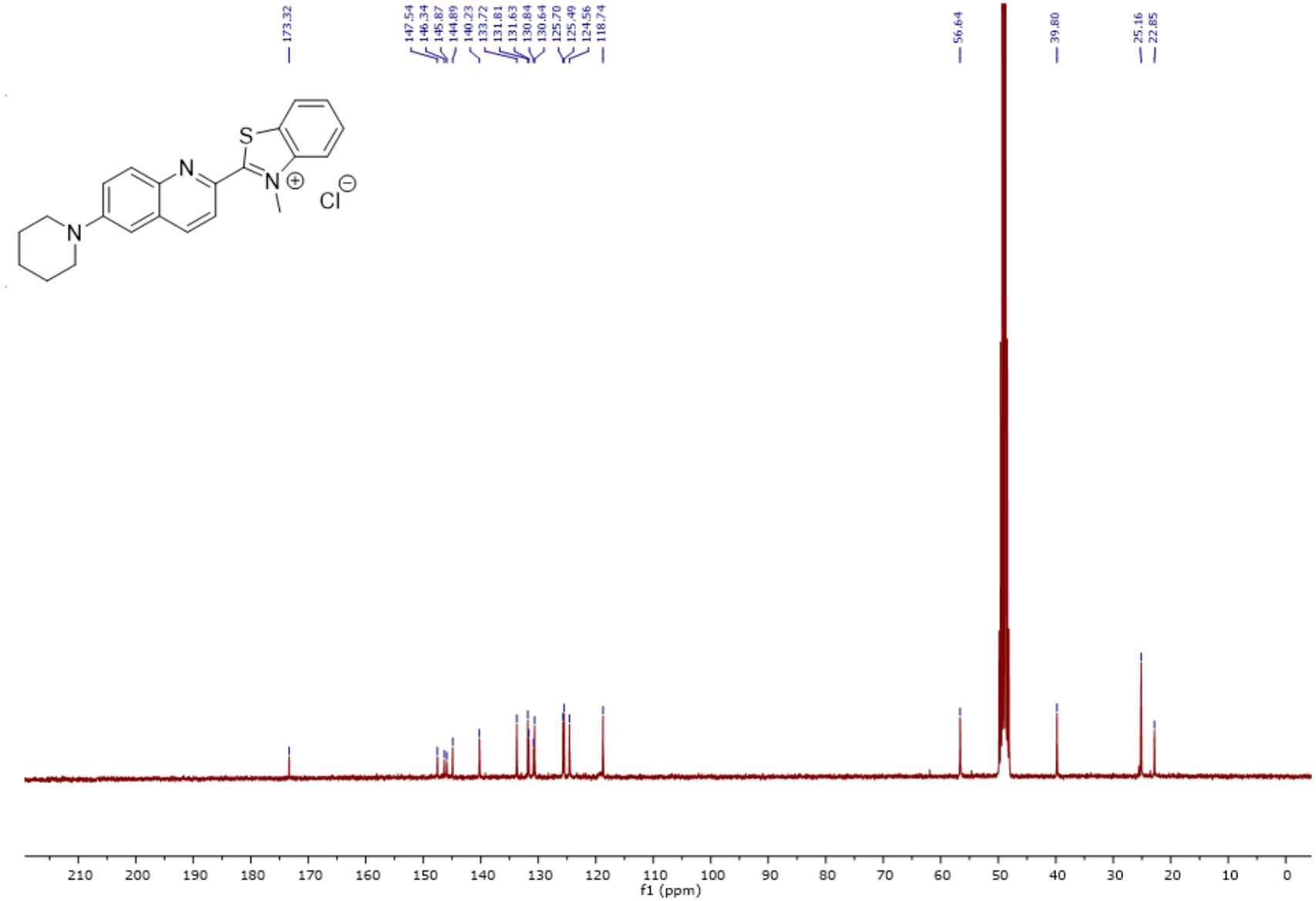

Chapter 3

Spectrum 42. Compound 29 ^{1}H NMR

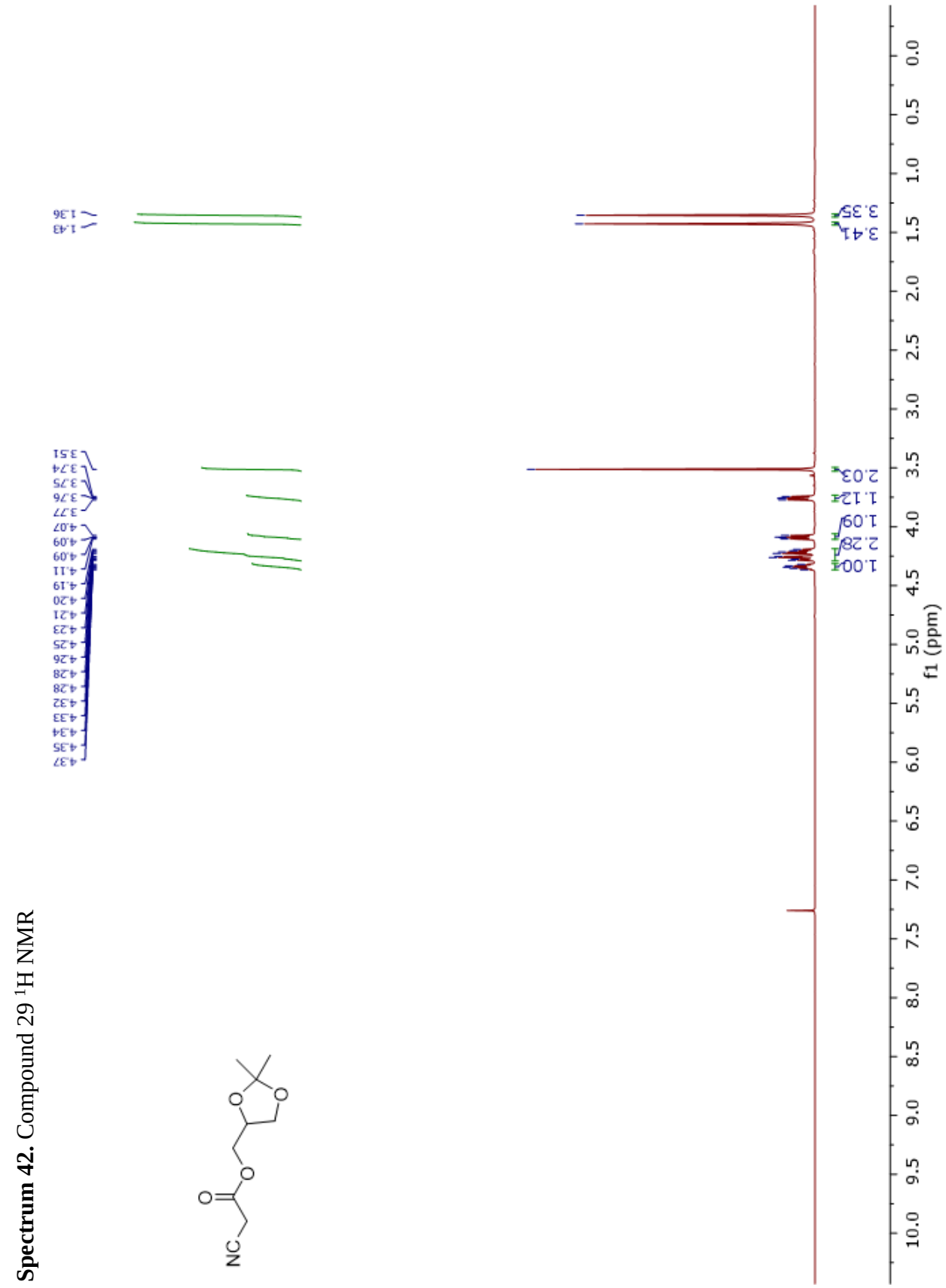

Spectrum 43. Compound 34 ^{1}H NMR

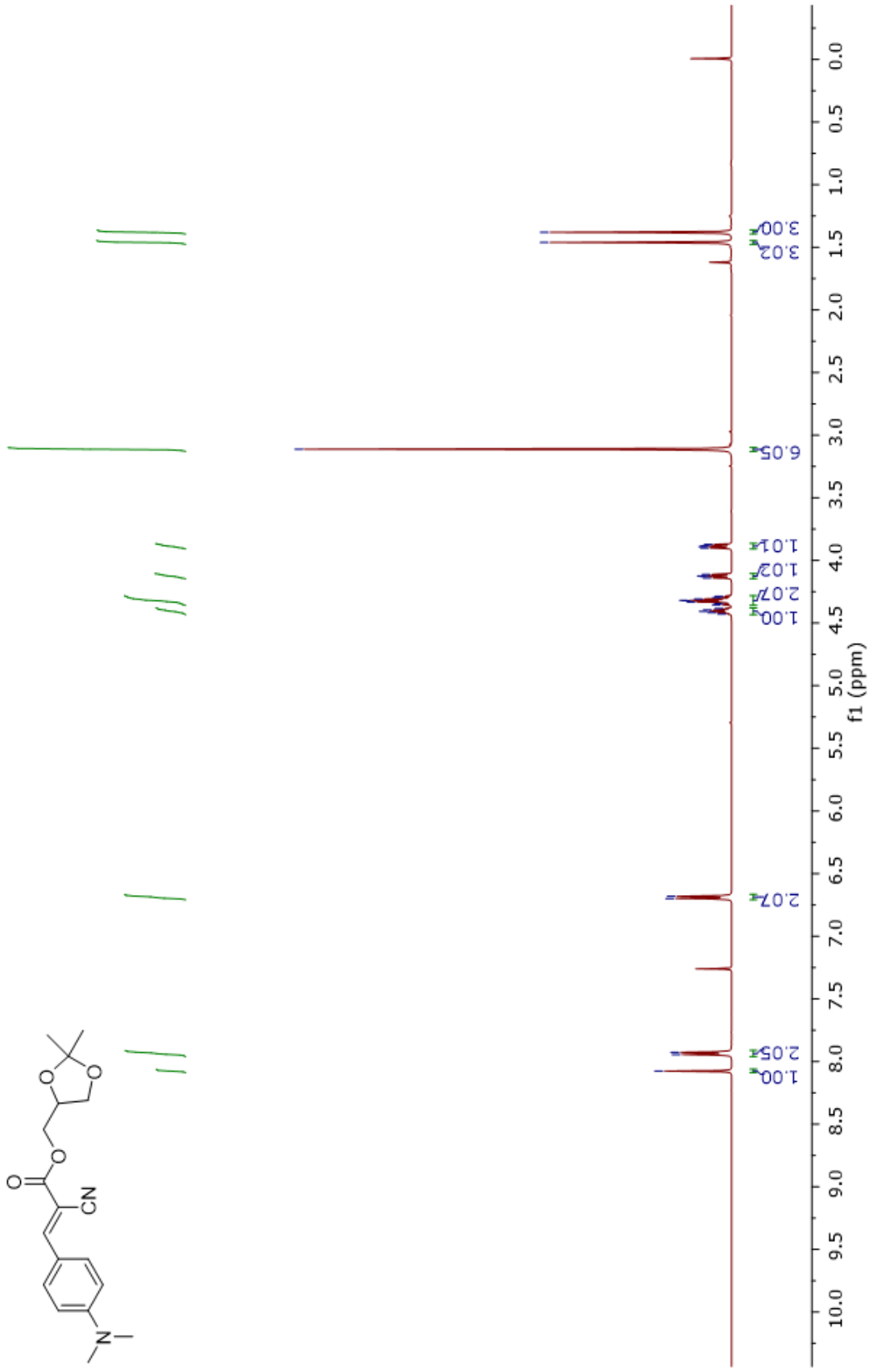

Spectrum 44. Compound 34 ^{13}C NMR

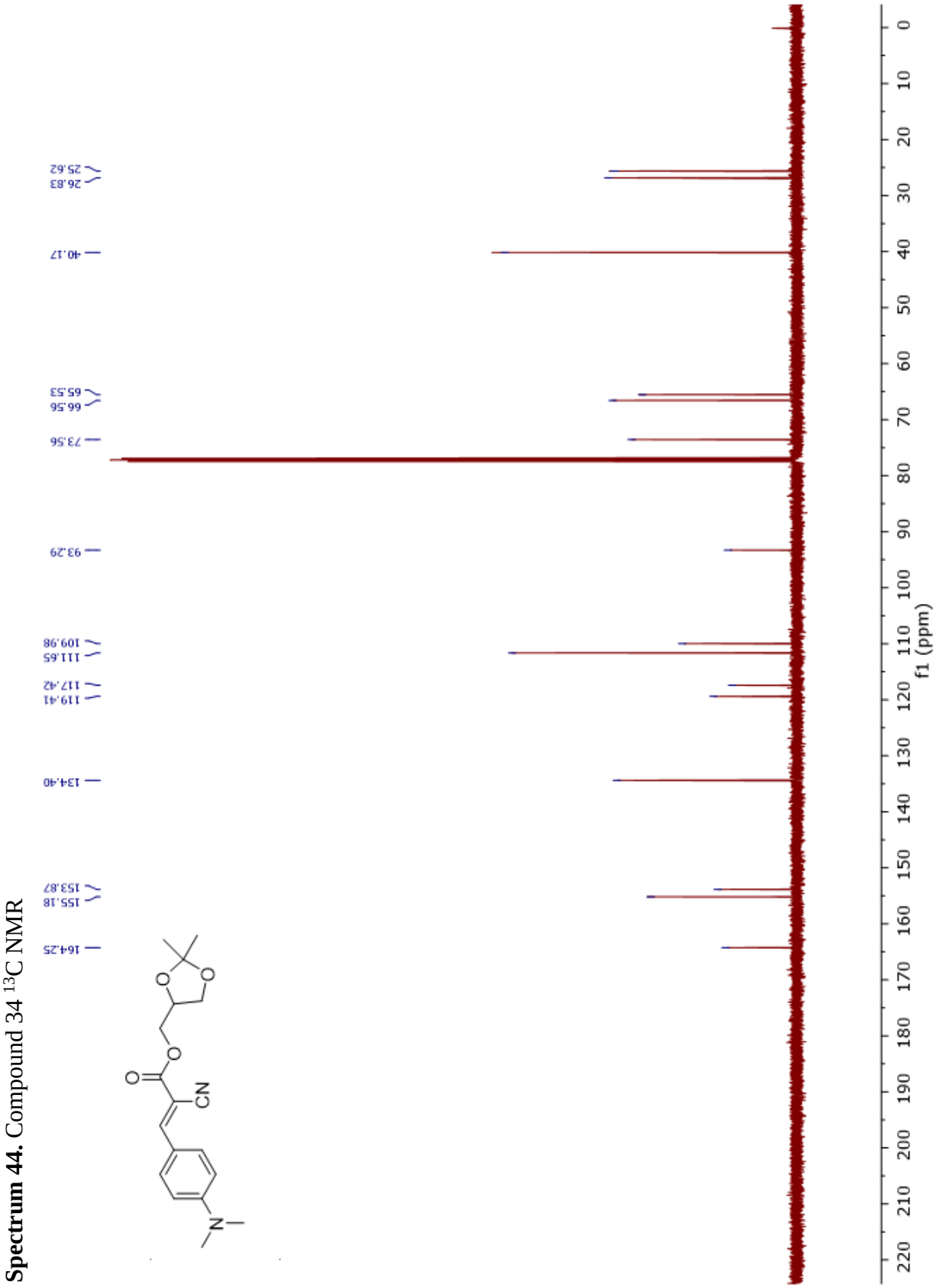

Spectrum 45. Compound 38 ^{1}H NMR

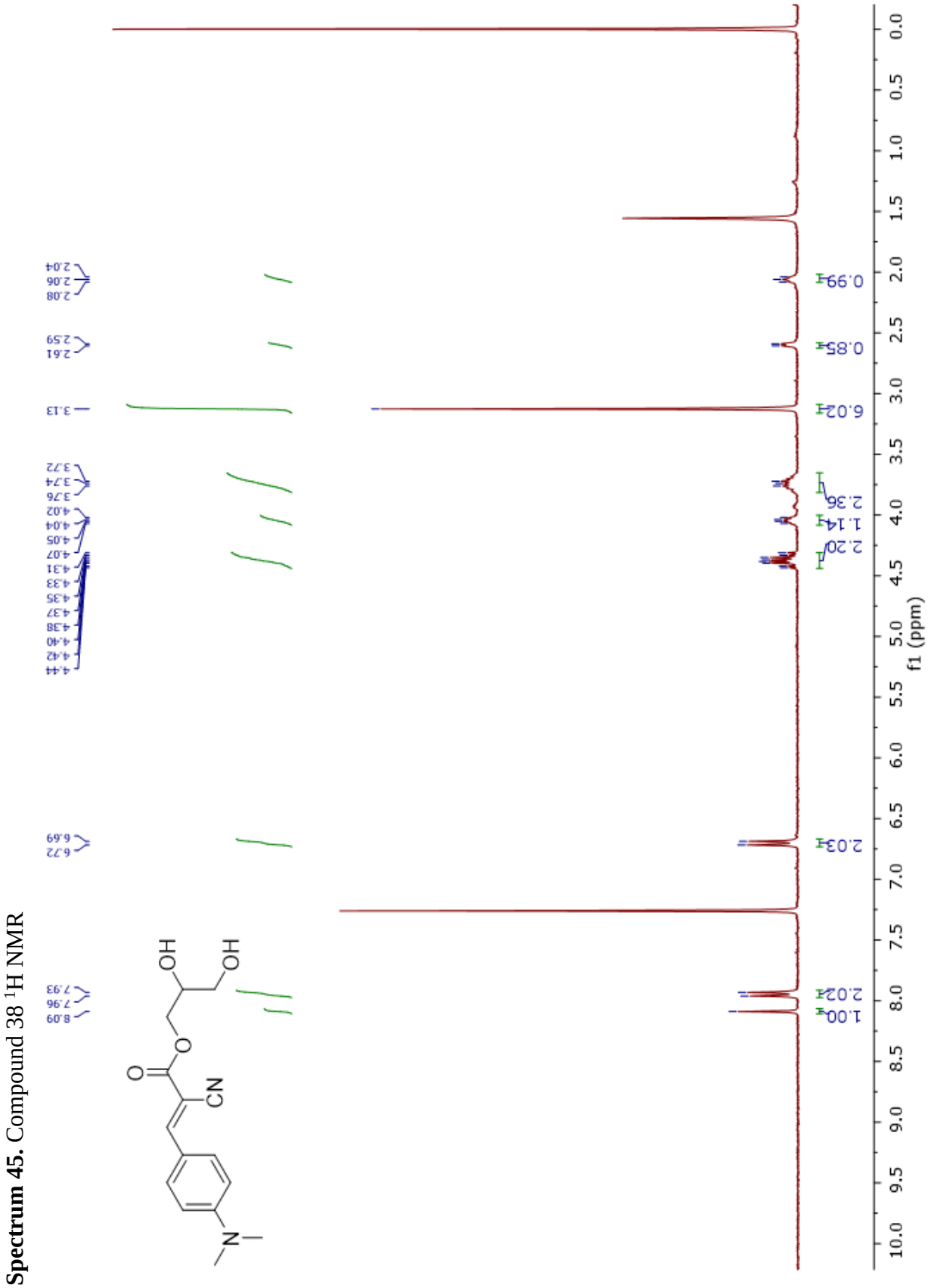

Spectrum 46. Compound 38 ^{13}C NMR

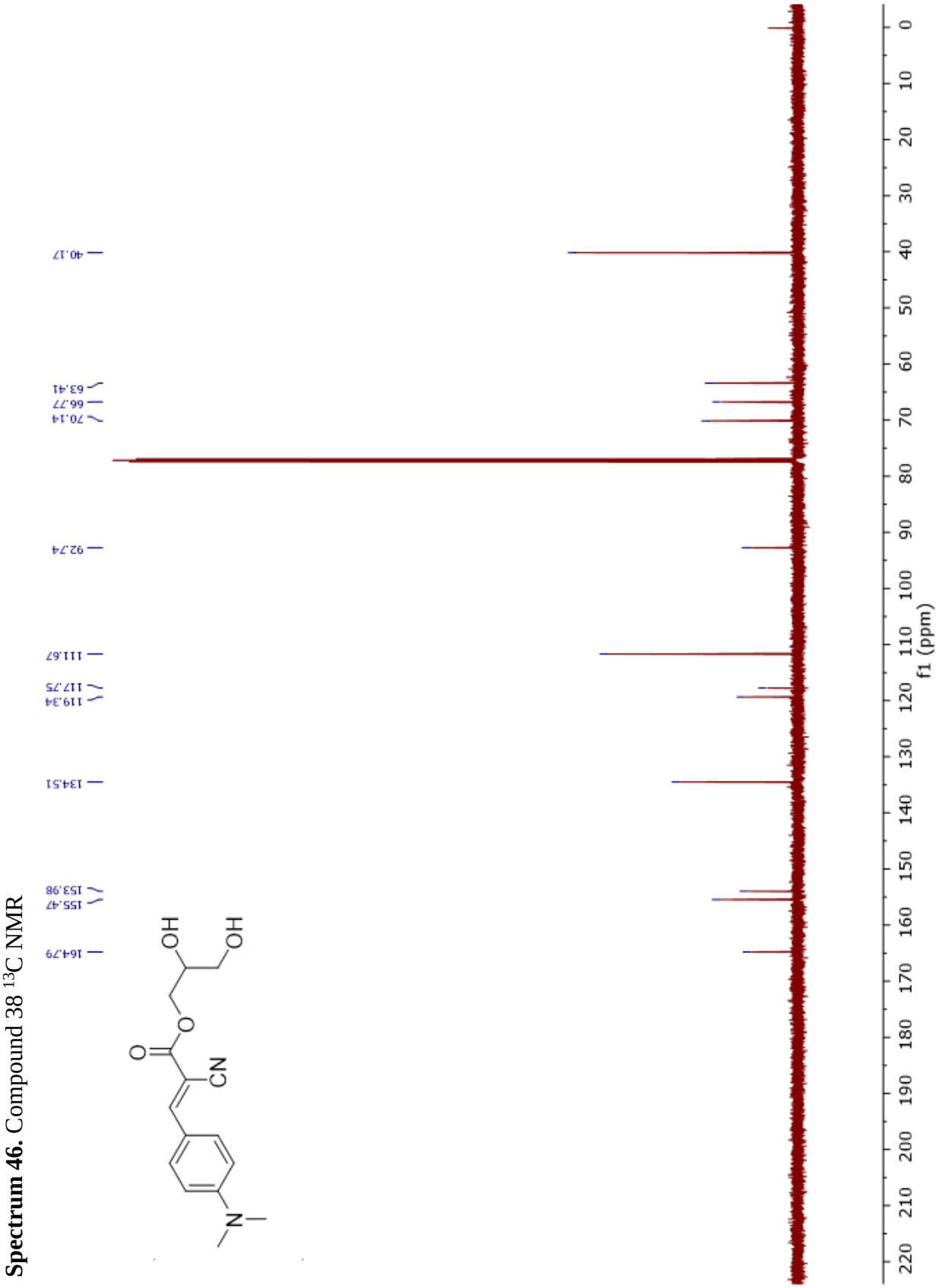

Spectrum 47. Compound 30 ^{1}H NMR

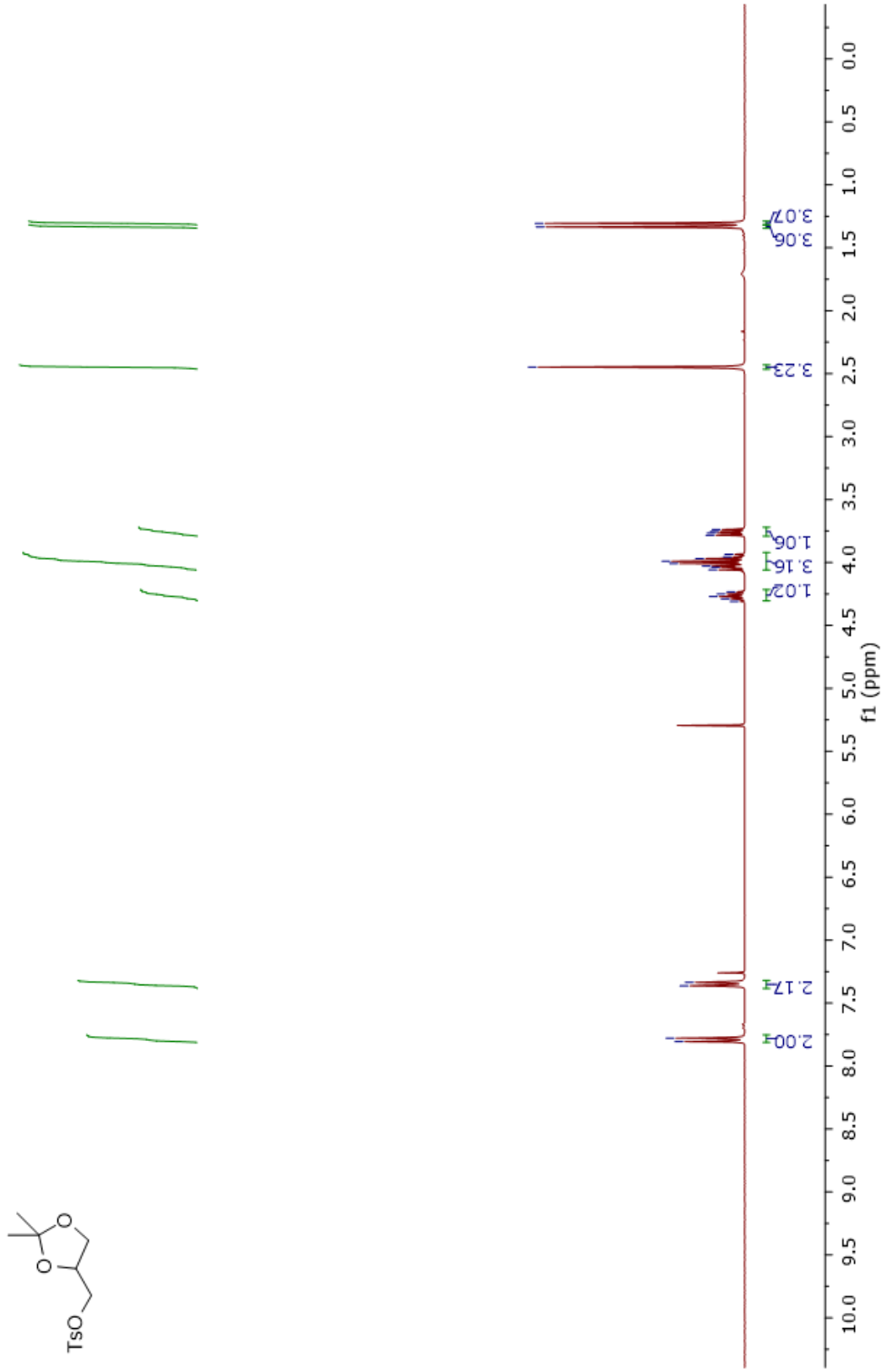

Spectrum 48. Compound 31 ^{1}H NMR

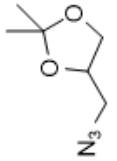

Spectrum 49. Compound 32 ^{1}H NMR

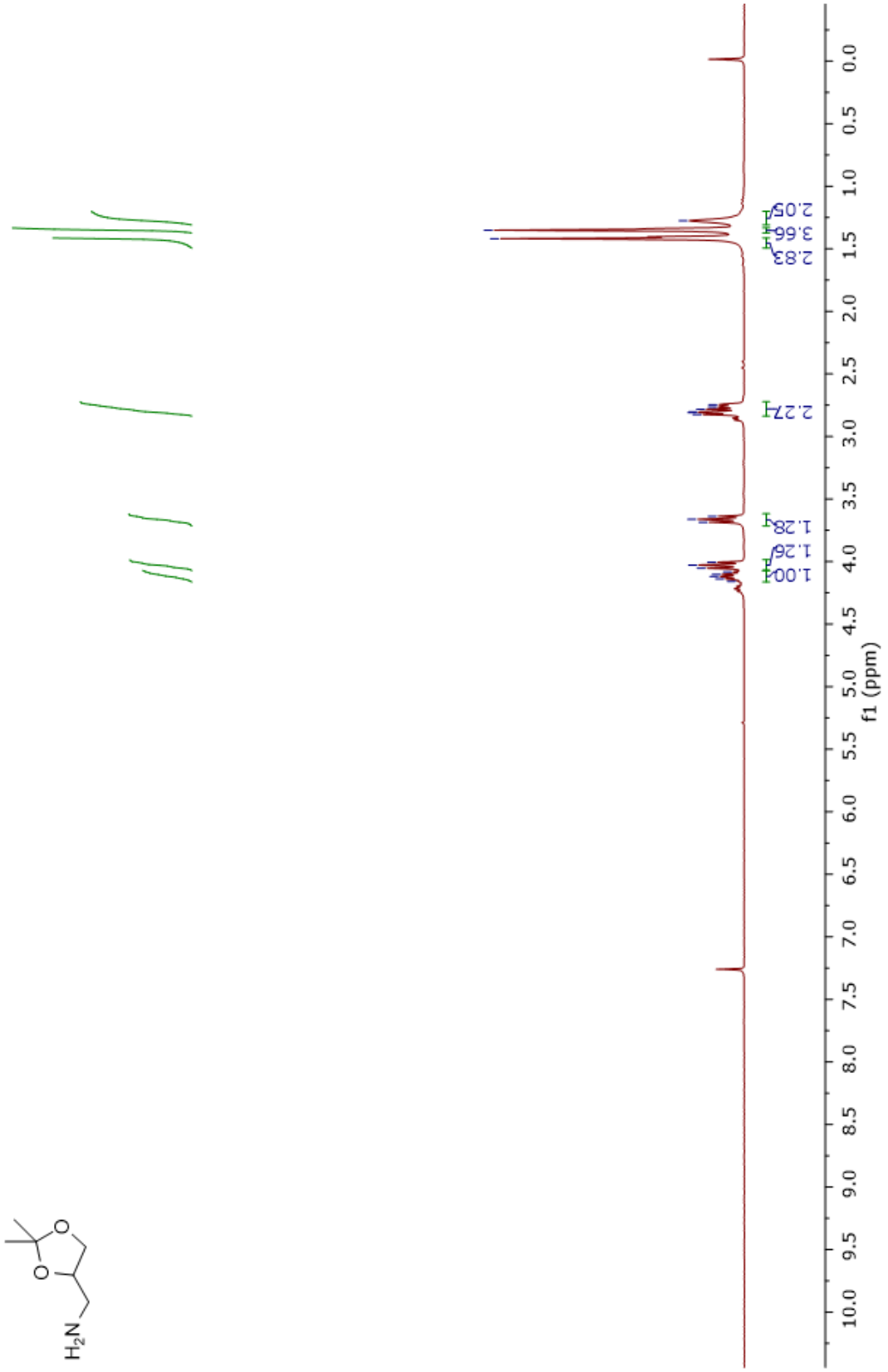

Spectrum 50. Compound 33 ^{1}H NMR

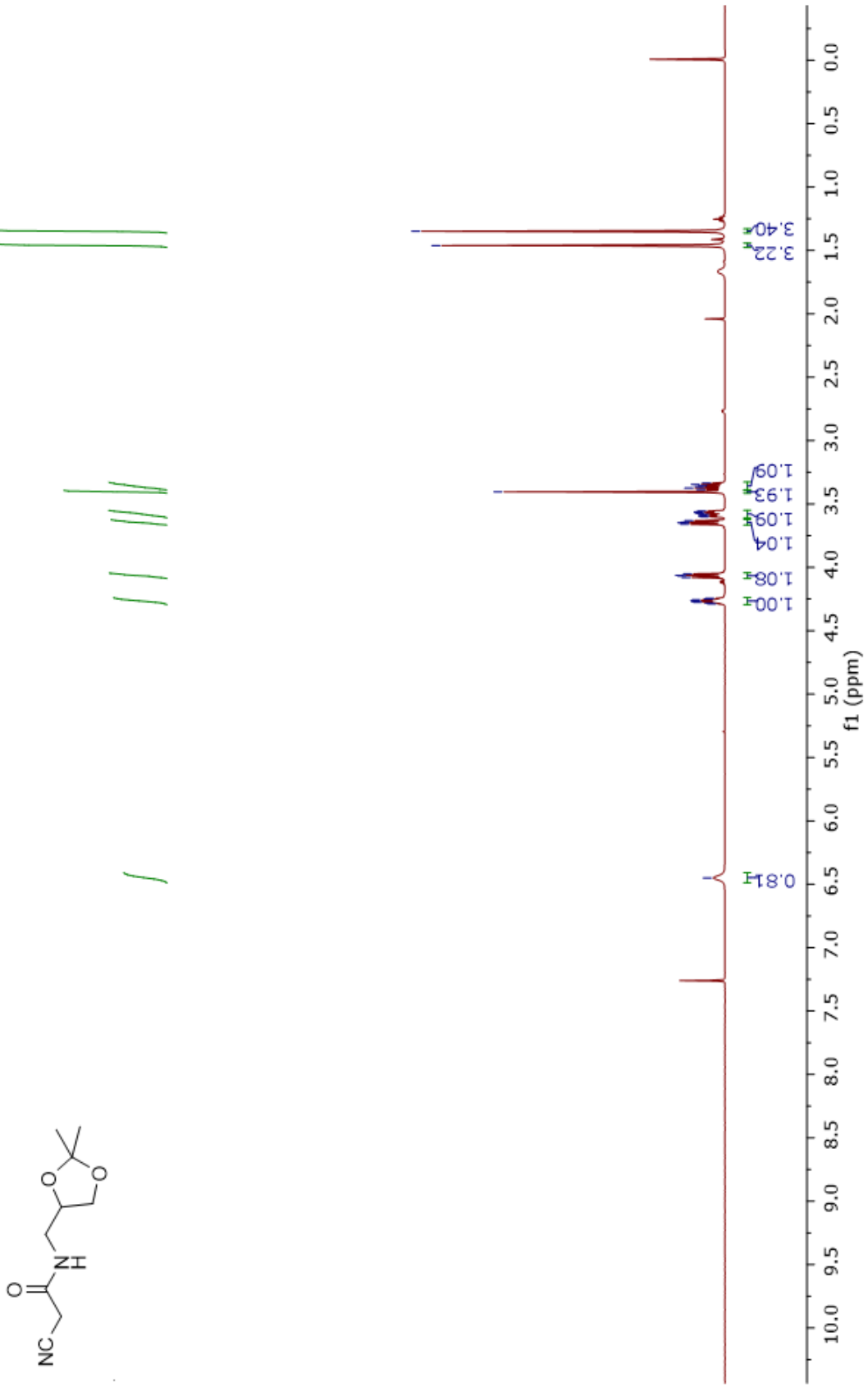

Spectrum 51. Compound 35 ^{1}H NMR

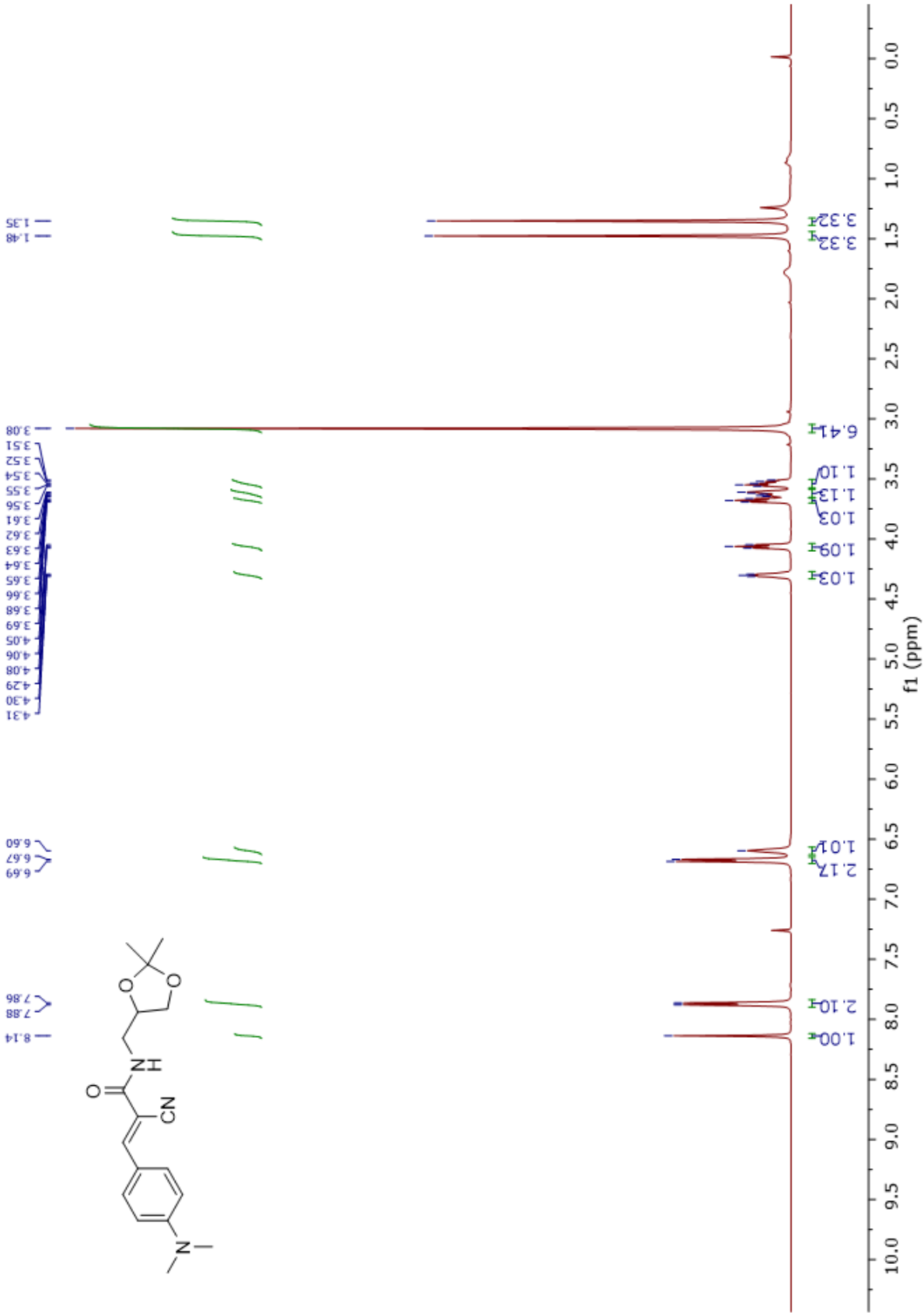

Spectrum 52. Compound 35 ^{13}C NMR

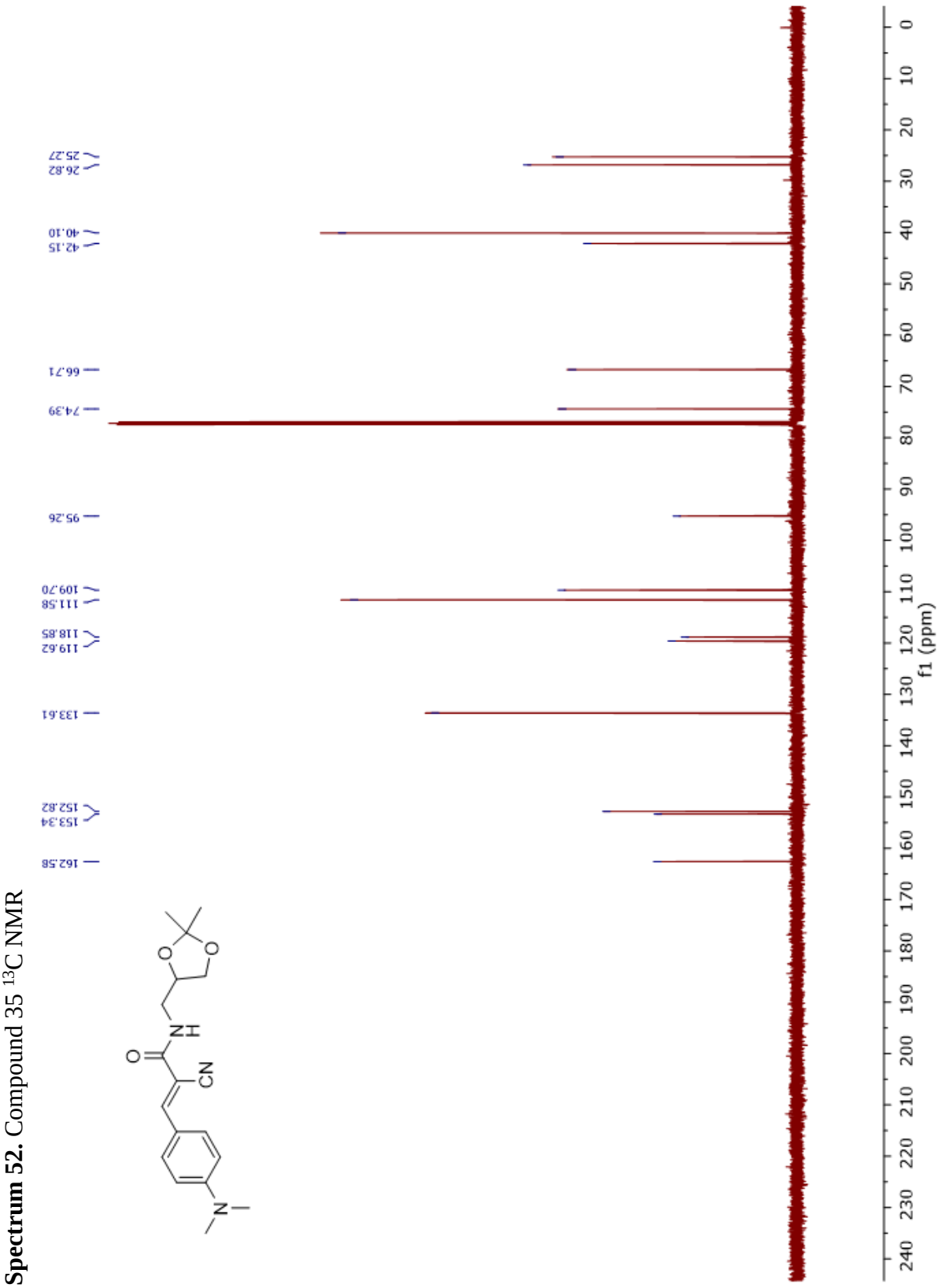

Spectrum 53. Compound 39 ^{1}H NMR

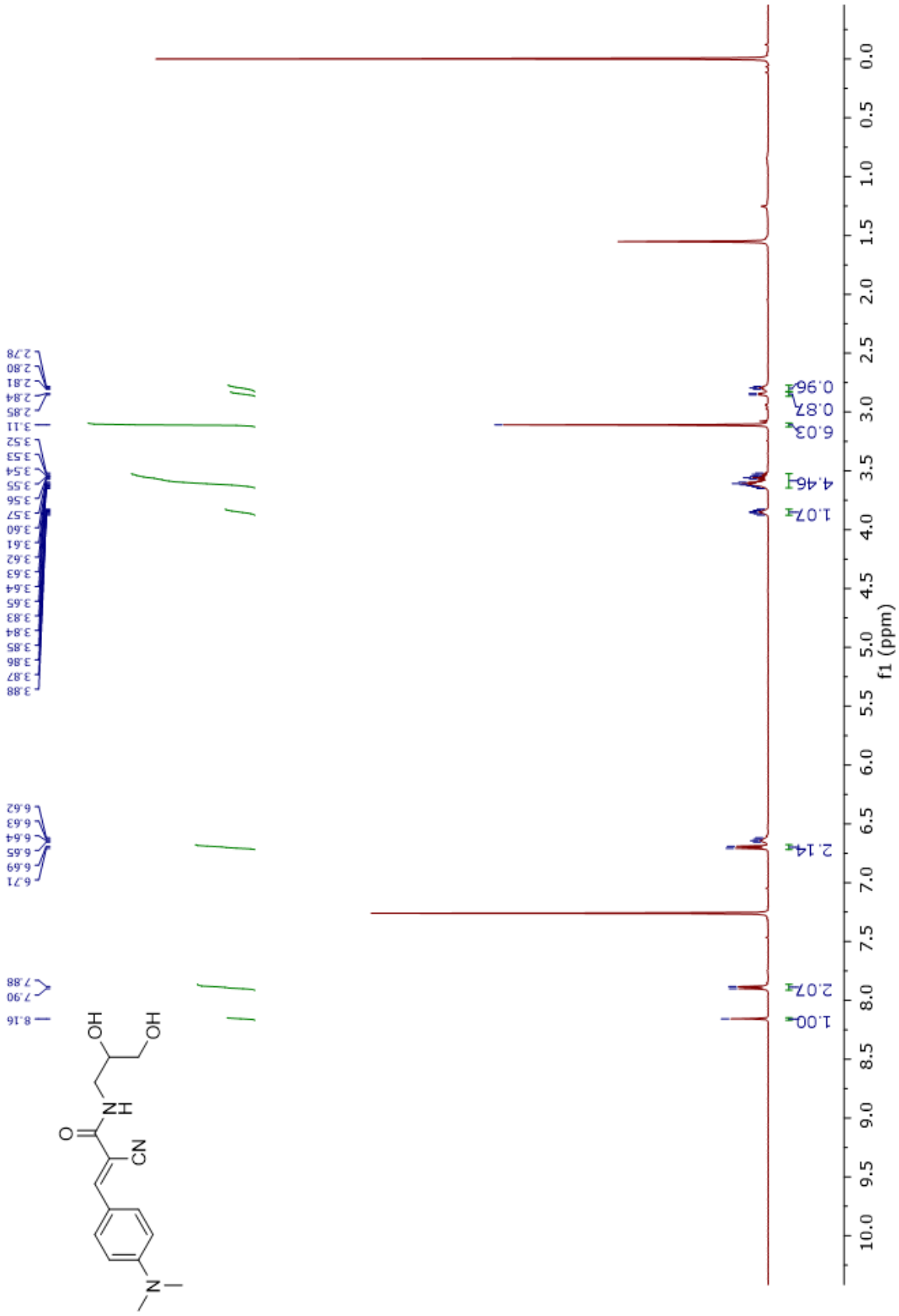

Spectrum 54. Compound 39 ^{13}C NMR

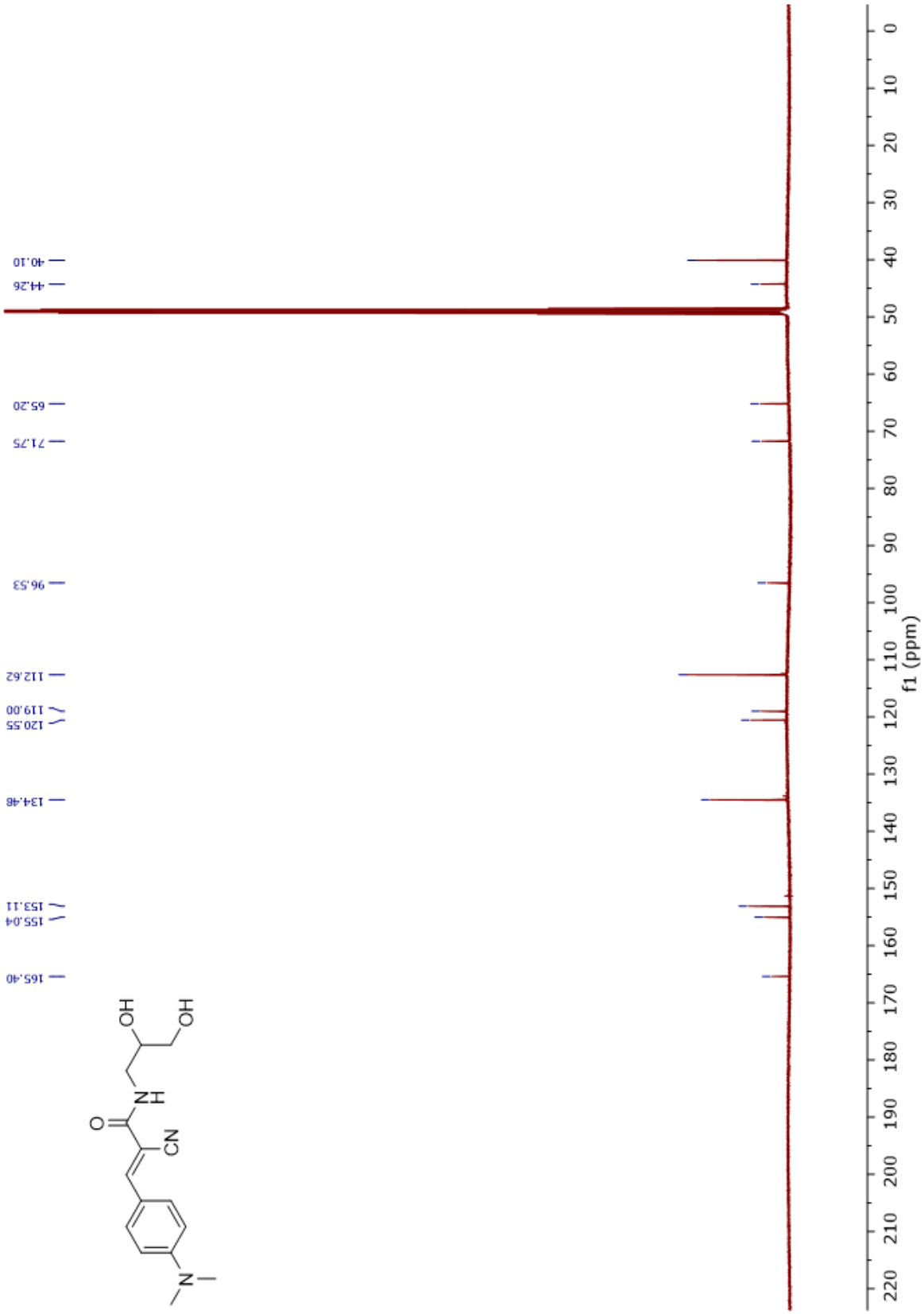

Spectrum 55. Compound 36 ^{13}C NMR

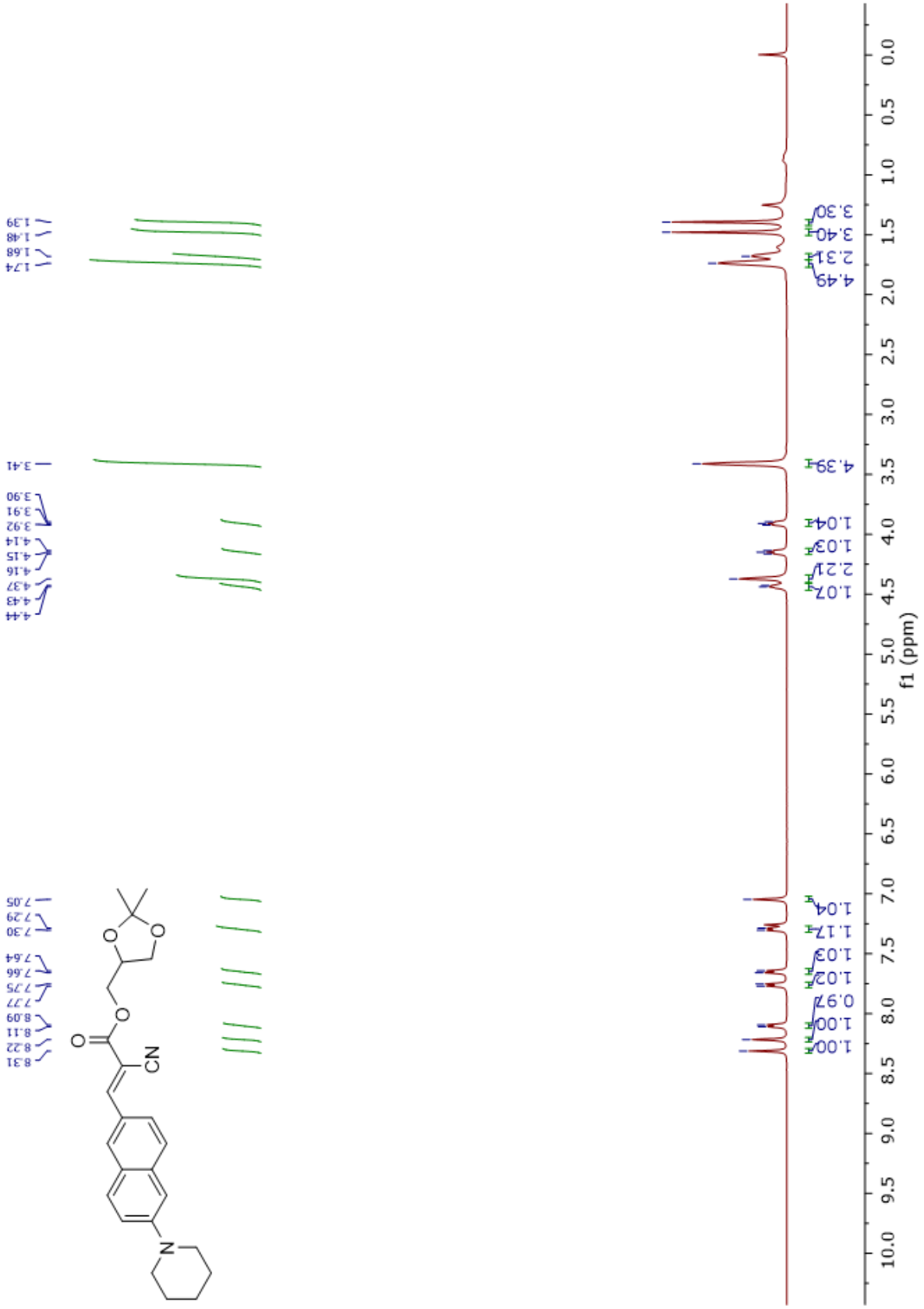

Spectrum 56. Compound 36 ^{13}C NMR

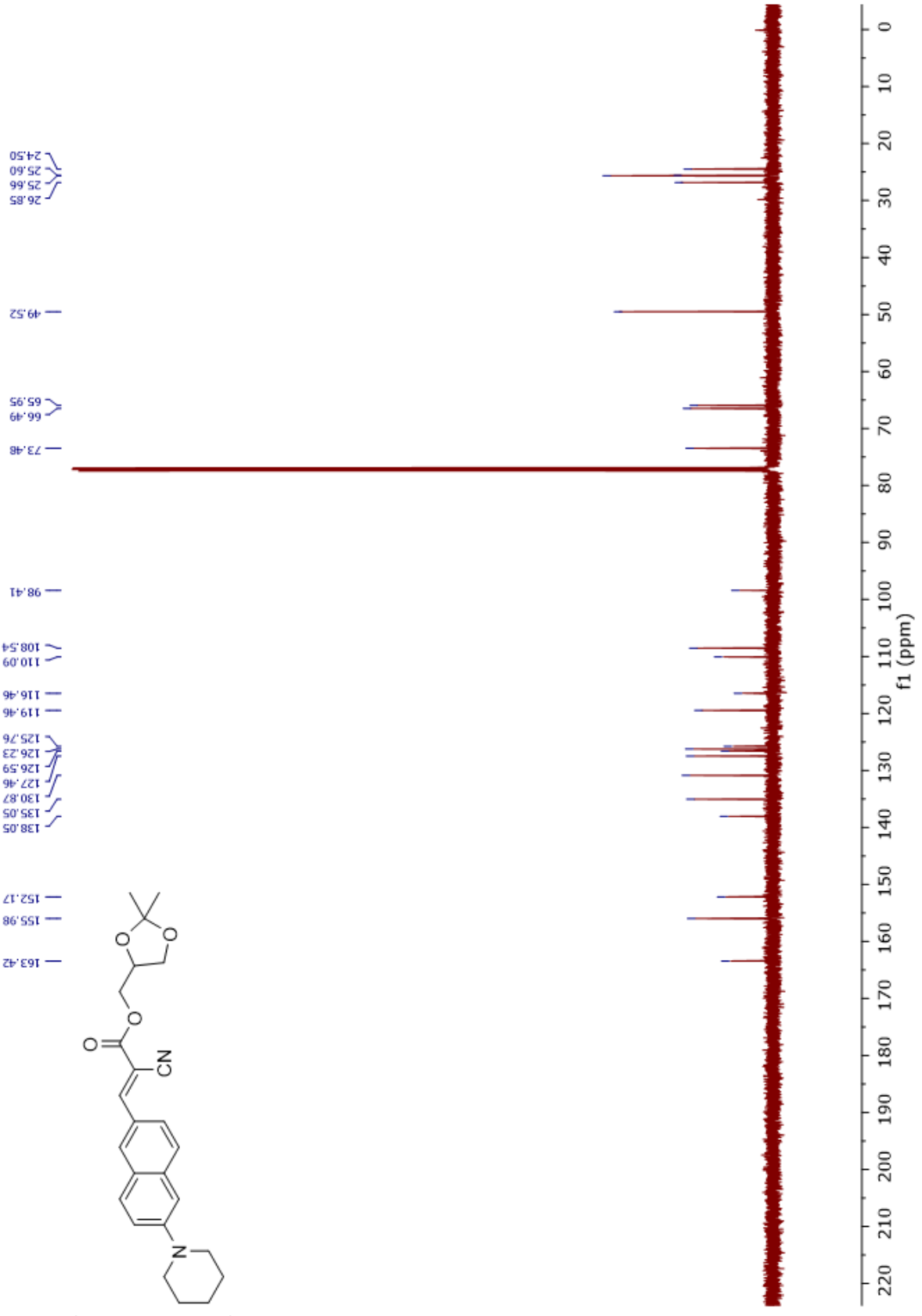

Spectrum 57. Compound 40 ^{1}H NMR

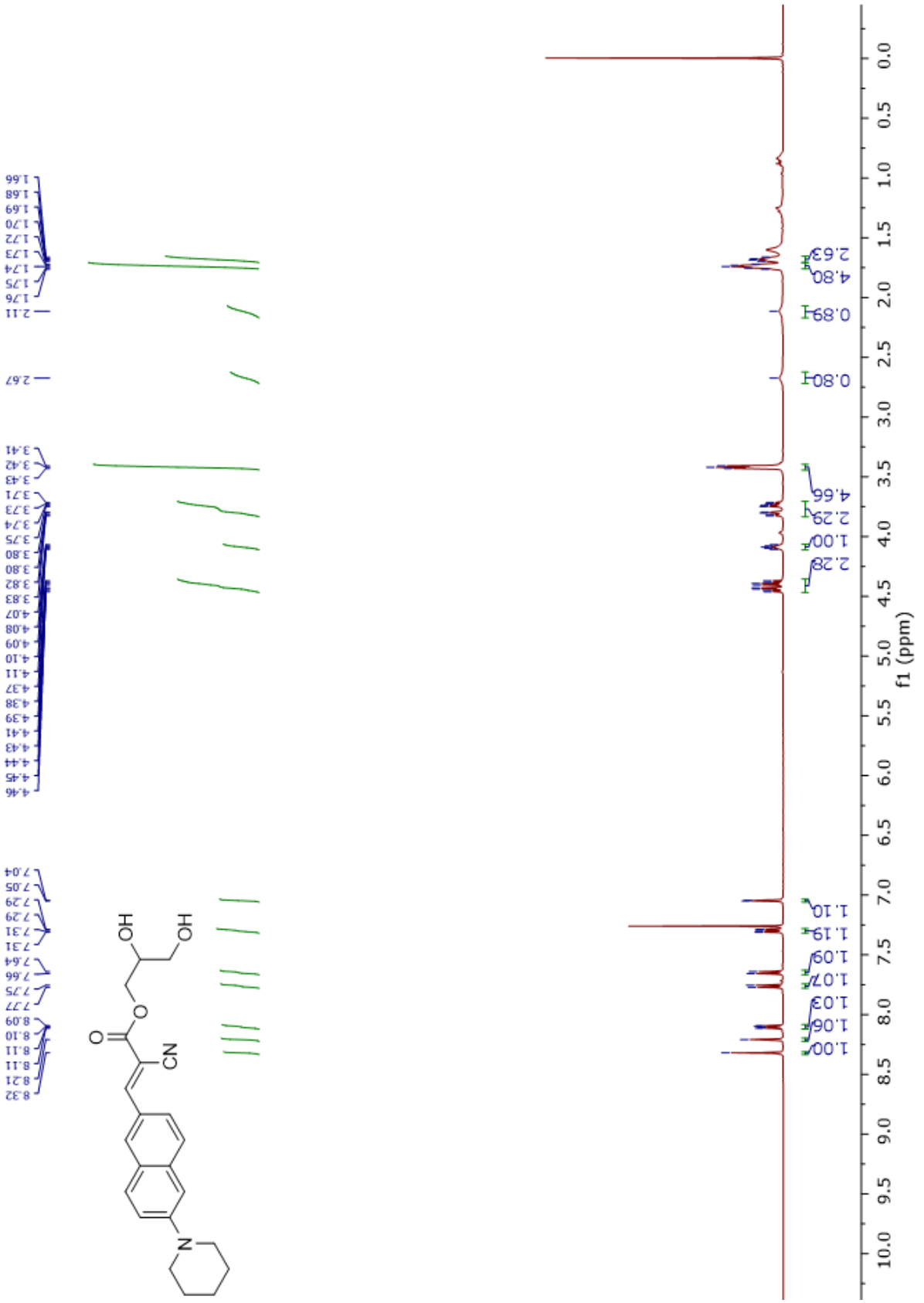

Spectrum 58. Compound 40 ^{13}C NMR

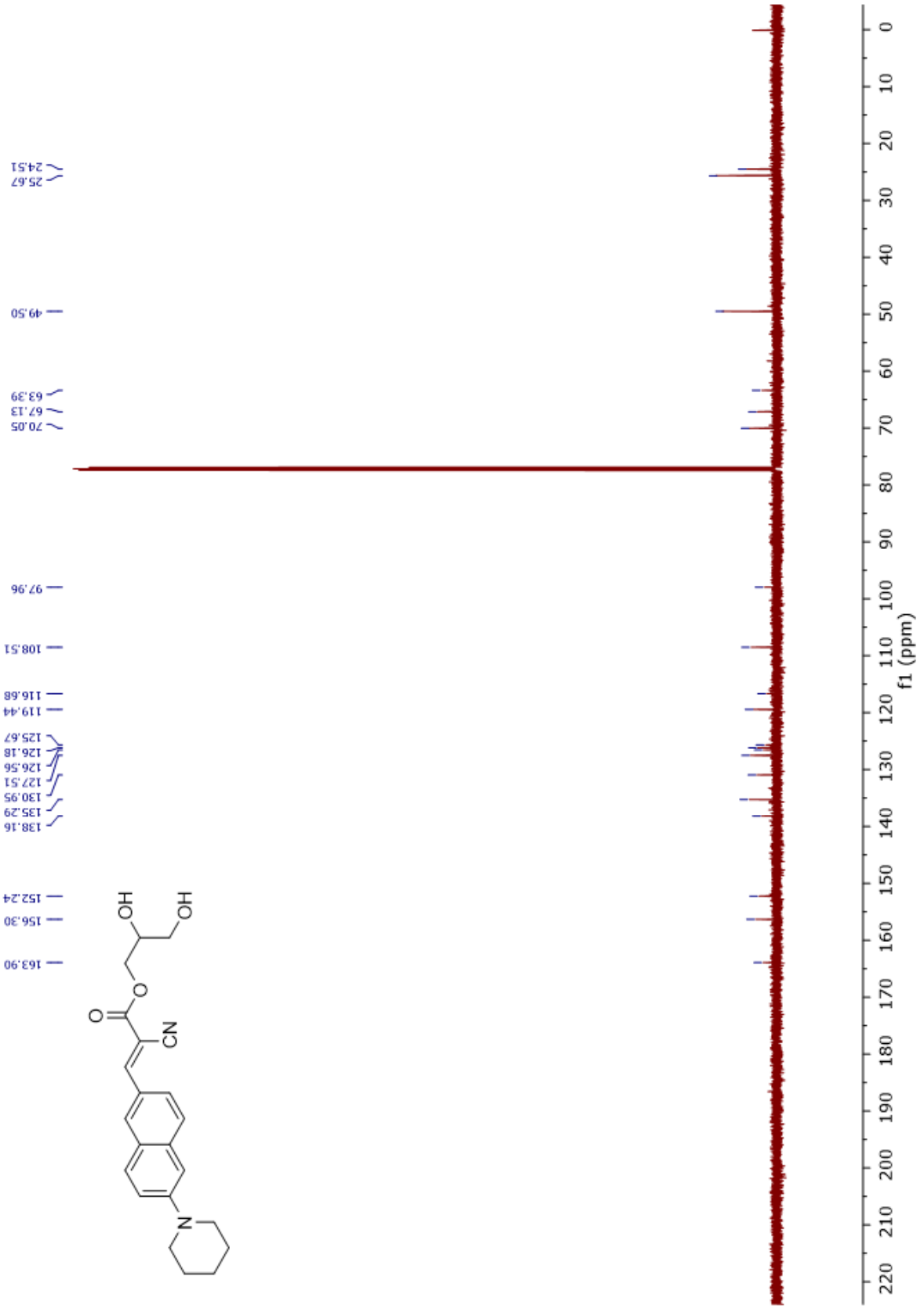

Spectrum 59. Compound 37 ^{1}H NMR

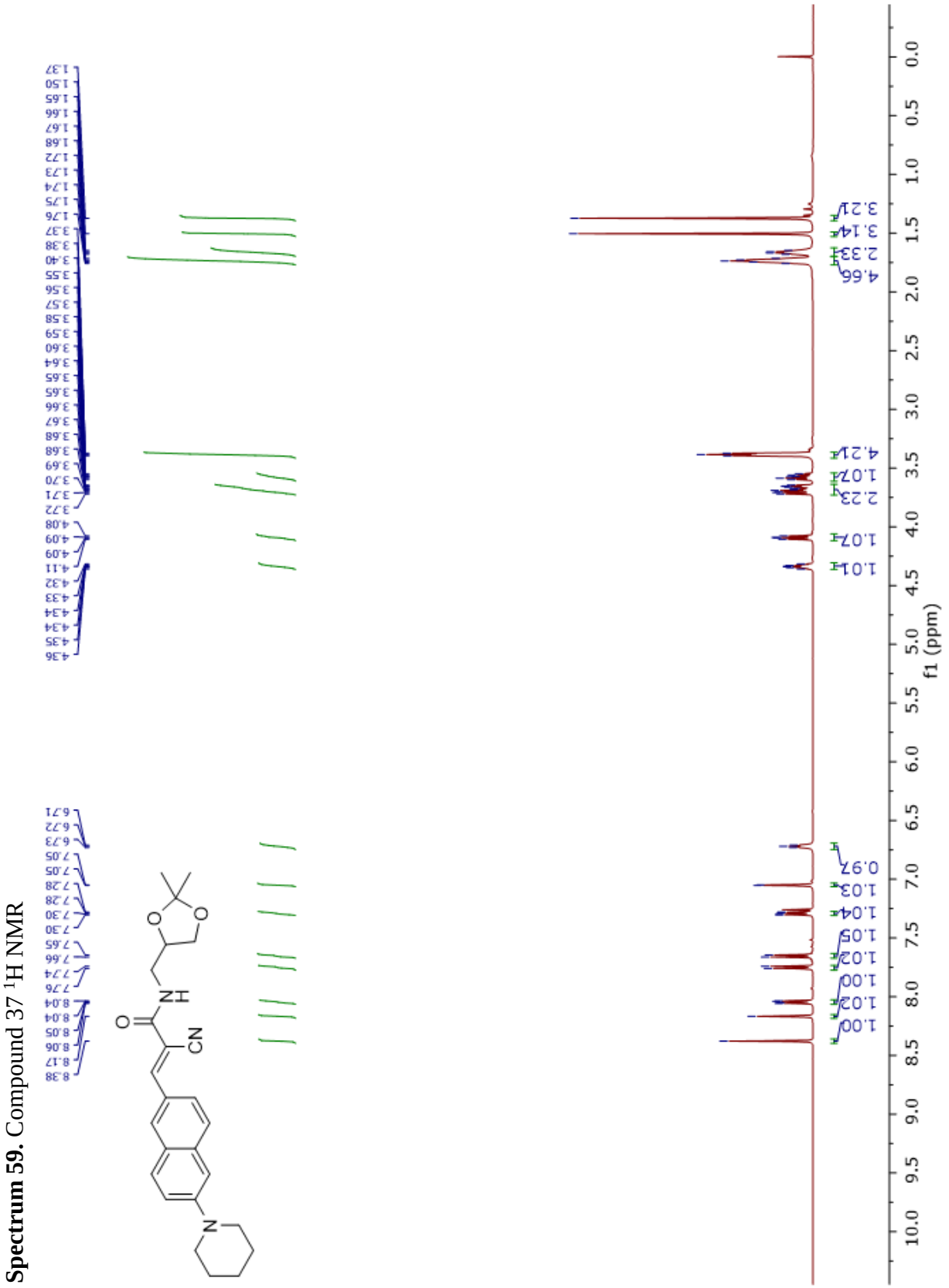

Spectrum 60. Compound 37 ^{13}C NMR

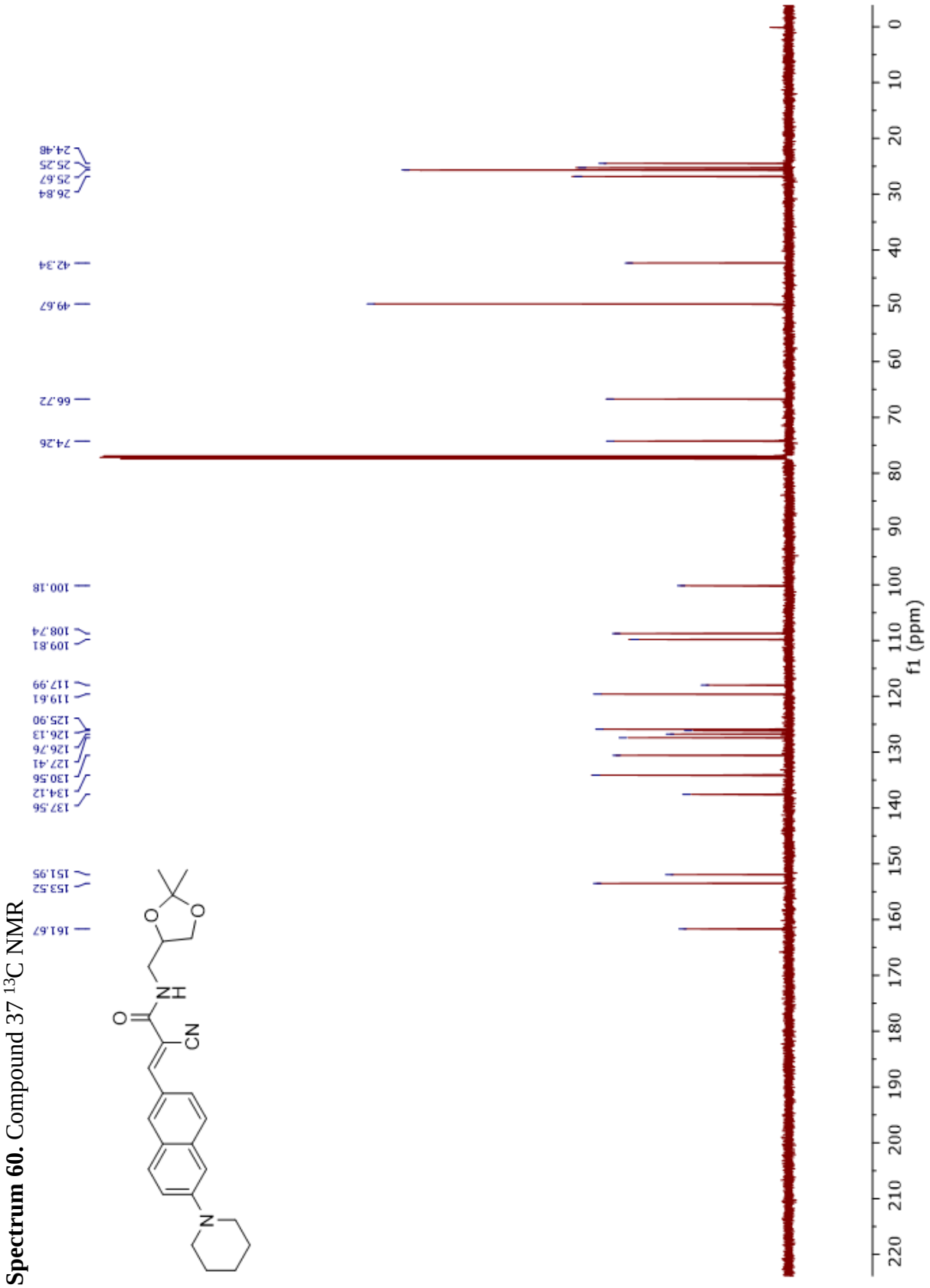

Spectrum 61. Compound 41 ^{1}H NMR

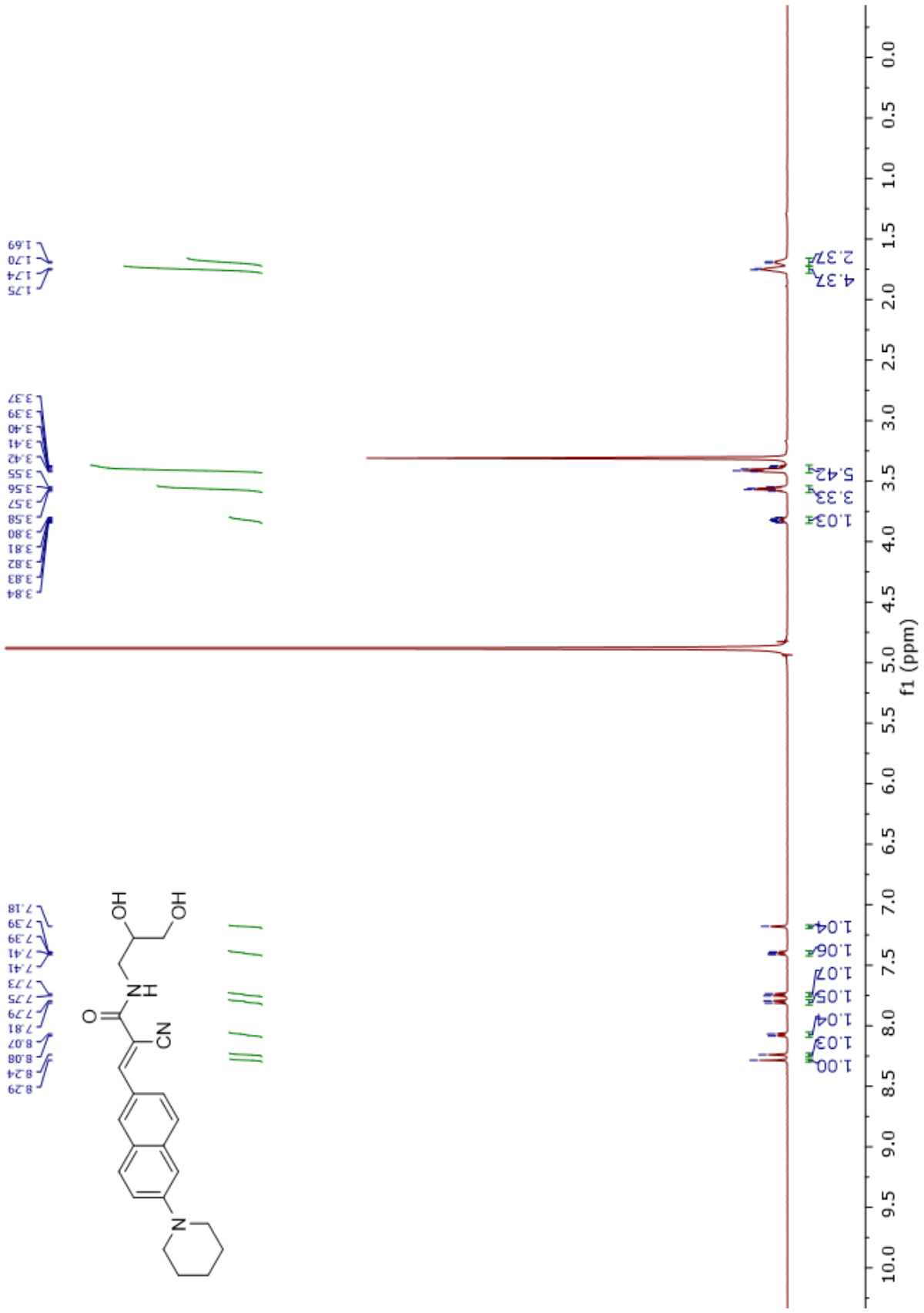

Spectrum 62. Compound 41 ^{13}C NMR

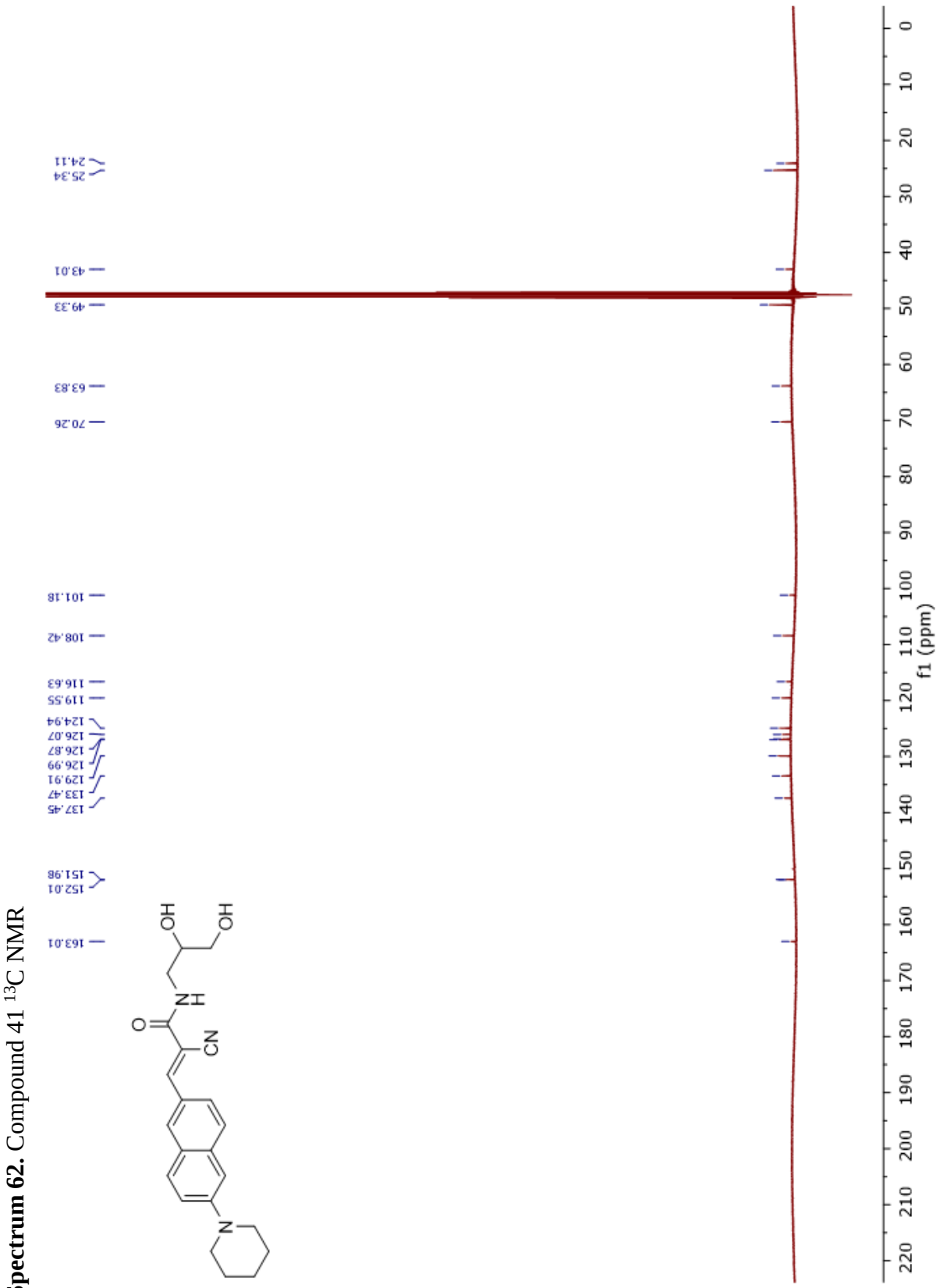

Spectrum 63. Compound 51 ^{1}H NMR

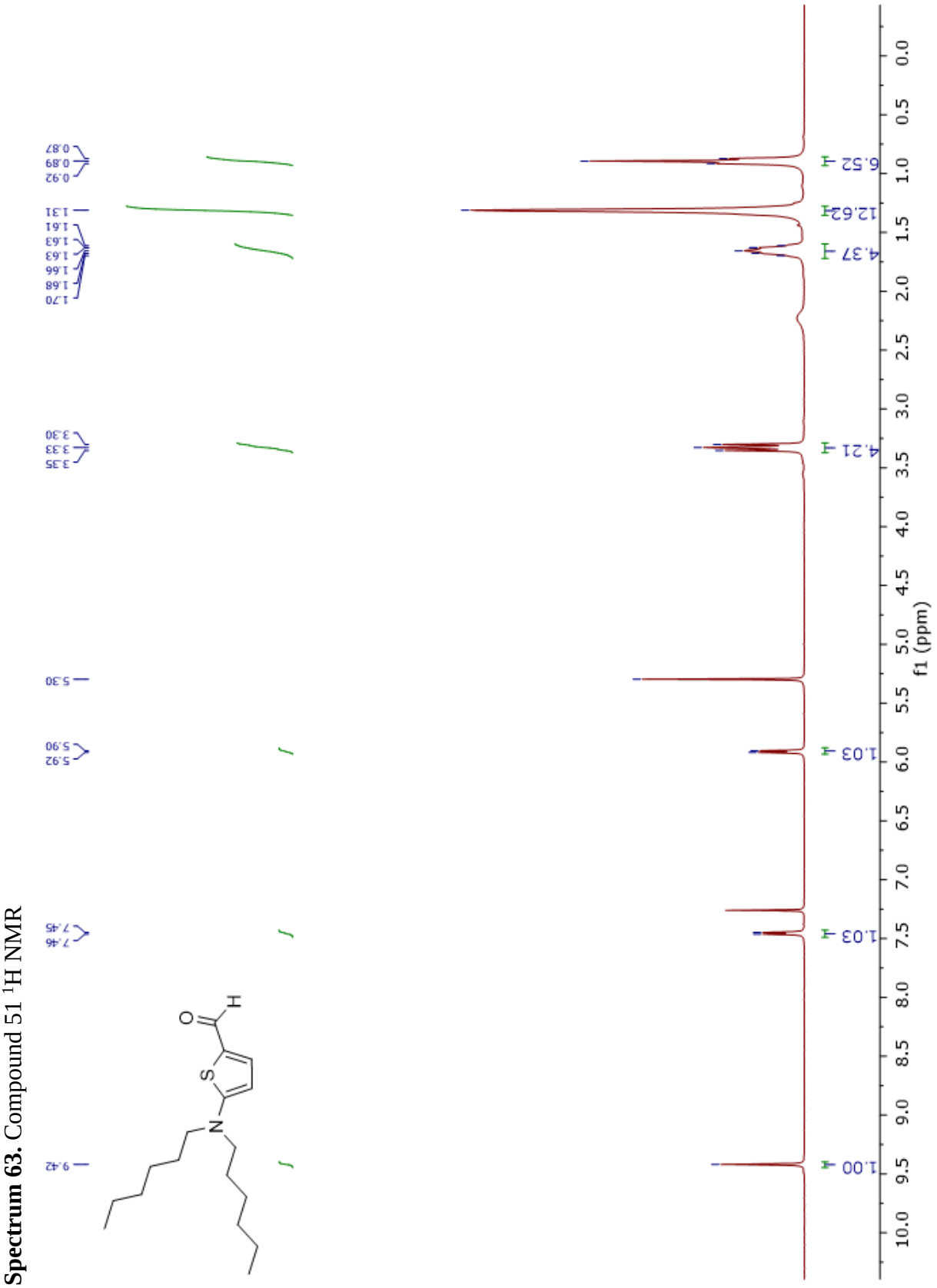

Spectrum 64. Compound 43 ^{1}H NMR

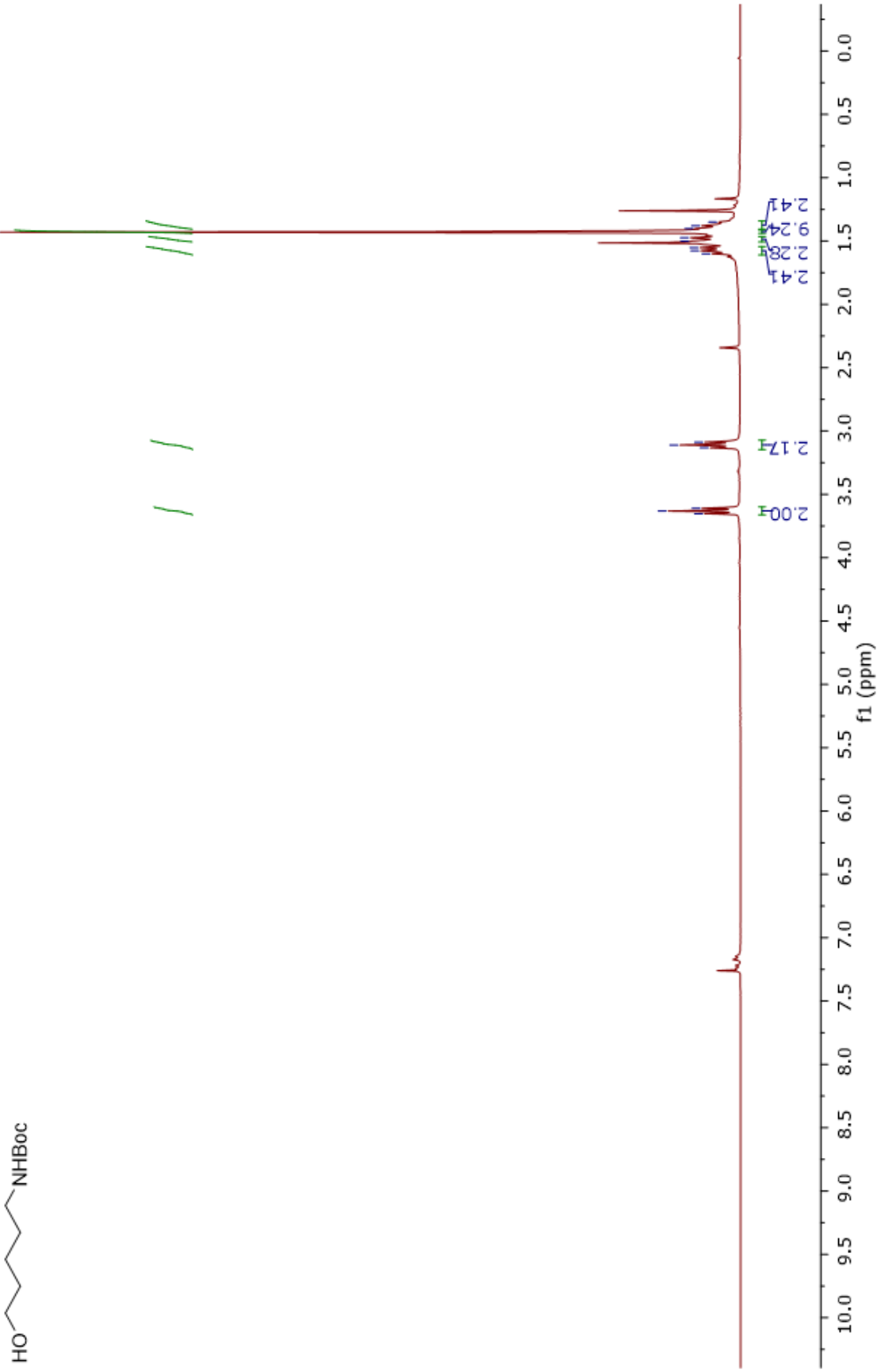

Spectrum 65. Compound 44 ^{1}H NMR

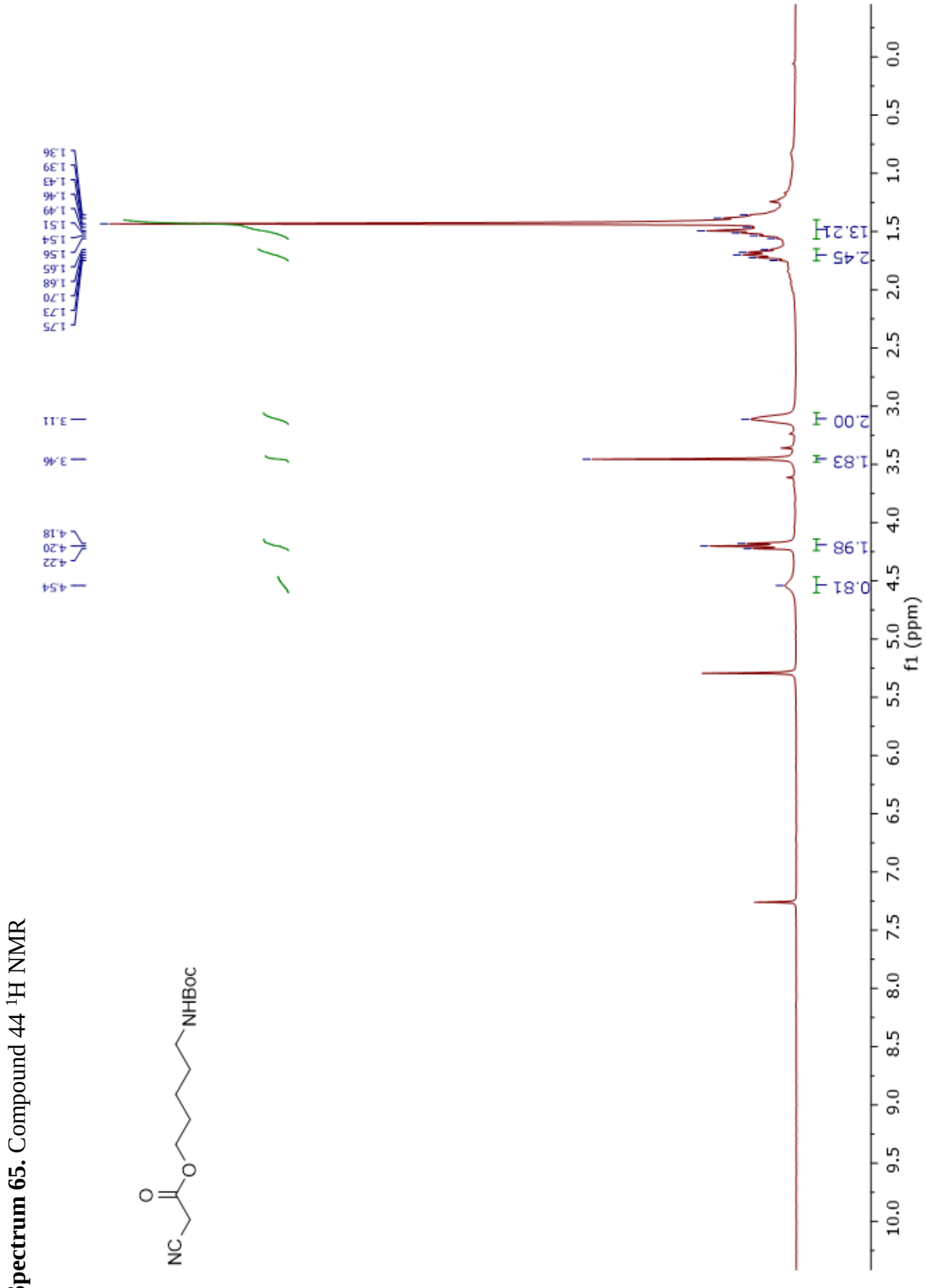

Spectrum 66. Compound 52 ^{1}H NMR

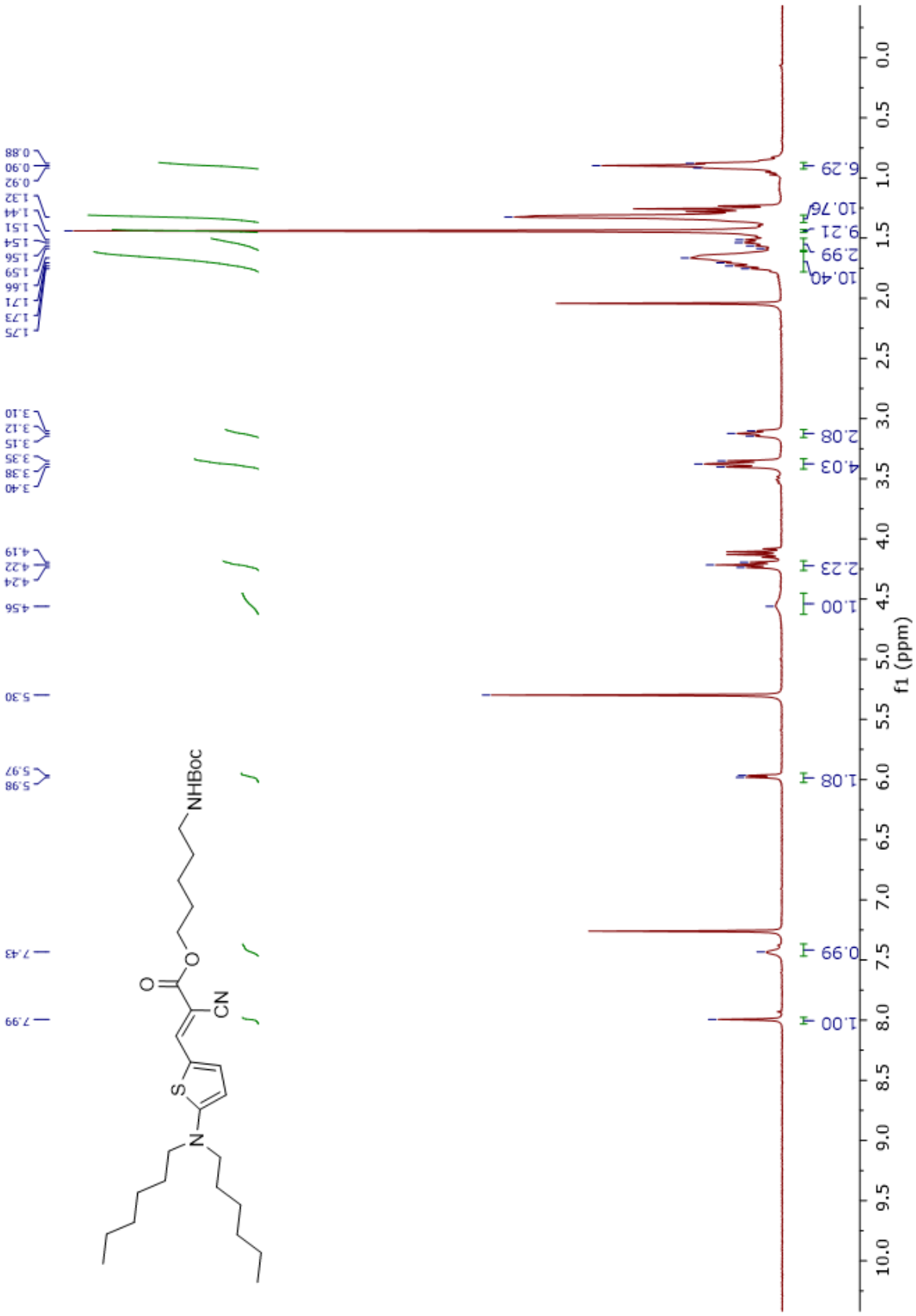

Spectrum 67. Compound 54 ^{1}H NMR

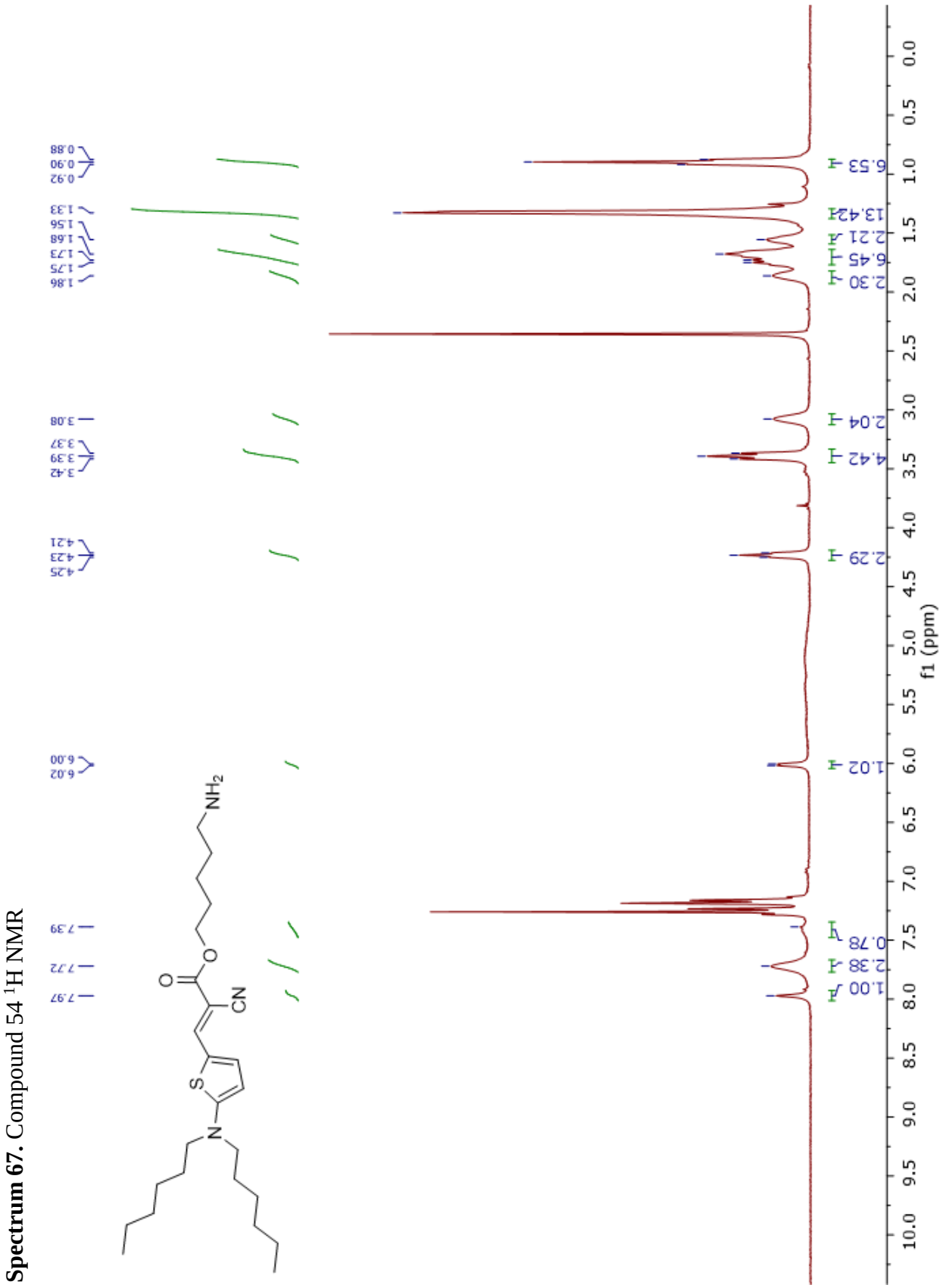

Spectrum 68. Compound 49 ^{1}H NMR

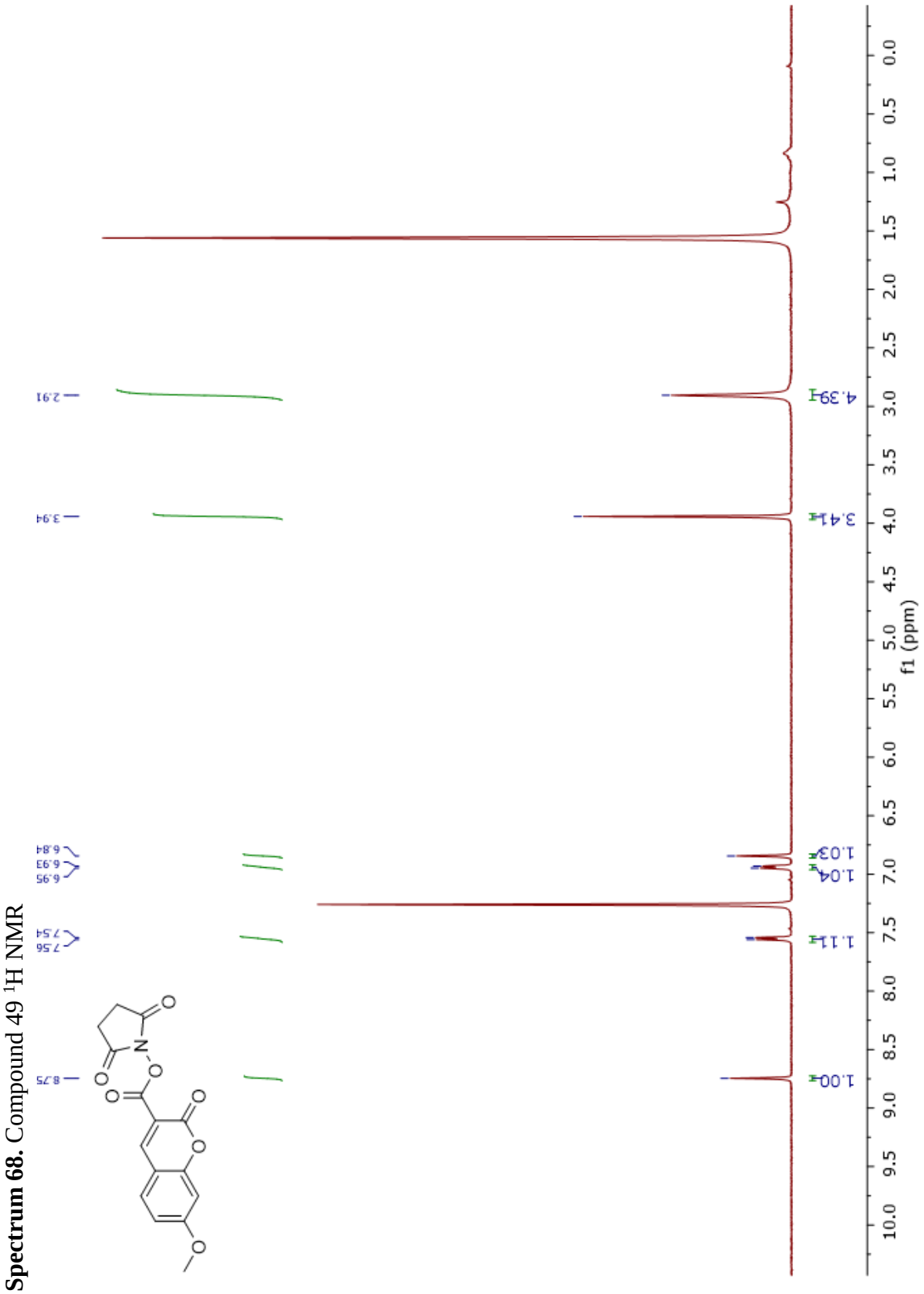

Spectrum 69. Compound 56 ^{1}H NMR

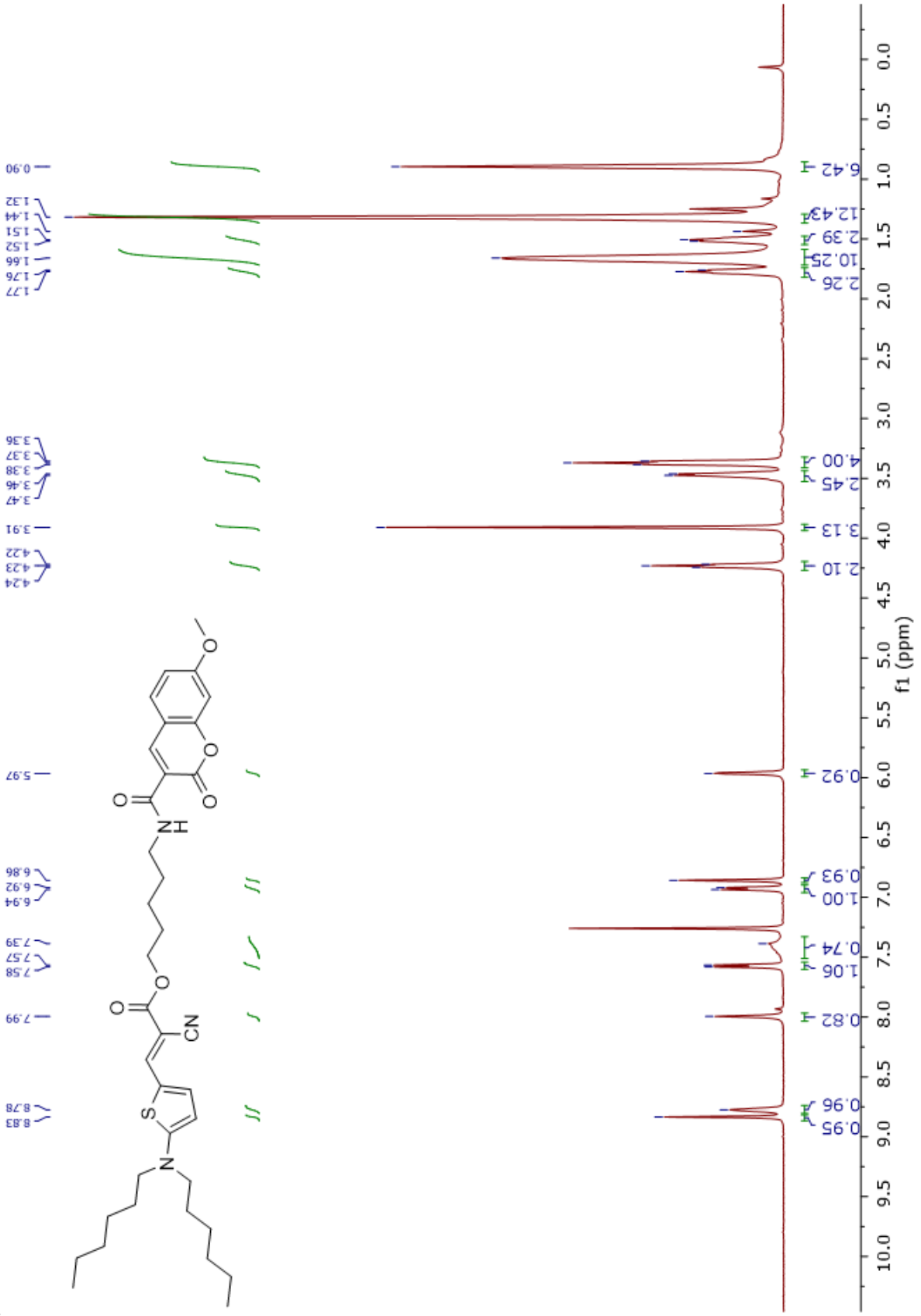

Spectrum 70. Compound 46 ^{1}H NMR

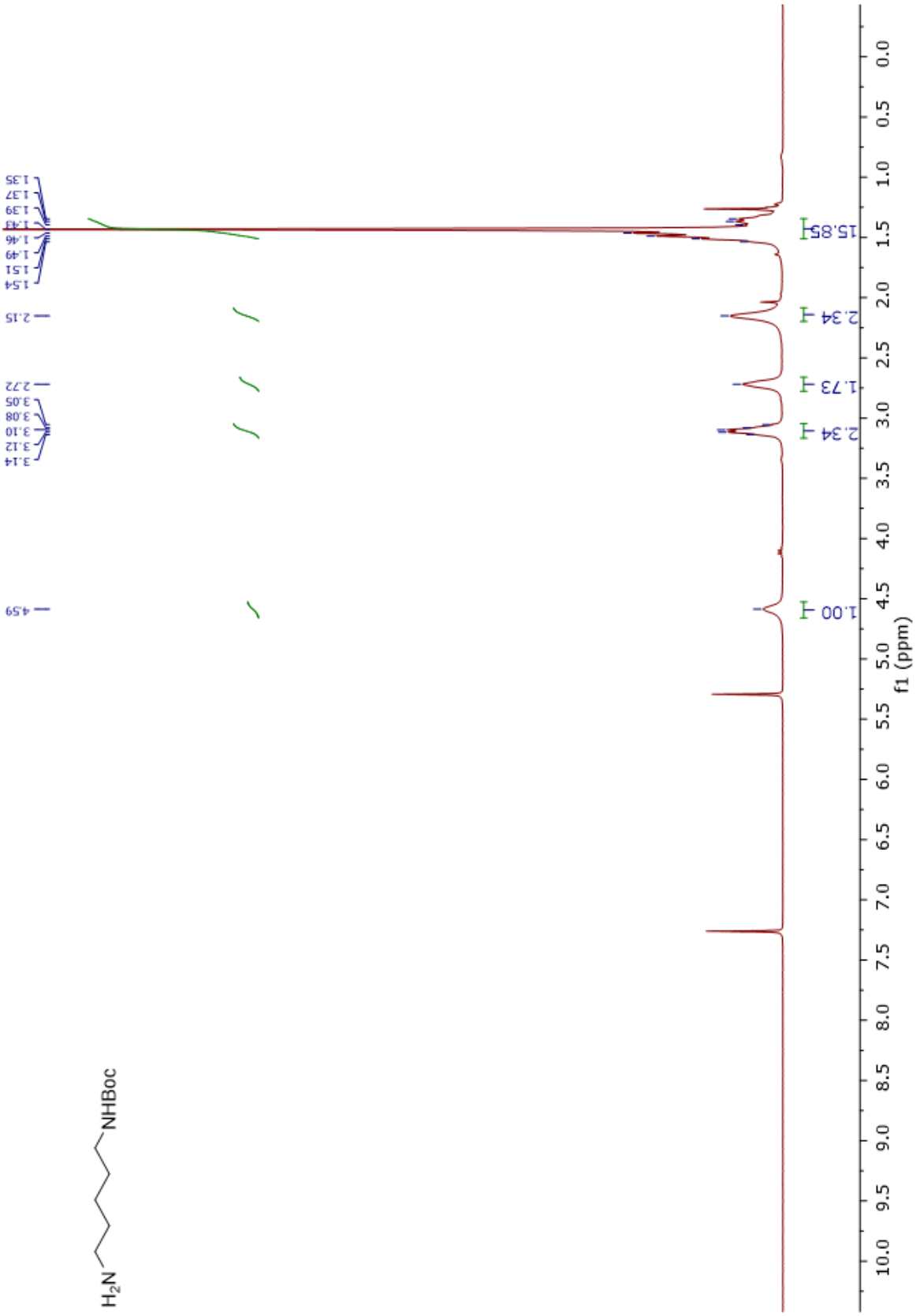

Spectrum 71. Compound 47 ^{1}H NMR

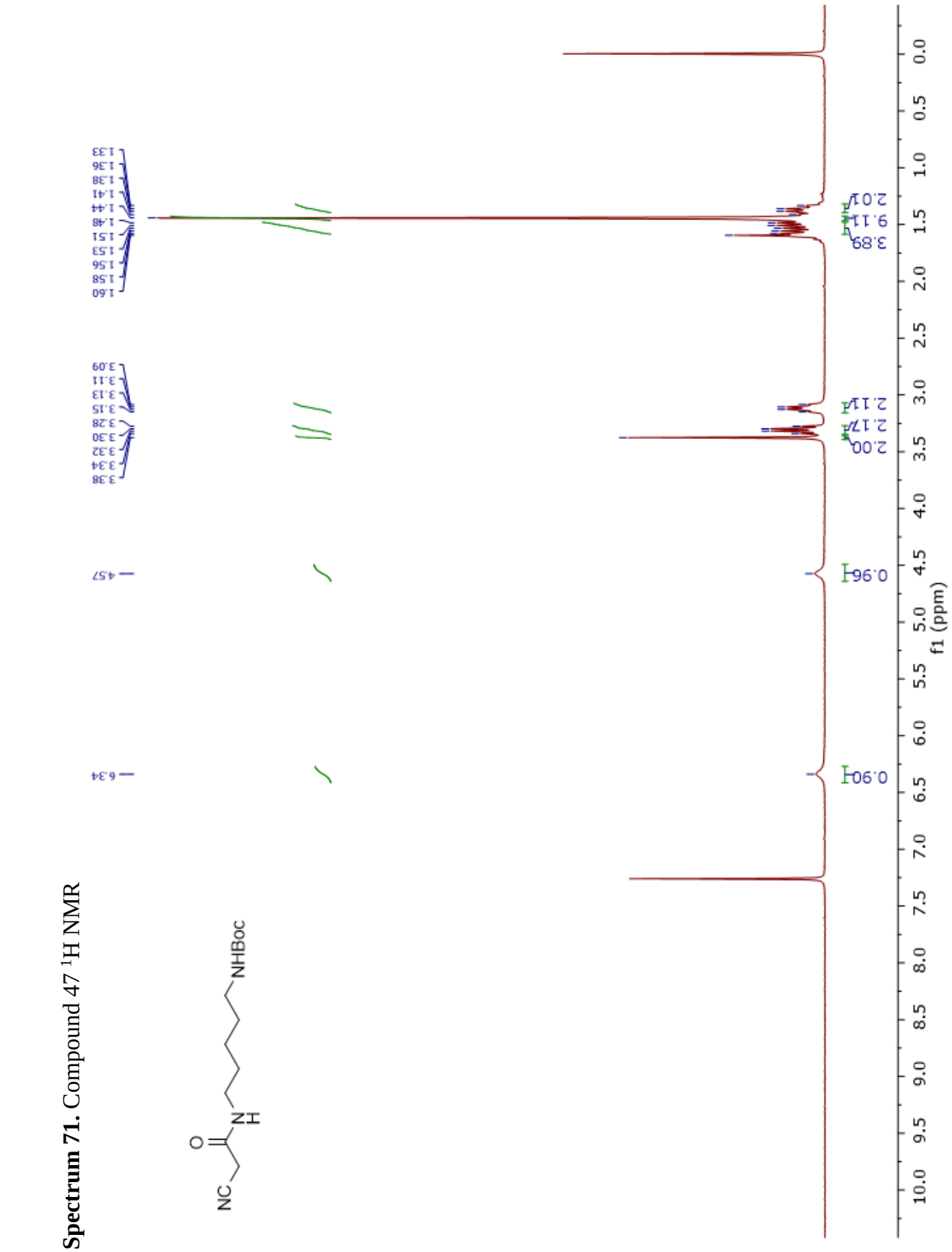

Spectrum 72. Compound 53 ^{1}H NMR

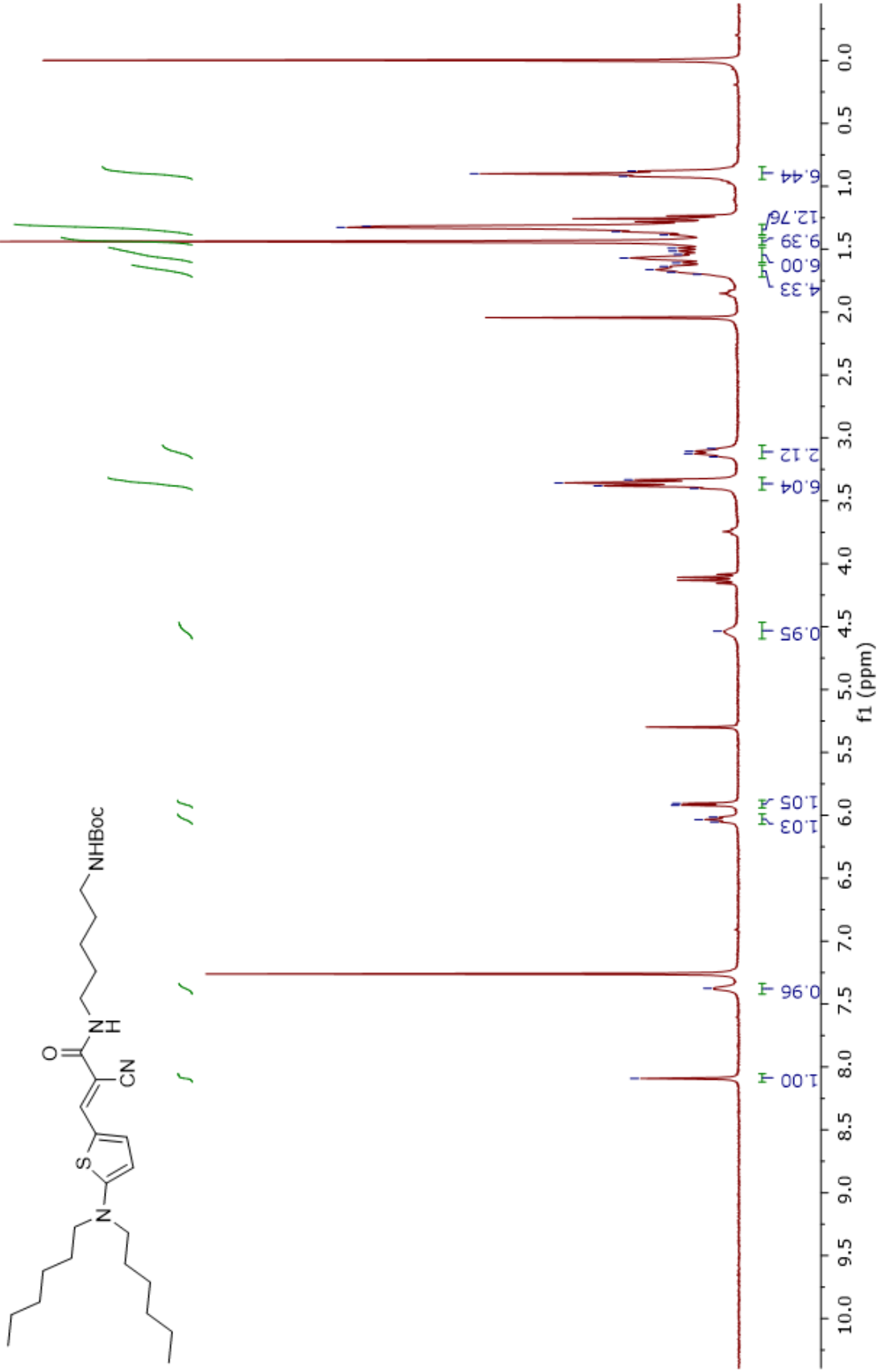

Spectrum 73. Compound 55 ^{1}H NMR

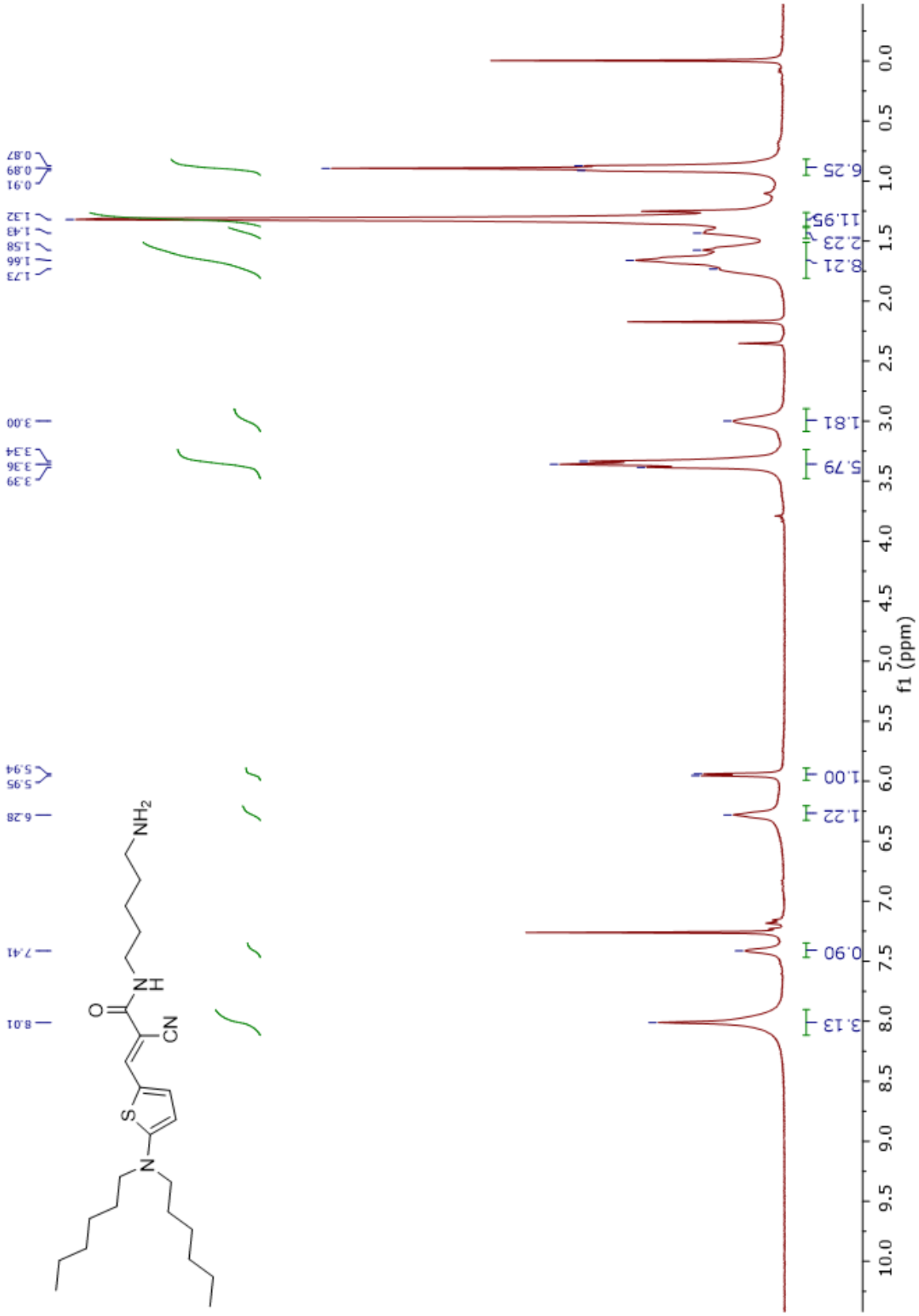

Spectrum 74. Compound 57 ^{1}H NMR

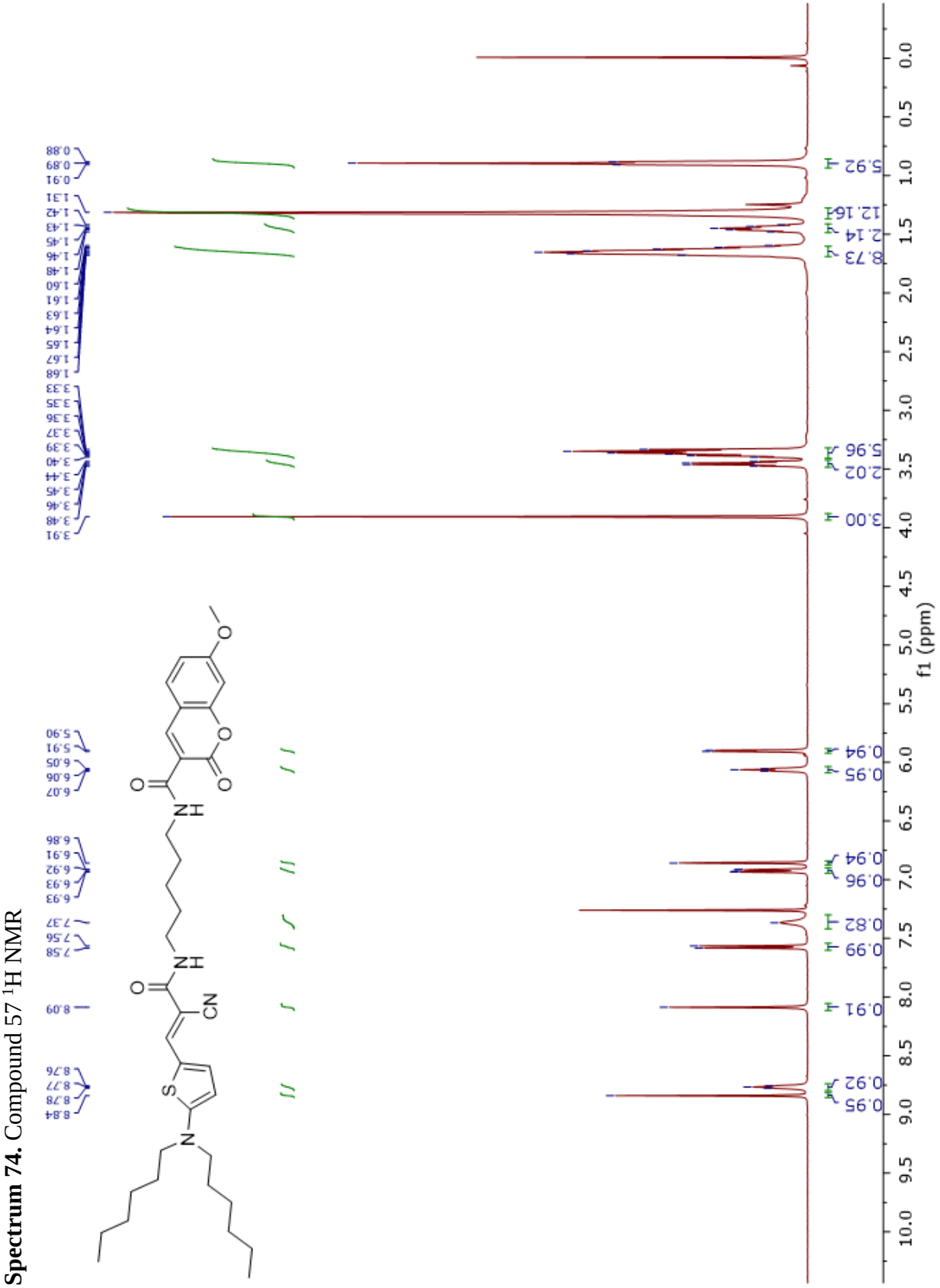

Spectrum 75. Compound 57 ^{1}H NMR

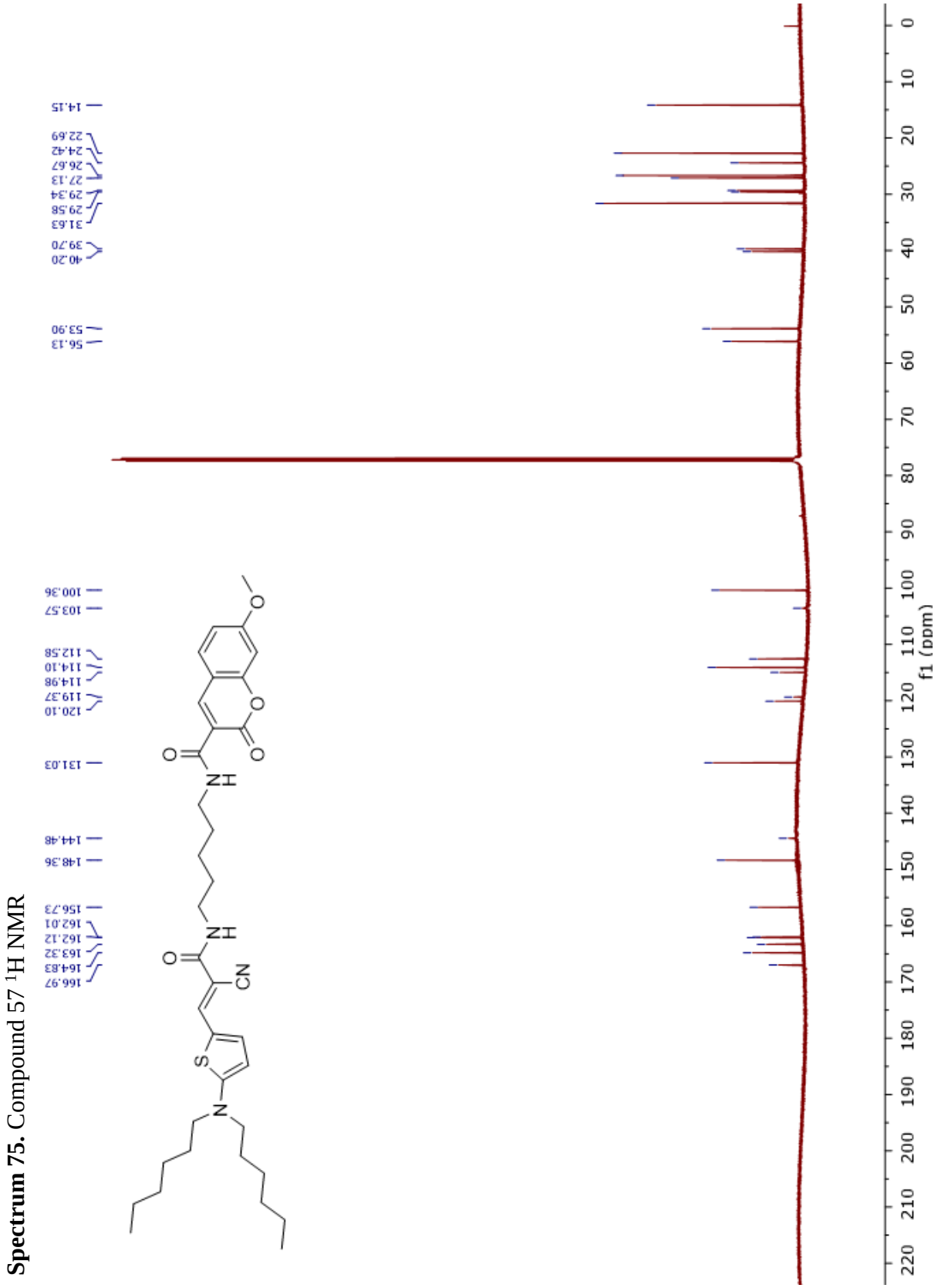

REFERENCES

(1) Lakowicz, J. R. *Principles of Fluorescence Spectroscopy*; 2006. https://doi.org/10.1007/978-0-387-46312-4.

(2) Lichtman, J. W.; Conchello, J. A. Fluorescence Microscopy. *Nat. Methods* **2005**, *2* (12), 910–919. https://doi.org/10.1038/nmeth817.

(3) Limpouchová, Z.; Procházka, K. *Theoretical Principles of Fluorescence Spectroscopy*; 2016. https://doi.org/10.1007/978-3-319-26788-3_4.

(4) Lakowicz, J. R.; Malicka, J.; Gryczynski, I.; Gryczynski, Z.; Geddes, C. D. Radiative Decay Engineering: The Role of Photonic Mode Density in Biotechnology. *J. Phys. D. Appl. Phys.* **2003**, *36* (14). https://doi.org/10.1088/0022-3727/36/14/203.

(5) Piatkevich, K. D.; Verkhusha, V. V. *Guide to Red Fluorescent Proteins and Biosensors for Flow Cytometry*, Second Edi.; Elsevier Inc., 2011; Vol. 102. https://doi.org/10.1016/B978-0-12-374912-3.00017-1.

(6) Horváth, P.; Šebej, P.; Šolomek, T.; Klán, P. Small-Molecule Fluorophores with Large Stokes Shifts: 9-Iminopyronin Analogues as Clickable Tags. *J. Org. Chem.* **2015**, *80* (3), 1299–1311. https://doi.org/10.1021/jo502213t.

(7) Mertz, E. L.; Tikhomirov, V. A.; Krishtalik, L. I. Stokes Shift as a Tool for Probing the Solvent Reorganization Energy. *J. Phys. Chem. A* **1997**, *101* (19), 3433–3442. https://doi.org/10.1021/jp963042b.

(8) Stopel, M. H. W.; Blum, C.; Subramaniam, V. Excitation Spectra and Stokes Shift Measurements of Single Organic Dyes at Room Temperature. *J. Phys. Chem. Lett.* **2014**, *5* (18), 3259–3264. https://doi.org/10.1021/jz501536a.

(9) Wang, L.; Frei, M. S.; Salim, A.; Johnsson, K. Small-Molecule Fluorescent Probes for Live-Cell Super-Resolution Microscopy. *J. Am. Chem. Soc.* **2019**, *141* (7), 2770–2781. https://doi.org/10.1021/jacs.8b11134.

(10) Sinkeldam, R. W.; Greco, N. J.; Tor, Y. Fluorescent Analogs of Biomolecular Building Blocks: Design, Properties, and Applications. *Chem. Rev.* **2010**, *110* (5), 2579–2619. https://doi.org/10.1021/cr900301e.

(11) Sarder, P.; Maji, D.; Achilefu, S. Molecular Probes for Fluorescence Lifetime Imaging. *Bioconjug. Chem.* **2015**, *26* (6), 963–974. https://doi.org/10.1021/acs.bioconjchem.5b00167.

(12) Gao, P.; Pan, W.; Li, N.; Tang, B. Fluorescent Probes for Organelle-Targeted Bioactive Species Imaging. *Chem. Sci.* **2019**, *10* (24), 6035–6071. https://doi.org/10.1039/c9sc01652j.

(13) Miao, W.; Yu, C.; Hao, E.; Jiao, L. Functionalized BODIPYs as Fluorescent Molecular Rotors for Viscosity Detection. *Front. Chem.* **2019**, *7* (November), 1–6. https://doi.org/10.3389/fchem.2019.00825.

(14) Klymchenko, A. S. Solvatochromic and Fluorogenic Dyes as Environment-Sensitive Probes: Design and Biological Applications. *Acc. Chem. Res.* **2017**, *50* (2), 366–375. https://doi.org/10.1021/acs.accounts.6b00517.

(15) Haidekker, M. A.; Nipper, M.; Mustafic, A.; Lichlyter, D.; Dakanali, M.; Theodorakis, E. A. *Dyes with Segmental Mobility: Molecular Rotors*; 2010. https://doi.org/10.1007/978-3-642-04702-2_8.

(16) Kuimova, M. K. Molecular Rotors Image Intracellular Viscosity. *Chimia (Aarau).* **2012**, *66* (4), 159–165. https://doi.org/10.2533/chimia.2012.159.

(17) Lee, S. C.; Heo, J.; Woo, H. C.; Lee, J. A.; Seo, Y. H.; Lee, C. L.; Kim, S.; Kwon, O. P. Fluorescent Molecular Rotors for Viscosity Sensors. *Chem. - A Eur. J.* **2018**, *24* (52), 13706–13718. https://doi.org/10.1002/chem.201801389.

(18) Vyšniauskas, A.; Kuimova, M. K. A Twisted Tale: Measuring Viscosity and Temperature of Microenvironments Using Molecular Rotors. *Int. Rev. Phys. Chem.* **2018**, *37* (2), 259–285. https://doi.org/10.1080/0144235X.2018.1510461.

(19) Haidekker, M. A.; Theodorakis, E. A. Environment-Sensitive Behavior of Fluorescent Molecular Rotors. *J. Biol. Eng.* **2010**, *4*, 1–14. https://doi.org/10.1186/1754-1611-4-11.

(20) Bureš, F. Fundamental Aspects of Property Tuning in Push-Pull Molecules. *RSC Adv.* **2014**, *4* (102), 58826–58851. https://doi.org/10.1039/c4ra11264d.

(21) Li, B.; Zhao, M.; Zhang, F. Rational Design of Near-Infrared-II Organic Molecular Dyes for Bioimaging and Biosensing. *ACS Mater. Lett.* **2020**, *2* (8), 905–917. https://doi.org/10.1021/acsmaterialslett.0c00157.

(22) Ulrich, G.; Goeb, S.; De Nicola, A.; Retailleau, P.; Ziessel, R. Chemistry at Boron: Synthesis and Properties of Red to near-IR Fluorescent Dyes Based on Boron-Substituted Diisoindolomethene Frameworks. *J. Org. Chem.* **2011**, *76* (11), 4489–4505. https://doi.org/10.1021/jo200246q.

(23) Ni, Y.; Wu, J. Far-Red and near Infrared BODIPY Dyes: Synthesis and Applications for Fluorescent PH Probes and Bio-Imaging. *Org. Biomol. Chem.* **2014**, *12* (23), 3774–3791. https://doi.org/10.1039/c3ob42554a.

(24) Su, D.; Teoh, C. L.; Gao, N.; Xu, Q. H.; Chang, Y. T. A Simple Bodipy-Based Viscosity Probe for Imaging of Cellular Viscosity in Live Cells. *Sensors (Switzerland)* **2016**, *16* (9). https://doi.org/10.3390/s16091397.

(25) López-Duarte, I.; Truc Vu, T.; Izquierdo, M. A.; Bull, J. A.; Kuimova, M. K. A Molecular Rotor for Measuring Viscosity in Plasma Membranes of Live Cells. *Chem. Commun.* **2014**, *50* (40), 5282–5284. https://doi.org/10.1039/c3cc47530a.

(26) Polishchuk, V.; Stanko, M.; Kulinich, A.; Shandura, M. D–π–A–π–D Dyes with a 1,3,2-Dioxaborine Cycle in the Polymethine Chain: Efficient Long-Wavelength Fluorophores. *European J. Org. Chem.* **2018**, *2018* (2), 240–246. https://doi.org/10.1002/ejoc.201701466.

(27) Karpenko, I. A.; Niko, Y.; Yakubovskyi, V. P.; Gerasov, A. O.; Bonnet, D.; Kovtun, Y.

P.; Klymchenko, A. S. Push-Pull Dioxaborine as Fluorescent Molecular Rotor: Far-Red Fluorogenic Probe for Ligand-Receptor Interactions. *J. Mater. Chem. C* **2016**, *4* (14), 3002–3009. https://doi.org/10.1039/c5tc03411f.

(28) Chongzhao, R.; Xiaoyin, X.; Raymond, S. B.; Ferrara, B. J.; Neal, K.; Bacskai, B. J.; Medarova, Z.; Moore, A. Design, Synthesis, and Testing of Difluoroboron-Derivatized Curcumins as near-Infrared Probes for in Vivo Detection of Amyloid-β Deposits. *J. Am. Chem. Soc.* **2009**, *131* (42), 15257–15261. https://doi.org/10.1021/ja9047043.

(29) Miller, E. W. Small Molecule Fluorescent Voltage Indicators for Studying Membrane Potential. *Curr. Opin. Chem. Biol.* **2016**, *33*, 74–80. https://doi.org/10.1016/j.cbpa.2016.06.003.

(30) Kang, J.; Lhee, S. M.; Lee, J. K.; Zare, R. N.; Nam, H. G. Restricted Intramolecular Rotation of Fluorescent Molecular Rotors at the Periphery of Aqueous Microdroplets in Oil. *Sci. Rep.* **2020**, *10* (1), 1–10. https://doi.org/10.1038/s41598-020-73980-7.

(31) Peng, X.; Yang, Z.; Wang, J.; Fan, J.; He, Y.; Song, F.; Wang, B.; Sun, S.; Qu, J.; Qi, J.; Yan, M. Fluorescence Ratiometry and Fluorescence Lifetime Imaging: Using a Single Molecular Sensor for Dual Mode Imaging of Cellular Viscosity. *J. Am. Chem. Soc.* **2011**, *133* (17), 6626–6635. https://doi.org/10.1021/ja1104014.

(32) Kung, C. E.; Reed, J. K. Fluorescent Molecular Rotors: A New Class of Probes for Tubulin Structure and Assembly. *Biochemistry* **1989**, *28* (16), 6678–6686. https://doi.org/10.1021/bi00442a022.

(33) Kung, C. E.; Reed, J. K. Microviscosity Measurements of Phospholipid Bilayers Using Fluorescent Dyes That Undergo Torsional Relaxation. *Biochemistry* **1986**, *25* (20), 6114–6121. https://doi.org/10.1021/bi00368a042.

(34) Yang, Z.; He, Y.; Lee, J. H.; Park, N.; Suh, M.; Chae, W. S.; Cao, J.; Peng, X.; Jung, H.; Kang, C.; Kim, J. S. A Self-Calibrating Bipartite Viscosity Sensor for Mitochondria. *J. Am. Chem. Soc.* **2013**, *135* (24), 9181–9185. https://doi.org/10.1021/ja403851p.

(35) Guo, R.; Yin, J.; Ma, Y.; Wang, Q.; Lin, W. A Novel Mitochondria-Targeted Rhodamine Analogue for the Detection of Viscosity Changes in Living Cells, Zebra Fish and Living Mice. *J. Mater. Chem. B* **2018**, *6* (18), 2894–2900. https://doi.org/10.1039/c8tb00298c.

(36) Chen, B.; Li, C.; Zhang, J.; Kan, J.; Jiang, T.; Zhou, J.; Ma, H. Sensing and Imaging of Mitochondrial Viscosity in Living Cells Using a Red Fluorescent Probe with a Long Lifetime. *Chem. Commun.* **2019**, *55* (51), 7410–7413. https://doi.org/10.1039/c9cc03977e.

(37) Xu, M. M.; Ren, W. M.; Tang, X. C.; Hu, Y. H.; Zhang, H. Y. Advances in Development of Fluorescent Probes for Detecting Amyloid-β Aggregates. *Acta Pharmacol. Sin.* **2016**, *37* (6), 719–730. https://doi.org/10.1038/aps.2015.155.

(38) Ran, K.; Yang, J.; Nair, A. V.; Zhu, B.; Ran, C. Cranad-28: A Robust Fluorescent Compound for Visualization of Amyloid Beta Plaques. *Molecules* **2020**, *25* (4), 1–8. https://doi.org/10.3390/molecules25040863.

(39) Nyström, S.; Bäck, M.; Nilsson, K. P. R.; Hammarström, P. Imaging Amyloid Tissues Stained with Luminescent Conjugated Oligothiophenes by Hyperspectral Confocal

Microscopy and Fluorescence Lifetime Imaging. *J. Vis. Exp.* **2017**, *2017* (128), 1–7. https://doi.org/10.3791/56279.

(40) Cui, M.; Ono, M.; Watanabe, H.; Kimura, H.; Liu, B.; Saji, H. Smart Near-Infrared Fluorescence Probes with Donor-Acceptor Structure for in Vivo Detection of β-Amyloid Deposits. *J. Am. Chem. Soc.* **2014**, *136* (9), 3388–3394. https://doi.org/10.1021/ja4052922.

(41) Ono, M.; Watanabe, H.; Kimura, H.; Saji, H. BODIPY-Based Molecular Probe for Imaging of Cerebral β-Amyloid Plaques. *ACS Chem. Neurosci.* **2012**, *3* (4), 319–324. https://doi.org/10.1021/cn3000058.

(42) Hong, M. C.; Kim, Y. K.; Choi, J. Y.; Yang, S. Q.; Rhee, H.; Ryu, Y. H.; Choi, T. H.; Cheon, G. J.; An, G. Il; Kim, H. Y.; Kim, Y.; Kim, D. J.; Lee, J. S.; Chang, Y. T.; Lee, K. C. Synthesis and Evaluation of Stilbene Derivatives as a Potential Imaging Agent of Amyloid Plaques. *Bioorganic Med. Chem.* **2010**, *18* (22), 7724–7730. https://doi.org/10.1016/j.bmc.2010.06.044.

(43) Borelli, M.; Iasilli, G.; Minei, P.; Pucci, A. Fluorescent Polystyrene Films for the Detection of Volatile Organic Compounds Using the Twisted Intramolecular Charge Transfer Mechanism †. *Molecules* **2017**, *22* (8), 13–18. https://doi.org/10.3390/molecules22081306.

(44) Iasilli, G.; Martini, F.; Minei, P.; Ruggeri, G.; Pucci, A. Vapochromic Features of New Luminogens Based on Julolidine-Containing Styrene Copolymers. *Faraday Discuss.* **2017**, *196*, 113–129. https://doi.org/10.1039/c6fd00151c.

(45) Paczkowski, J.; Neckers, D. C. New Fluorescence Probes for Monitoring the Kinetics of Laser-initiated Polymerization. *J. Polym. Sci. Part A Polym. Chem.* **1993**, *31* (3), 841–846. https://doi.org/10.1002/pola.1993.080310330.

(46) Ortyl, J.; Fiedor, P.; Chachaj-Brekiesz, A.; Pilch, M.; Hola, E.; Galek, M. The Applicability of 2-Amino-4,6-Diphenyl-Pyridine-3-Carbonitrile Sensors for Monitoring Different Types of Photopolymerization Processes and Acceleration of Cationic and Free-Radical Photopolymerization under near UV Light. *Sensors (Switzerland)* **2019**, *19* (7). https://doi.org/10.3390/s19071668.

(47) Sasaki, S.; Drummen, G. P. C.; Konishi, G. I. Recent Advances in Twisted Intramolecular Charge Transfer (TICT) Fluorescence and Related Phenomena in Materials Chemistry. *J. Mater. Chem. C* **2016**, *4* (14), 2731–2743. https://doi.org/10.1039/c5tc03933a.

(48) Chen, Q.; Ikemori, F.; Mochida, M. Light Absorption and Excitation-Emission Fluorescence of Urban Organic Aerosol Components and Their Relationship to Chemical Structure. *Environ. Sci. Technol.* **2016**, *50* (20), 10859–10868. https://doi.org/10.1021/acs.est.6b02541.

(49) Alhassawi, F. M.; Corradini, M. G.; Rogers, M. A.; Ludescher, R. D. Potential Applications of Luminescent Molecular Rotors in Food Science and Engineering. *Crit. Rev. Food Sci. Nutr.* **2018**, *58* (11), 1902–1916. https://doi.org/10.1080/10408398.2017.1278583.

(50) Biancalana, M.; Koide, S. Molecular Mechanism of Thioflavin-T Binding to Amyloid Fibrils. *Biochim. Biophys. Acta - Proteins Proteomics* **2010**, *1804* (7), 1405–1412. https://doi.org/10.1016/j.bbapap.2010.04.001.

(51) Larkin, J. W.; Zhai, X.; Kikuchi, K.; Redford, S. E.; Prindle, A.; Liu, J.; Greenfield, S.; Walczak, A. M.; Garcia-Ojalvo, J.; Mugler, A.; Süel, G. M. Signal Percolation within a Bacterial Community. *Cell Syst.* **2018**, *7* (2), 137-145.e3. https://doi.org/10.1016/j.cels.2018.06.005.

(52) Liu, J.; Prindle, A.; Humphries, J.; Gabalda-Sagarra, M.; Asally, M.; Lee, D. Y. D.; Ly, S.; Garcia-Ojalvo, J.; Süel, G. M. Metabolic Co-Dependence Gives Rise to Collective Oscillations within Biofilms. *Nature* **2015**, *523* (7562), 550–554. https://doi.org/10.1038/nature14660.

(53) Prindle, A.; Liu, J.; Asally, M.; Ly, S.; Garcia-Ojalvo, J.; Süel, G. M. Ion Channels Enable Electrical Communication in Bacterial Communities. *Nature* **2015**, *527* (7576), 59–63. https://doi.org/10.1038/nature15709.

(54) Zhai, X.; Larkin, J. W.; Kikuchi, K.; Redford, S. E.; Roy, U.; Süel, G. M.; Mugler, A. Statistics of Correlated Percolation in a Bacterial Community. *PLoS Comput. Biol.* **2019**, *15* (12), 1–19. https://doi.org/10.1371/journal.pcbi.1007508.

(55) Mancini, L.; Terradot, G.; Tian, T.; Pu, Y.; Li, Y.; Lo, C.; Bai, F.; Pilizota, T. Escherichia Coli's Physiology Can Turn Membrane Voltage Dyes into Actuators. *Bull. Am. Phys. Soc.* **2019**, *Volume 64*, 1–15. https://doi.org/10.1101/607838.

(56) Barbon, S. M.; Staroverov, V. N.; Gilroy, J. B. Effect of Extended π Conjugation on the Spectroscopic and Electrochemical Properties of Boron Difluoride Formazanate Complexes. *J. Org. Chem.* **2015**, *80* (10), 5226–5235. https://doi.org/10.1021/acs.joc.5b00620.

(57) Senerovic, L.; Opsenica, D.; Moric, I.; Aleksic, I.; Spasić, M.; Vasiljevic, B. Quinolines and Quinolones as Antibacterial, Antifungal, Anti-Virulence, Antiviral and Anti-Parasitic Agents. *Adv. Exp. Med. Biol.* **2020**, *1282* (September 2019), 37–69. https://doi.org/10.1007/5584_2019_428.

(58) Grimm, J. B.; Muthusamy, A. K.; Liang, Y.; Brown, T. A.; Lemon, W. C.; Patel, R.; Lu, R.; Macklin, J. J.; Keller, P. J.; Ji, N.; Lavis, L. D. A General Method to Fine-Tune Fluorophores for Live-Cell and in Vivo Imaging. *Nat. Methods* **2017**, *14* (10), 987–994. https://doi.org/10.1038/nmeth.4403.

(59) Grimm, J. B.; English, B. P.; Chen, J.; Slaughter, J. P.; Zhang, Z.; Revyakin, A.; Patel, R.; Macklin, J. J.; Normanno, D.; Singer, R. H.; Lionnet, T.; Lavis, L. D. A General Method to Improve Fluorophores for Live-Cell and Single-Molecule Microscopy. *Nat. Methods* **2015**, *79* (3), 244–250. https://doi.org/10.1038/nmeth.3256.A.

(60) Sibrian-Vazquez, M.; Escobedo, J. O.; Lowry, M.; Fronczek, F. R.; Strongin, R. M. Field Effects Induce Bathochromic Shifts in Xanthene Dyes. *J. Am. Chem. Soc.* **2012**, *134* (25), 10502–10508. https://doi.org/10.1021/ja302445w.

(61) Guan, Y.; Cao, K. J.; Cantlon, A.; Elbel, K.; Theodorakis, E. A.; Walsh, D. M.; Yang, J.;

Shah, J. V. Real-Time Monitoring of Alzheimer's-Related Amyloid Aggregation via Probe Enhancement-Fluorescence Correlation Spectroscopy. *ACS Chem. Neurosci.* **2015**, *6* (9), 1503–1508. https://doi.org/10.1021/acschemneuro.5b00176.

(62) Haidekker, M. A.; Brady, T. P.; Lichlyter, D.; Theodorakis, E. A. A Ratiometric Fluorescent Viscosity Sensor. *J. Am. Chem. Soc.* **2006**, *128* (2), 398–399. https://doi.org/10.1021/ja056370a.

(63) Haidekker, M. A.; Brady, T. P.; Chalian, S. H.; Akers, W.; Lichlyter, D.; Theodorakis, E. A. Hydrophilic Molecular Rotor Derivatives - Synthesis and Characterization. *Bioorg. Chem.* **2004**, *32* (4), 274–289. https://doi.org/10.1016/j.bioorg.2004.04.002.

(64) Dakanali, M.; Do, T. H.; Horn, A.; Chongchivivat, A.; Jarusreni, T.; Lichlyter, D.; Guizzunti, G.; Haidekker, M. A.; Theodorakis, E. A. Self-Calibrating Viscosity Probes: Design and Subcellular Localization. *Bioorganic Med. Chem.* **2012**, *20* (14), 4443–4450. https://doi.org/10.1016/j.bmc.2012.05.026.

(65) Barnard, R.; Barnard, A.; Salmon, G.; Liu, W.; Sreckovic, S. Histamine-Induced Actin Polymerization in Human Eosinophils: An Imaging Approach for Histamine H4 Receptor. *Cytom. Part A* **2008**, *73* (4), 299–304. https://doi.org/10.1002/cyto.a.20514.

(66) Fujiwara, I.; Zweifel, M. E.; Courtemanche, N.; Pollard, T. D. Latrunculin A Accelerates Actin Filament Depolymerization in Addition to Sequestering Actin Monomers. *Curr. Biol.* **2018**, *28* (19), 3183-3192.e2. https://doi.org/10.1016/j.cub.2018.07.082.

(67) Lee, M. H.; Kim, J. S.; Sessler, J. L. Small Molecule-Based Ratiometric Fluorescence Probes for Cations, Anions, and Biomolecules. *Chem. Soc. Rev.* **2015**, *44* (13), 4185–4191. https://doi.org/10.1039/c4cs00280f.